The role of human ORC2 in DNA replication, mitosis and organization of the nucleus

A Dissertation Presented

by

Hsiang-Chen Chou

to

The Graduate School

in Partial Fulfillment of the

Requirements

for the Degree of

Doctor of Philosophy

in

Molecular and Cellular Biology

Stony Brook University

August 2021

Stony Brook University

The Graduate School

Hsiang-Chen Chou

We, the dissertation committee for the above candidate for the

Doctor of Philosophy degree, hereby recommend

acceptance of this dissertation.

Bruce Stillman, Ph.D. – Dissertation Advisor
Professor, President & CEO, Cold Spring Harbor Laboratory, MCB

Ed Luk, Ph.D. – Chairperson of Defense
Associate Professor of Biochemistry and Cell Biology

Leemor Joshua-Tor, Ph.D.
Professor & HHMI Investigator, Cold Spring Harbor Laboratory, MCB

Rob Martienssen, Ph.D.
Professor & HHMI Investigator, Cold Spring Harbor Laboratory, MCB

Susan Smith, Ph.D. – Outside member
Professor of Pathology, NYU School of Medicine

This dissertation is accepted by the Graduate School

Eric Wertheimer
Dean of the Graduate School

Abstract of the Dissertation

The role of human ORC2 in DNA replication, mitosis and organization of the nucleus

by

Hsiang-Chen Chou

Doctor of Philosophy

in

Molecular and Cellular Biology

(MCB)

Stony Brook University

2021

In eukaryotic cells, the entire genome is duplicated only once each cell division cycle during S-phase and is followed by segregation of the sister chromatids to the two daughter cells. A pre-Replication Complex (pre-RC) is assembled at every origin prior to replication initiation and is assembled in a stepwise manner. It begins with the hexameric Origin Recognition Complex (ORC) 1-6 subunits binding to replication origins. Unlike yeast *Saccharomyces cerevisiae* ORC that remains a stable complex throughout the entire cell division cycle, in human cells the ORC complex dissociates soon after the pre-RC is activated at the beginning of S phase and the ORC1 subunit is degraded. Reports in the literature suggest that ORC1 and ORC2 in human cells are not entirely essential, however, CRISPR/Cas9 screens with guide RNAs that target the entire open reading frame of ORC1-6, CDC6, CDT1 and MCM2-7 showed that these proteins are all essential to cell survival. Indeed, the CRISPR/Cas9 screening points to essential domains in each of these proteins.

Previous studies showed depletion of ORC2 or ORC3 in human cells using siRNA caused defects in S-phase and also during mitosis, however, depletion of these proteins using

siRNA is a slow process. Here I used the auxin regulated mAID degron system to construct cell lines in which ORC2 or ORC3 were removed from cells and the resulting cell cycle phenotypes investigated. First, human cells were transduced with LTR-mAID-ORC2, which is resistant to a specific CRISPR-mediated single guide RNA (sgRNA) via retrovirus transduction into cell lines expressing the OsTIR1 protein, a ubiquitin ligase from rice that promotes degradation of proteins linked to an auxin inducible domain (mAID). Then the endogenous *ORC2* gene was mutated using a CRISPR/Cas9 with a sgRNA that inactivates the gene. The primary defects in the absence of ORC2 were cells encountering difficulty in initiating DNA replication or progressing through the cell division cycle due to reduced MCM2-7 loading onto chromatin in G1 phase. This abnormal cell division phenotype then persists through mitosis causing abnormal chromosome segregation including the presence of lagging chromosomes, micronuclei and eventually apoptosis. The nuclei of ORC2 deficient cells were also large, with decompacted heterochromatin. ORC1 knockout cells also demonstrated extremely slow cell proliferation and abnormal cell and nuclear morphology. Thus, ORC proteins and CDC6 are indispensable for normal cellular proliferation and contribute to DNA replication, chromosomes segregation and nuclear organization.

Dedication Page

I dedicate this thesis to my parents who have always supported me throughout my education. I am truly grateful for their support and belief in me.

Table of Contents

List of Figures

List of Tables

List of Abbreviations

Abs	antibodies
ACS	ARS consensus sequence
AD	annotated domain
ANOVA	analysis of variance
ARS	autonomously replicating sequences
ATAC-seq	assay for transposase accessible chromatin with high-throughput sequencing
ATM	Ataxia telangiectasia mutated
ATP	Adenosine triphosphate
ATR	Ataxia telangiectasia and RAD3-related
BAH	bromo-adjacent homology
BiFC	bimolecular fluorescence molecular complementation
BioID	biotin identification
bp	base pair
BSA	bovine serum albumin
BUB1B	mitotic checkpoint serine/threonine-protein kinase BUB1 beta
BUB3	Mitotic checkpoint protein BUB3
BUBR1	Mitotic spindle checkpoint protein BUBR1
$CaCl_2$	calcium chloride
CAF-1	chromatin assembly factor 1
Cas9	CRISPR associated protein 9
CCNE1	G1/S-specific cyclin-E1
CD	chromodomain
Cdc45	cell division control protein 45
Cdc5	cell division cycle 5
CDC6	cell division control 6
CDK	cyclin dependent kinase
CDT	DNA replication factor Cdt1
CENP-C	Centromere protein C

CENP-E	centrosome-associated protein E
ChIP	chromatin Immunoprecipitation
CHK1	checkpoint kinase 1
CHK2	Serine/threonine-protein kinase Chk2
Chp2	Calcineurin B homologous protein 2
CKHS	CRISPR Knockout Hypersensitive
CNVs	copy number variations
CRISPR	clustered regularly interspaced short palindromic repeats
CSD	chromoshadow domain
Ct	cycle threshold
CTE	C-terminal extension
DAPI	4′,6-diamidino-2-phenylindole
DDK	Dbf4 dependent kinase
DMEM	Dulbecco's Modified Eagle Medium
DNA	deoxyribonucleic acid
Dox	doxycycline
Dpb11	DNA replication regulator DPB11
DSB	double strand break
dsDNA	double strand DNA
E2F1	E2F Transcription Factor 1
EDTA	ethylenediaminetetraacetic acid
EdU	5-Ethynyl-2′-deoxyuridine
EGTA	ethylene glycol-bis(β-aminoethyl ether)-N,N,N′,N′-tetraacetic acid
EtOH	ethanol
FACS	fluorescence-activated cell sorting
FC	fold change
FC	fluorescent protein
FSC	forward scatter
GFP	green fluorescent protein
GINS	go-ichi-ni-san

GTP	guanosine-5'-triphosphate
HCl	hydrochloric acid
HEPES	4-(2-hydroxyethyl)-1-piperazineethanesulfonic acid
HP1	heterochromatin protein 1
IDR	intrinsic disordered region
IgG	immunoglobulin G
INPPL1	phosphatidylinositol 3,4,5-trisphosphate 5-phosphatase
IP	immunoprecipitation
IPTG	Isopropyl β- d-1-thiogalactopyranoside
iTRAQ	Isobaric tags for relative and absolute quantitation
KAP-1	KRAB-associated protein 1
KCl	potassium chloride
KOH	potassium hydroxide
LFC	log fold change
LRWD1	Leucine-rich repeat and WD repeat-containing protein 1
Mad2	mitotic spindle checkpoint component MAD2
mAID	mini auxin-inducible degron
MCM	minichromosome maintenance
Mec1	Serine/threonine-protein kinase MEC1
$MgCl_2$	magnesium chloride
MGS	Meier–Gorlin syndrome
MIR	MOD1-interacting region
MNase	micrococcal nuclease
MOI	multiplicity of infection
MS	mass spectrometry
MUMs	maximal unique matches
NaCl	sodium chloride
NAD	non-annotated domain
NGS	normal goat serum
NTE	N-terminal extension

OCCM	ORC-Cdc6-Cdt1-MCM
ONT	Oxford Nanopore Technologies
ORC	origin recognition complex
OsO4	osmium tetraoxide
OsTIR1	Oryza sativa transport inhibitor response 1
P	pellet
PACT	pericentrin-AKAP450 centrosomal targeting
PAM	protospacer adjacent motif
PBS	Phosphate-buffered saline
PCR	Polymerase chain reaction
PFA	paraformaldehyde
PGP	P-Glycoprotein
PI3K	phosphoinositide 3-kinase
PLK1	Polo-like kinase 1
PP1	protein phosphatase 1
Pre-RC	pre-replicative complex
PTPMT1	Phosphatidylglycerophosphatase and protein-tyrosine phosphatase 1
Rad53	Serine/threonine-protein kinase RAD53
RB	retinoblastoma
RBBP5	retinoblastoma-binding protein
RNAi	ribonucleic acid interference
rpm	revolutions per minute
RT-PCR	reverse transcription polymerase chain reaction
SA-β-gal	senescence-associated β-galactosidase
Scc2	sister chromatid cohesion protein 2
SDS	sodium dodecyl sulfate
SEPT2	Septin-2
sgRNA	single guide RNA
SIPS	stress-induced premature senescence
Sir	silent information regulator

siRNA	small interfering RNA
SLiMs	short linear protein motifs
SMASH	short multiply aggregated sequence homologies
SNP	Single nucleotide polymorphism
SSC	side scatter
sup	supernatant
SUV39H1	suppressor of variegation 3-9 homolog 1
SVs	structural variations
TEM	transmission electron microscopy
TFIIB	transcription initiation factor IIB
TFRC	transferrin receptor protein 1
TGUH	Tail-Greedy Unbalanced Haar
TRF2	telomeric repeat-binding factor 2
WHD	winged helix domain

Acknowledgments

When I first came to the US in 2013 to pursue my PhD degree, I'd never thought of how it will totally change my life, both personally and professionally. I received so much guidance, support and company from people that I couldn't imagine going through the journey without them. I would like to take this opportunity to thank all of them.

First of all, I want to express my deepest gratitude and utmost respect to my dissertation advisor, Dr. Bruce Stillman, for his constant guidance and support, and always taking time out of his busy schedule to discuss about the experiments and projects. At the beginning I often felt frustrated because things hadn't work for a period of time, but he kept encouraging me, giving insightful suggestions and directed me to explore new possibilities. His wealth of knowledge and the passion for research has always inspired me to become a better scientist. It would not have been possible to finish this thesis and acquire the Ph.D. without his guidance.

I also want to thank my committee members, Dr. Ed Luk, Dr. Leemor Joshua-Tor, and Dr. Rob Martienssen for spending time to discuss my research with me and providing me with constructive and invaluable advice to make sure that I was on the right track. I feel honored to have a committee composed of members who are respectable scientists in different fields and have helped me improve my research along the way.

I would also like to thank all Stillman lab members, Yi-Jun Sheu, Manzar Hossain, Kuhulika Bhalla, Mike Tramantano, Elaine Hu, Farhana Nasrin, Meng Ouyang, Jenn Shapp, Narges Zali, and Carol Link for their generous help, discussion, and friendships. I want to especially thank Kuhulika, who led the pre-RC CRIPSR screening projects and allowed me to integrate the data into my dissertation. I also want to thank my classmates, Dongyan Song and Zhumin Liu, who accompanied me on the way to CSHL from SBU when I just got the license. Those trips were filled with scientific discussion and unforgettable happiness. I sincerely cherished our friendships.

Last but not least, I want to thank my family for their endless support and belief in me. My parents have taught me and given me the strength to face any challenges in life. My sister, Lori, has always been there when I needed someone to talk to. I also want to share my deepest appreciation to my husband, Peter, for always being by my side and also encouraging me to try different things no matter at work or daily life. I'm also thankful for my son, Ollie, who brings the most happiness in my life, and also keeps reminding me of that world is a wonderful place and I should make every effort to become a better person and contribute my skills to improve human's health.

I am beyond grateful for all of the support I had throughout my Ph.D. and without them, all of this would not have happened.

Publications

Chou H-C, Bhalla K, El Demerdesh O, Klingbeil O, Hanington K, Aganezov S, Andrews P, Alsudani H, Chang K, Vakoc CR, Schatz MC, McCombie WR, Stillman B. 2021. The human Origin Recognition Complex is essential for pre-RC assembly, mitosis and maintenance of nuclear structure. Elife 10:e61797. doi:10.7554/elife.61797

Data availability:

DNA sequencing data including Tiling-sgRNA CRISPR screen, CNV analysis by SMASH and ONT Nanopore long-read sequencing are available in the Dryad database.

Chou H-C., Bhalla K., El Demerdesh O., Klingbeil O., Hanington K., Aganezov S., Andrews P., Alsudani H., Chang K., Vakoc C. R., Schatz M., McCombie W. R., and Stillman B. (2020) Dryad Digital Repository Data from: The human Origin Recognition Complex is essential for pre-RC assembly, mitosis and maintenance of nuclear structure. https://doi.org/10.5061/dryad.59zw3r25f

Chapter One- Background

1. Pre-RC complex and DNA replication

Cell division requires DNA to be synthesized once and only once in the cell cycle, and the process is complex and highly regulated by multiple proteins. In budding yeast *S. cerevisiae*, in which the mechanism and regulation of DNA replication has been characterized most in depth, origin firing has also been reconstituted in vitro with purified proteins (Yeeles et al., 2015) **(Figure 1-1)**. It begins with the Origin Recognition Complex ORC1-6 hexamer binding to every potential origin. ORC acts as a landing pad and recruits Cdc6, Cdt1, and the Mcm2-7 helicase, forming the ORC-Cdc6-Cdt1-MCM (OCCM) intermediate. Next, upon ATP hydrolysis and release of Cdt1, an ORC-MCM (OM) intermediate is formed, and a second Cdc6 and Cdt1-Mcm2-7 complex is recruited to assemble the two Mcm2-7 hexamers in a head-to-head double hexamer (Evrin et al., 2009; Fernández-Cid et al., 2013; Miller et al., 2019; Remus et al., 2009; Ticau et al., 2015). This multi-protein complex, also termed the pre-replicative complex (pre-RC), is an inactive helicase (Donovan and Diffley, 1996; Remus et al., 2009; Rowley et al., 1995; Siddiqui et al., 2013). Activation of DNA helicase requires binding and loading of other proteins and the activation of two conserved protein kinases, Cyclin dependent kinase (CDK) and Dbf4 dependent Cdc7 kinase (DDK), both of which play essential and critical roles in this process. The assembly of pre-replicative complex happens following exit from mitosis and into G1 phase and when the CDK activity is low (Amin et al., 2019; Diffley, 1996; Weinreich et al., 1999). CDK phosphorylation of ORC, Cdc6, and MCM subunits prevent pre-RC assembly outside of G1 and DNA re-replication (Nguyen et al., 2001). With the onset of S phase, MCM is phosphorylated by DDK, which recruits Sld3/7 and Cdc45. CDK-dependent phosphorylation of Sld2 and Sld3 further recruit Sld2, Dpb11, GINS, pol ε and Mcm10 to form the active CMG (Cdc45-MCM-GINS) helicase (Araki et al., 2009; Mailand and Diffley, 2005; Muramatsu et al., 2010; Tak et al., 2006; Yeeles et al., 2015). The single strand DNA is stabilized by RPA protein, thereby allowing the salt-stable CMG complexes to move along efficiently, forming bi-directional forks, unwinding DNA, and allowing DNA polymerase to bind and initiate replication (Kose et al., 2019).

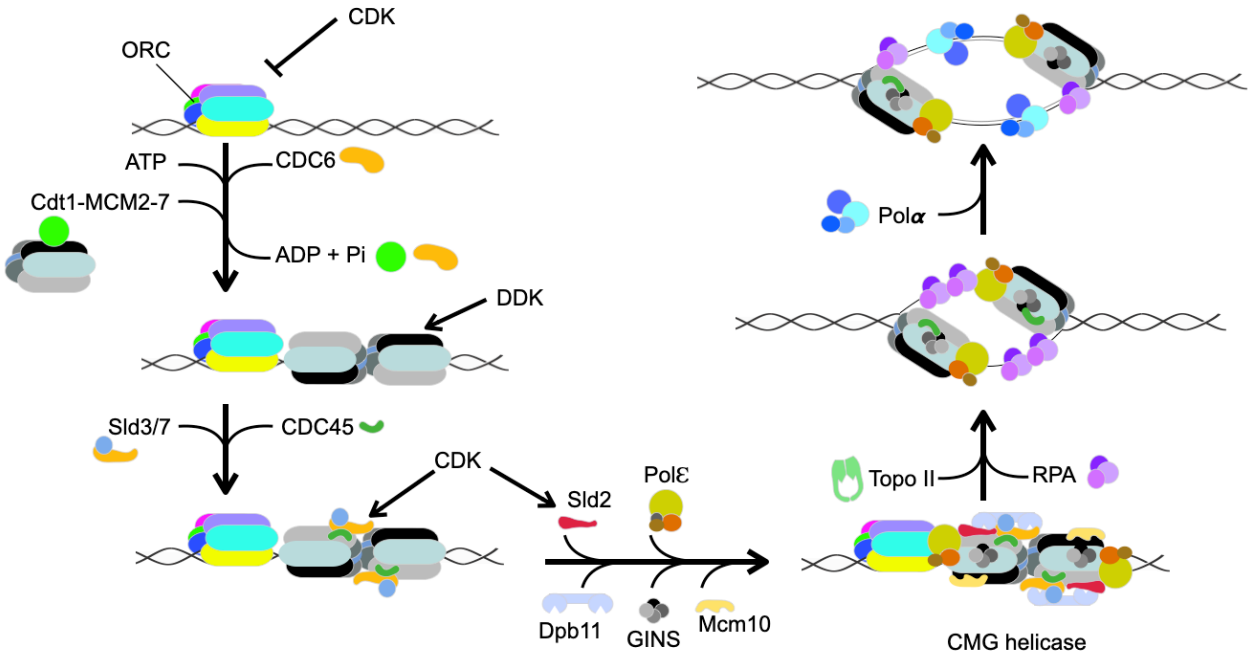

Figure 1-1. **Cartoon illustrating stepwise eukaryotic DNA replication initiation.** The figure was adapted from (Yeeles et al., 2015).

Although the mechanism and the proteins involved in DNA replication initiation are highly conserved in eukaryotes, the DNA sequences where ORC binds are not. In yeast, there are about 350-400 DNA origins throughout the genome, whereas in human there are about 40,000-80,000 origins in order for the large genome to be replicated in a timely manner. In budding yeast *S. cerevisiae*, replication origins are determined by specific DNA sequence motifs. These DNA sequence elements, also termed autonomously replicating sequences (ARSs), consist of about 150 bp of DNA and can maintain extrachromosomal replication when put in a plasmid and transformed into yeast (Stinchcomb et al., 1979). The ARS is composed of an A element that contains the essential ~11 bp AT-rich ARS consensus sequence (ACS) and three B elements, B1, B2, and B3, and ORC binds to A and B1 elements in yeast (Broach et al., 1983; Marahrens and Stillman, 1992; Newlon and Theis, 1993; Palzkill et al., 1986; Rao and Stillman, 1995; Rowley et al., 1995; Shirahige et al., 1993; Theis and Newlon, 1997). In addition, the replication origins are mostly found in nucleosome-free regions, making it more accessible for other replication initiation factors to join (Eaton et al., 2010). In several structural studies, an Orc4 α-helix and Orc2 loop are shown to contact with DNA and are necessary for origin specificity (Hu et al., 2020; Li et al., 2018; Yuan et al., 2017). A structure of the *S. cerevisiae* pre-RC intermediate complex ORC-Cdc6-Cdt1-MCM (OCCM) determined at 3.9-Å-resolution has revealed that an Orc2 loop inserts into the DNA minor groove, and an Orc4 α-helix inserts into the DNA major groove (Yuan et al., 2017). Recent studies in *S. cerevisiae* ORC have found that the Orc4 α-helix is essential for origin recognition specificity and Orc2 loop is essential for replication initiation (Hu et al., 2020; Lee et al., 2021). Loss of the Orc4 α-helix or Orc2 loop is lethal, and the Orc4 α-helix mutations in yeast lead to different levels of growth defects and alter the genome-wide origin firing map (Hu et al., 2020). The α-helix within Orc4 is absent in other budding yeast, *S. pombe*, plants, human and other eukaryotes. In fission yeast *S. pombe*, no specific sequence, but several A-T rich sequences ranging from 20 to 50 bp were found to be important for origin function (Clyne and Kelly, 1995). Binding of ORC to origins in *S. Pombe* is mediated via the AT-hook located in the N-terminal domain of Orc4 DNA, but this is only found in some fungi and thus how origins are specified in most eukaryotes is not known (Chuang and Kelly, 1999).

In other eukaryotes, including plants, animals, and human, replication origins also show no sequence specificity. In fact, in human cells, any fragment of DNA that has sufficient length

can initiate replication (Vashee, 2003). Similar to yeast, not all origins activate at the same time in S phase or have the same efficiency (O'Keefe et al., 1992), and only a subset of origins fire during each cell cycle, depending on the genomic loci, cell type, development and environmental stress, etc. Time-lapse live imaging microscopy revealed that ORC1, being the first ORC subunit binding to the DNA replication origins, localizes to mitotic chromosomes during early mitosis, showing different chromatin binding patterns at different times during G1 and acts as a nucleating center for recruiting other ORC subunits and the assembly of pre-RC (Kara et al., 2015; Okuno et al., 2001). ORC selectively binds to nucleosome depleted regions such as active promoters at transcription start sites, GC-rich DNA, CpG islands, and are also found at cohesion binding sites (Blin et al., 2019; Karnani et al., 2010; MacAlpine et al., 2009; Miotto et al., 2016). ORC tends to localize to open chromatin enriched with H3.3, H2A.Z, or active chromatin marks (Hossain and Stillman, 2016; Kuo et al., 2012; Long et al., 2019; MacAlpine et al., 2009). Active chromatin enriched with acetylation of histone H3 at lysine 27 (H3K27ac) and di-methylation of histone H3 at lysine 4 (H3K4me2) are correlated with ORC-associated DNA origins (Miotto et al., 2016). ORC1, CDT1 and MCM2 also bind to the MYST family histone acetyltransferase HBO1 (KAT7) which is responsible for acetylation of H3K14 and H4 (Burke et al., 2001; Iizuka and Stillman, 1999; Kueh et al., 2019; Miotto and Struhl, 2008). The methylated histone H4 lysine 20 mark (H4K20) enriched at replication origins also binds specifically to ORC and can potentially stabilize the ORC-chromatin interaction. The histone H4K20 have three states of methylation: mono, di, and tri-methylation, and each state is catalyzed by different enzymes (Jørgensen et al., 2013). ORC1 preferentially binds to H4K20me2 which is catalyzed by Suv4-20H1, and mutation in the ORC1 BAH domain disrupts the binding of ORC1 to H4K20me2, and therefore diminishing ORC occupancy at the origins (Kuo et al., 2012).

In eukaryotes, protein sequence analysis of ORC suggests that ORC1-5 subunits contain a AAA+ or a AAA+-like domain and a winged helix domain responsible for DNA binding (Bleichert et al., 2017; Chen et al., 2008; Li et al., 2018; Tocilj et al., 2017). A classical AAA+ domain consists of a RecA-fold which contains Walker-A and Walker-B motifs, but ORC2 and ORC3 have diverged RecA-folds and are therefore considered AAA+-like (Jaremko et al., 2020; Li et al., 2018; Tocilj et al., 2017; Yuan et al., 2017). Although the AAA+ domain exists in ORC1-5 subunits, ATP hydrolysis occurs only at the ORC1-ORC4 ATP-binding site (Bell and

Stillman, 1992; Bowers et al., 2004; Speck et al., 2005). ORC1 has an N-terminal bromo-adjacent homology domain (BAH) which recognizes and interacts with histone modifications, such as H3K9me3, H3K27me3, and H4K20me2, and a pericentrin-AKAP450 centrosomal targeting PACT domain (768–851 amino acids) at the C-terminus that targets ORC1 to centrosomes to regulate centriole duplication (Hossain and Stillman, 2012; Kuo et al., 2012; Müller et al., 2010; Noguchi et al., 2006). ORC1 has an intrinsic disordered region (IDR; amino acids 180-480) which contains multiple short linear protein motifs (SLiMs) that mediate nuclear localization and other regulatory functions (Davey et al., 2011, 2007; Hossain et al., 2021). During late G1 phase Cyclin A-CDK2 binds to a motif within the IDR and recruits the SCF^{SKP2} ubiquitin ligase that modifies ORC1 for degradation. Separately, Cyclin A-CDK2 phosphorylates ORC1 when it is resynthesized just before mitosis and during mitotic exit. Protein phosphatase 1 (PP1) binds to a motif within the ORC1 IDR and de-phosphorylates ORC1 as well as promotes pre-RC assembly (Hossain et al., 2021). A SLiM in the ORC1 IDR that overlaps with the cyclin-binding motif (Cy motif) binds to CDC6 and also mediates the ORC1 intra- and inter-molecular interactions (Hossain et al., 2021). The ORC1 IDR is also involved in DNA-dependent liquid phase separation (Parker et al., 2019). ORC2 also harbors a predicted intrinsic disordered region within the N-terminus but is not required for phase separation (Parker et al., 2019). ORC6 is poorly conserved in eukaryotes and lacks the AAA+ domain. ORC6 contains two transcription initiation factor-IIB-like domains and a C-terminal domain which is essential for chromosome segregation and cytokinesis in metazoans (Balasov et al., 2009; Chesnokov et al., 2009, 2003; Liu et al., 2011; Prasanth et al., 2002; Semple et al., 2006). CDC6, which is closely related in amino acid sequence to ORC1, also has an AAA+ domain that binds to ATP and a C-terminal winged helix domain. ATP hydrolysis in CDC6 is not required for binding to DNA but is required for dissociating from the pre-RC complex to prevent re-replication (Chang et al., 2015; Perkins and Diffley, 1998; Randell et al., 2006; Tiengwe et al., 2012; Weinreich et al., 1999). CDC6 also has a predicted IDR and potentially involved in DNA-dependent liquid-liquid phase separation (Parker et al., 2019), although, unlike ORC1, CDC6 cannot phase separate on its own (Hossain et al., 2021).

In human cells, the initiation of replication is similar to that in budding yeast, however some differences exist. Yeast ORC forms a stable hexamer and associates with chromatin at all

times during the cell division cycle (Bell and Stillman, 1992; Diffley, 1994). Yeast Cdc6 is degraded from the G1-S boundary until mitosis via SCF^{Cdc4} mediated proteolysis controlled by Clb/Cdk28 kinases (Perkins et al., 2001; Piatti et al., 1996). In contrast, human ORC2-5 form a core complex, and ORC1 and ORC6 binds to the core complex transiently during the G1 phase of the cell cycle. One or more human ORC subunits dissociate from the DNA after pre-RC assembly. In human cells, the largest ORC1 subunit is targeted for degradation at G1/S transition by SCF^{Skp2}-mediated ubiquitination, and is re-synthesized in late G2, and then binds to mitotic chromosomes during mitosis (DePamphilis, 2004; Kara et al., 2015; Méndez et al., 2002; Ohta et al., 2003; Tatsumi et al., 2003). Human CDC6 undergoes proteasome degradation during late mitosis via $SCF^{cyclinF}$ and during early G1 phase by the anaphase-promoting complex/cyclosome (APC/C)/Cdh1 complex and is stabilized during mid-G1 by Cyclin E-CDK2 dependent phosphorylation (Duursma and Agami, 2005; Mailand and Diffley, 2005; Petersen et al., 2000; Walter et al., 2016). Later during S phase CDC6 is phosphorylated by CyclinA-CDK2 and is exported from the nucleus (Jiang et al., 1999; Petersen et al., 1999; Saha et al., 1998). Human ORC2 and ORC3 form stable heterodimers in the cells (Dhar et al., 2001; Jaremko et al., 2020; Vashee, 2003). In human cells, localization of ORC and CDC6 to the nucleus or cytoplasm is regulated by their phosphorylation. Geminin also plays a critical role in regulating replication by targeting CDT1, and loss of this protein results in re-replication (Ballabeni et al., 2013; McGarry and Kirschner, 1998; Wohlschlegel et al., 2000).

2. ORC and gene silencing and heterochromatin structure

The human genome contains two copies of about 3 billion base pairs that are arranged into a linear DNA that is packaged into 23 chromosome pairs and a mitochondria genome. To fit all this genetic material in the nucleus and retain its ability to replicate and transcribe correctly, DNA condenses and wraps around histone proteins to form chromatin. Interphase chromatin is

classified into two groups, euchromatin and heterochromatin. Euchromatin if straightened looks like beads on a string under the microscope, and these beads are the nucleosomes which contain DNA and histones. Each nucleosome consists of eight histones (two copies of each histone core H2A, H2B, H3, and H4) with 147 bps of DNA wrapping around them. Nucleosomal wrapping in euchromatin is loose, resulting in a more accessible and transcriptionally active chromatin.

Heterochromatin was first discovered by Emil Heitz in 1928 by the cytological staining pattern of mitotic chromosomes in liverworts *Marchantia polymorpha.* Heterochromatin is a more condensed form of chromatin with tightly packed nucleosomes, making it less accessible and mostly transcriptionally silent. There are two types of heterochromatin, facultative heterochromatin and constitutive heterochromatin. The former is able to change its structural conformation during the cell cycle and has the potential for gene expression during development. The latter remains condensed throughout the cell cycle and contains highly repetitive DNA sequences called satellite DNA that is mostly found at the centromeres and telomeres. Constitutive heterochromatin plays a role in chromosome organization, chromosome segregation, telomere protection, and it also prevent genome instability (Allshire and Madhani, 2018; Canudas et al., 2011; Cheutin et al., 2003; Fanti et al., 1998; Grewal and Jia, 2007; Janssen et al., 2018; Perrini et al., 2004; Zeng et al., 2010). Heterochromatin is usually found near the nuclear membrane in the nucleus and localizes to pericentromeric and telomeric regions of chromosomes (Canudas et al., 2011; Frydrychova et al., 2008; Kumar and Kono, 2020; Luijsterburg et al., 2009; Nielsen et al., 2001; Perrini et al., 2004; Prasanth et al., 2010; Yi et al., 2018; Zeng et al., 2010). In mammals, the telomere capping Shelterin protein recruits ORC subunits to telomeric replication origins, and one of the Shelterin subunits, protein telomeric repeat-binding factor 2 (TRF2), directly binds and recruits ORC1 and ORC2 (Atanasiu et al., 2006; Deng et al., 2009, 2007; Higa et al., 2017; Tatsumi et al., 2008). Cells expressing a TRF2 mutant that is unable to bind ORC results in loss of telomeric repeats and leads to telomeric dysfunction (Drosopoulos et al., 2020).

Heterochromatin is enriched for satellite DNA and marked with di- and trimethylated histone H3 lysine 9 (H3K9me2 and H3K9me3) which is catalyzed by SUV39 methyltransferases. It is also enriched for heterochromatin protein 1 (HP1) (Eymery et al., 2009;

Saksouk et al., 2015; Schueler and Sullivan, 2006). HP1 protein is evolutionarily conserved in most eukaryotes from yeast, plants to humans, and they play important roles not only in maintenance of heterochromatic structure, but also in genome stability, gene silencing, DNA replication and repair, sister chromatid cohesion, heterochromatin and telomere maintenance (Canudas et al., 2011; Cheutin et al., 2003; Chow et al., 2018; Fanti et al., 1998; Frydrychova et al., 2008; Inoue et al., 2008; Kang et al., 2011; Maison and Almouzni, 2004; Perrini et al., 2004; Singh et al., 1991; Yi et al., 2018). In fission yeast, there are two HP1 paralogs, Swi6 and Chp2 (Canzio et al., 2014). Mammalian cell HP1 has three homologs, HP1α, HP1β, and HP1γ (Jones et al., 2000). These three isoforms show strong redundancy in terms of their functions in heterochromatic organization and structure, but each of these also has different localization in chromatin, binding partners, and functions in genome stability (Kwon and Workman, 2011; Maison and Almouzni, 2004; Minc et al., 1999). All isoforms localize to the pericentric heterochromatin, and HP1β and HP1γ also localize to euchromatin. During mitosis, HP1α and HP1β localize to the centromere region while HP1γ localizes to the chromosome arms.

The structure of HP1 consists of the N-terminal extension (NTE), the chromodomain (CD) that binds to H3K9me2/3, the connecting disordered hinge region (HR) that binds to nucleic acids, the chromoshadow domain (CSD) that mediates protein-protein interactions as well as self-dimerization, and the C-terminal extension (CTE) (Aasland et al., 1995; Bannister et al., 2001; Lachner et al., 2001; Maison and Almouzni, 2004; Meehan et al., 2003; Nielsen et al., 2001; Nishibuchi and Nakayama, 2014; Paro and Hogness, 1991; Ye et al., 1997). During mitosis, replicated DNA is evenly transmitted into two daughter cells and the chromatin structure is also propagated to pass on epigenetic information (Groth et al., 2007). This process is facilitated by the binding of HP1 to SUV39H1 methyltransferase and methylated DNA, H3K9me3 and histone deacetylases (Aagaard et al., 1999; Bannister et al., 2001; Fischer et al., 2009; Lachner et al., 2001; Motamedi et al., 2008). By recursive HP1 and SUV39H1 binding, histone methylation and deacetylation, the heterochromatin begins to form on DNA. HP1 also interacts with the PxVxL motif-containing chromatin assembly factor 1 (CAF-1) protein via HP1 chromoshadow domain for the assembly of nucleosomes after DNA synthesis (Huang et al., 2010; Quivy et al., 2004, 2008; Richart et al., 2012; Thiru et al., 2004; Yan et al., 2018).

DNA methylation and histone post translational modifications are two key players for maintaining chromatin structure, and it is very important that this information can be passed on to newly synthesized cells when cells replicate. Chromatin organization is coupled with DNA replication when cells duplicate, but how ORC is involved in heterochromatin organization still remains unclear. ORC in budding yeast directly binds to silencer sequences and the large ORC subunit Orc1 binds directly to the Silent Information Regulator protein Sir1 protein, bringing it to the mating type loci *HMR* and *HML* where SIR-mediated silencing takes place (Bell et al., 1993; Foss et al., 1993; Fox et al., 1995; Gardner and Fox, 2001; Hou et al., 2005; Triolo and Sternglanz, 1996). ORC-Sir1 then recruits and stabilizes the remaining SIR complex including the histone deacetylase Sir2 which is essential for gene silencing. The ORC-Sir-mediated transcriptional gene silencing pathway is not present in most other eukaryotes such as *S. pombe*, *Drosophila*, plants and human, but these species have acquired RNAi for gene silencing and also obtain HP1 protein (Castel et al., 2014; Drinnenberg et al., 2009; Ellahi and Rine, 2016; Hu et al., 2020; Martienssen and Moazed, 2015).

Human, *Drosophila* and *Xenopus* ORC bind to HP1 and plays an important role in gene regulation and heterochromatin maintenance (Chou et al., 2021; Pak et al., 1997; Pflumm and Botchan, 2001; Prasanth et al., 2010, 2004; Shen and Prasanth, 2012). Human ORC1, ORC2, ORC3 and ORC5 localize to heterochromatin foci in G1 and early S phase, and ORC1 and ORC3 subunits directly interact with the HP1 chromoshadow domain (Prasanth et al., 2010). HP1 binds to ORC1 via an N-terminal region and binds to ORC3 through the N-terminal coiled-coil domain and the MOD1-interacting region (MIR; 213-218 aa). Depletion of ORC1 or ORC5 with siRNA led to re-distribution of the HP1 protein, which then localized to the periphery of the nucleoli (Prasanth et al., 2010). During G2 and M phase, ORC2 and ORC3 localize predominantly to the centromeric region of the sister chromatids. Disruption of the ORC2 subunits results in defects in HP1 localization, decompaction of heterochromatic foci and chromosome 9 α-satellite repeats DNA, and large nuclei, although the mechanism is yet to be further investigated (Chou et al., 2021; Giri et al., 2016; Prasanth et al., 2010, 2004). It was also shown that rapid ORC2 depletion in G1-phase for 16 hr did not result in abnormal heterochromatic phenotypes, and therefore the heterochromatic defects could be cell cycle dependent, or the outcome of a failure to load cohesion during S phase (Zheng et al., 2018).

Fluorescence recovery after photobleaching (FRAP) analysis showed that ORC2, ORC3, and HP1 have similar fluorescence recovery rates suggesting that their interaction with heterochromatin is highly dynamic (Prasanth et al., 2010). On the other hand, ORC1 has a slow and incomplete fluorescence recovery, suggesting that ORC1 binds to heterochromatin in a more stable manner. ORC1 also binds to RB and SUV39H1 methyltransferase which tri-methylates histone H3K9 to repress E2F1-dependent transcription of the *CCNE1* gene which encodes Cyclin E (Hossain and Stillman, 2016). HP1 is also involved in liquid-liquid phase-separation to form heterochromatin structure and can form liquid droplets *in vitro* (Larson et al., 2017; Strom et al., 2017). This compact and phase-separated environment can potentially maintain the association of heterochromatin structure with nuclear lamina and protect the significant amounts of repetitive sequences present within the heterochromatin (Janssen et al., 2018; Strom et al., 2017). Recent studies showed that in the presence of DNA, *Drosophila* ORC1 and CDC6 undergoes liquid-liquid phase separation (LLPS) (Parker et al., 2019). In human cells, it was also shown that ORC1 can phase separate with or without DNA, while CDC6 can phase separate only in presence of DNA-bound ORC1 (Hossain et al., 2021). The function of ORC undergoing phase separation is not clear, but it could be related to regulation of ORC protein level in nucleus (Hossain et al., 2021), or be involved in heterochromatin and nuclear organization since ORC subunits colocalize with HP1 protein in vivo.

3. Additional functions of ORC

In metazoan species, in addition to its function in DNA replication initiation, ORC subunits are also involved in various processes during the cell cycle in addition to its well-studied role in DNA replication initiation. ORC subunits localize to kinetochores, centromeres, centrosomes, heterochromatin, and the ORC6 subunit localizes to the cytokinesis cleavage furrows (Bernal and Venkitaraman, 2011; Chesnokov et al., 2009, 2003; Gillingham and Munro, 2000; Hemerly et al., 2009; Pflumm and Botchan, 2001; Popova et al., 2018; Prasanth et al., 2010, 2004, 2002; Shimada and Gasser, 2007). ORC subunits are found to be important in several mitotic phase

events, including chromosome condensation, kinetochore-microtubule alignments, sister-chromatid cohesin-mediated pairing, chromosome congression and cytokinesis (Chesnokov, 2007; Craig et al., 2003; Hossain and Stillman, 2012; Popova et al., 2018; Prasanth et al., 2010, 2004; Sasaki and Gilbert, 2007; Zheng et al., 2018). Mutations in ORC1, ORC4, ORC6, CDT1, and CDC6 are found in Meier–Gorlin syndrome (MGS) patients. MGS is an autosomal recessive microcephalic primordial dwarfism syndrome in which patients have small ears, short stature, and absent or very small patellae, but usually for microcephalic syndromes have near normal intelligence (Bicknell et al., 2011a; Sonja A. de Munnik et al., 2012; Munnik et al., 2015).

Centrosomes are organizing centers that nucleate microtubules that bind to centromeres to ensure correct chromosome segregation and are an important organelle required for efficient and symmetric cell division in animals and for signal transduction. Ablating one centrosome during early mitosis in mammalian cells could still create a bipolar spindle and normal anaphase, however the cells have higher failure rate in cytokinesis (Khodjakov et al., 2000; Khodjakov and Rieder, 2001). Many animal oocytes that naturally do not have centrosomes or somatic cells that are depleted of centrosomes by manipulation show formation of anastral spindles and asymmetric cell division (Bonaccorsi et al., 1998; Khodjakov and Rieder, 2001; Matthies et al., 1996; Megraw et al., 2001). Human ORC1 and ORC2 localize to centrosomes. During G1 phase in human cells, binding of Cyclin A to the Cy motif in ORC1 promotes ORC1 localization to centrosomes via centrosome-targeting domain PACT, and also prevents Cyclin E–CDK2 dependent re-duplication of centrioles (Hemerly et al., 2009; Hossain and Stillman, 2012). Several mutations associated with MGS were found in Cyclin E binding sites within ORC1 BAH domain, and overexpressing these MGS ORC1 mutant proteins in cells results in re-duplication of centrioles and centrosomes (Bicknell et al., 2011b; Hossain and Stillman, 2012; Kuo et al., 2012; Munnik et al., 2015; Sonja A de Munnik et al., 2012).

ORC subunits in yeast *Saccharomyces cerevisiae* may have functional roles in mitosis besides initiation of DNA replication (Dillin and Rine, 1998). Temperature-sensitive haploid *Orc5* mutants arrest with 2C DNA content in early M phase (Dillin and Rine, 1998). When synchronizing the *Orc5* mutants in G2/M phase with nocodazole, switching to a non-permissive temperature and then released cells from the block, cells could exit mitosis normally but arrested

in G1/S phase (Dillin and Rine, 1998). Moreover, expressing wild type Orc5 in G1 did not let cells recover from the G1/S arrest. This study shows that ORC is required for pre-RC formation during late mitosis to G1 and is required for the onset of normal M phase, but when cells are already in M phase, ORC is not required for mitosis exit. Later, it was shown that in budding yeast, depleting Orc2 following the complete formation of pre-RC impairs sister-chromatid cohesion, resulting in both DNA damage and Mad2-spindle checkpoint activation in mitosis (Shimada and Gasser, 2007). In a normal cell cycle, Securin binds and inhibits separase protease which is responsible for cleaving the sister chromatid cohesin rings until the onset of anaphase (Hornig et al., 2002; Nasmyth, 2001; Uhlmann, 2001). Orc2 depletion in yeast results in DNA damage that activates the checkpoint kinase Mec1-Ddc2, and thus phosphorylates its effector kinase Chk1, which, in turn, phosphorylates and stabilizes Securin and prevents mitotic exit (Chen et al., 2009). Mec1 also phosphorylates a second effector kinase Rad53, which prevents anaphase entry by targeting Polo-like kinase Cdc5 (Liang and Wang, 2007; Schleker et al., 2010). Incorrect kinetochore-microtubule attachment triggers the Mad2-spindle checkpoint and inhibits Cdc20, resulting in stabilization of Securin, and arrest at the metaphase to anaphase transition (Clarke and Giménez-Abián, 2000; Sanchez et al., 1999). In *Drosophila*, ORC subunits localize to centromeric heterochromatin in mitosis, and *Orc2* and *Orc5* mutants died at late larval stages with cells arrested in G1 and mitosis (Pflumm and Botchan, 2001). Those mitotic arrest mutant cells had short and disorganized chromosomes that could not align correctly at the metaphase plate and also showed impaired sister chromatids cohesion.

In human, ORC2 and ORC3 bind to centromeres or kinetochores of the sister chromatids in mitosis (Craig et al., 2003; Prasanth et al., 2010, 2004). Small interfering RNA (siRNA) knockdown of ORC2 or ORC3 results in cells arresting in both G1 and M phase (Prasanth et al., 2004). ORC2 depleted cells have slow S phase and significantly less PCNA loading on chromatin. The rounded cells arrested in mitosis were mostly in early M phase with multipolar or asymmetric asters and multiple centrosomes, and the metaphase spread showed thick short chromosomes, possibly due to a defect in condensin. These findings suggested that ORC subunits might play a role in spindle organization, centrosome duplication, sister chromatid condensation, and chromosome segregation in mitosis. However, these abnormal phenotypes were observed in cells treated with ORC2 siRNA for 72 hr, and therefore some phenotypes

might not have been direct outcomes of ORC2 depletion but rather a secondary effect due to incomplete replication or activation of cell cycle checkpoints. My thesis work utilized the auxin-induced degradation system to rapidly knockdown ORC2 in 4 hr and demonstrated that ORC2 depleted cells arrested in late S/G2 phase, underwent aberrant mitosis, and showed abnormal nuclear structure, which is described in more detail in Chapter four.

The smallest ORC subunit, Orc6, localizes to cell membranes and the cleavage furrow during cytokinesis, and its C-terminal domain binds Pnut protein, which is a member of the GTP-binding protein septin family important for cell division in *Drosophila* (Chesnokov et al., 2003; Neufeld and Rubin, 1994). In addition, the replication function is genetically separable from the cytokinesis function, and expression of the Pnut interacting domain-deleted mutant protein in cells resulted in multinucleated cells with readily replicated DNA. In human cells, ORC6 localizes to outer kinetochores in M phase, and some ORC6 localizes to the midbody and binds septins at the intracellular bridge during cytokinesis (Prasanth et al., 2002). Depleting ORC6 in HeLa cells with Orc6 siRNA caused polyploidy and multinucleated cells, and cells with multipolar spindles and aberrant mitosis. The phenotypes of ORC6 depleted cells are similar to those of chromosomal passenger and cell cycle checkpoint protein depleted cells, suggesting that ORC6 might play an important role in coordinating multiple cell cycle events and signal cell cycle checkpoints by localizing to replication origins, kinetochores, and cleavage furrows. Recently a study performed in chicken DT40 cells using a temperature-sensitive degron version of avian Orc6 showed that its replication function is separate from its cytokinesis function, because Orc6 depletion in mitosis alone caused abscission defects (Bernal and Venkitaraman, 2011).

The function of ORC in DNA replication initiation has been thoroughly researched in the *Saccharomyces cerevisiae*, but more evidence is showing that ORC subunits are also involved in other cellular activities in yeast or higher eukaryotes. In addition, ORC subunits dissociate from the replication origins upon S phase entry and form sub-complexes in human cells allowing them to localize to different organelles and play multiple roles in cells. The goal of my thesis is to uncover the roles of ORC2 subunit, and I found that ORC2 depletion results in replication defect, aberrant mitosis, and fail to maintain heterochromatin organization.

Chapter two: Materials and methods

Most of the text of this chapter is taken directly from a manuscript published in *eLife* with slight changes. (All experiments were conducted by me, unless otherwise noted in the text.)

Chou, H.-C., Bhalla, K., El Demerdesh, O., Klingbeil, O., Hanington, K., Aganezov, S., Andrews, P., Alsudani, H., Chang, K., Vakoc, C.R., et al. (2021). The human Origin Recognition Complex is essential for pre-RC assembly, mitosis and maintenance of nuclear structure. Elife 10, e61797.

Cell Culture

HCT116 (WT $p53^{+/+}$), U2OS, RPE-1, Plat-E cells and HEK293T cell lines were cultured in DMEM (Gibco) supplemented with 10% Fetal bovine serum and 1 % Penicillin/Streptomycin. IMR-90 cell line was cultured in EMEM supplemented with 10 % Fetal bovine serum and 1 % Penicillin/Streptomycin. Plat-E and HEK293T cells were used for retroviral and lentiviral production respectively. HCT116 ($p53^{-/-}$), HCT116 *ORC1*$^{-/-}$ ($p53^{-/-}$ background, clone B14), HCT116 *ORC2*$^{-/-}$ ($p53^{-/-}$ background, clone P44) were a kind gift from Dr. Anindya Dutta (University of Virginia, Charlottesville, VA, USA). Tet-OsTIR1 HCT116 (TO-HCT116) cell line was a kind gift from Dr. Masato Kanemaki (National Institute of Genetics, Mishima, Japan). All gifted cell lines were cultured in McCoys 5A (Gibco) supplemented with 10 % fetal bovine serum and 1% Penicillin/Streptomycin. All cell lines were cultured at 37 °C with 5 % CO_2. All of the cell lines used in this study were tested for mycoplasma and were negative.

Tiling-sgRNA guide design (Done by Dr. Kuhulika Bhalla and Dr. Kenneth Chang))

Every possible guide directly upstream of a sp-Cas9 canonical PAM (NGG) sequence in the 5'->3' direction was extracted from the target exon sequences. Guides with the canonical PAM (NGG) were aligned to the GRCh38 genome using the BatMis exact k-mismatch aligner (Tennakoon et al., 2012). A maximum of three mismatches were considered for off-target evaluation. The resulting alignment file was parsed, and each off-target location assigned a penalty according to the number of mismatches to the target sequence and the exact position of each mismatch in the guide, where the farther the mismatch is from the PAM the higher the penalty, and based on the proximity of the mismatches to each other; assigning higher penalties to mismatches that are farther apart.

The resulting penalties from each assessed off-target site were then combined into a single off-target score for each guide (Hsu et al., 2013) with 1.00 as the maximum possible score for guides not having any off-target site with up to three mismatches. The final results included the guide sequence, the PAM, the number of off-target sites in the genome with 0, 1, 2 and 3 mismatches, the cut site location, the calculated off-target score, and any RefSeq genes (O'Leary et al., 2016) located at the off-target sites.

Plasmid construction and sgRNA cloning (Performed with Dr. Kuhulika Bhalla)

HCT116-Cas9 and RPE-1-Cas9 expressing cell lines were gifts from Dr. Chris Vakoc and Dr. Jason Sheltzer, respectively (Cold Spring Harbor Laboratory, NY, USA). In this study, all the sgRNAs targeting genes of interest as well as controls were cloned into LRG2.1 plasmid [derived from U6-sgRNA-GFP, Addgene: 108098 - as described (Tarumoto et al., 2018)]. Single sgRNAs were cloned by annealing sense and anti-sense DNA oligos followed by T4 DNA ligation into a BsmB1-digested LRG2.1 vector. To improve U6 promoter transcription efficiency, an additional 5' G nucleotide was added to all sgRNA oligo designs that did not already start with a 5' G.

For an unbiased tiling-sgRNA CRISPR screen, pooled sgRNA libraries were constructed. All designed sgRNAs including positive/negative controls were synthesized in duplicate or triplicate in a pooled format on an array platform (Twist Bioscience) and then PCR cloned into the Bsmb1-digested LRG2.1 vector using Gibson Assembly. To ensure the representation and

identity of sgRNA in the pooled lentiviral libraries, a MiSeq analysis was performed (Illumina) and we verified that 100 % of the designed sgRNAs were cloned in the LRG2.1 vector and that the abundance of >95 % of the sgRNA constructs was within 5-fold of the mean.

For *ORC2* CRISPR complementation assays, sgRNA resistant synonymous mutations were introduced to ORC2 by PCR mutagenesis using Phusion high fidelity DNA polymerase (NEB). Amplified Guide RNA resistant ORC2 ($ORC2^{gr}$) was cloned into NheI-digested mAID-mCherry2-NeoR plasmid (mAID-mCherry2-NeoR, Addgene 72830) to add mAID degron sequence to the N-terminus. The mAID-$ORC2^{gr}$ was then PCR amplified and assembled into BglII/XhoI digested pMSCV-hygro retroviral vector (TaKaRa #634401). Cloning was done using In-Fusion cloning system (TaKaRa). In this experiment, sgRNAs targeting ORC2 and control sgRNAs were cloned into BsmB1digested LgCG_cc88 lentiviral vector (Vakoc laboratory, CSHL) by the same sgRNA cloning strategy described above.

To create *ORC2* CRISPR/Cas9 knock out TO-HCT116 cells, we used sgRNA_ORC2-1-epCas9-1.1-mCherry plasmid for transient transfection. Sequence of sgRNA_ORC2-1 was cloned into epCas9-1.1-mCherry plasmid which was a kind gift from Dr. David Spector (Cold Spring Harbor Laboratory, NY, USA). sgRNAs were cloned by annealing sense and anti-sense DNA oligos followed by T4 DNA ligation into a BbsI-digested epCas9-1.1-mCherry vector.

To construct a lentiviral vector that constitutively expresses H2B-mCherry in TO-HCT116 and ORC2_H-2 cells, H2B-mCherry sequence was PCR amplified and cloned into BamHI/BspDI -digested pHAGE-CMV-MCS-IZsGreen vector which was a kind gift from Dr. Alea Mills (Cold Spring Harbor Laboratory, NY, USA).

Viral Transductions

Lentiviruses were produced in HEK293T cells by co-transfecting target plasmid and helper packaging plasmids psPAX2 and pVSVG with polyethylenimine (PEI 25000, Polysciences cat# 23966-100) transfection reagent. Plasmids were mixed in the ratio of 1:1.5:2 of psPAX2, pVSVG and target plasmid DNA in OptiMEM (Gibco, Cat# 31985062). 1 mg/mL PEI was added, mixed and incubated, before addition to the cells. Cell culture medium was

changed 7 h after transfection, and viral supernatant collected at 36 and 72 h following transfection. For the high throughput lentiviral screening, viral supernatant was concentrated with Lenti-X™ Concentrator (Takara, #631231) following manufacturer's protocol.

Retroviruses were produced in Plat-E cells by co-transfecting target plasmid and packaging plasmids pCL-Eco and pVSVG in the ratio of 1.25:1:9 with PEI. Cell culture medium was changed 7 h after transfection, and the supernatant was collected at 36 hr post-transfection.

For either lenti (gRNAs) or retroviral transductions (mAID-ORC2^{gr}), target cells were mixed with viral supernatant, supplemented with 8 µg/mL polybrene and centrifuged at 1700 rpm for 30 min at room temperature. Fresh medium was added 24 h after transduction. Where selection was required, antibiotics - 1 µg/mL puromycin; 10 µg/mL of blasticidin; 200 µg/ml of hygromycin - were added 72 h post infection.

Cytospin and metaphase spread

Prepare in advance less than 2-month-old acid-washed coverslips (stored in 100 % EtOH). Dry and put into the 6-well plate. Make fresh KCM (120mM KCl, 20mM NaCl, 10mM Tris-HCL, 0.3mM EDTA, 0.1 % Trixon X-100) and wash buffer (1% BSA or normal goat serum (NGS) in PBS). Prewarm 75 KCl in 37-degree water bath. Cells were treated for 2-4 hours with colcemid or nocodazole at 0.05-0.1 µg/ml. Cells were pelleted by centrifugation at 1,000 rpm for 5 minutes at, washed twice with PBS and count the cells. Spin down at 1000 rpm and remove PBS. Tap the tube to resuspend cells in residual PBS. Add 75 mM KCl at 2×10^5 cells/ml and left at room temperature for 30 mins. Aliquots (~150µl) of the swollen cell suspension were spun onto coverslips at 1,800 rpm for 10 minutes in a Shandon Cytospin. Coverslips were then immersed for 10 minutes at room temperature in KCM buffer. To rinse, coverslips were immersed in PBS for 5 mins at room temperature. Next, coverslips were fixed with 2% PFA for 5 mins at room temperature in dark. After fixation, coverslips were washed with PBS for five minutes 3 times. Coverslips were then immersed in blocking buffer (5 % BSA or NGS in PBS with 0.1 % Tween) for 1 hour. Coverslips were incubated with primary antibodies (anti-ORC2 #CS205, 1:200; anti-BUBR1 #BD612503, 1:200; anti-CENP-E; anti-Aurora B kinase #ab2254, 1:200; anti-CENP-A #, 1:200) overnight in cold room. The next day, wash the coverslips with

PBS+1%BSA+0.1 % Tween for 15 mins 3 times. Incubate coverslips with secondary Abs for 1-1.5 hour at room temperature in dark. Wash with PBS+1 % BSA+0.1 % Tween-20 10 mins 2 times. Dilute DAPI (1ug/ml) in PBS. Immersed the coverslips in 1DAPI for 1-2 minutes. Wash with PBS for 5 mins 3 times. Mount the coverslips onto ethanol cleaned slides.

ORC2 immunoprecipitation for iTRAQ analysis

First, the rabbit IgG and anti-ORC2 rabbit polyclonal CS205 antibody were crosslinked to GammaBind Plus Sepharose respectively using DMP crosslinker following lab protocol. HeLa Cells were treated with nocodazole to arrest in G2/M phase. Mitotic cells were collected by mitotic shake-off method and the remaining cells (G2) were harvested by trypsin digestion. Cells were lysed with lysis buffer 1(20mM pH8 HEPES-KOH, 100mM NaCl, 1mM EDTA, 0.1% NP-40) for 40 min in the cold room rotated. Next, lysates were centrifuged at 14000 rpm for 15 mins and the supernatant (sup1) was collected. The pellet was resuspended with lysis buffer2(20 mM pH8 HEPES-KOH, 200 mM NaCl, 5 mM $MgCl_2$, 1 mM EDTA, 0.3 % NP-40, 3 mM $CaCl_2$) for 30 min in the cold room rotated. Next, the lysates were aliquoted into 200 ul lysates per tube and warmed in 37 degrees for 1 min. 120U MNase was added into each tube and incubated for 10 mins at 37 degree. Next, EGTA was added to stop the reaction. Finally, the lysates were centrifuged at 14000 rpm for 15 mins and the supernatant (sup2) and pellet (P) were collected separately. For ORC2 immunoprecipitation, sup1 and sup2 were precleared with beads first and then incubated with 20 ul of antibody-conjugated sepharose beads for 2 hours in cold room. The beads were washed with 500 ul wash buffer for 3 times (change to new tubes after first wash) and followed by boiling for western blotting or enzymatic digestion done by mass spectrometry facility.

Pooled sgRNA screening (Performed with Dr. Kuhulika Bhalla, Kaarina Hanington, and Dr. Kenneth Chang)

CRISPR-based negative selection screens using sgRNA libraries targeting proteins ORC1-6, CDC6 as well as positive and negative controls, were performed in stable Cas9-expressing HCT116 ($p53^{+/+}$) and RPE-1 cell lines. The screens were performed as previously described (Lu et al., 2018; Miles et al., 2016; Shi et al., 2015) with a few optimizations for scale.

Briefly, to ensure a single copy sgRNA transduction per cell, multiplicity of infection (MOI) was set to 0.3-0.35. To achieve the desired representation of each sgRNAs during the screen, the total number of cells infected was determined such that while maintaining the MOI at ~0.3, each guide would yield at least 2000 counts at the beginning with Illumina NGS. Cells were harvested at day 3 post-infection and served as the initial time-point (P1) of the pooled sgRNA library, representing all guides transduced to begin with. Cells were cultured for 10 population doublings (P10) and harvested as the final time point. Genomic DNA was extracted using QIAamp DNA midi kit (QIAGEN) according to the manufacturer's protocol. Data from a total of 3 screens (HCT116: n=2; RPE-1: n=1) is presented in this study.

Next Generation Sequencing (NGS) library was constructed based on a newly developed protocol. To quantify the sgRNA abundance at P1 and P10, the sgRNA cassette was PCR amplified from genomic DNA using Amplitaq Gold DNA Polymerase (Invitrogen, 4311820) and primers (F2: TCTTGTGGAAAGGACGAAACACCG; R2: TCTACTATTCTTTCCCCTGCACTGT). The resulting DNA fragment (~ 242 bp) was gel purified. In a 2nd PCR reaction Illumina-compatible P7 and custom stacked barcodes which included the standard Illumina P5 forward primer, were introduced into samples by PCR amplification and the final product was gel purified (~180-200 bp). Samples were quantified by Agilent Bioanalyzer DNA High-sensitivity Assay (Agilent 5067-4626) and pooled together in equal molar ratios and analyzed by Illumina. Libraries were sequenced with a single-end 76 cycle NextSeq 500/550 kit on the NextSeq mid-output platform.

Quantification and analysis of screen data (Performed by Dr. Kuhulika Bhalla, Dr. Osama El Demerdesh, and Dr. Olaf Klingbeil)

The quantification of guides was done using a strict exact match to the forward primer, sample barcode, and guide sequence. MAGeCK was used for the identification of essential sgRNAs by running the "mageck test" command on the P1 and P10 raw sgRNA counts. MAGeCK employs median normalization followed by a Negative Binomial modeling of the counts and provides the log fold change (LFC) and p-values at both the individual guide and gene levels (Li et al., 2014).

We used Protiler (https://github.com/MDhewei/ProTiler-1.0.0), a computational method for the detection of CRISPR Knockout Hypersensitive (CKHS) regions from high-throughput tiling screens, to call and visualize the essential domains (He et al., 2019). Protiler uses denoising methods to mitigate the off-target effects and inactive sgRNAs, then applies a wavelet-based changing point detection algorithm to delineate the boundaries of sensitive regions. We separately input averaged LFC values from the two replicates of HCT116 or RPE-1 computed from MAGeCK, and analyzed the dataset at default values for all parameters except -t2/--threshold2. This threshold detects changing points using TGUH method described in this pipeline and we identified CKHS regions at thresholds of 0.25 and 0.5 for each target protein.

GFP competition and sgRNA complementation assay

TO-HCT116, TO-HCT116_mAID-ORC2^{gr}, U2OS, U2OS_mAID-ORC2^{gr}, HCT116 *p53*$^{-/-}$, HCT116 *p53*$^{-/-}$_mAID-ORC2^{gr}, *ORC2*$^{-/-}$ p44, and *ORC2* p44$^{-/-}$_ mAID-ORC2^{gr} cells were transduced with individual sgRNA-Cas9-GFP lentiviruses at an MOI of 0.3-0.4 to ensure one copy of sgRNA per cell. Cells were passaged every 3 days beginning day 3 (P1) till day 21(P7) post-transduction. At each passage, GFP percentage were evaluated by guava easyCyte™ flow cytometer. Three technical repeats were measured for each datapoint. Measured values were normalized to GFP percentages at P1 for each sgRNA. All experiments were performed as a set of 3 biological replicates.

Generating endogenous ORC2 KO mAID-ORC2^{gr} cell lines

To construct TO-HCT116-mAID-ORC2^{gr} cells, TO-HCT116 cells were transduced with mAID-ORC2^{gr} retrovirus and selected with 200 μg/ml of hygromycin. sgRNA_ORC2-1-epCas9-1.1-mCherry plasmid was transiently transfected into TO-HCT116-mAID-ORC2^{gr} cells using Lipofectamine 2000 Transfection Reagent (ThermoFisher #11668019) following manufacturer's protocol. Cells were harvest by 0.25% trypsin-EDTA after 24 hr, washed once with PBS, and resuspended into sorting buffer containing 2% FBS, 2 mM EDTA, and 25mM HEPES pH7.0. Single cells were FACS sorted and expanded.

Cell Proliferation assays

TO-HCT116, ORC2_H-2, ORC2_H-4, and ORC2_H-5 cell lines were seeded 24 hr before the experiment in either base medium or medium containing 0.75μg/ml doxycycline. For each cell line, 150,000 cells were seeded on day 1, and medium was changed every day. We harvested 3 replicates for each time point. Cells stained with 0.4 % trypan blue solution were counted using an automated cell counter. Similarly, cell proliferation assays for HCT116 *p53*$^{+/+}$, HCT116 *p53*$^{-/-}$, *ORC1*$^{-/-}$ and *ORC2*$^{-/-}$ cells were done starting at a seeding density of 100,000 cells.

Immunoprecipitation, Immunoblotting and quantitation

Cells were incubated in RIPA buffer (150 mM NaCl, 1 % NP-40, 0.5 % Sodium deoxycholate, 0.1 % SDS, 25 mM Tris-HCl PH 7.4) on ice for 15 minutes. Laemmli buffer was then added and samples analyzed by western blotting to detect proteins with antibodies. Primary antibodies: anti-ORC2 (rabbit polyclonal #CS205, in-house), anti-ORC3 (rabbit polyclonal #CS1980, in-house), anti-ORC1 (mouse monoclonal #pKS1-40, in-house), anti-CDC6 (mouse monoclonal #DCS-180, EMD Millipore), anti-ATM (rabbit monoclonal #ab32420, abcam), anti-pATM(S1981) (rabbit monoclonal #ab81292, abcam), anti-CHK1 (rabbit monoclonal #ab40866, abcam), anti-pCHK1(S345) (rabbit monoclonal #2348, Cell Signaling), anti-pCHK2(T68) (rabbit monoclonal #2197, Cell Signaling), anti-ATR (rabbit polyclonal #ab2905, abcam), anti-pATR(T1989) (rabbit polyclonal #ab227851, abcam), anti-pATR(S428) (rabbit polyclonal #2853, Cell Signaling), anti-p-γH2AX(S139) (rabbit monoclonal #9718, Cell Signaling), anti-β-Actin (mouse monoclonal #3700, Cell Signaling). Secondary antibodies: ECL^{TM} anti-Rabbit IgG Horseradish Peroxidase linked whole antibody (#NA934V, GE Healthcare) and ECL^{TM} anti-mouse IgG Horseradish Peroxidase linked whole antibody (#NA931V, GE Healthcare).

Relative ORC2 (or mAID-ORC2^{gr}), ORC3, ORC1, and CDC6 protein levels in each cell line was quantified by normalizing band area to β-Actin of each cell line and then normalized to HCT116 cells using ImageJ software.

Cell cycle analysis and pulse EdU label

For double-thymidine block and release experiments, cells were first incubated with 2 mM thymidine for 18 hr. After PBS washes, cells were released into fresh medium, with or without (0.75 μg/ml) doxycycline, for 9 hr. Next, 2 mM thymidine were added into the medium for 16 hr. Where needed 500 nM of auxin was added into the medium 4.5 hr before final release. Prior to harvest, all cells were pulse labeled with 10 μM EdU for 2 hours. Once released from the second thymidine block, 0 hr time point cells were harvested, and the remaining were released into fresh medium ±dox and auxin and collected at indicated time points. Samples for analysis were prepared using Click-iT™ EdU Alexa Fluor™ 488 Flow Cytometry Assay Kit following manufacturer's protocol (ThermoFisher #C10420). FxCycle™ Violet Stain (ThermoFisher #F10347) was used for DNA content analysis. Experiments were repeated >3 times.

For Palbociclib cell synchronization experiments, cells were incubated with medium containing 1μM Palbociclib (#S1116, Selleckchem) and 0.75 μg/ml doxycycline for 28 hr before first harvest. When needed auxin was added 4.5 hr prior to harvest. Another subset of cells was maintained in medium containing palbociclib and dox for another 12 hr (with or without auxin) for the second harvest.

Mitotic index flow cytometry

TO-HCT116 and ORC2_H-2 cells were pre-treated with doxycycline for 24 hr where needed in this experiment. Cells were harvested at different time points after auxin treatment, and immediately fixed with 4 % paraformaldehyde (PFA) in PBS for 15 min, mixed with 1 % BSA-PBS and centrifuged and supernatant discarded. Next, cells were permeabilized with 0.5 % Triton X -100 in 1 % BSA-PBS for 15 min at room temperature, mixed with 1% BSA-PBS and centrifuged and supernatant discarded. Samples were incubated with anti-pH3S10 antibody (mouse monoclonal #9706, Cell Signaling) for 45 min at 37℃. Cells were then washed with 1 % BSA-PBS + 0.1 % NP-40, and incubated with secondary antibody (Donkey anti-Mouse Alexa Fluor 647, #715-605-151, Jackson ImmunoResearch) for 50 min at 37℃ protected from light. Finally, DNA in cells were stained with FxCycle™ Violet Stain (ThermoFisher) and samples analyzed by flow cytometry.

Cell extraction and MCM2 flow cytometry

EdU pulse labeled asynchronous TO-HCT116, ORC2_H-2, ORC2_H-5 cells with or without doxycycline and auxin treatment were harvested, washed with PBS, and processed based on the previously described protocol (Matson et al., 2017) with minor optimizations. For non-extracted cells, cells were fixed with 4 % PFA in PBS for 15 min, and then centrifuged at 1000 xg for 7 min to remove fixation, then washed with 1 % BSA-PBS and centrifuged again. Next, cells were permeabilized with 0.5 % Triton X-100 in 1 % BSA-PBS for 15 min and then washed with 1% BSA-PBS. For chromatin extracted cells, cells were incubated in CSK buffer (10mM PIPES/KOH pH 6.8, 100 mM NaCl, 300 mM sucrose, 1 mM EGTA, 1 mM $MgCl_2$, 1 mM DTT) containing 0.5 % Triton X-100 with protease and phosphatase inhibitors, on ice for 5 min. Cells were centrifuged, washed with 1 % BSA-PBS and then fixed in 4% PFA in PBS for 15 min. After a PBS wash, samples were prepared using Click-iT™ EdU Alexa Fluor™ 488 Flow Cytometry Assay Kit manufacturer's manual (ThermoFisher #C10420), but instead of the kit's permeabilization and wash reagent, we used 1 % BSA-PBS + 0.1 % NP-40 for all washing steps. Next, cells were incubated with anti-MCM2 antibody (mouse monoclonal #610700, BD Biosciences) at 37℃ for 40 min protected from light. Cells were washed and then incubated with secondary antibody (Donkey anti-Mouse Alexa Fluor 647 #715-605-151 Jackson ImmunoResearch) at 37℃ for 50 min, protected from light. Finally, cells were washed and stained with FxCycle™ Violet Stain (ThermoFisher). >10,000 cells were quantified per condition. Gating for MCM negative cells was done based on unstained cell populations and secondary antibody only fluorescence controls.

Immunofluorescence Staining

TO-HCT116, ORC2_H-2, ORC2_H-4, and ORC2_H-5 cells were grown on coverslips for 48 hr with or without doxycycline and auxin treatment. Samples on coverslips were fixed in 4 % PFA for 10 min at room temperature. Next, coverslips were washed for 5 min with cold PBS. Cells were then permeabilized in 0.5 % Triton X-100 in PBS for 9 min. Following PBS washes, cells were blocked with 5 % normal goat serum in PBS + 0.1 % Tween (NGS-PBST) for 1 hr. For primary antibody incubation, antibodies were diluted in 1 % NGS-PBST and incubated for overnight at 4℃. Primary antibodies used include anti-CENP-C (Mouse monoclonal #ab50974, Abcam), anti-CENP-C (Rabbit polyclonal #ABE1957, Millipore), anti-HP1α (Mouse

monoclonal #MAB3584, Millipore), anti-pCHK1(S345) (rabbit polyclonal #2348, Cell Signaling), anti-p-γH2AX(S139) (rabbit monoclonal #9718, Cell Signaling), and anti-pATM(S1981) (Mouse monoclonal #ab36180, Abcam). Cells were washed with 1 % NGS-PBST before incubation with secondary antibody for 1 hr at room temperature. Secondary antibodies used include Goat Anti-Mouse IgG H&L Alexa Fluor® 647 (#ab150115, Abcam) and Goat Anti-Rabbit IgG H&L Alexa Fluor® 488 (#ab150077, Abcam). Finally, cells were stained with 1 µg/ml DAPI and coverslips mounted with VECTASHIELD® Antifade Mounting Medium (#H-1000-10, Vector Laboratories). Images were taken using a Perkin Elmer spinning disc confocal equipped with a Nikon-TiE inverted microscope using 60X objective oil lens with an Orca ER CCD camera. Images presented are maximum intensity projections of a z-stack (z=0.3µM).

To study the nuclear and cellular morphology HCT116 *p53*$^{+/+}$, HCT116 *p53*$^{-/-}$, *ORC1*$^{-/-}$ *(*B14) and *ORC2*$^{-/-}$ (P44) cells were grown on coverslips. Cells were fixed with 4% PFA and the method described above was followed. Primary antibody against Lamin B1 (Abcam ab16048) was used as a marker for nuclear envelope. Secondary antibody used is Goat Anti-Rabbit IgG Alexa Fluor® 594 (Abcam ab150084). In addition, Phalloidin iFluor® 488 (Abcam ab176753) was used to stain for cytoskeleton and DNA was detected with 1µg/ml Hoechst dye (ThermoFisher #62249). Mounted coverslips were imaged with Perkin Elmer spinning disc confocal equipped with a Nikon-TiE inverted microscope using 40X objective lens with an Orca ER CCD camera. Images presented are single channel average intensity projections or merged multi-channel maximum intensity projections of z-stacks.

Nuclear volume quantitation

Nuclei were fixed and stained with DRAQ5™ Fluorescent Probe Solution as per the manufacturer's guidelines (ThermoFisher #62251). Images were taken using a Perkin Elmer spinning disc confocal equipped with a Nikon-TiE inverted microscope using 60X objective lens with an Orca ER CCD camera. Images presented are maximum intensity projections of a z-stack (z=0.3µM). Nuclear size was analyzed with volocity software (version 6.3.1).

Live cell microscopy

TO-HCT116 and ORC2_H-2 cells were seeded in ibidi µ-Slide 8 Well Glass Bottom, in the presence or absence of 0.75 µg/ml doxycycline for 24 hr. Next, 2 mM thymidine was added, and samples incubated ±dox for 24 hr. Two hours prior to washing out thymidine, 500 nM auxin were added to the dox treated wells. Samples were then imaged beginning 4 hr after thymidine release and the timepoints reconstructed from time-lapse images using volocity software. Images were acquired approximately every 5 minutes on a Perkin Elmer spinning disc confocal equipped with a Nikon-TiE inverted microscope using 40X objective lens with an Orca ER CCD camera. Images presented are maximum intensity projections of a z-stack (z=3 µM).

Quantitative PCR

Total RNA of HCT116 *p53*$^{-/-}$ and *ORC2*$^{-/-}$ cells were extracted using Rneasy Mini Kit (Qiagen #74104) following manufacturer's handbook and quantified by Nanodrop (ThermoFisher). cDNA was made using TaqMan Reverse Transcription Reagents with either oligo(dT) or random hexamer primers (#N8080234, Applied Biosystems). Real-time quantitative PCR were performed using PowerSYBR Green PCR Master Mix (Applied biosystems #4367659) following manufacturer's protocol. Primer pairs for quantitative PCR were designed to PCR exon-exon junction and each PCR was performed as a triplicate. The delta-Ct (ΔCt) values were obtained from subtracting Actin mean Ct values from test samples. The delta-delta-Ct (ΔΔCt) value were calculated by subtracting HCT116 *p53*$^{-/-}$ ΔCt from ORC2$^{-/-}$ ΔCt for each primer pair individually. Data is represented as Log2 Fold change (FC) for each primer pair in *ORC2*$^{-/-}$ cells compared to HCT116 *p53*$^{-/-}$ cells.

Transmission electron microscopy (Performed with Dr. Habeeb Alsudani)

HCT116 *p53*$^{-/-}$ and *ORC1*$^{-/-}$ cells were pelleted and resuspended in 1 mL of 2.5 % glutaraldehyde in 0.1 M sodium cacodylate solution (pH 7.4) overnight at 4 °C. Fixative was removed, and in each step ~200 µl of the solution was left in the tubes. Pellet was washed with 0.1 M sodium cacodylate buffer. Next, 4 % low melting agarose solution was added and the tubes centrifuged immediately at 1,000 x g for 10 min at 30 °C, and transferred directly on ice for 20 min to solidify the agarose. Agarose was washed twice with 0.1 M cacodylate buffer. Next, 1 % osmium tetraoxide (OsO4) solution was added and left undisturbed for 1 hr followed

by three 0.1 M cacodylate buffer washes. Samples were then serially dehydrated using increasing amounts of ethanol (50 %, 60 %, 70 %, 80 %, 90 %, 95 %, 100 %, respectively). Finally, samples were embedded in 812 Embed resin and sectioned into 60-90 μm sections using Ultramicrotome. Hitachi H-7000 Transmission Electron Microscopy was used to image the sample.

Copy Number Variation Analyses by SMASH (Performed by Dr. Kuhulika Bhalla and Dr. Peter Andrews)

Copy number profiles were generated from input DNA using the SMASH sequencing protocol and analysis pipeline as described previously (Wang et al., 2016). Briefly, total cellular genomic DNA was isolated from HCT116 *p53*$^{+/+}$, HCT116 *p53*$^{-/-}$, *ORC1*$^{-/-}$ and *ORC2*$^{-/-}$ cell lines using QIAamp mini kit (Qiagen, 51104). Approximately 500 ng genomic DNA was enzymatically fragmented using dsDNA fragmentase (NEB, M0348L). Following end repair, fragments were joined to create chimeric fragments of DNA suitable for creating NGS libraries (300-700bp). The fragment size selection was done with Agencourt AMPure XP beads (Beckman Coulter, Cat. No. A63881). Illumina-compatible NEBNext Multiplex Dual Index Primer Pairs and adapters (New England Biolabs, Cat. No. E6440S) were ligated to the selected chimeric DNA fragments. These barcoded DNA fragments were then sequenced using an Illumina 300cycle MiSeqv2 kit on a MiSeq platform.

The SMASH analysis pipeline searches for Maximal Unique Matches (MUMs) to the human genome in all read pairs using a suffix array. These MUMs were then filtered to exclude short matches below 20bp, matches with less than 4bp of excess unique sequence, and matches on read 2 that are within 1000 bases of the genome coordinate of matches from read 1. The resulting 3-4 on average kept matches per read pair are then added to pre-computed empirically sized bins spanning the genome to generate a raw copy number profile. Regions with identical copy are expected to yield similar bin counts using these empirical bins. This profile is then corrected to remove GC content effects by normalizing counts based on LOWESS smoothing of count vs. GC content data in each bin. Final copy number profiles are normalized so that the autosome has an average copy number of 2. Plots were generated with G-Graph MUMdex

software - MUMdex Genome Alignment Anal. Softw. (https://mumdex.com/) (Andrews et al., 2016).

Oxford Nanopore Technologies (ONT) Long read sequencing and analysis (Performed by Dr. Kuhulika Bhalla, Dr. Sergey Aganezov and Dr. Michael C. Schatz)

High molecular weight DNA was isolated using the MagAttract kit (Qiagen # 67563). DNA was sheared to 50kb via Megarupter (diagenode). The quality of the DNA was then assessed on a Femtopulse (Agilent) to ensure DNA fragments were >40kb on average. After shearing, the DNA was size selected with an SRE kit (Circulomics) to reduce the fragments size to <20kb. After size selection, the DNA underwent a-tailing and damage repair followed by ligation to sequencing specific adapters.

Half of the prepared library was mixed with library loading beads and motor protein and then loaded on to an ONT PromothION PROM-0002 flow-cell and allowed to sequence for 24 hr. After 24 hr the flow-cell was treated with DNase to remove stalled DNA followed by a buffer flush. The second half of the library was then loaded and allowed to sequencing for 36 hr. The DNA was base called via Guppy 3.2 in High accuracy mode.

Long reads were aligned to the reference human genome using NGMLR (https://github.com/philres/ngmlr) and structural variants were identified using Sniffles (https://github.com/fritzsedlazeck/Sniffles) (Sedlazeck et al., 2018). The alignments and structural variants were then visualized using IGV (https://igv.org/).

Table 2-1. Reagents Table

Reagents Table				
Reagent type (species) or resource	**Designation**	**Source or reference**	**Identifiers**	**Additional information**
gene (*Homo sapiens*)	ORC1	GenBank	NM_004153.4	
gene (*Homo sapiens*)	ORC2	GenBank	NM_006190.5	
gene (*Homo sapiens*)	ORC3	GenBank	NM_181837.3	
gene (*Homo sapiens*)	ORC4	GenBank	NM_001190879.3	
gene (*Homo sapiens*)	ORC5	GenBank	NM_002553.4	
gene (*Homo sapiens*)	ORC6	GenBank	NM_014321.4	
gene (*Homo sapiens*)	CDC6	GenBank	NM_001254.4	
strain, strain background (*Escherichia coli*)	Stbl3	NEB	C3040	High efficiency chemically competent cells
cell line (*H. sapiens*)	HCT116 *p53*+/+	ATCC	Cat# CCL-247, RRID: CVCL_0291	Cell line maintained in B. Stillman Lab
cell line (*H. sapiens*)	RPE-1	ATCC	Cat# CRL-4000, RRID: CVCL_4388	Cell line maintained in B. Stillman Lab

cell line (*H. sapiens*)	HEK293T	ATCC	Cat# CRL-3216, RRID: CVCL_0063	Cell line maintained in B. Stillman Lab
cell line (*H. sapiens*)	HCT116 *p53-/-*	Bunz et al., 1998	RRID: CVCL_S744	Generous gift from Anindya Dutta (University of Virginia)
cell line (*H. sapiens*)	HCT116 *p53-/- ORC1-/-* (clone B14)	Shibata et al., 2016	N/A	Generous gift from Anindya Dutta (University of Virginia)
cell line (*H. sapiens*)	HCT116 *p53-/- ORC2-/-* (clone P44)	Shibata et al., 2016	N/A	Generous gift from Anindya Dutta (University of Virginia)
cell line (*H. sapiens*)	U2OS	ATCC	Cat# HTB-96, RRID: CVCL_0042	Cell line maintained in B. Stillman Lab
cell line (*H. sapiens*)	TO-HCT116 (Tet-OsTIR1 HCT116)	Natsume et al., 2016	N/A	Generous gift from Masato T. Kanemaki (National Institute of Genetics, Japan)
cell line (*H. sapiens*)	ORC2_H-2	This study	N/A	Cell line derived from TO-HCT116
cell line (*H. sapiens*)	ORC2_H-4	This study	N/A	Cell line derived from TO-HCT116

cell line (*H. sapiens*)	ORC2_H-5	This study	N/A	Cell line derived from TO-HCT116
Antibody	Lamin B1; Rabbit polyclonal	Abcam	Cat# ab16048, RRID: AB_10107828	IF – 0.2µg/ml
Antibody	ORC1, mouse monoclonal (pKS1-40)	CSHL In-house	N/A	IB – 1:1,000
Antibody	ORC2, rabbit polyclonal (CS205)	CSHL In-house	N/A	IB – 1:10,000
Antibody	ORC3, rabbit polyclonal (CS1980)	CSHL In-house	N/A	IB – 1:10,000
Antibody	CDC6, mouse monoclonal (DCS-180)	EMD Millipore	Cat# 05-550 RRID: AB_2276118	IB – 1:1,000
Antibody	ATM, rabbit monoclonal (Y170)	Abcam	Cat# ab32420 RRID: AB_725574	IB – 1:1,000
Antibody	p-ATM(S1981), rabbit monoclonal (EP1890Y)	Abcam	Cat# ab81292 RRID: AB_1640207	IB – 1:1,000 IF – 1:200
Antibody	CHK1, rabbit monoclonal (EP691Y)	Abcam	Cat# ab40866 RRID: AB_726820	IB – 1:1,000
Antibody	p-CHK1(S345), rabbit monoclonal (133D3)	Cell Signaling	Cat# 2348 RRID: AB_331212	IB – 1:1,000 IF – 1:200

Antibody	p-CHK2(T68), rabbit monoclonal (C13C1)	Cell Signaling	Cat# 2197 RRID: AB_2080501	IB – 1:1,000
Antibody	p-γH2AX(S139), rabbit monoclonal (20E3)	Cell Signaling	Cat# 9718 RRID: AB_2118009	IB – 1:1,000 IF – 1:200
Antibody	ATR, rabbit polyclonal	abcam	Cat# ab2905 RRID: AB_303400	IB – 1:1,000
Antibody	p-ATR(T1989), rabbit polyclonal	abcam	Cat# ab227851 (discontinued)	IB – 1:1,000
Antibody	p-ATR(S428), rabbit polyclonal	Cell Signaling	Cat# 2853 RRID: AB_2290281	IB – 1:1,000
Antibody	β-Actin, mouse monoclonal (8H10D10)	Cell Signaling	Cat# 3700 RRID: AB_2242334	IB – 1:10,000
Antibody	CENP-C, Mouse monoclonal (2159C5a)	Abcam	Cat# ab50974 RRID: AB_869095	IF – 1:200
Antibody	HP1α, Mouse monoclonal (2HP-1H5)	Millipore	Cat# MAB3584 RRID: AB_94938	IF – 1:500
Antibody	ECL™ anti-Rabbit IgG Horseradish Peroxidase linked whole antibody	GE Healthcare	Cat# NA934V	IB – 1:10,000
Antibody	ECL™ anti-mouse IgG Horseradish Peroxidase linked whole antibody	GE Healthcare	Cat# NA931V	IB – 1:10,000

Antibody	Goat Anti-Mouse IgG H&L Alexa Fluor® 647	Abcam	Cat# ab150115 RRID: AB_2687948	IF – 1:1000
Antibody	Goat Anti-Rabbit IgG H&L Alexa Fluor® 488	Abcam	Cat# ab150077 RRID: AB_2630356	IF – 1:1000
Antibody	Goat Anti-Rabbit IgG H&L (Alexa Fluor® 594)	Abcam	Cat# ab150084, RRID: AB_2734147	IF – 1:1000
Antibody	MCM2 (BM28); mouse monoclonal	BD Biosciences	Cat #610700 RRID: AB_2141952	FC – 1:200
Antibody	Alexa Fluor 647 donkey anti-mouse antibody	Jackson ImmunoResearch Labs	Cat# 715-605-151, RRID: AB_2340863	FC – 1:1000
Antibody	Phospho-Histone H3 (Ser10), Mouse monoclonal (6G3)	Cell Signaling Technology	Cat# 9706, RRID: AB_331748	FC – 1:25
recombinant DNA reagent	LentiV_Cas9_puro (plasmid)	Addgene	RRID: Addgene_108100	Lentiviral expression of cDNA with puromycin resistance gene – used for making RPE-1 cas9 puro (generous gift from Jason Sheltzer, CSHL)
recombinant DNA reagent	LentiV_Cas9_Blast (plasmid)	Addgene	RRID: Addgene_125592	Lentiviral expression of cDNA with blasticidin resistance

				gene – used for making HCT116 cas9 blast (generous gift from Chris Vakoc CSHL)
recombinant DNA reagent	LRG2.1 (plasmid)	Addgene	RRID: Addgene_108098	BsmBI digestion for sgRNA cloning
recombinant DNA reagent	LgCG_cc88 lentiviral vector (plasmid)	N/A	N/A	Lentiviral expression of Cas9-sgRNA-GFP – used for dropout CRISPR/Cas9 experiment (generous gift from Chris Vakoc, CSHL)
recombinant DNA reagent	epCas9-1.1-mCherry (plasmid)	Chang et al., 2020	N/A	Generous gift from David Spector (CSHL)
recombinant DNA reagent	pHAGE-CMV-MCS-IZsGreen (plasmid)	N/A	N/A	Lentiviral expression vector – used to construct pHAGE-CMV-H2B-mCherry
recombinant DNA reagent	mAID-mCherry2-NeoR (plasmid)	Addgene	RRID: Addgene_72830	The plasmid was used to construct mAID-ORC2 transgene
recombinant DNA reagent	pMSCV-hygro retroviral (plasmid)	TaKaRa	Cat #634401	Retroviral expression of

				cDNA with hygromycin resistance gene – used to construct pMSCV-hygro-mAID-ORC2 to express mAID-ORC2 in cells
transfected construct (*H. sapiens*)	pMSCV-hygro-mAID-ORC2 (plasmid)	This study	N/A	Retroviral construct for transduction and express mAID-ORC2
transfected construct (*H. sapiens*)	sgRNA_ORC2-1-epCas9-1.1-mCherry (plasmid)	This study	N/A	Construct to transfect and express Cas9 and sgRNA ORC2-1 in human cells
transfected construct (*H. sapiens*)	pHAGE-CMV-H2B-mCherry (plasmid)	This study	N/A	Lentiviral construct for transduction and express H2B-mCherry in human cells
sequence-based reagent	F2	This study	PCR primer for amplification of sgRNA cassette	TCTTGTGG AAAGGACG AAACACCG
sequence-based reagent	R2	This study	PCR primer for amplification of sgRNA cassette	TCTACTATT CTTTCCCCT GCACTGT
commercial assay or kit	NEBuilder® HiFi DNA Assembly Cloning Kit	NEB	Cat# E5520S	

commercial assay or kit	Click-iT™ EdU Alexa Fluor™ 488 Flow Cytometry Assay Kit	Invitrogen	Cat# C10420	
Commercial assay or kit	DNeasy Blood and Tissue kit	Qiagen	Cat# 69504	
Commercial assay or kit	RNeasy Mini kit	Qiagen	Cat# 74104	
Software, algorithm	Volocity 3D Image Analysis Software	Perkin Elmer	RRID: SCR_002668	
Software, algorithm	GraphPad Prism 9	GraphPad	RRID: SCR_002798	
Software, algorithm	Model-based Analysis of Genome-wide CRISPR-Cas9 Knockout (MAGeCK)	Li, et al. MAGeCK enables robust identification of essential genes from genome-scale CRISPR/Cas9 knockout screens. Genome Biology 15:554 (2014)	N/A	https://sourceforge.net/p/mageck/wiki/Home/
Software, algorithm	Protiler Analysis	He et al. De novo identification of essential protein domains from CRISPR-Cas9 tiling-sgRNA knockout screens. Nat Commun 10, 4547(2019)	N/A	https://github.com/MDhewei/protiler

Software, algorithm	FlowJo	BD	RRID:SCR_008520	
Software, algorithm	ImageJ	NIH	RRID:SCR_003070	
Chemical compound, drug	Palbociclib	Selleckchem	Cat# S1116	1 μM
Chemical compound, drug	Thymidine	Millipore Sigma	Cat# 89270	2 mM
Chemical compound, drug	Doxycycline	CalBiochem	Cat# 324385	0.75 ug/ml
Chemical compound, drug	Auxin (Indole-3-acetic acid sodium salt)	Millipore Sigma	Cat# 15148	500 nM
Chemical compound, drug	DAPI	Life Technologies	Cat# D1306	1μg/ml
Chemical compound, drug	FxCycle™ Violet Stain	ThermoFisher	Cat# F10347	1:1000
Chemical compound, drug	Hoechst dye	ThermoFisher	Cat# 62249	1μg/ml
Chemical compound, drug	Phalloidin iFluor® 488	Abcam	Cat# ab176753	1:1000
Chemical compound, drug	Polyethylenimine (PEI 25000)	Polysciences	Cat# 23966-100	1 mg/mL

Chapter three: The human Origin Recognition Complex is essential for pre-RC assembly, mitosis and maintenance of nuclear structure.

The text of this chapter is taken directly from a manuscript published in *eLife*.
Chou, H.-C., Bhalla, K., El Demerdesh, O., Klingbeil, O., Hanington, K., Aganezov, S., Andrews, P., Alsudani, H., Chang, K., Vakoc, C.R., et al. (2021). The human Origin Recognition Complex is essential for pre-RC assembly, mitosis and maintenance of nuclear structure. Elife 10, e61797.

I carried out all the experiments in the manuscript, unless otherwise noted in the text or figure legends.

1. Introduction

Cell division requires the entire genome to be duplicated once and only once during S-phase of the cell cycle, followed by segregation of the sister chromatids into two daughter cells. To ensure complete and correct duplication of genomes, the initiation of DNA replication is highly regulated and begins with the assembly of a pre-Replication Complex (pre-RC) at origins of DNA replication throughout the genome (Bell and Labib, 2016). Among eukaryotes, *Saccharomyces cerevisiae* is the best characterized system, from which individual proteins involved in DNA replication have been identified and studied extensively, including functional reconstitution of the entire pre-RC assembly and the regulated initiation of DNA replication from these pre-RCs with purified proteins (Evrin et al., 2009; Remus et al., 2009; Yeeles et al., 2015). In *S. cerevisiae*, pre-RC assembly begins with the Origin Recognition Complex (ORC), comprising Orc1-6 subunits, binding to each potential DNA replication origin (Bell et al., 1993; Bell and Labib, 2016; Bell and Stillman, 1992; Gibson et al., 2006). Chromatin-bound ORC then provides a platform for the assembly and recruitment of other pre-RC proteins. Cdc6 binds to ORC, followed by the binding of Cdt1-Mcm2-7 to form head-to-head Mcm2-7 double hexamers to complete the formation of the pre-RC (Araki, 2011; Bell and Labib, 2016; Bleichert et al., 2017; Evrin et al., 2009; Heller et al., 2011; Remus et al., 2009). The Mcm2-7 double hexamer helicase precursor complex remains bound to DNA in an inactive state until it is activated by additional proteins and protein kinases (Bell and Labib, 2016). During S phase, Cyclin-dependent protein kinase (CDK) and the Cdc7-Dbf4-dependent protein kinase (DDK), Sld2, Mcm10, Dpb11, Sld3/7, DNA polymerase ε, Cdc45 and the GINS complex are recruited to activate MCM2-7 helicase (Araki, 2016, 2011; Araki et al., 2009, 1995; Kamimura et al., 1998; Takayama et al., 2003; Yeeles et al., 2015). The functional helicase consists of Cdc45-Mcm2-7-GINS (CMG) and when activated it unwinds the DNA in a bidirectional and temporally regulated manner from each origin (Bleichert et al., 2017).

In all eukaryotes, including *S. cerevisiae* and human cells, the ORC1-5 subunits contain a AAA+ or a AAA+-like domain and a winged-helix domain (WHD) (Bleichert et al., 2017; Chen et al., 2008; Jaremko et al., 2020; Li and Stillman, 2012; Ocaña-Pallarès et al., 2020; Tocilj et al., 2017). In yeast, Orc1-6 remains as a stable complex bound to the chromatin throughout the cell

division cycle (Aparicio et al., 1997; DePamphilis, 2003; Weinreich et al., 1999). ORC binds to A and B1 DNA sequence elements within the Autonomously Replicating Sequence (ARS), which contains a conserved ARS Consensus Sequence (ACS) (Bell and Labib, 2016; Bell and Stillman, 1992; Celniker et al., 1984; Deshpande and Newlon, 1992; Marahrens and Stillman, 1992; Rao and Stillman, 1995; Rowley et al., 1995). On the other hand, in human cells, there is no apparent sequence-specific binding of ORC to DNA, and the binding of ORC to chromosomes is dynamic (Vashee et al., 2001). ORC subunits do, however, localize to specific sites within the chromosome, most likely via interactions with modified histones or other chromatin interacting proteins (Higa et al., 2017; Hossain and Stillman, 2016; Kuo et al., 2012; Long et al., 2019; Miotto et al., 2016; Tatsumi et al., 2008). One or more of the human ORC subunits dissociate from the complex soon after the pre-RC is formed. For example, in human cells ORC1 is ubiquitinated by the SCF^{skp2} ubiquitin ligase and is degraded during the G1-S transition and early S phase, and then re-appears as cells enter mitosis (Kara et al., 2015; Kreitz et al., 2001; Méndez et al., 2002; Ohta et al., 2003). In human cells, ORC1 is the first ORC subunit to bind to mitotic chromosomes and is inherited into the daughter cells where it recruits other ORC subunits and CDC6 to form new pre-RCs (Kara et al., 2015; Okuno et al., 2001).

ORC is a conserved complex in eukaryotes, and it is essential for DNA replication in *S. cerevisiae, S. pombe, Xenopus and Drosophila*, since mutation or depletion of ORC prevents CDC6 binding and MCM loading onto DNA (Aparicio et al., 1997; Chuang et al., 2002; Pak et al., 1997; Pflumm and Botchan, 2001; Romanowski et al., 1996; Speck et al., 2005). Besides its function in the initiation of DNA replication, ORC protein subunits also have other important roles that vary with species. In budding yeast, Orc1 directly interacts with silencing regulator Sir1 at the silent mating type loci to mediate transcriptional gene silencing and maintain heterochromatin (Bell et al., 1993; Foss et al., 1993; Fox et al., 1995; Hou et al., 2005; Triolo and Sternglanz, 1996). ORC1 also plays a role in transcriptional gene silencing of the human *CCNE1* locus in human cells (Hossain and Stillman, 2016). ORC also interacts with heterochromatin protein HP1 and is required for maintenance of heterochromatin (Pak et al., 1997; Pflumm and Botchan, 2001; Prasanth et al., 2010, 2004; Shen et al., 2012).

ORC2 depletion after pre-RC assembly resulted in spindle and DNA damage checkpoint activation, and impaired sister-chromatid cohesion (Shimada and Gasser, 2007). In *Drosophila*, Orc2 mutants showed reduced S phase cells, increased number of mitotic cells with abnormally condensed chromosomes and chromosome alignment defects, and more importantly, those mutants could not survive at late larval stage (Loupart et al., 2000; Pflumm and Botchan, 2001). In humans, mutations in ORC1, ORC4, ORC6, CDT1, and CDC6 are detected in Meier-Gorlin syndrome (MGS) patients (Bicknell et al., 2011b, 2011a; Guernsey et al., 2011; Hossain and Stillman, 2012; Munnik et al., 2015). ORC1 and ORC2 localize to centrosomes and ORC1 regulates the re-duplication of the centriole (Hemerly et al., 2009; Prasanth et al., 2004). ORC also localizes to telomeres via the TRF2 shelterin protein (Deng et al., 2009; Tatsumi et al., 2008). It was also shown that siRNA knockdown or CRISPR/Cas9 knockout of ORC1 resulted in loss of MCM2-7 from chromatin, abnormal duplication of centrioles, and a change in cell cycle stage distribution (Hemerly et al., 2009; Kara et al., 2015; McKinley and Cheeseman, 2017). ORC1, ORC2, ORC3, and ORC5 associate with heterochromatin, and depletion of ORC subunits disrupt localization of heterochromatin and also causes abnormal heterochromatin decondensation in cells (Giri et al., 2016; Prasanth et al., 2010, 2004). ORC2 and ORC3 also specifically localize to centromeric heterochromatin during late S phase, G2 and mitosis and removal of these proteins causes decondensation of centromeric α-satellite (Greil et al., 2003; Prasanth et al., 2010, 2004).

There is an emerging debate, however, about the essential nature of ORC in human cells (Bell, 2017). ORC is overexpressed in numerous cancerous cell lines (McNairn and Gilbert, 2005) and HCT116 colorectal cancer cells can survive with only 10% of the ORC2 protein level (Dhar et al., 2001). More importantly, it was reported that HCT116 *p53*$^{-/-}$ (*TP53*$^{-/-}$, but we henceforth use *p53*$^{-/-}$) cells in which expression of either ORC1 or ORC2 subunit was eliminated using CRISPR-Cas9 mediated gene ablation could still proliferate (Shibata et al., 2016). Here, we developed a genetic method to address the function of the pre-RC proteins ORC and CDC6, particularly focusing on the ORC1 and ORC2 subunits. We demonstrate that ORC proteins are essential for normal cell proliferation and survival of human cells. Moreover, ORC1 or ORC2 depleted cells showed multiple defects in progression through cell division cycle, including DNA replication and mitosis, as well as defects in nuclear structure.

2. Results

2.1. ORC1-6 and CDC6 are essential for cell survival (This part was written by Dr. Bhalla)

To address the issue of essentiality and to identify functional domains within the ORC and CDC6 proteins, we used unbiased tiling-sgRNA CRISPR negative selection screens. Evaluation of CRISPR knock-out (CRISPR-KO) strategies have shown that targeting regions within protein domains typically show significantly higher degree of negative selection phenotypes (He et al., 2019; Hsu et al., 2018; Montalbano et al., 2017; Munoz et al., 2016; Shi et al., 2015; Wang et al., 2019). This is because both frameshift and more crucially in-frame mutations within functionally active regions of a protein result in genetic nulls (Munoz et al., 2016; Shi et al., 2015). Off-target effects notwithstanding, targeting known domains that contribute to protein function have informed the design of pooled whole-genome CRISPR screens like GeCKO and Avana. Similarly, applying CRISPR-KO strategies to individual proteins requires selection of a single or a few sgRNAs that target known functional domains and have a considerably low off-target score. However, at least in the case of ORC, CRISPR-based ablation of individual subunits of the complex have reported different phenotypic outcomes. For example, in DepMap, the database that summarizes results from whole-genome CRISPR screens (GeCKO 19Q1 and Avana 20Q2 libraries) (Meyers et al., 2017; Tsherniak et al., 2017), *ORC1* is listed as a common essential gene while *ORC2* is listed as non-essential in tested cell types **(Figure 3-1a)**. Other members of the pre-RC proteins – *ORC3*, *ORC4*, *CDC6*, *MCM2-7* and *CDT1* show variability between GeCKO and Avana screens in being described as common essential or not. In 2015, *ORC1*, *ORC4* and *MCM4* were reported as essential in murine cells by using guides that targeted the AAA+ or WH domains of the proteins (Shi et al., 2015). Subsequently, in human colorectal carcinoma cell line HCT116, *ORC1* and *ORC2* were reported to be non-essential for cell proliferation (Shibata et al., 2016).

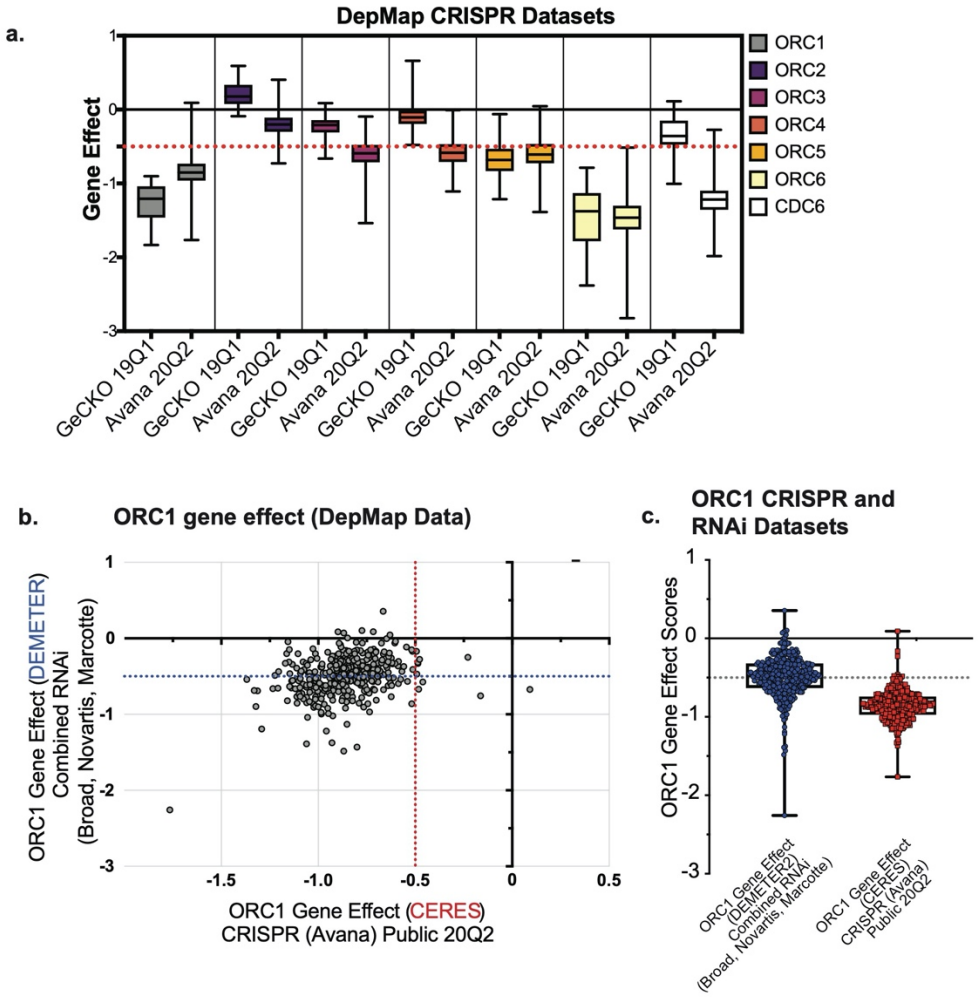

Figure 3-1. DepMap analyses of *ORC1* data. (Provided by Dr. Kuhulika Bhalla) (a) Distribution of Gene Effect scores of *ORC1-6* and *CDC6* across all the cell lines used in either the GeCKO 19Q1 or Avana 20Q2 CRISPR screens reported on DepMap [DepMap, Broad (2019): DepMap GeCKO 19Q1. figshare. Dataset. https://doi.org/10.6084/m9.figshare.7668407.v1, DepMap, Broad (2020): DepMap 20Q2 Public. figshare. Dataset. https://doi.org/10.6084/m9.figshare.12280541.v4, (Meyers et al., 2017)]. Each box plot represents gene effect range displayed in the tested cell lines. The red dotted line represents the gene effect score below which genes are scores as essential. (b) *ORC1* gene effect values for CRISPR [CERES; (Meyers et al., 2017) vs RNAi (McFarland et al., 2018)] mapped as xy scatter for ~390 common cell lines used in the screens. Red dotted line bifurcates the plot at CRISPR based gene effect score of less than -0.5 is considered essential to cell line. Blue dotted line bifurcates the plot at RNAi based gene effect score of less than -0.5 is considered essential to cell line. (c) Distribution of *ORC1* gene effect scores across all the cell lines used in CRISPR Avana 20Q2 and RNAi datasets respectively (McFarland et al., 2018; Meyers et al., 2017).

The rationale for using a pooled tiling-sgRNA CRISPR screen approach was – (a) since essential protein domains correlate with higher negative selection phenotype, we hypothesized that analyzing the effect of every possible guide RNA target site in the ORF might uncover new functional regions, and (b) a high-throughput screen of this nature would provide incontrovertible evidence about the essentiality of ORC and CDC6 proteins, at least in the cell lines tested. A recent study validated this approach by analyzing tiling-sgRNA data from Munoz et. al. and found that up to 17.7% of the regions that displayed a CRISPR knockout hyper-sensitive (CKHS) phenotype, did not overlap with previously annotated domain or known function (He et al., 2019; Munoz et al., 2016). Thus, guide RNAs targeting every possible PAM sequence 5′-NGG-3′ (S*treptococcus pyogenes* Cas9) across each exon of *ORC1-6* and *CDC6* were designed and synthesized. Pooled CRISPR libraries also included control guide RNAs targeting either known core essential genes such as *CDK1*, *PCNA* etc. as positive controls, or those targeting non-essential gene loci or no loci at all as negative controls (Miles et al., 2016). The total library comprised 882 guides targeting *ORC1-6* and *CDC6*, 1602 negative controls [Used in GeCKO V2 library - "NeGeCKO" (Sanjana et al., 2014), negative controls used in The Sabatini/Lander CRISPR pooled library (Park et al., 2017), *Rosa26*, CSHL in-house negatives (Lu et al., 2018; Tarumoto et al., 2018) and 43 positive controls; with a median of 3 pre-validated guides targeting known essential genes *CDK1*, *CDK9*, *RPL9*, *PCNA* etc.] Parallel screens were done in the colorectal cancer derived HCT116-Cas9 cells and human diploid RPE-1-Cas9 cells and the relative depletions of guide RNAs in the cell populations between Day 3 and Day 21 were compared using the guide read counts generated by Illumina based next-generation sequencing (n=2 for HCT116, n=1 for RPE-1) and the data was analyzed with MAGeCK (Li et al., 2014). The screens performed well as shown by the consistent log fold change (LFC) pattern of depletion or relative enrichment of positive and negative controls respectively - although the absolute values and the range of LFCs were cell-line specific. The LFC threshold of 'essentiality' for each cell line was set at the value at which a guide RNA was depleted more than every negative control as well as ≥ to the median depletion of guides targeting each positive control **(Figure 3-2b-d, red line)**. In HCT116, LFC ≤ -1 and LFC ≤ -5 in RPE-1 were found to be the cut-off for log fold depletion.

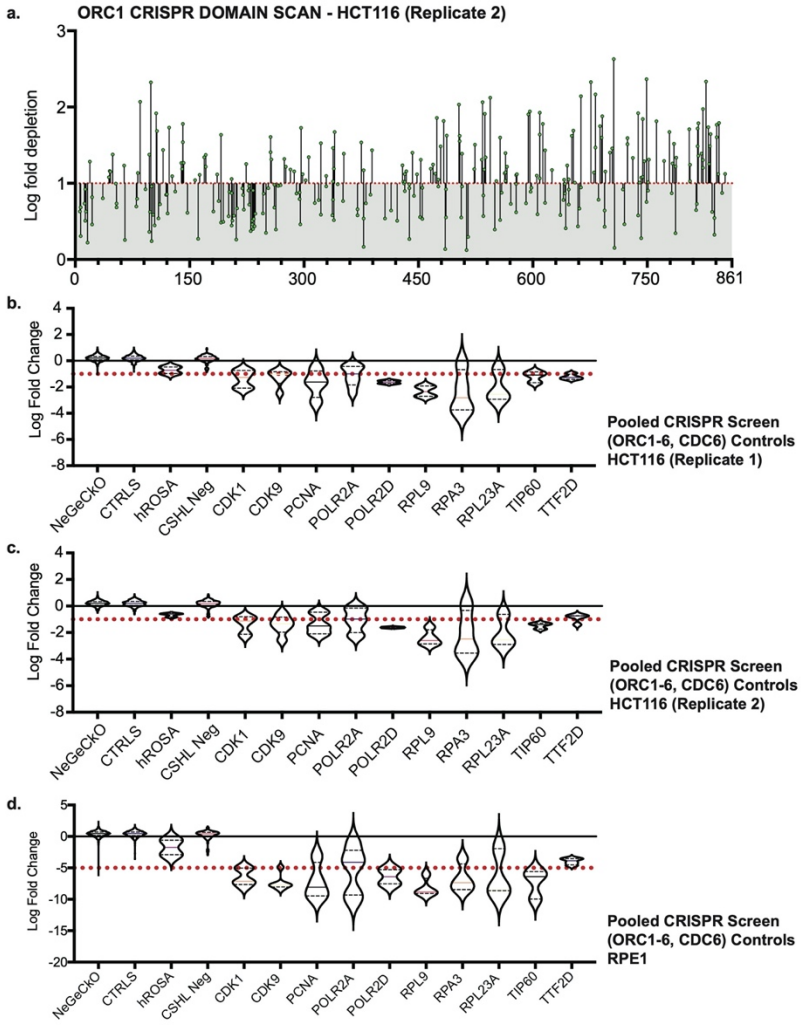

Figure 3-2. Tiling-sgRNA CRISPR screen data and controls. (Provided by Dr. Kuhulika Bhalla) (a) tiling-sgRNA map of ORC1 (replicate 2) in HCT116. Mapped as Log fold depletion (inverted LFC scale) as calculated by MaGeCK (Li et al., 2014) on y axis vs the amino acid disrupted by that guide RNA on the x axis. Effect of guide RNA is interpreted as essential if its depletion is more than 1 log fold (red dotted line). Data mapped on 1 Log fold depletion pseudo-axis for clarity. (b) tiling-sgRNA controls for HCT116 (replicate 1). Violin plots mapped as distribution of Log fold depletion (MaGeCK) for each guide RNA from negative (NeGeCKO, CTRLS, hROSA, and CSHL-neg library) or positive control (CDK1, CDK9, PCNA, POLR2A, POLR2D, RPL9, RPA3, RPL23A, TIP60, TTF2D) subsets. The median and quartiles of LFC for each subset are indicated within their violin plots. Cut-off of essentiality is LFC $\geq$ 1 (log fold depletion), indicated by red dotted line (Highest log fold depletion value of all negative controls and more than the median of positive controls. (c) tiling-sgRNA controls for HCT116 (replicate 2). (d) tiling-sgRNA controls for RPE-1. Cut-off of essentiality is LFC $\geq$ 5, indicated by red dotted line.

The results showed significant depletion of guide RNAs that target regions within structurally defined domains **(Figure 3-3a-b, f, Figure 3-4a-c, Figure 3-5a-c, g, Figure 3-6a-c, g, h-j, n, Figure 3-7a-c, g, h-j, n)**. To visualize the tiling-sgRNA data relative to amino acid conservation and intrinsic disorder, we used NCBI RefSeq coding sequences (NP_004144.2, NP_006181.1, NP_862820.1, NP_859525.1, NP_002544.1, NP_055136.1, NP_001245.1) for three analyses - (1) FrPred (Adamczak et al., 2004; Fischer et al., 2008) (https://toolkit.tuebingen.mpg.de/frpred) server that calculates a conservation score based on amino acid variability as well as the probability of it being a functional ligand binding or catalytic site at each amino acid position of the input sequence **(Figure 3-3c, Figure 3-5d, Figure 3-6d, k, Figure 3-7d, k, Figure 3-8b)**; (2) Consurf (Ashkenazy et al., 2016) (https://consurf.tau.ac.il/) server which analyses the probability of structural and functional conservation despite amino acid variability for any given position of input **sequence (Figure 3-3d, 3-5e, Figure 3-6e, l, Figure 3-7e, l, Figure 3-8c)**. We ran these analyses with default parameters except for the number of species to include. In one analysis we chose 50 representative homologues with maximum and minimum percent identity set to 95 and 50 across species. In the other, we increased the species to 150 and set max. and min. percent identity to 95 and 35 to compare a larger evolutionary subset. In both analyses the UNIREF90 database was used, which consists of cluster sequences that have at least 90% sequence identity with each other into a single UniRef entry, thus increasing the representative diversity of species considered in the output. And lastly, 3) Disopred tool (Buchan and Jones, 2019; Jones and Cozzetto, 2015) (http://bioinf.cs.ucl.ac.uk/psipred/) that scores for intrinsically disordered regions (IDRs) that are usually not well conserved yet found to be functionally essential in many proteins **(Figure 3-3e, Figure 3-5f, Figure 3-6f, m, Figure 3-7f, m, Figure 3-8d)**.

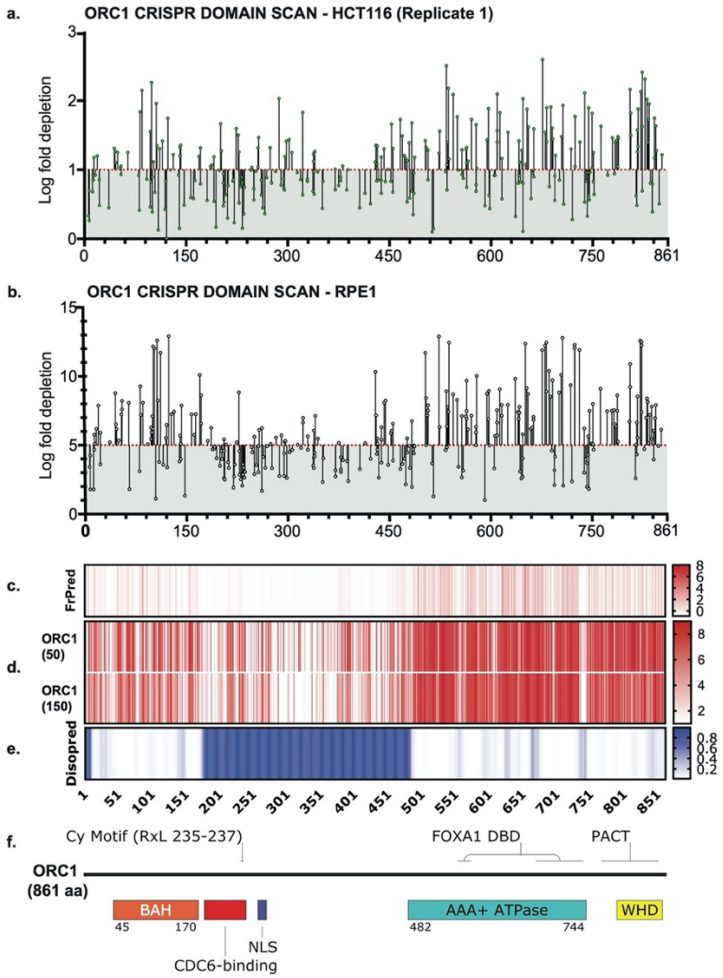

Figure 3-3. ORC1 is essential to HCT116 and RPE-1 cell lines. (Provided by Dr. Kuhulika Bhalla) (a) Tiling-sgRNA map ORC1 (replicate 1) in HCT116. Mapped as Log fold depletion (inverted LFC scale) of guide RNAs as calculated by MaGeCK (Li et al., 2014) on y axis vs the amino acid(s) disrupted by that guide RNA on the x axis. Effect of guide RNA is interpreted as essential if its depletion is more than 1 log fold (red dotted line). Data mapped on 1 Log fold depletion pseudo-axis for clarity. (b) Tiling-sgRNA map of ORC1 in RPE-1. Effect of guide RNA is interpreted as essential if its depletion is more than 5 log fold (red dotted line). Data mapped on 5 Log fold depletion pseudo-axis for clarity. (c) FrPred (https://toolkit.tuebingen.mpg.de/frpred) of hORC1 (NP_004144.2) shown as gradient heat map of conservation score vs amino acid position. (d) Consurf (https://consurf.tau.ac.il/) of hORC1 – (upper) ORC1 (50) subset (50 HMMER Homologues collected from UNIREF90 database, Max sequence identity = 95%, Min sequence identity 50, Other parameters = default), and (lower) ORC1 (150) subset (150 HMMER Homologues collected from UNIREF90 database, Max sequence identity = 95%, Min sequence identity 35, Other parameters = default). Data represented as heat map of Conservation scores of each amino acid position. (e) Disopred (http://bioinf.cs.ucl.ac.uk/psipred/) plot of hORC1 – heat map representing amino acids within intrinsically disordered regions of the protein. (f) Schematic of domain architecture of ORC1.

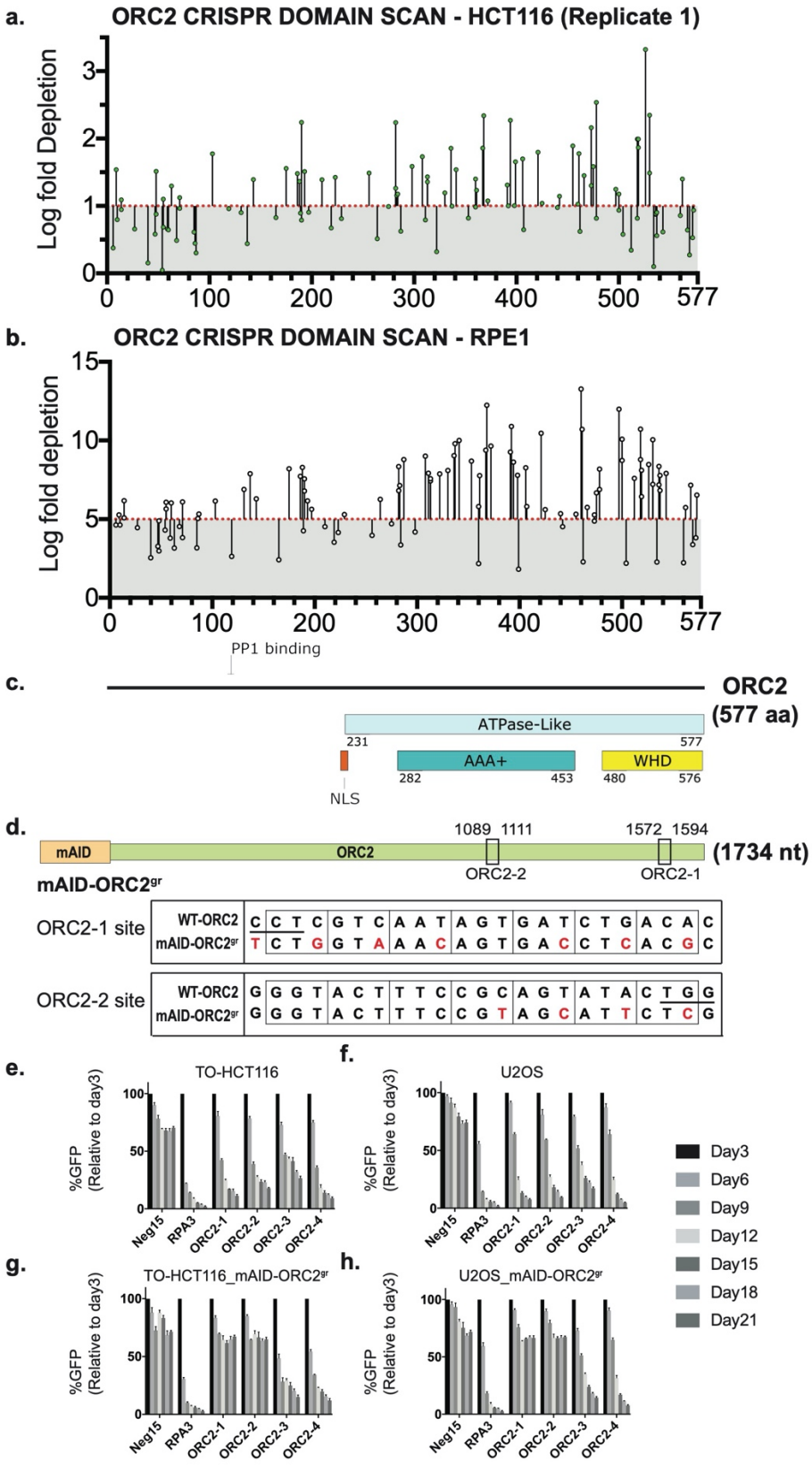
a.
ORC2 CRISPR DOMAIN SCAN - HCT116 (Replicate 1)
Log fold Depletion
b.
ORC2 CRISPR DOMAIN SCAN - RPE1
Log fold depletion
PP1 binding
c.
ORC2
(577 aa)
ATPase-Like
231
577
AAA+
282
453
WHD
480
576
NLS
d.
1089 1111
1572 1594
mAID
ORC2
(1734 nt)
ORC2-2
ORC2-1
mAID-ORC2gr
ORC2-1 site
WT-ORC2
mAID-ORC2gr
C C T C G T C A A T A G T G A T C T G A C A C
T C T G G T A A A C A G T G A C C T C A C G C
ORC2-2 site
G G G T A C T T T C C G C A G T A T A C T G G
G G G T A C T T T C C G T A G C A T T C T C G
e.
TO-HCT116
%GFP (Relative to day3)
Neg15
RPA3
ORC2-1
ORC2-2
ORC2-3
ORC2-4
f.
U2OS
Day3
Day6
Day9
Day12
Day15
Day18
Day21
g.
TO-HCT116_mAID-ORC2gr
h.
U2OS_mAID-ORC2gr

Figure 3-4. *ORC2* is essential in HCT116 and RPE-1 by tiling-sgRNA. (a) Tiling-sgRNA map of *ORC2* (replicate 1) in HCT116. (Provided by Dr. Kuhulika Bhalla) Mapped as Log fold depletion (inverted LFC scale) of guide RNAs as calculated by MaGeCK (Li et al., 2014) on y axis vs the amino acid(s) disrupted by that guide RNA on the x axis. Effect of guide RNA is interpreted as essential if its depletion is more than 1 log fold (red dotted line). Data mapped on 1 log fold depletion pseudo-axis for clarity. (b) Tiling-sgRNA map of *ORC2* for RPE-1. Data mapped on 5 Log fold depletion pseudo-axis for clarity. (c) Schematic of ORC2 protein showing annotated structural or functional domains. (d) The top panel is the schematic of the mAID degron fused to ORC2 transgene at the N-terminus, and the two black rectangles indicate ORC2-1 and ORC2-2 sgRNAs targeting regions. The numbers represent nucleotide positions in the ORC2 cDNA. The lower two panels show the silent mutations (in red) around the sgRNA target sites introduced into mAID-ORC2gr compared to wild type ORC2. Protospacer-adjacent motif (PAM) site is underlined in the wild type sequence. (e-h) Negative-selection time course assay that plots the percentage of GFP positive cells over time following transduction with the indicated sgRNAs. Experiments were performed in (e) TO-HCT116, (f) U2OS, (g) TO-HCT116_mAID-ORC2gr, and (h) U2OS_mAID-ORC2gr cell lines. The GFP positive percentages were normalized to the Day3 measurement. n = 3. Error bars, mean ± SD.

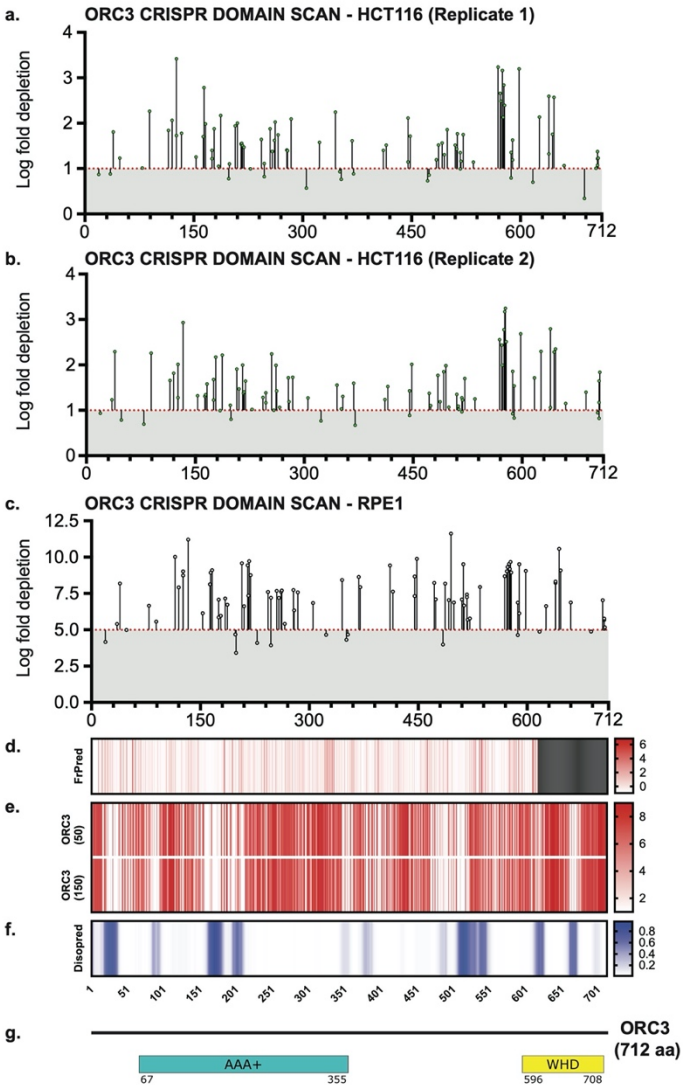

Figure 3-5. Tiling-sgRNA CRISPR screen data contd. (Provided by Dr. Kuhulika Bhalla) (a) tiling-sgRNA map of *ORC3* in HCT116 (replicate 1). Mapped as Log fold depletion as calculated by MaGeCK on y axis vs the amino acid(s) disrupted by that guide RNA on the x axis. Effect of guide RNA is interpreted as essential if its depletion is more than 1 log fold (red dotted line). (b) tiling-sgRNA map of ORC3 for HCT116 (replicate 2). (c) tiling-sgRNA map of ORC3 for RPE-1 cell line. Cutt-off of essentiality is LFC ≥ -5, indicated by red dotted line. (d) FrPred of hORC3 (NP_862820.1) shown as gradient heat map of conservation score vs amino acid position. (e) Consurf of hORC3 – (upper) ORC3 (50) subset (50 HMMER Homologues collected from UNIREF90 database, Max sequence identity = 95%, Min sequence identity 50, Other parameters = default), and (lower) ORC3 (150) subset (150 HMMER Homologues collected from UNIREF90 database, Max sequence identity = 95%, Min sequence identity 35, Other parameters = default). Data represented as heatmap of Conservation scores of each amino acid position. (f) Disopred plot of hORC3 – heatmap representing amino acids within intrinsically disordered regions of the protein. (g) Schematic of domain architecture of ORC3.

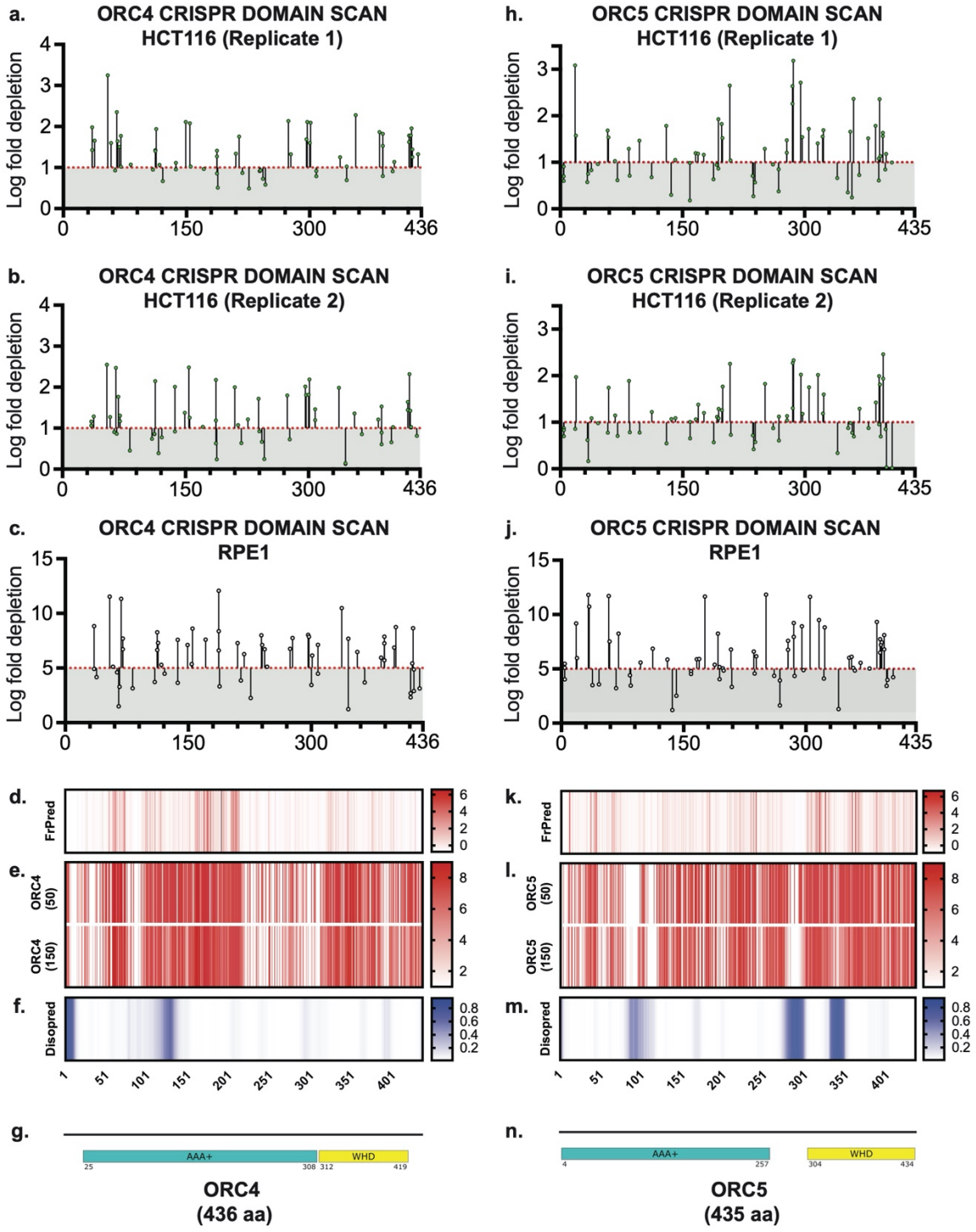
a.
ORC4 CRISPR DOMAIN SCAN
HCT116 (Replicate 1)
Log fold depletion
b.
ORC4 CRISPR DOMAIN SCAN
HCT116 (Replicate 2)
Log fold depletion
c.
ORC4 CRISPR DOMAIN SCAN
RPE1
Log fold depletion
h.
ORC5 CRISPR DOMAIN SCAN
HCT116 (Replicate 1)
Log fold depletion
i.
ORC5 CRISPR DOMAIN SCAN
HCT116 (Replicate 2)
Log fold depletion
j.
ORC5 CRISPR DOMAIN SCAN
RPE1
Log fold depletion
d.
FrPred
e.
ORC4 (50)
ORC4 (150)
f.
Disopred
k.
FrPred
l.
ORC5 (50)
ORC5 (150)
m.
Disopred
1 51 101 151 201 251 301 351 401
g.
AAA+
WHD
25 308 312 419
ORC4
(436 aa)
n.
AAA+
WHD
4 257 304 434
ORC5
(435 aa)

Figure 3-6. Tiling-sgRNA CRISPR screen data contd. (Provided by Dr. Kuhulika Bhalla) (a) tiling-sgRNA map of *ORC4* in HCT116 (replicate 1). Mapped as Log fold depletion as calculated by MaGeCK on y axis vs the amino acid(s) disrupted by that guide RNA on the x axis. Effect of guide RNA is interpreted as essential if its depletion is more than 1 log fold (red dotted line). (b) tiling-sgRNA map of ORC4 for HCT116 (replicate 2). (c) tiling-sgRNA map of ORC4 for RPE-1 cell line. Cutt-off of essentiality is LFC ≥ -5, indicated by red dotted line. (d) FrPred of hORC4 (NP_859525.1) shown as gradient heat map of conservation score vs amino acid position. (e) Consurf of hORC4 – (upper) ORC4 (50) subset (50 HMMER Homologues collected from UNIREF90 database, Max sequence identity = 95%, Min sequence identity 50, Other parameters = default), and (lower) ORC4 (150) subset (150 HMMER Homologues collected from UNIREF90 database, Max sequence identity = 95%, Min sequence identity 35, Other parameters = default). Data represented as heatmap of Conservation scores of each amino acid position. (f) Disopred plot of hORC4 – heatmap representing amino acids within intrinsically disordered regions of the protein. (g) Schematic of domain architecture of ORC4. (h) tiling-sgRNA map of *ORC5* in HCT116 (replicate 1). (i) tiling-sgRNA map of ORC5 for HCT116 (replicate 2). (j) tiling-sgRNA map of ORC5 for RPE-1 cell line. (k) FrPred of hORC5 (NP_002544.1) shown as gradient heat map of conservation score vs amino acid position. (e) Consurf of hORC5 – (upper) ORC5 (50) subset and (lower) ORC5 (150) subset. Data represented as heatmap of Conservation scores of each amino acid position. (f) Disopred plot of hORC5 – heatmap representing amino acids within intrinsically disordered regions of the protein. (g) Schematic of domain architecture of ORC5.

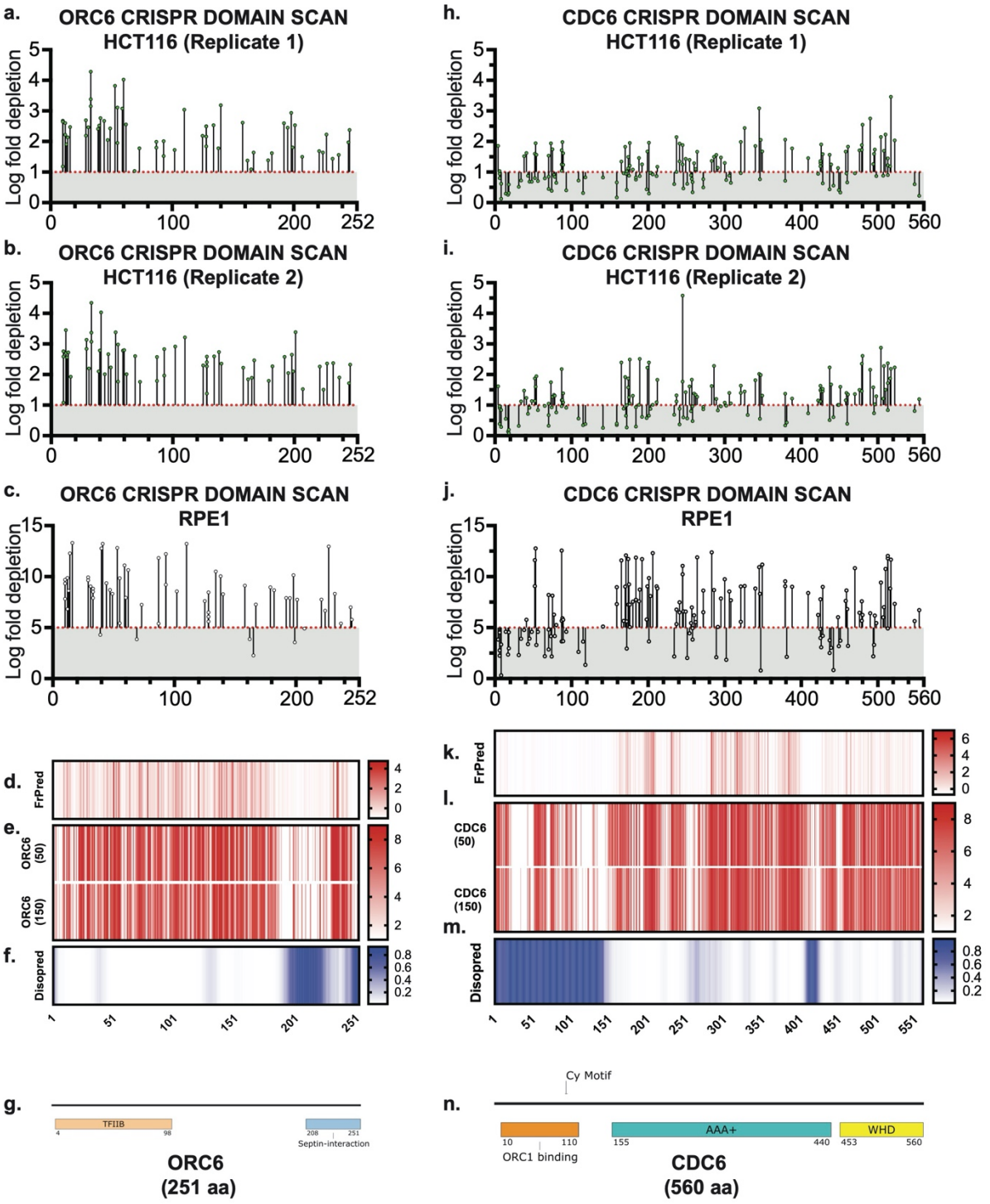
a.
ORC6 CRISPR DOMAIN SCAN
HCT116 (Replicate 1)
Log fold depletion
b.
ORC6 CRISPR DOMAIN SCAN
HCT116 (Replicate 2)
c.
ORC6 CRISPR DOMAIN SCAN
RPE1
d.
FrPred
e.
ORC6 (50)
ORC6 (150)
f.
Disopred
g.
TFIIB
Septin-interaction
ORC6
(251 aa)
h.
CDC6 CRISPR DOMAIN SCAN
HCT116 (Replicate 1)
i.
CDC6 CRISPR DOMAIN SCAN
HCT116 (Replicate 2)
j.
CDC6 CRISPR DOMAIN SCAN
RPE1
k.
FrPred
l.
CDC6 (50)
CDC6 (150)
m.
Disopred
n.
Cy Motif
AAA+
WHD
ORC1 binding
CDC6
(560 aa)

Figure 3-7. Tiling-sgRNA CRISPR screen data contd. (Provided by Dr. Kuhulika Bhalla) (a) Tiling-sgRNA map of *ORC6* in HCT116 (replicate 1). Mapped as Log fold depletion as calculated by MaGeCK on y axis vs the amino acid(s) disrupted by that guide RNA on the x axis. Effect of guide RNA is interpreted as essential if its depletion is more than 1 log fold (red dotted line). (b) Tiling-sgRNA map of ORC6 for HCT116 (replicate 2). (c) Tiling-sgRNA map of ORC6 for RPE-1 cell line. Cutt-off of essentiality is LFC ≥ -5, indicated by red dotted line. (d) FrPred of hORC6 (NP_055136.1) shown as gradient heat map of conservation score vs amino acid position. (e) Consurf of hORC6 – (upper) ORC6 (50) subset and (lower) ORC6 (150) (f) Disopred plot of hORC6-heatmap representing amino acids within intrinsically disordered regions of the protein. (g) Schematic of domain architecture of ORC6. (h) tiling-sgRNA map of *CDC6* in HCT116 (replicate 1). (i) Tiling-sgRNA map of CDC6 for HCT116 (replicate 2). (j) Tiling-sgRNA map of CDC6 for RPE-1 cell line. (k) FrPred of hCDC6 (NP_001245.1) shown as gradient heat map of conservation score vs amino acid position. (e) Consurf of hCDC6 – (upper) CDC6 (50) subset and (lower) ORC5 (150) subset. Data represented as heatmap of Conservation scores of each amino acid position. (f) Disopred plot of hCDC6 – heatmap representing amino acids within intrinsically disordered regions of the protein. (g) Schematic of domain architecture of hCDC6.

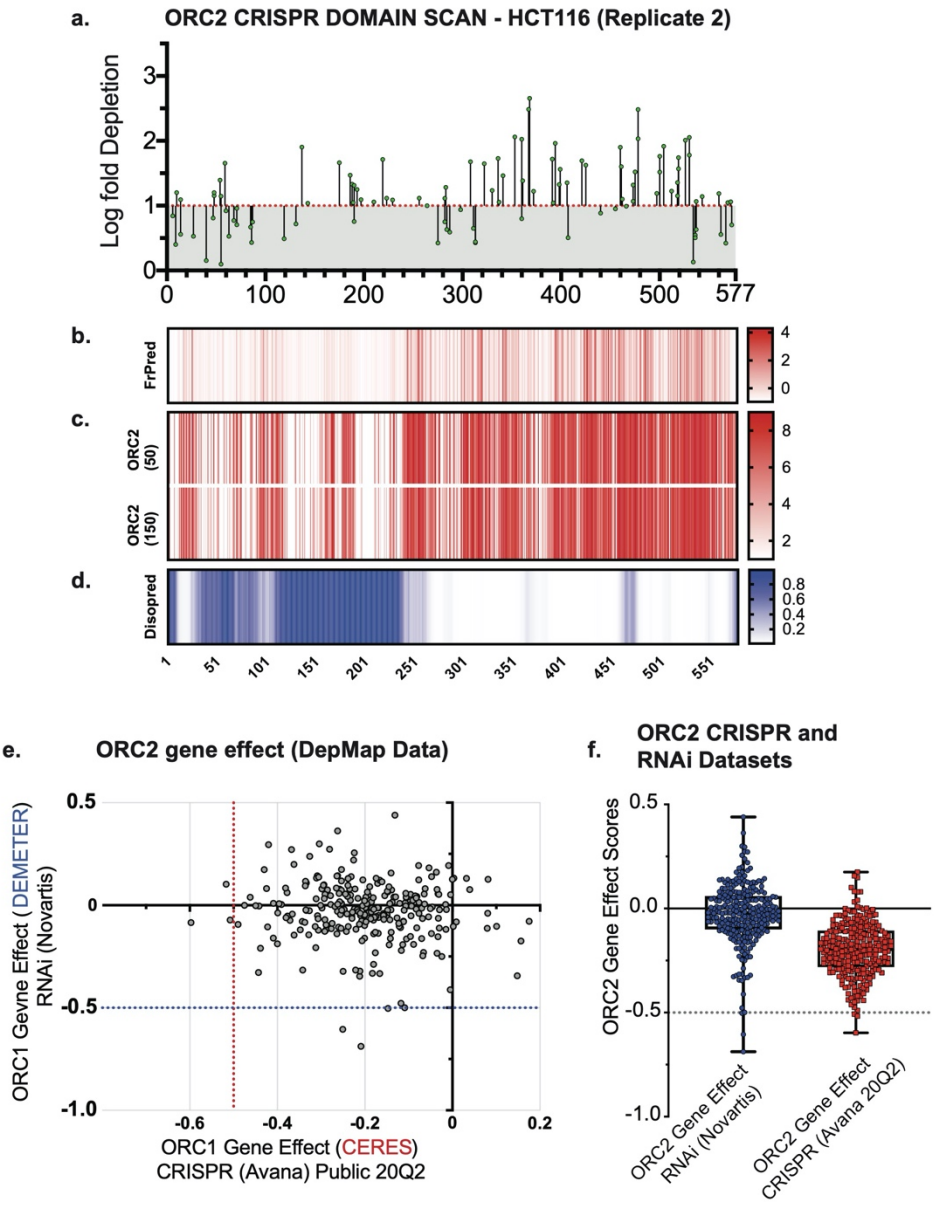

Figure 3-8. Tiling-sgRNA CRISPR screen data contd. (Provided by Dr. Kuhulika Bhalla) (a) Tiling-sgRNA map of *ORC2* (replicate 2) in HCT116. (b) FrPred (https://toolkit.tuebingen.mpg.de/frpred) of hORC2 (NP_006181.1) shown as gradient heat map of conservation score vs amino acid position. (d) Consurf (https://consurf.tau.ac.il/) of hORC2 – (upper) ORC2 (50) subset (50 HMMER Homologues collected from UNIREF90 database, Max sequence identity = 95%, Min sequence identity 50, Other parameters = default), and (lower) ORC2 (150) subset (150 HMMER Homologues collected from UNIREF90 database, Max sequence identity = 95%, Min sequence identity 35, Other parameters = default). Data represented as heatmap of Conservation scores of each amino acid position. (e) Disopred (http://bioinf.cs.ucl.ac.uk/psipred/) plot of hORC2 – heatmap representing amino acids within intrinsically disordered regions of the protein.

When the DepMap CRISPR Achilles (Avana 20Q2 library) dataset was compared to a combined RNAi dataset of cell lines, it indicated that using the CRISPR method, with a gene effect score of less than -0.5, *ORC1* classified as common essential in > 90 percent of the cell lines, while with RNAi datasets with that same cut-off, it classified as essential in only about 45 percent of the same cell lines **(Figure 3-9b-c)**. It is evident that the method of choice did have a bearing on the phenotypic outcome of the knock-down. The study by Shibata et al. (2016) that found *ORC1* and *ORC2* to be non-essential also used CRISPR editing as the method of knock-down, but also performed long term selection for cell proliferation to obtain $ORC1^{-/-}$ of $ORC2^{-/-}$ cells. We therefore determined if our screen had guide RNAs that were used in either of the DepMap dataset or used in the directed study (Shibata et al., 2016). For *ORC1* and *ORC2* sgRNAs that were used in DepMap datasets, there was a variation in their phenotype as measured by LFC values, with some guides classifying *ORC1* and *ORC2* as essential and others not **(Figure 3-10a-c)**. Of note is the fact that the guide used to target *ORC2* in the Shibata et al. (2016) study showed activity very close to the cut-off in HCT116 cells and scored as non-essential in RPE-1. It is important to note that when a guide targeting a relatively non-essential region allows for the cells to proliferate, no conclusion can be made about the protein being essential. The Shibata et al. (2016) study used that single guide to insert a gene encoding blasticidin resistance and a poly A cassette into the locus, with the aim of disrupting transcription, while our single-guide-per-locus type of screen did not introduce such large insertions. We find that *ORC1-6* and *CDC6* are all essential in both cell lines tested, and that the dynamic range of depletion of these proteins was greater in diploid RPE-1 cells **(Figure 3-11)**. Comparison of the results from our screens and the published DepMap, especially about *ORC2*, suggest that using too few guides to target proteins can lead to artifactual observations both in terms of essentiality or non-essentiality, and that overall, the gene-effect is influenced by the combination of the choice of guide RNA and the cell line studied.

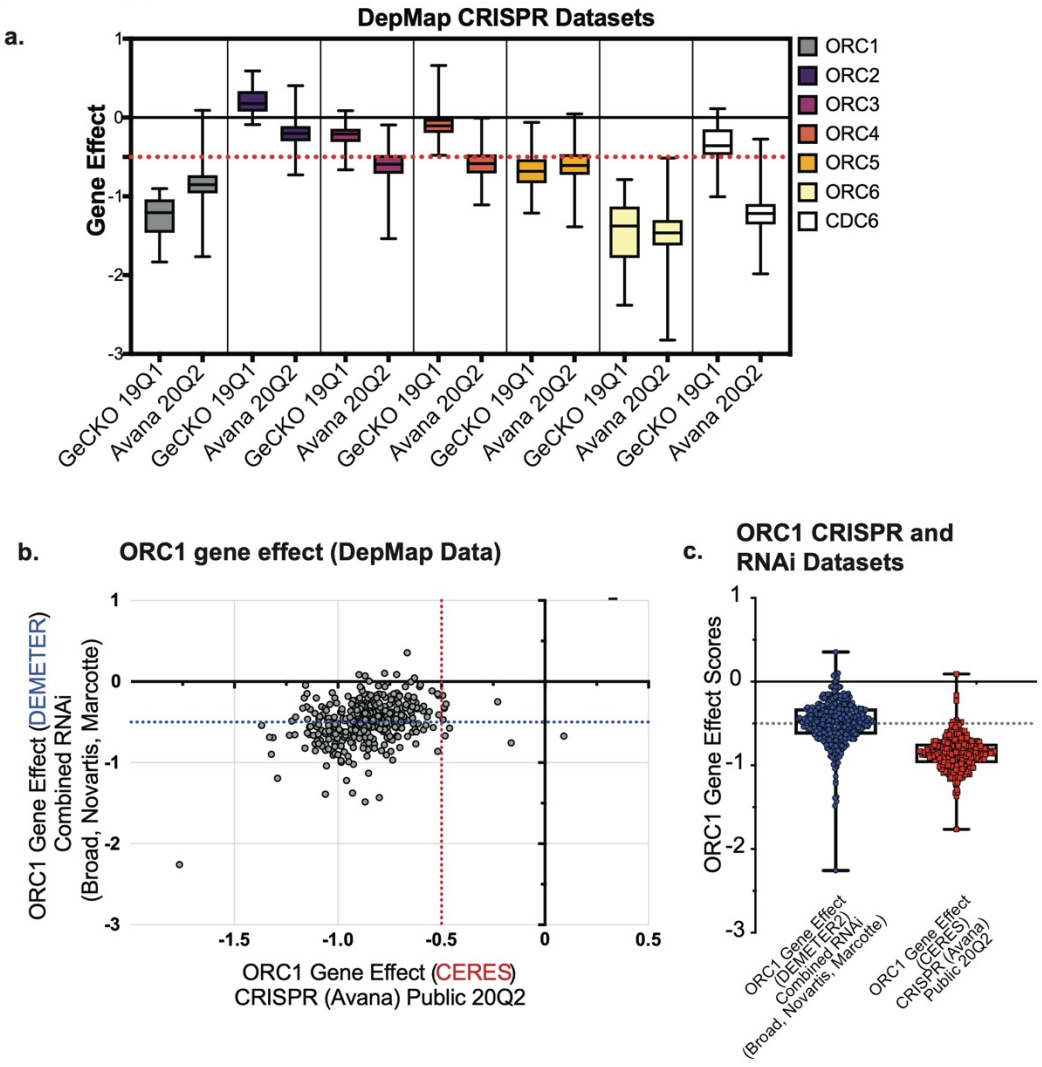

Figure 3-9. DepMap analyses of *ORC1* data. (Provided by Dr. Kuhulika Bhalla) (a) Distribution of Gene Effect scores of *ORC1-6* and *CDC6* across all the cell lines used in either the GeCKO 19Q1 or Avana 20Q2 CRISPR screens reported on DepMap [DepMap, Broad (2019): DepMap GeCKO 19Q1. figshare. Dataset. https://doi.org/10.6084/m9.figshare.7668407.v1, DepMap, Broad (2020): DepMap 20Q2 Public. figshare. Dataset. https://doi.org/10.6084/m9.figshare.12280541.v4, (Meyers et al., 2017)]. Each box plot represents gene effect range displayed in the tested cell lines. The red dotted line represents the gene effect score below which genes are scores as essential. (b) *ORC1* gene effect values for CRISPR [CERES; (Meyers et al., 2017) vs RNAi (McFarland et al., 2018)] mapped as xy scatter for ~390 common cell lines used in the screens. Red dotted line bifurcates the plot at CRISPR based gene effect score of less than -0.5 is considered essential to cell line. Blue dotted line bifurcates the plot at RNAi based gene effect score of less than -0.5 is considered essential to cell line. (c) Distribution of *ORC1* gene effect scores across all the cell lines used in CRISPR Avana 20Q2 and RNAi datasets respectively (McFarland et al., 2018; Meyers et al., 2017).

a. **GeCkO library: ORC1 and ORC2 sgRNA**

No.	Gene	sgRNA	HCT116 (LFC; ≤-1)	RPE1 (LFC; ≤-5)
1	ORC1	TGTACTCGAGCACGTTTCTT	-1.837	-7.1963
3	ORC1	AGAAACGTGCTCGAGTACAG	-2.149	-8.0847
5	ORC1	ACCGAGATTCACATCCAGAT	-1.1019	-6.1747
6	ORC1	ACCACATCCTTTGGGGCTAA	-0.92417	-3.82
7	ORC2	GAACCTTGTCTGAAGCAGAA	-1.3909	-4.6301
9	ORC2	TCTTCCTCCAAATCATATTC	-0.68492	-4.2515

b. **Avana 20Q2 library: ORC1 and ORC2 sgRNA**

No.	Gene	sgRNA	HCT116 (LFC; ≤-1)	RPE1 (LFC; ≤-5)
1	ORC1	TTACCCCAAGAGCCAGAAAG	-0.81863	-2.8709
2	ORC1	AGAAACGTGCTCGAGTACAG	-2.149	-8.0847
3	ORC1	AGTTTGGCGAGATTTGGAGG	-0.83692	-1.9165
4	ORC1	TCTGGTTTCAGAATCACGGA	-0.76629	-2.3272
5	ORC1	ATTCTCCAGGAAGAATAAAA	-0.98108	-6.2369
6	ORC1	AAGTCTGCTGGGACATCTGA	-0.99435	-4.8626
8	ORC2	AAGTTCGGCAGAAAAGGAAG	-0.75093	-6.8116
9	ORC2	GGTTGCACAGGAACATGAAG	-1.094	-5.625
10	ORC2	TTTGGAGGAAGATGACCAGG	-0.6455	-6.6874
12	ORC2	ATATTCTGCTTCCAACTCAG	-1.4795	-9.1468

c.

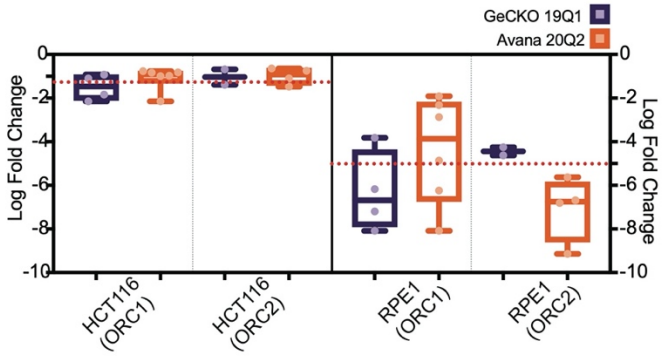

d. **ORC2 guides used in this study**

Gene	sgRNA	aa	HCT116-I (LFC; ≤-1)	HCT116-II (LFC; ≤-1)	RPE1 (LFC≤-5)
ORC2-1	GTGTCAGATCACTATTGACG	526	-3.3226	-2.0084	-8.468
ORC2-2	GGGTACTTTCCGCAGTATAC	367	-1.8567	-2.4848	-9.3786
ORC2-3	GGATGATGAAGGGGTTGCAC	193	-1.5095	-1.2495	-6.1627
ORC2-4	AAAGCACAATGTTGAACCCA	308	-1.7298	-1.6785	-8.9999
Shibata 2016	GAAGGAGCGAGCGCAGCTTT	40	-1.5134	-1.1548	-4.4581

Figure 3-10. (a) Table listing guide RNA sequences used in GeCKO 19Q1 library against *ORC1* and *ORC2* that were also present in our tiling-sgRNA screen; columns HCT116(LFC ≤ -1) and RPE-1(LFC ≤-5) show the LFC of the GeCKO guides in our screen. (b) Table listing guide RNA sequences used in Avana 20Q2 library against *ORC1* and *ORC2* that were also present in our tiling-sgRNA screen; columns HCT116(LFC ≤ -1) and RPE-1(LFC ≤-5) show the LFC of the GeCKO guides in our screen. Rows highlighted blue represent the only common guide against *ORC1* used between GeCKO and Avana screens (c) Distribution of the LFC values for the GeCKO and Avana guides in HCT116 and RPE-1 (graphical representation of the tables (a) & (b). (d) *ORC2* guides selected for single guide studies. Row highlighted yellow – guide RNA sequence used in the Shibata et. al 2016 study.

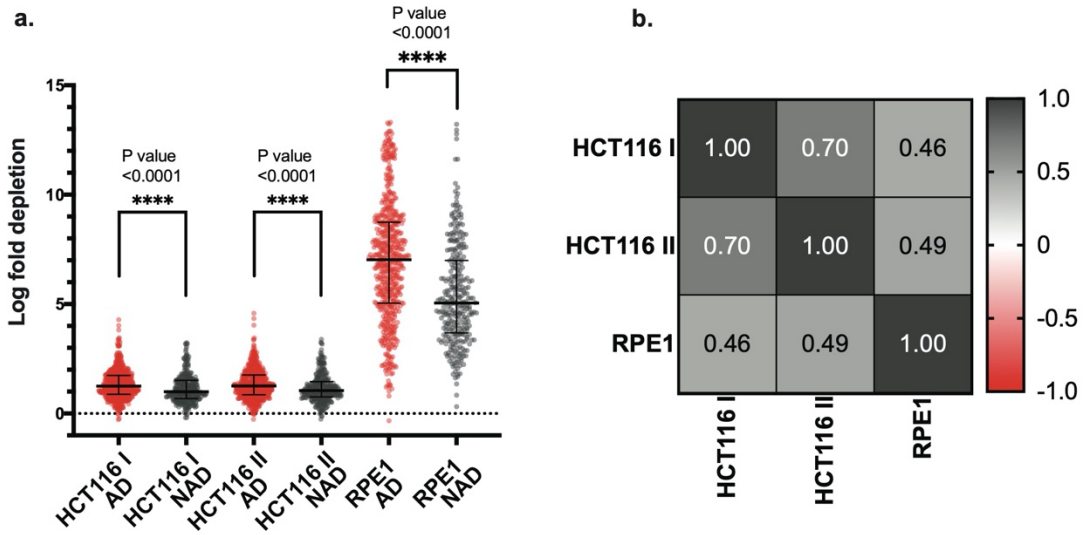

Figure 3-11. Guide RNAs targeting annotated domains show a higher negative selection phenotype. (Provided by Dr. Kuhulika Bhalla) (a) Distribution of LFC values of all guide RNAs (ORC1-6, CDC6) targeting all annotated domains (AD) (red) or non-annotated domains (NAD) (grey) regions. Significance (P value) calculated using non-parametric Mann-Whitney t-test to compare ranks. Error bars depict median and interquartile ranges of distributions. (b) Heatmap of correlation matrix for the 3 tiling-sgRNA screens. r values were computed by Spearman Correlation for each pair at a confidence interval of 99%.

When we evaluate the distribution of LFC for all sgRNAs we saw a negative correlation with annotated domains (AD) – that is sgRNAs targeting AD regions showed significantly higher depletion compared to those targeting non-annotated domain (NAD) regions **(Figure 3-11a, Figure 3-12a)**. This finding is consistent the only previous study that used tiling-sgRNA negative CRISPR screens (Munoz et al., 2016). Moreover, we see a high correlation between our datasets from both HCT116 replicates ($r \approx 0.7$) as well as between HCT116 and RPE-1 ($r \approx 0.47$), which is also consistent with the previous study that compared three cell lines **(Figure 3-11b)**. For each ORC subunit (and CDC6), ≥50% of designed sgRNAs target annotated domain (AD) regions **(Figure 3-12a)**, with the exception of *ORC4*, which is entirely structured, and thus none of the sgRNAs target non-annotated domain (NAD) regions. For all other genes, the fraction of NAD targeting sgRNAs that scored as essential, as well as their locations within these regions were comparable between cell lines rather than between proteins **(Figure 3-12b-h)**. This suggests there are functional modules within the NADs and indeed, at least in some cases, we found that sgRNA dropouts in our screens agree with recent functional studies about these regions. For example, in *ORC1*, in HCT116 we saw depletion of sgRNAs targeting regions between 300 – 450 aa. In humans and *Drosophila*, this N-terminal region is an unstructured IDR, required for ATP-independent chromatin recruitment of ORC and drives protein phase-separation with DNA *in vitro* (Bleichert et al., 2018; Hossain et al., 2021; Parker et al., 2019). In yeast, this region of Orc1 has been shown to be critical for interacting with ARS DNA as well, but is completely structured unlike metazoan ORC1(Hu et al., 2020; Kawakami et al., 2015; Li et al., 2018). Another example is ORC6 in which the N-terminus harbors a structured TFIIB domain, but we noticed sgRNA depletions in the remaining regions, especially the C-terminal extremity, which is a septin-binding region essential for cytokinesis and mutations in a conserved C-terminal motif have also been linked to Meier-Gorlin Syndrome (Akhmetova et al., 2014; Balasov et al., 2020, 2015, 2007; Bicknell et al., 2011a; Prasanth et al., 2002; Xu et al., 2020).

a.

Protein	Annotated Domains (AD) aa region		No. Of sgRNA targeting AD	No. of sgRNA targeting NAD	Subtotal
ORC1	BAH AAA+/WHD	45 - 171 501 - 861	169	137	306
ORC2	AAA+/WHD	280 - 577	70	40	110
ORC3	AAA+ WHD	67 - 355 596 - 708	55	37	92
ORC4	AAA+ WHD	25 -308 312 - 419	62	0	62
ORC5	AAA+ WHD	4 - 257 304 - 434	58	10	68
ORC6	TFIIB	4 - 98	32	29	61
CDC6	AAA+ WHD	155 - 440 435 - 560	106	47	153
Total			**552**	**300**	**852**

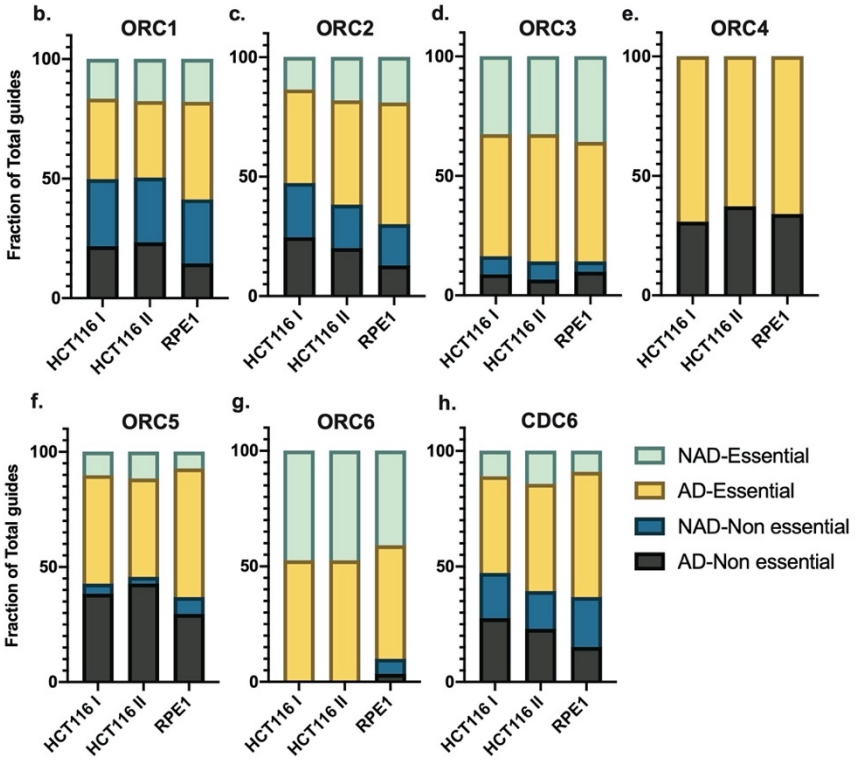

Figure 3-12. Analysis of ORC1-6, CDC6 tiling-sgRNA CRISPR screens. (Provided by Dr. Kuhulika Bhalla) (a) Table listing annotated domains from Pfam database and structural studies in ORC1-6 and CDC6. It also lists the number of guides recovered in our sequencing datasets targeting either Annotated Domain (AD) regions or Non-Annotated Domain (NAD) regions (Total input library was 882 guides; ~ 30 guides from the *ORC3* library were consistently absent in the initial time harvest to start with). (b-h) Fractions of AD and NAD targeting guide RNAs classified as essential or non-essential in the tiling-sgRNA CRISPR screens. Data represented as percent of total guide RNAs targeting the protein. Stacked histograms represent individual screens - HCT116 I (replicate 1), HCT116 II (replicate 2) and RPE-1.

Limitations like variability of sgRNA efficiency, target gene copy number, *p53* status of the cell, post-translational modifications, local structure of the gene locus can confound analyses from high-throughput tiling-sgRNA CRISPR screening (Haapaniemi et al., 2018; Munoz et al., 2016). To determine similarities or differences in 'regions of essentiality' in ORC and CDC6 between HCT116 and RPE-1 cell lines, we used the computational tool Protiler, developed specifically for tiling-sgRNA CRISPR screens (He et al., 2019). This tool takes into account local outliers due to inactive sgRNA or additive effects, and maps sgRNA depletion signals to amino acids of the target proteins to identify functionally essential regions based on their CRISPR-knockout hyper-sensitivity (CKHS). MAGeCK LFC values for combined HCT116 replicates and RPE-1 were put through this pipeline at two different -t2/--thresholds, 0.25 and 0.5, which detect changing points using the TGUH method described in this study. Almost all annotated domains or their boundaries overlapped with CKHS regions **(Figure 3-13, Figure 3-14, Figure 3-15, Figure 3-16, Figure 3-17, Figure 3-18)**. In addition, in ORC1, ORC2, ORC3, ORC6 and CDC6 NAD regions were also determined to be CKHS. Some of the newly identified CKHS regions are in agreement with studies that have found that the N-terminal IDR region of ORC1, ORC2 and CDC6, and a small C-terminal region of ORC6, to be functionally important and therefore indispensable (Akhmetova et al., 2014; Balasov et al., 2007; Hossain et al., 2021; Lidonnici et al., 2004; Parker et al., 2019; Prasanth et al., 2002; Shen et al., 2012).

At this point we selected sgRNAs that fall within regions of AD and CKHS overlap to target *ORC2* and characterize the phenotype of such ablation **(Figure 3-10d)**. We also received *ORC1* and *ORC2* deficient stable cell lines from the authors of the previous study (Shibata et al., 2016) for further analysis.

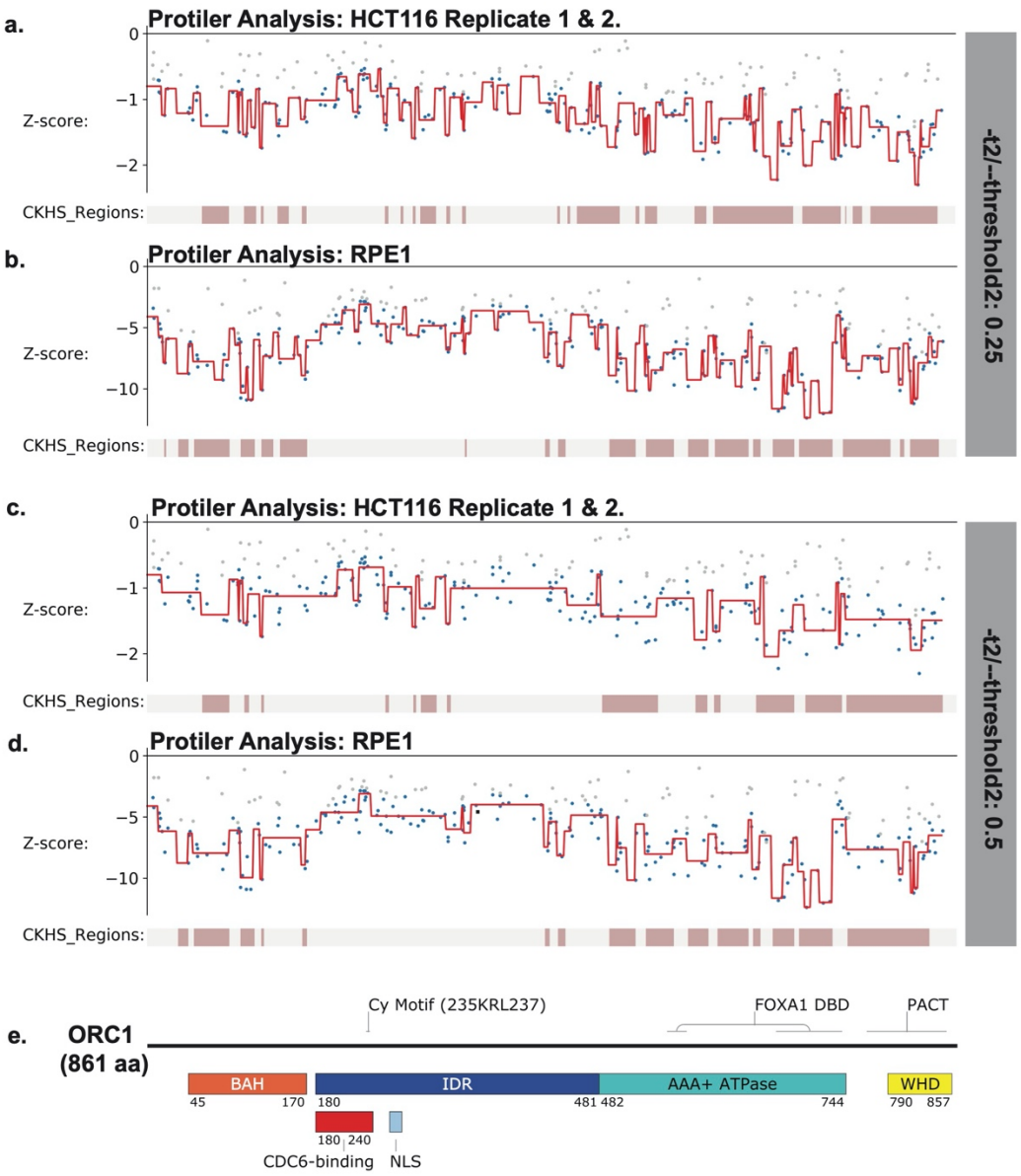

Figure 3-13. Identification of CKHS regions in *ORC1* using Protiler. (Provided by Dr. Kuhulika Bhalla) Protiler computational pipeline was run on LFC values of guide RNAs for either for the average of the two HCT116 replicates or RPE-1 at two different TGUH thresholds. (a-b) -t2/--threshold2 = 0.25. (c-d) -t2/--threshold2 = 0.5. (e) Schematic of ORC1 highlighting annotated domains, IDRs and regions of known function.

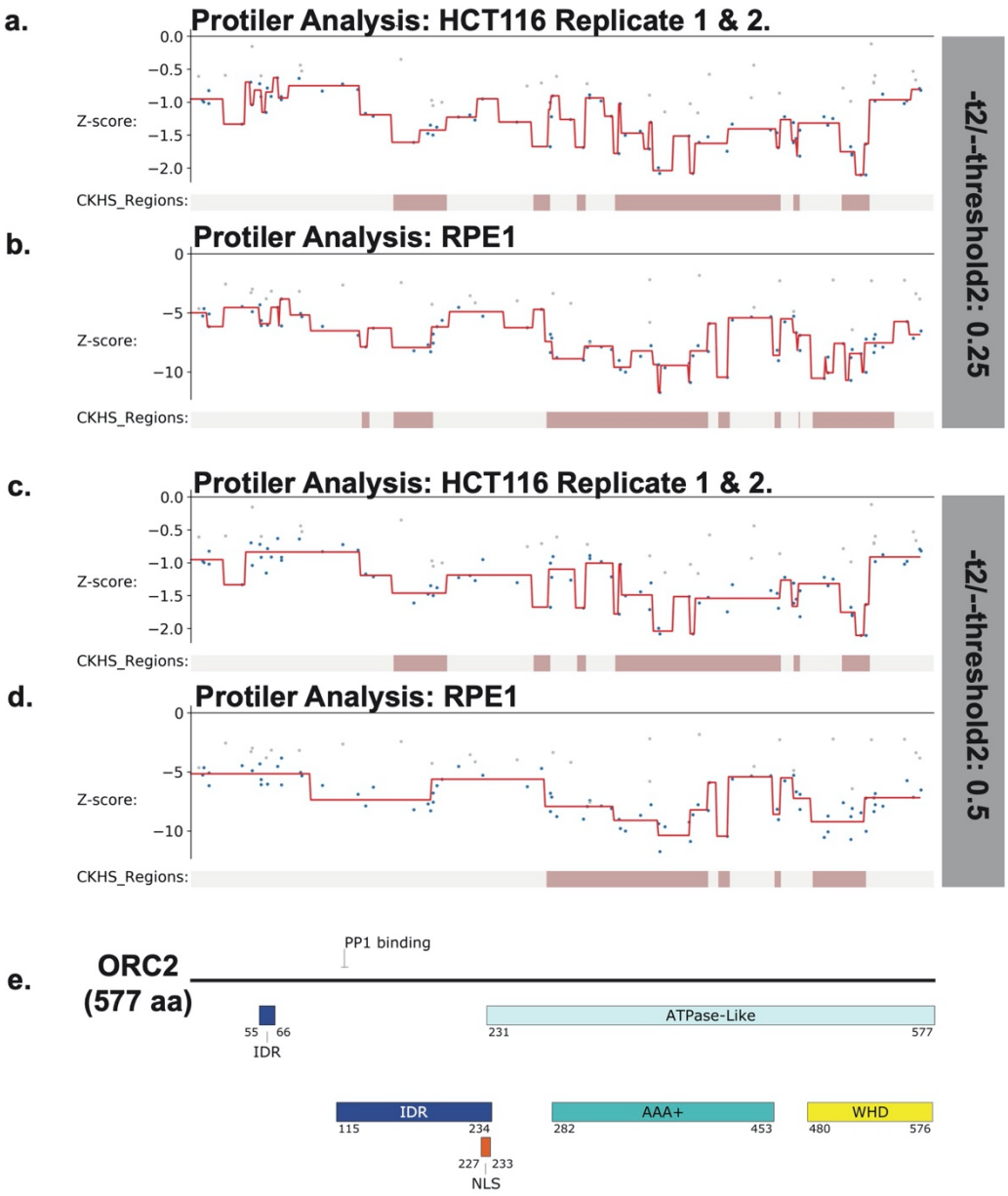

Figure 3-14. Identification of CKHS regions in *ORC2* using Protiler. (Provided by Dr. Kuhulika Bhalla) Protiler computational pipeline was run on LFC values of guide RNAs for either for the average of the two HCT116 replicates or RPE-1 at two different TGUH thresholds. (a-b) -t2/--threshold2 = 0.25. (c-d) -t2/--threshold2 = 0.5. (e) Schematic of ORC2 highlighting annotated domains, IDRs and regions of known function.

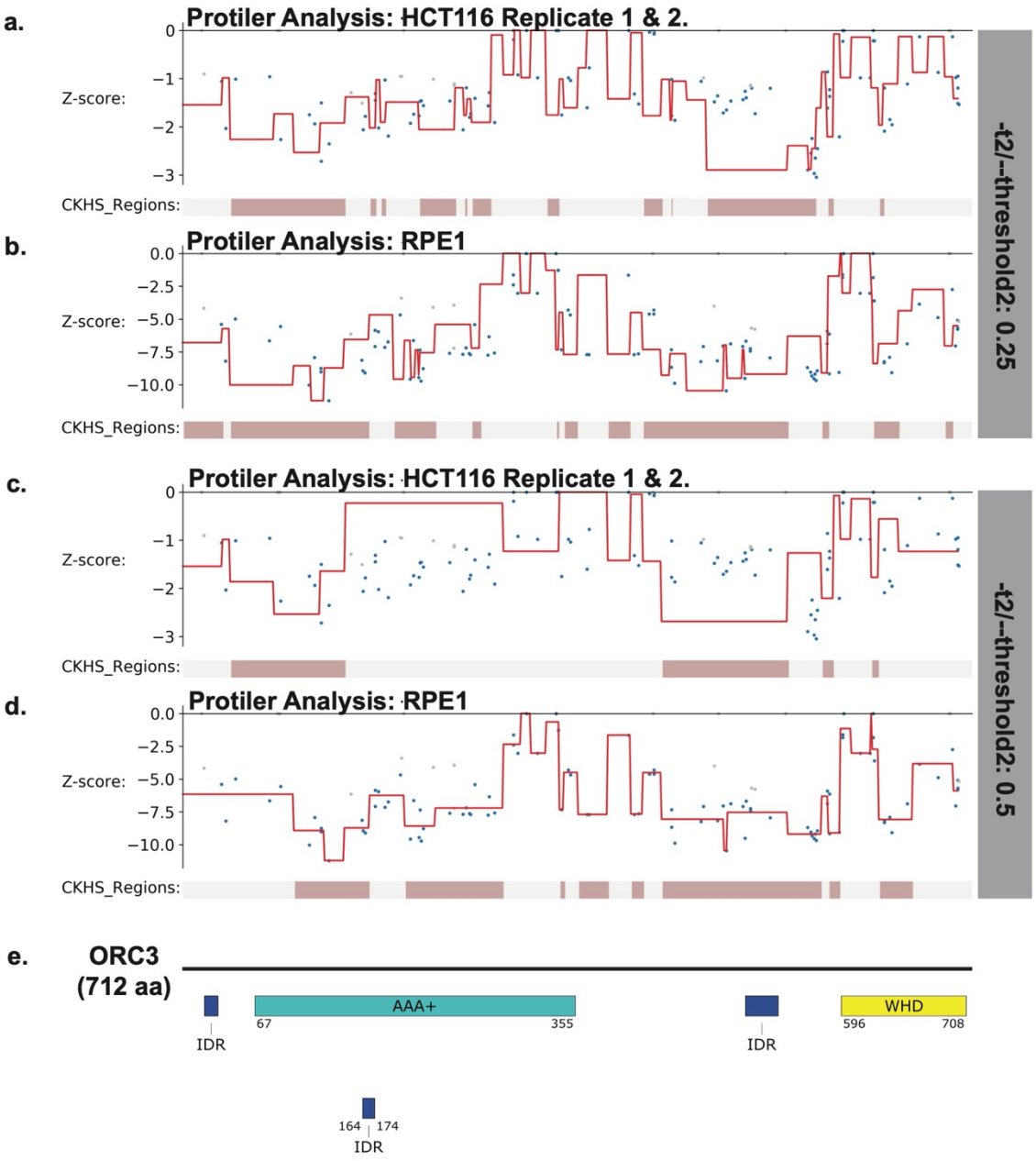

Figure 3-15. Identification of CKHS regions in *ORC3* using Protiler. (Provided by Dr. Kuhulika Bhalla) Protiler computational pipeline was run on LFC values of guide RNAs for either for the average of the two HCT116 replicates or RPE-1 at two different TGUH thresholds. (a-b) -t2/--threshold2 = 0.25. (c-d) -t2/--threshold2 = 0.5. (e) Schematic of ORC3 highlighting annotated domains, IDRs and regions of known function.

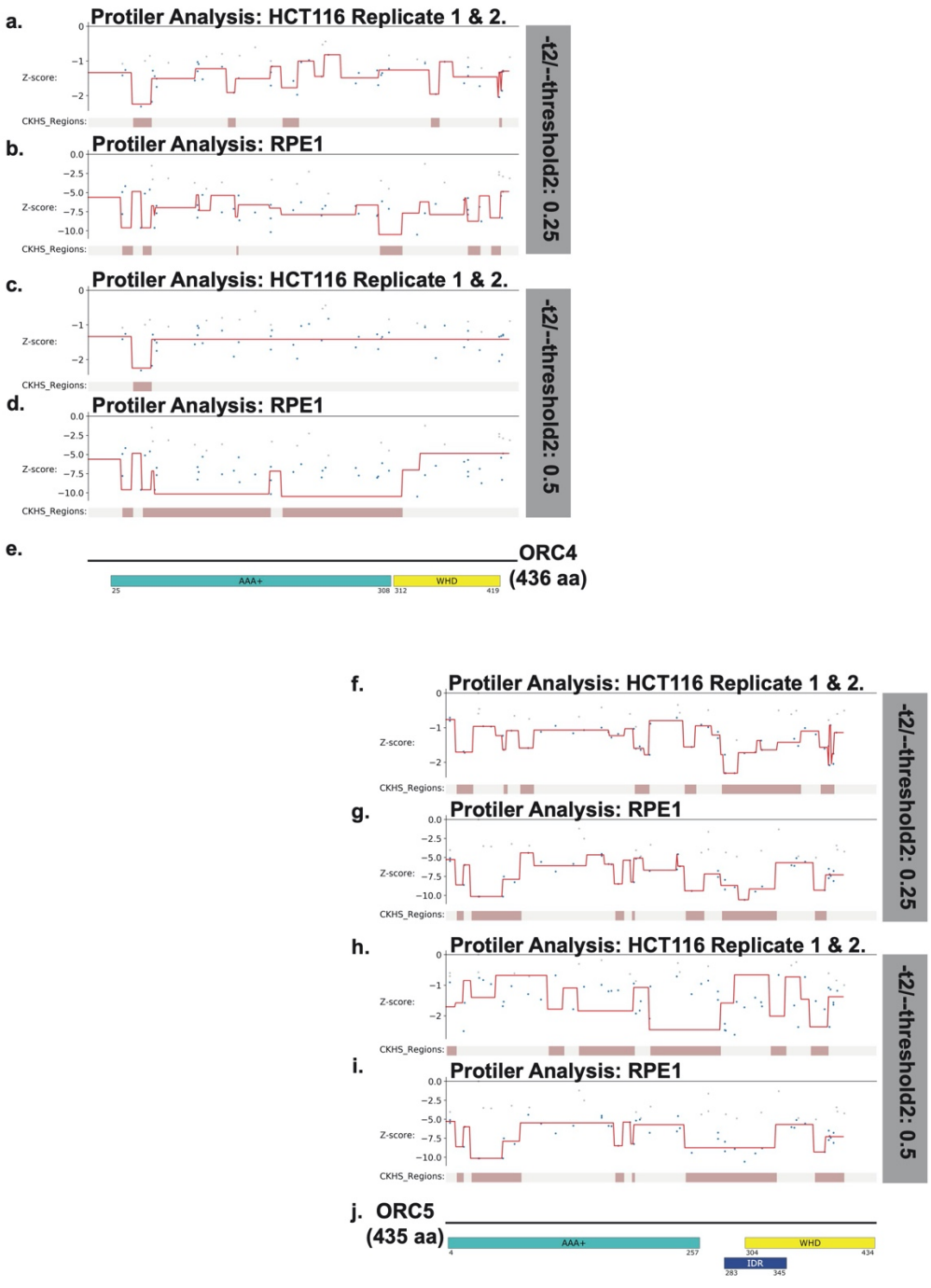

Figure 3-16. Identification of CKHS regions in *ORC4* and *ORC5* using Protiler. (Provided by Dr. Kuhulika Bhalla) Protiler computational pipeline was run on LFC values of guide RNAs for either for the average of the two HCT116 replicates or RPE-1 at two different TGUH thresholds. ORC4 (a-b) -t2/--threshold2 = 0.25. (c-d) -t2/--threshold2 = 0.5. (e) Schematic of ORC4 highlighting annotated domains, IDRs and regions of known function. ORC5 (f-g) -t2/--threshold2 = 0.25. (h-i) -t2/--threshold2 = 0.5. (j) Schematic of ORC4 highlighting annotated domains, IDRs and regions of known function.

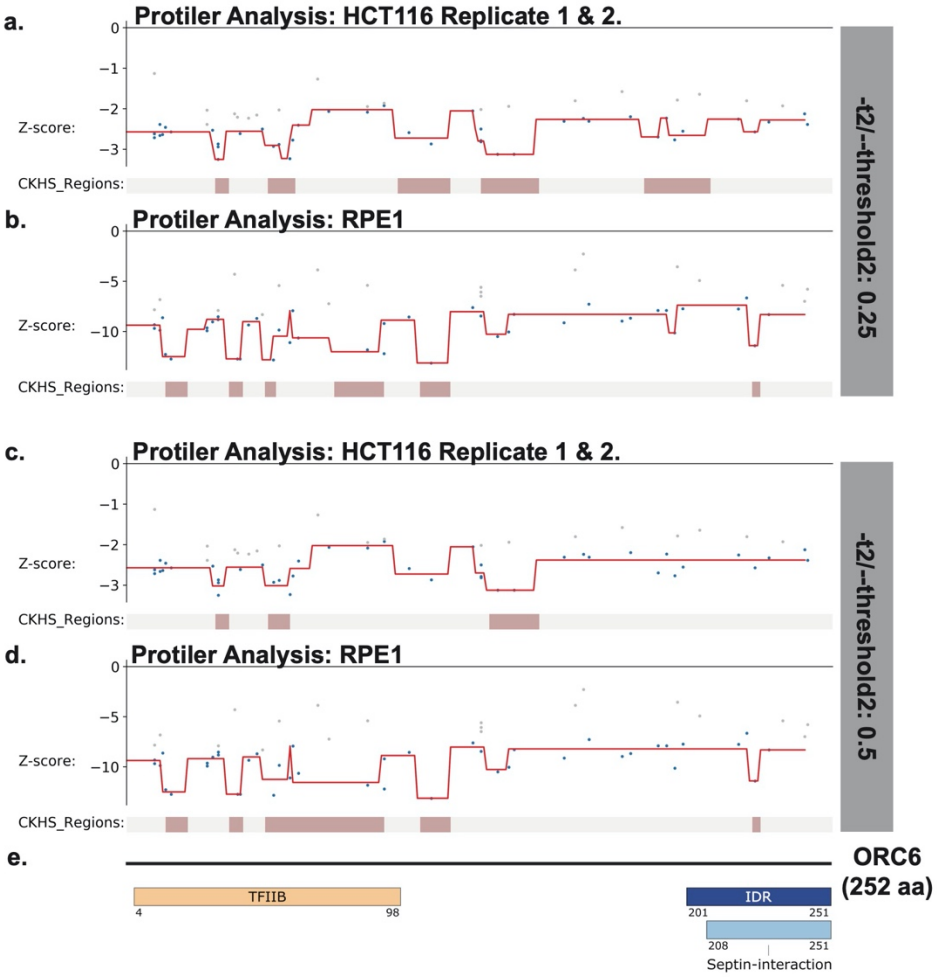

Figure 3-17. Identification of CKHS regions in *ORC6* using Protiler. (Provided by Dr. Kuhulika Bhalla) Protiler computational pipeline was run on LFC values of guide RNAs for either for the average of the two HCT116 replicates or RPE-1 at two different TGUH thresholds. (a-b) -t2/--threshold2 = 0.25. (c-d) -t2/--threshold2 = 0.5. (e) Schematic of ORC6 highlighting annotated domains, IDRs and regions of known function.

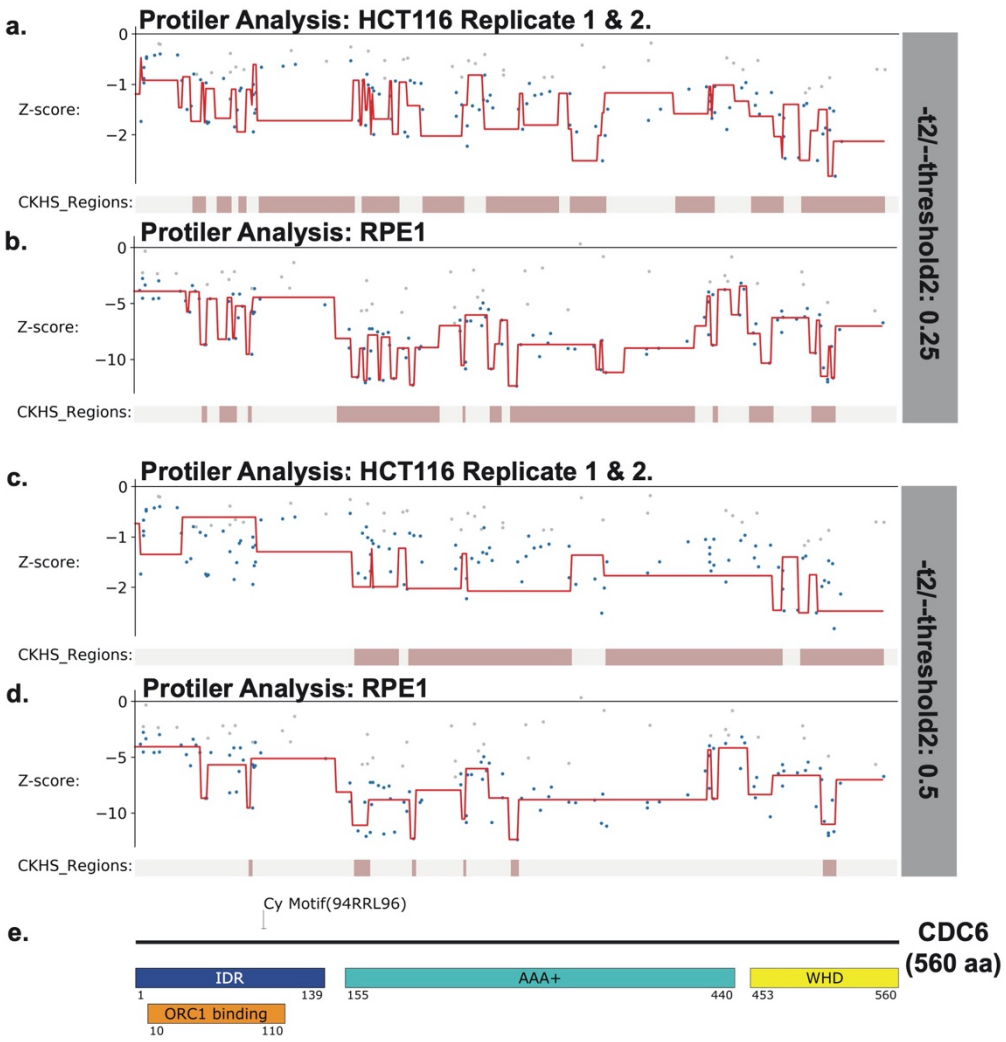

Figure 3-18. Identification of CKHS regions *CDC6* using Protiler. (Provided by Dr. Kuhulika Bhalla) Protiler computational pipeline was run on LFC values of guide RNAs for either for the average of the two HCT116 replicates or RPE-1 at two different TGUH thresholds. ORC4 (a-b) -t2/--threshold2 = 0.25. (c-d) -t2/--threshold2 = 0.5. (e) Schematic of CDC6 highlighting annotated domains, IDRs and regions of known function.

2.2. Rapid ORC2 removal in cancer cells impedes cell growth and causes DNA damage

Knock-down of *ORC2* with an siRNA approach was a slow process that took at least 24-48 hours, however, using this method we have observed various defective phenotypes, including G1 arrest, S-phase defects, abnormally condensed chromosomes as well as defects in mitosis (Prasanth et al., 2010, 2004). These phenotypes can be outcomes of accumulated errors that happen during any phase of the cell cycle and thus it is hard to distinguish between primary and secondary phenotypes associated with the loss of ORC2. Therefore, we used CRISPR/Cas9 in combination with an auxin inducible degron (mAID) tagged ORC2 to construct cell lines in which endogenous ORC2 could be knocked out by CRISPR, and the complementing CRISPR-resistant mAID-ORC2 could then be rapidly removed from cells, allowing exploration of the importance of ORC2 at different stages of cell division cycle (Natsume et al., 2016; Nishimura et al., 2009). To mediate the endogenous ORC2 knockout, four sgRNAs, hereafter named ORC2-1, ORC2-2, ORC2-3 and ORC2-4, were selected for on-target single guide validation. For complementation, N-terminally tagged mAID-sgRNA resistant ORC2 (mAID-ORC2^{gr}) was constructed, and the *ORC2* cDNA was edited to harbor multiple mismatches based on two of the four sgRNAs, ORC2-1 and ORC2-2 **(Figure 3-4d)**. To perform ORC2 depletion or genetic complementation, mAID-ORC2^{gr} constructs were transduced into two cell lines, TO-HCT116 cell line, which expresses a doxycycline-inducible *Oryza sativa* (Asian rice) *TIR1* (OsTIR1) gene that encodes a plant auxin-binding receptor that interacts with the conserved E3 ubiquitin ligase SCF complex to degrade mAID-tagged proteins and the U2OS cell line. In the dropout CRISPR/Cas9 experiment, cells expressing a positive control RPA3 sgRNA and all four ORC2 sgRNAs, but not the negative control Neg15 sgRNA (CSHL in-house negatives), showed depletion over 3 weeks of cell culture **(Figure 3-4e,f)**. The effects of ORC2-1 and ORC2-2 sgRNAs could be rescued by mAID-ORC2^{gr} in both TO-HCT116_mAID-ORC2^{gr} and U2OS_mAID-ORC2^{gr} cell lines confirming target specificity **(Figure 3-4g,h)**.

To acquire clonal cells to study ORC2 depletion phenotypes, TO-HCT116_mAID-ORC2^{gr} cells were depleted of the endogenous *ORC2* gene with sgRNA ORC2-1 and single clones were isolated by flow sorting. Five cell lines, ORC2_H-1, ORC2_H-2, ORC2_H-3, ORC2_H-4, and ORC2_H-5, were obtained from two independent CRISPR/Cas9 knockout

experiments done about 6 months apart. Sequencing of the target sites showed that the ORC2_H-1 and H-3 cell lines had heterozygous mutations at the sgRNA targeting site which led to premature stop codons downstream of the target site **(Figure 3-19a)**. On the other hand, the H-2, H-4, and H-5 cell lines were homozygous with an identical two-nucleotide-deletion, creating a nonsense mutation at the sgRNA targeting site. Although the ORC2-1 sgRNA targets the C-terminus of ORC2, no truncated form of protein was detected by western blot. Our ORC2 rabbit polyclonal antibody was raised against the N-terminal half of ORC2 protein. The LTR-driven mAID-ORC2^{gr} protein expressed at lower levels compared to endogenous ORC2 in TO-HCT116, RPE-1 and IMR90 cells, but was sufficient to complement the loss of endogenous ORC2 **(Figure 3-20a)**.

For further analysis of the effects of auxin-induced ORC2 depletion in cells, ORC2_H-2, H-4, and H-5 cell lines were used because of their genetically identical deletions at the CRISPR cut-site and because they showed efficient depletion of mAID-ORC2^{gr} after auxin treatment **(Figure 3-20)**. We excluded off-target effects by confirming the ORC2_H-2 cell line was resistant to both ORC2-1 and ORC2-2 sgRNAs, but not to the ORC2-3 and ORC2-4 sgRNAs **(Figure 3-19b)**. Compared with parental TO-HCT116 cell line, the human diploid cell RPE-1 expressed ~50% less ORC2, while IMR-90 cells expressed ~75% less **(Figure 3-20a)**. The relative levels of ORC3 reflect the levels of ORC2 since they are known to form a cognate complex throughout the cell cycle (Dhar et al., 2001; Jaremko et al., 2020; Vashee et al., 2001). ORC2_H-2, H-4, and H-5 cells had no detectable endogenous ORC2, and ORC3 showed stoichiometrically comparable expression to mAID-ORC2^{gr} levels **(Figure 3-20a)**. In addition, ORC2_H-2 cells expressed mAID-ORC2^{gr} at only about 5% that of endogenous ORC2 levels in TO-HCT116, while H-4 and H-5 cells expressed marginally more at about 10%. It is known that cancer cells can proliferate normally with 10% of the levels of ORC2 (Dhar et al., 2001).

Next, we compared the proliferation rates in these cell lines. In normal medium the ORC2_H-2, H-4, and H-5 cells grew slightly slower than the parental TO-HCT116 cells **(Figure 3-20b)**. When doxycycline was added to induce OsTIR1 expression, proliferation of all cell lines decreased by similar rates, possibly either due to some toxicity to doxycycline or the expression of OsTIR1 protein itself **(Figure 3-20c)**. It is important to note that auxin alone did not affect the

proliferation rate of wild type TO-HCT116, H-4, and H-5 cells, but it reduced the proliferation rate of H-2 cells substantially **(Figure 3-20d)**. This phenotype was probably caused by the leaky expression of Tet-OsTIR1 in ORC2_H-2 cells. Finally, when both doxycycline and auxin were added, all three ORC2 KO cell lines stopped proliferating entirely, whereas the parental TO-HCT116 cells continued to proliferate **(Figure 3-20e)**.

Concomitant with the lack of cell proliferation, we observed altered cell cycle profiles after mAID-ORC2^{gr} was depleted from these cells. Cells were treated with doxycycline and auxin to deplete mAID-ORC2^{gr} for 0 hr, 4 hr, 24 hr, and 50 hr. At the 50 hr time point, all three ORC2 KO cell lines had less cells progressing from G1 into S phase, and more cells accumulated in late S phase or the G2/M phase **(Figure 3-20f, Figure 3-21)**. Cells with a 4C DNA peak (late S/G2/M phase) continued to incorporate EdU, suggesting that DNA replication was not complete, even though the bulk of the genome was duplicated. This phenotype was consistent with previous observations that cells treated with *ORC2* siRNA arrested in interphase (70%) or as rounded, mitotic-like cells (30%) (Prasanth et al., 2004).

To analyze whether the cell cycle arrest was due to checkpoint activation in response to DNA damage, cell extracts were prepared from doxycycline and auxin treated cells and analyzed by immunoblotting for various DNA damage markers. CHK1 is essential for the DNA damage response and the G2/M checkpoint arrest and is primarily phosphorylated by ATR, although phosphorylation by ATM has also been reported (Gatei et al., 2003; Goto et al., 2019; Jackson et al., 2000; Liu et al., 2000; Wilsker et al., 2008). ORC3 and mAID-ORC2^{gr} proteins in ORC2_H-2, H-4, and H-5 cell lines were depleted following 4 hours of auxin treatment **(Figure 3-20g)**. A nonspecific smaller band was detected but this band did not co-immunoprecipitate with ORC3 **(Figure 3-21c)**. When no auxin was added, ORC1 levels in all four cell lines were similar, but the level gradually decreased after mAID-ORC2^{gr} depletion, which could be an effect of the phase in which cells ultimately arrest at the 50 hr time point **(Figure 3-22b)**. On the other hand, CDC6 protein level increased 1.3 to 1.7-fold in mutant cell lines at 0 hr time point, indicating cells might favor higher CDC6 level when ORC is low **(Figure 3-22c)**. Phosphorylation of ATM(S1981), ATR(T1989), and CHK1(S345) were detected in H-2, H-4, and H-5 cell lines after 50 hr of auxin treatment, but not in the parental TO-HCT116 **(Figure 3-20g, Figure 3-22a)**.

Higher levels of P-γH2AX(S139) in H-2, H-4, and H-5 cells were detected even when no auxin was added **(Figure 3-20g)**. This showed that although cells can divide with only 5-10 % of ORC2, a certain degree of replication stress exists. In our experiments, when parental and ORC2 mutant cells were treated with doxycycline and auxin, phospho-CHK2(T68) level increased slightly in all four cell lines, suggesting the phosphorylation could be associated with the drug treatment but not depletion of mAID-ORC2^{gr} itself. These observations were also supported by results from immunofluorescent staining of individual cells. When cells were treated with doxycycline and auxin for 48 hr, substantially more ATM(S1981) and CHK1(S345) phosphorylation were detected in all three ORC2 mutant cell lines **(Figure 3-20h, i, Figure 3-22d-e)**. In the absence of doxycycline and auxin, the P-γH2AX(S139) signal was more abundant in ORC2_H-2, H-4, and H-5 cells than in wild type **(Figure 3-22f)**. To conclude, insufficient ORC2 protein in cells resulted in abnormal DNA replication and DNA damage, and in response to DNA damage, CHK1 was activated and cells arrested in G2 phase.

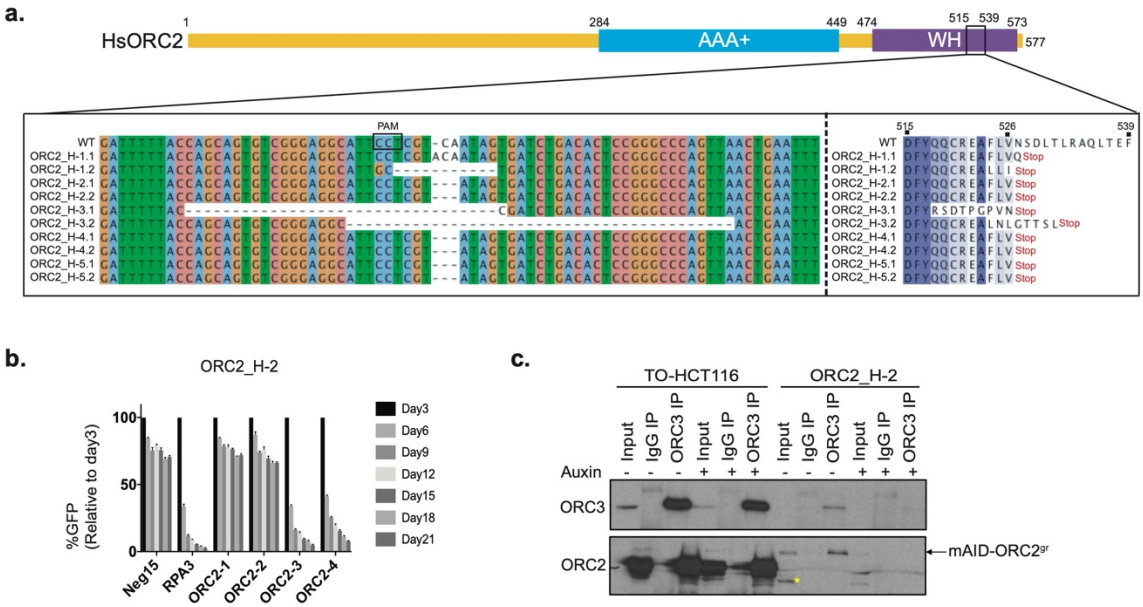

Figure 3-19. Validation of CRISPR/Cas9 knockout in ORC2_H-2 cell line. (a) Nucleotide and amino acid alignments near the ORC2-1 sgRNA targeting site in parental TO-HCT116 and five cloned ORC2 KO cell lines. (b) the ORC2_H-2 cell line is resistant to ORC2_1 and ORC2_2 sgRNAs. Negative-selection time course assays that plot the percentage of GFP positive cells over time following transduction with indicated sgRNAs/Cas9. The GFP positive percentage was normalized to Day3 measurement. N=3. Error bars, mean ± SD. (c) ORC3 immunoprecipitation in TO-HCT116 and ORC2_H-2 cell lines. Cell lysates were incubated with mouse IgG or ORC3 mouse monoclonal antibody for immunoprecipitation, followed by western blotting and detected with antibodies against ORC2 and ORC3. Input ~ 2.5% and IP ~ 30 % of total lysate. Asterisks (*) indicates the non-specific smaller band detected in ORC2_H-2 cell line.

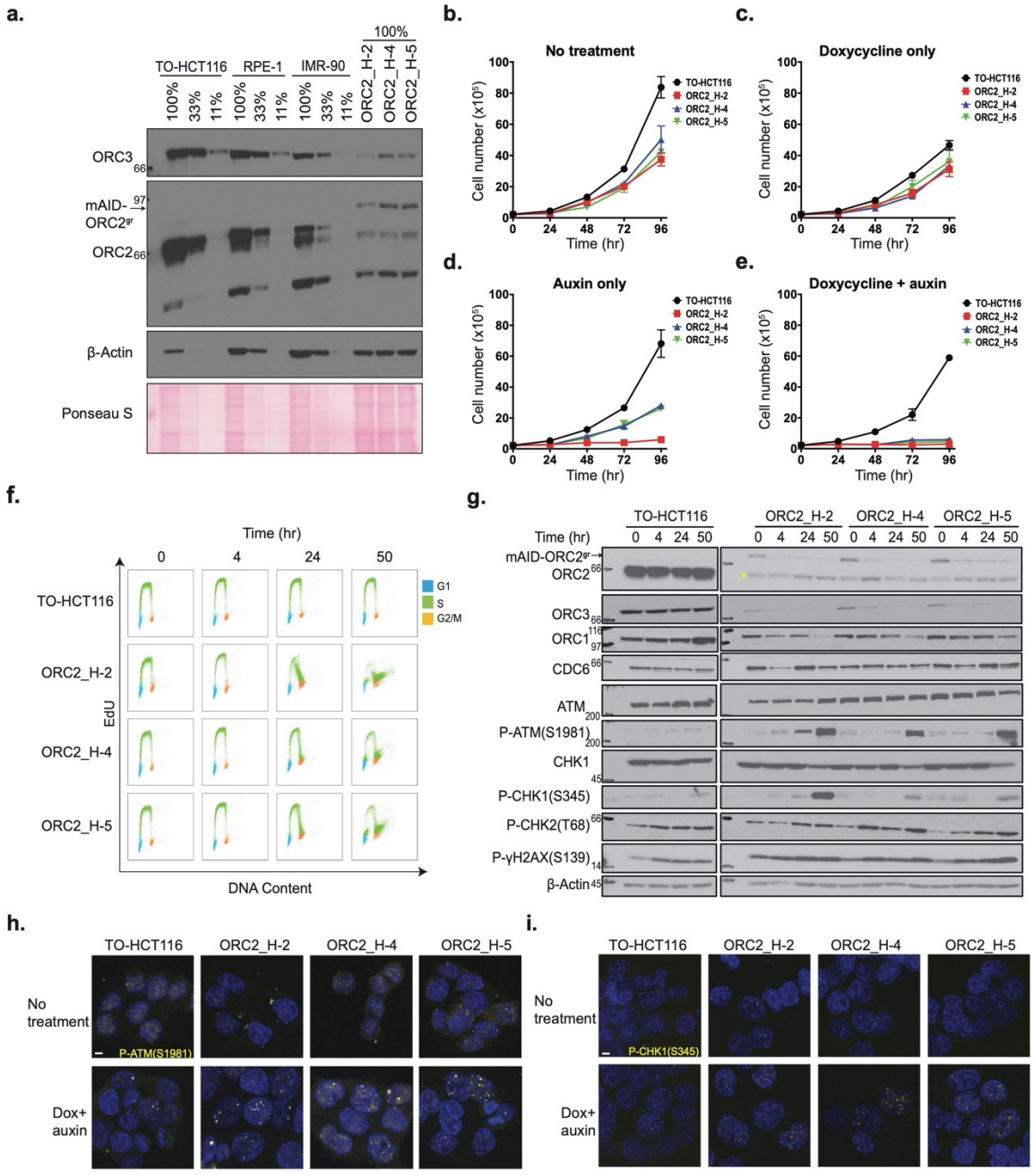
a.
TO-HCT116
RPE-1
IMR-90
100%
100%
33%
11%
ORC2_H-2
ORC2_H-4
ORC2_H-5
ORC3
mAID-ORC2
ORC2
β-Actin
Ponseau S
b.
No treatment
c.
Doxycycline only
d.
Auxin only
e.
Doxycycline + auxin
Cell number (x10⁵)
Time (hr)
f.
Time (hr)
TO-HCT116
ORC2_H-2
ORC2_H-4
ORC2_H-5
G1
S
G2/M
EdU
DNA Content
g.
Time (hr)
mAID-ORC2
ORC2
ORC3
ORC1
CDC6
ATM
P-ATM(S1981)
CHK1
P-CHK1(S345)
P-CHK2(T68)
P-γH2AX(S139)
β-Actin
h.
No treatment
Dox+ auxin
P-ATM(S1981)
i.
P-CHK1(S345)

Figure 3-20. Characterization of CRISPR/Cas9 ORC2 knockout and complementation with sgRNA resistant ORC2. (a) ORC2, mAID-ORC2^{gr}, and ORC3 protein levels in human TO-HCT116, RPE-1, human diploid IMR-90, and three ORC2 KO cell lines. (b-e) Growth curves of cell lines under (b) normal condition, (c) doxycycline only, (d) auxin only, and (e) dox+auxin containing media, respectively. The x axis indicates hours after addition of doxycycline or auxin if any. The y axis reflects the cell number (x10^5). n=3 (biological repeats). Error bars, mean ± SD. (f) Cell cycle analysis of TO-HCT116, ORC2_H-2, ORC2_H-4, and ORC2_H-5 cell lines following mAID-ORC2^{gr} depletion. Cells were treated with 0.75 μg/ml of doxycycline for 24 hours before auxin treatment. Cells were pulse labeled with 10 μM EdU for 2 hours before harvesting at 0, 4, 24, and 50 hr time points. The x axis indicates DNA content, and the y axis represents EdU incorporation. Color legend for cell cycle phases - G1-blue; S-green; G2/M-orange. >10,000 cells were analyzed per condition. (g) Protein expression profiles of mAID-ORC2^{gr}, ORC2, ORC1, ORC3, CDC6, ATM, p-ATM(S1981), CHK1, p-CHK1(S345), p-CHK2(T68), and p-γH2AX(S139) in four cell lines after dox and auxin treatment for 0, 4, 24, and 50 hr. Cells were treated with doxycycline for 24 hr prior to auxin treatment. Asterisks (*) indicates the non-specific band detected in mutant cell lines. Immunoblot of each protein was developed on the same film at the same time for comparison between all four cell lines. Quantification of ORC1 and CDC6 levels are shown in Figure 3-22b,c. (h) Immunofluorescence staining of p-ATM(S1981) in four cell lines with or without dox+auxin treatment. Quantification of p-ATM(S1981) foci is shown in Figure 3-22d. (i) Immunofluorescence staining of p-CHK1(S345) in four cell lines with or without dox+auxin treatment. For (h) and (i), dox+auxin treated cells were stained after incubation with doxycycline for 24 hr followed by addition of auxin for 48 hours. Quantification of p-CHK1(S345) foci is shown in Figure 3-22e. Scale bar indicated 4 μM.

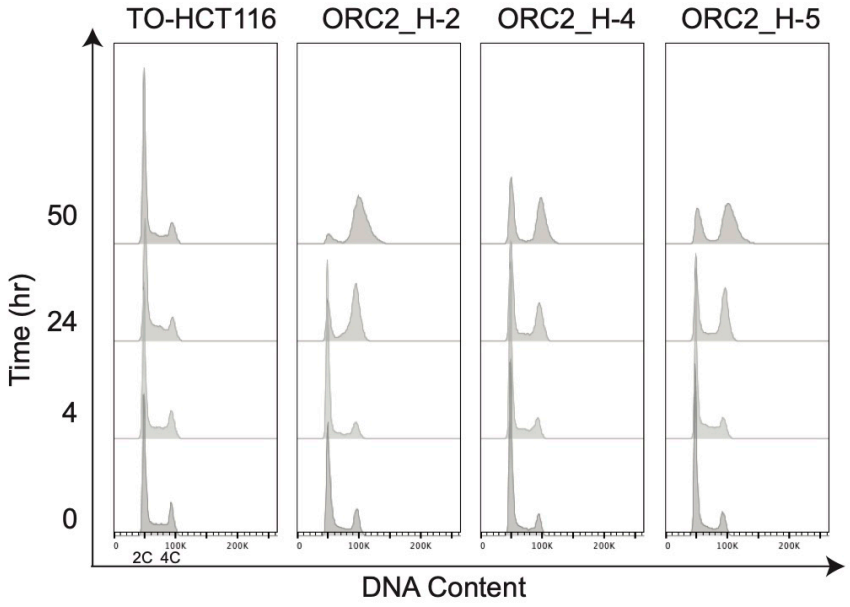

Figure 3-21. Cell cycle analysis after dox and auxin treatment in TO-HCT116, ORC2_H-2, ORC2_H-4, and ORC2_H-5 cell lines. Flow cytometry histogram plots with DNA content plotted on the x axis. Pseudo-Y axis represents time points (hr) following auxin treatment.

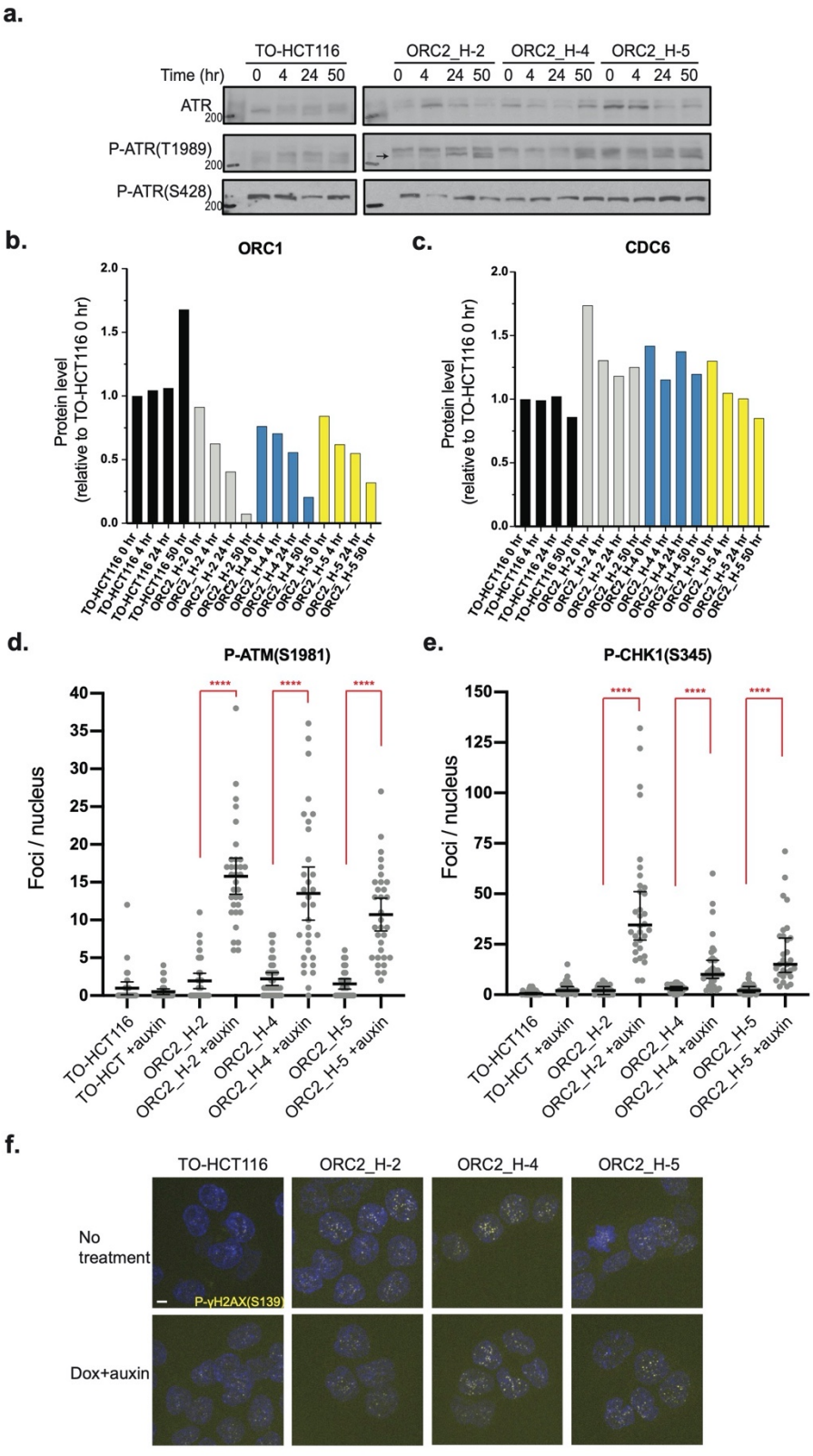
a.
TO-HCT116
ORC2_H-2
ORC2_H-4
ORC2_H-5
Time (hr)
0 4 24 50
ATR
P-ATR(T1989)
P-ATR(S428)
b.
ORC1
Protein level (relative to TO-HCT116 0 hr)
c.
CDC6
d.
P-ATM(S1981)
Foci / nucleus
e.
P-CHK1(S345)
TO-HCT116
TO-HCT +auxin
ORC2_H-2
ORC2_H-2 +auxin
ORC2_H-4
ORC2_H-4 +auxin
ORC2_H-5
ORC2_H-5 +auxin
f.
No treatment
Dox+auxin
P-γH2AX(S139)

Figure 3-22. DNA damage checkpoint is activated in auxin-treated ORC2_H-2, ORC2_H-4, and ORC2_H-5 cell lines. (a) ATR(T1989) was phosphorylated in ORC2_H-2, -4, -5 cell lines after dox and auxin treatment for 50 hr. There was no change in p-ATR(S428) level. (b) Relative ORC1 levels in four cell lines at different time points after auxin treatment. (c) Relative CDC6 level in four cell lines at different time points after auxin treatment. Protein levels in all cases were normalized to actin loading control and then compared to TO-HCT116 cells 0 hr time point. (d) Quantification of phospho-ATM(S1981) foci per nucleus in four cell lines in the absence or presence of dox and auxin. TO-HCT116, n=31; TO-HCT116 with dox+auxin, n=33; ORC2_H-2, n=33; ORC2_H-2 with dox+auxin, n=33; ORC2_H-4, n=34; ORC2_H-4 with dox+auxin, n=32; ORC2_H-5, n=30; ORC2_H-5 with dox+auxin, n=32. Statistical analysis was performed using unpaired t-test: **** $p<0.0001$. (e) Quantification of phospho-CHK1(S345) foci per nucleus in four cell lines either in the absence or presence of dox and auxin. TO-HCT116, n=30; TO-HCT116 with dox+auxin, n=34; ORC2_H-2, n=32; ORC2_H-2 with dox+auxin, n=32; ORC2_H-4, n=37; ORC2_H-4 with dox+auxin, n=32; ORC2_H-5, n=33; ORC2_H-5 with dox+auxin, n=30. Statistical analysis was performed using unpaired t-test: **** $p<0.0001$. (f) Phosphorylation of γH2AX(S139) was seen in ORC2_H-2, H-4, and H-5 cells either in the absence or presence of dox and auxin for 48 hrs.

2.3. Loss of ORC2 results in heterochromatin decompaction and abnormal nuclear morphology

The ORC2 depleted ORC2_H-2 and ORC2_H-5 cells had twice the nuclear volume following treatment with doxycycline and auxin for 48 hr **(Figure 3-23a-b)** compared to cells without treatment. The average volume of nuclei was greater than the volume of the largest parental cells, and thus the large nuclear phenotype could not be explained by their arrest in G2 phase with a 4C DNA content. However, since ORC2 depletion using siRNA decondenses centromere associated α-satellite DNA (Prasanth et al., 2010), this phenotype could be due to cells arrested in late S and G2 phase with decompacted heterochromatin. During interphase, ORC2 and ORC3 localize to the heterochromatin foci and interact with heterochromatin protein 1α (HP1α) through ORC3 (Pak et al., 1997; Pflumm and Botchan, 2001; Prasanth et al., 2004). To detect heterochromatin decompaction, immunofluorescent staining of the centromeric protein C (CENP-C) and heterochromatin protein 1 α (HP1α) was performed. In TO-HCT116 cells, CENP-C staining showed multiple, compact foci, but in the doxycycline and auxin treated cells that were dependent on mAID-ORC2^{gr}, CENP-C foci were larger and more prominent **(Figure 3-23c, Figure 3-24a-b)**. In doxycycline-treated control TO-HCT116, ORC2_H-2, and ORC2_H-5 cells, normal HP1α foci were observed and most of them localized adjacent to the CENP-C foci. However, in the doxycycline and auxin treated ORC2 mutant cells, HP1α foci were more decompacted, shown by an expanded pattern of staining rather than discrete foci found in the parental cells **(Figure 3-25a-f)**. This phenotype was observed in cells that also showed the large CENP-C foci phenotype. HP1α is involved in phase separation of heterochromatin (Larson et al., 2017; Strom et al., 2017), and removing ORC (ORC2 in this case) from the heterochromatin might affect the overall compaction. These HP1α fluorescence patterns were different from those previously observed when ORC was removed using an siRNA approach in HeLa cells (Prasanth et al., 2010, 2004). This difference is most likely because HeLa, being hyper tetraploid cells, have a different nuclear organization of HP1α compared to that found in HCT116 cells. HeLa cell HP1α foci are more intense and discrete and colocalize with CENP-C **(Figure 3-25g)**.

To understand if the heterochromatin decompaction phenotype was a direct outcome of the loss of ORC2, we synchronized cells using Palbociclib, a CDK4/6 inhibitor that arrests cells in G1 phase. TO-HCT116 and ORC2_H-2 cells were incubated with Palbociclib and doxycycline for 28 hr, with auxin added during the last 4.5 hr in G1 phase, then cells were harvested after a further 12 hr incubation **(Figure 3-26a)**. The second harvest time point was 40 hr after Palbociclib treatment and 16.5 hr after auxin treatment. The nuclear volume was determined, and we found that it remained unchanged in both cell types **(Figure 3-26b)**. CENP-C and HP1α staining was also unaffected (data not shown). Thus, loss of ORC2 in G1 phase did not induce nuclear chromatin decompaction. One possibility is that the absence of ORC2 during S phase affects sister chromatid cohesion loading (Zheng et al., 2018), which leads to decompaction of centromeric and heterochromatin regions in late S/G2 phase.

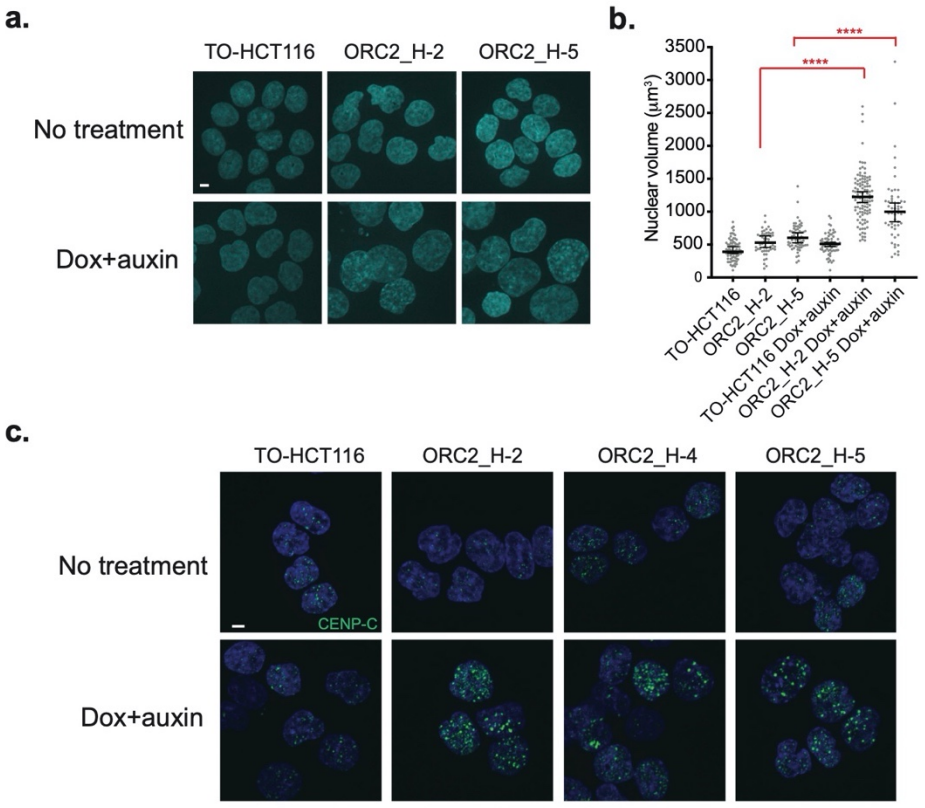

Figure 3-23. Auxin-treated ORC2_H2, H-4, and H-5 cells have abnormal nuclear phenotypes. (a) Nuclear morphology of TO-HCT116, ORC2_H-2 and H-5 cells after 48 hr of auxin treatment. Scale bar indicated 4 µM. (b) Scatter plot illustrating the nuclear volume after 48 hr of auxin treatment. Untreated: TO-HCT116, n=77; ORC2_H-2, n=52; ORC2_H-5, n=63. Dox and auxin treated: TO-HCT116, n=66; ORC2_H-2, n=110; ORC2_H-5, n=54. Error bars, medium ± 95% CI. Nuclear volume decreased significantly in both dox and auxin treated ORC2_H-2 and H-5 cells. Statistical analysis was performed using Student's t-test: **** $p<0.0001$. All singlets in each field captured have been measured, resulting in different but unbiased sample size selection. (c) Immunofluorescence staining of CENP-C after mAID-ORC2^{gr} depletion for 50 hr.

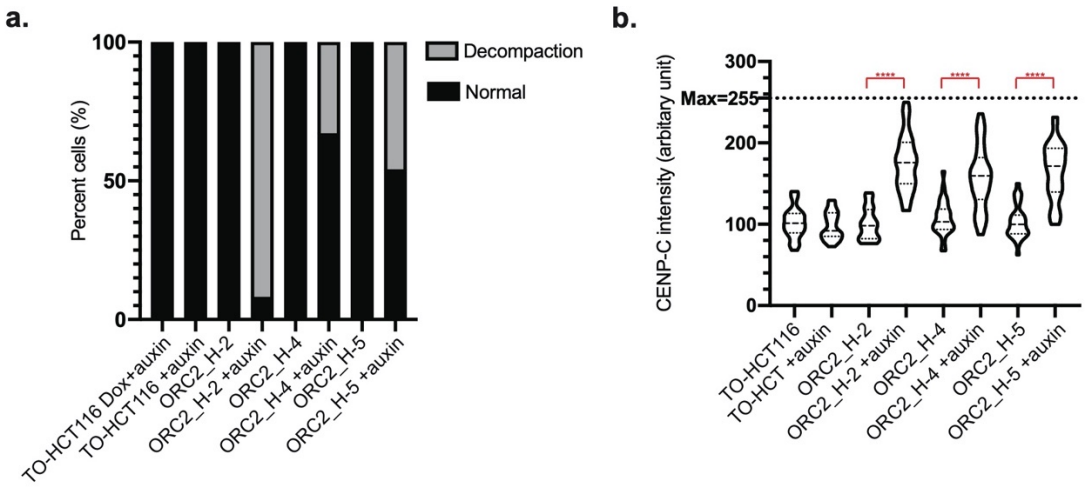

Figure 3-24. Quantification of CENP-C foci. (a) Quantitation of cells with large CENP-C foci in each experimental group. N=30 for all groups. (b) Violin plot illustrating CENP-C intensity per nucleus in four cell lines either in the absence or presence of dox and auxin. The y-axis represents mean intensity of CENP-C in each nucleus. Mean intensity of CENP-C foci per nucleus was calculated by averaging intensity of five foci in each nucleus by imageJ software. N=30 nuclei for all groups.

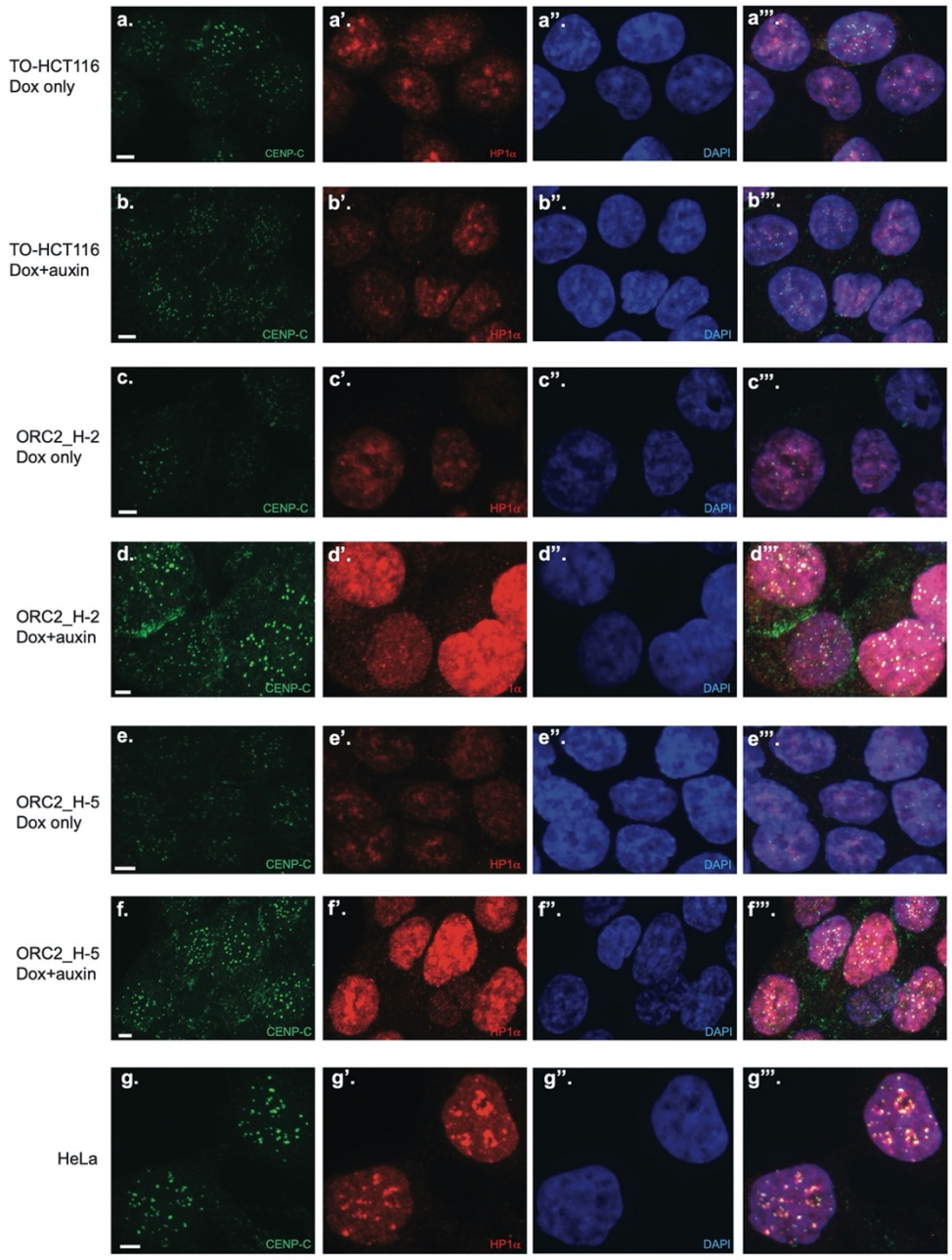

Figure 3-25. Centromeric foci and heterochromatin are decondensed in ORC2 depleted ORC2_H-2 and H-5 cells. Endogenous CENP-C and HP1α foci were detected by indirect immunofluorescence. Merged images include nuclear DAPI staining. Panels top to bottom: doxycycline-treated TO-HCT116 cells (a, a', a'', and a'''), dox+auxin treated TO-HCT116 cells (b, b', b'', and b'''), dox-treated ORC2_H-2 cells (c, c', c'', and c'''), dox+auxin treated ORC2_H-2 cells (d, d', d'', and d'''), dox-treated ORC2_H-5 cells (e, e', e'', and e'''), dox+auxin treated ORC2_H-5 cells (f, f', f'', and f'''), and untreated HeLa cells (g, g', g'', and g'''). For dox+auxin groups, cells were treated with dox for 24 hr followed by addition of auxin for another 48 hr before harvest. All Scale bars indicate 4 μM.

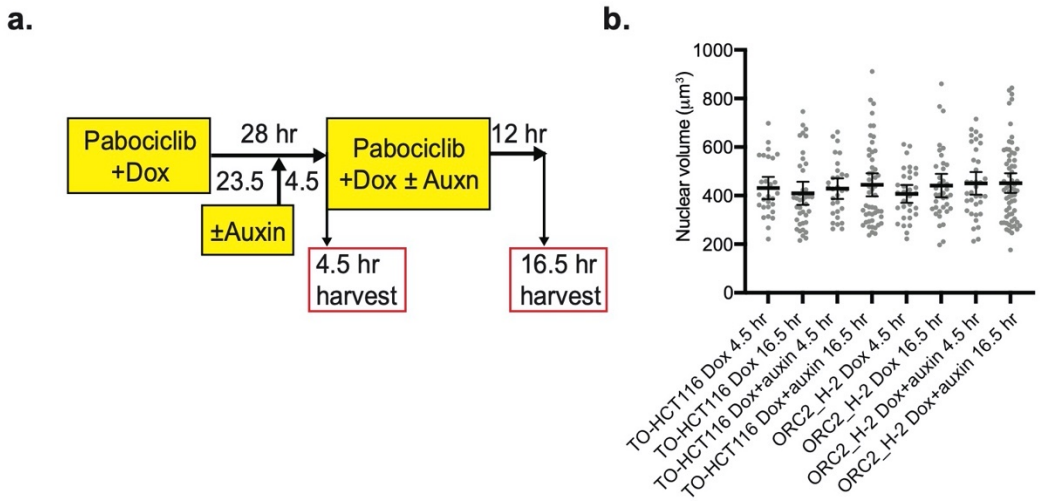

Figure 3-26. Palbociclib synchronization of TO-HCT116 and ORC2_H-2 cell lines. (a) Experimental scheme of TO-HCT116 and ORC2_H-2 cells synchronization by a Palbociclib block. (b) Scatter plot illustrating the nuclear volume after incubating cells in Palbociclib with doxycycline and different times of auxin treatment, in TO-HCT116 and ORC2_H-2 cell lines. For TO-HCT116 cells, Dox 4.5 hr, n=28; Dox 16.5 hr, n=39; Dox+auxin 4.5 hr, n=30; Dox+auxin 16.5 hr, n=50. For ORC2_H-2 cells, Dox 4.5 hr, n=32; Dox 16.5 hr, n=37; Dox+auxin 4.5 hr, n=36; Dox+auxin 16.5 hr, n=63. Error bars, median ± 95% CI. All singlets in each field captured have been measured, resulting in different but unbiased sample size selection.

2.4. ORC2 is essential for initiation of DNA replication

When cells were treated with siRNA against *ORC2* for 72 hours, 30% of the cells arrested in a mitosis-like state (Prasanth et al., 2004). This observation led to the conclusion that ORC2 is not only required for the initiation of DNA replication, but also during mitosis. To examine the role of ORC2 in G1 and mitosis following acute depletion, TO-HCT116 and the ORC2_H-2 cells were synchronized at the G1-early S phase boundary with a 2C DNA content by a double thymidine block, with doxycycline being added during the second thymidine block. Where indicated, auxin was added 4.5 hours before the release from the second thymidine block **(Figure 3-27a)**. Synchronized cells were then released and allowed to progress through two cell division cycles. Cells were pulse labeled with EdU for two hours and harvested at several timepoints after release. The mAID-ORC2^{gr} protein was depleted upon release from second thymidine block, and the depletion persisted until the final collection at 48 hr in the auxin-treated ORC2_H-2 cells **(Figure 3-28a, lane 23-28)**.

During the first cell cycle following release into S phase, no obvious change in DNA content and EdU labeling was observed in both cell lines, irrespective of whether or not they were treated with doxycycline and auxin **(Figure 3-27b-c; Figure 3-28b)**. During the second cell cycle however, doxycycline and auxin-treated TO-HCT116 cells progressed through S phase only slightly slower than the untreated cells. By contrast, starting from the second cell cycle, serious defects were observed in ORC2_H-2 auxin-treated cells compared to untreated cells **(Figure 3-27b-c)**. First, auxin treated ORC2_H-2 cells exhibited a very slow S phase, indicating that cells were struggling to completely replicate their DNA. Second, cells arrested with a 4C DNA content, which could either be late S or G2/M phase. Third, after 48 hours following release from the double thymidine block, some cells arrested in G1 phase and could not enter S phase. We suggest that in the first cell cycle, although mAID-ORC2^{gr} was depleted just before release, the pre-RCs were already formed and the cells were primed to replicate the complete genome. However, starting from the second cell cycle, since ORC2 was entirely lost from cells following cell cycle progression through the previous S, G2 and M phase, the cells began to accrue cell cycle defects. Most ORC2 depleted cells then either arrested in G1 or went through an incomplete S phase and arrested at the G2/M phase, but did not progress further. This

experiment indicated ORC2 primarily functions in establishing DNA replication initiation, but based on the results thus far, we could not conclude a role during mitosis because in the first cycle ORC2 depleted cells with a 4C DNA content, progressed through G2/M phase and cell division into the next G1.

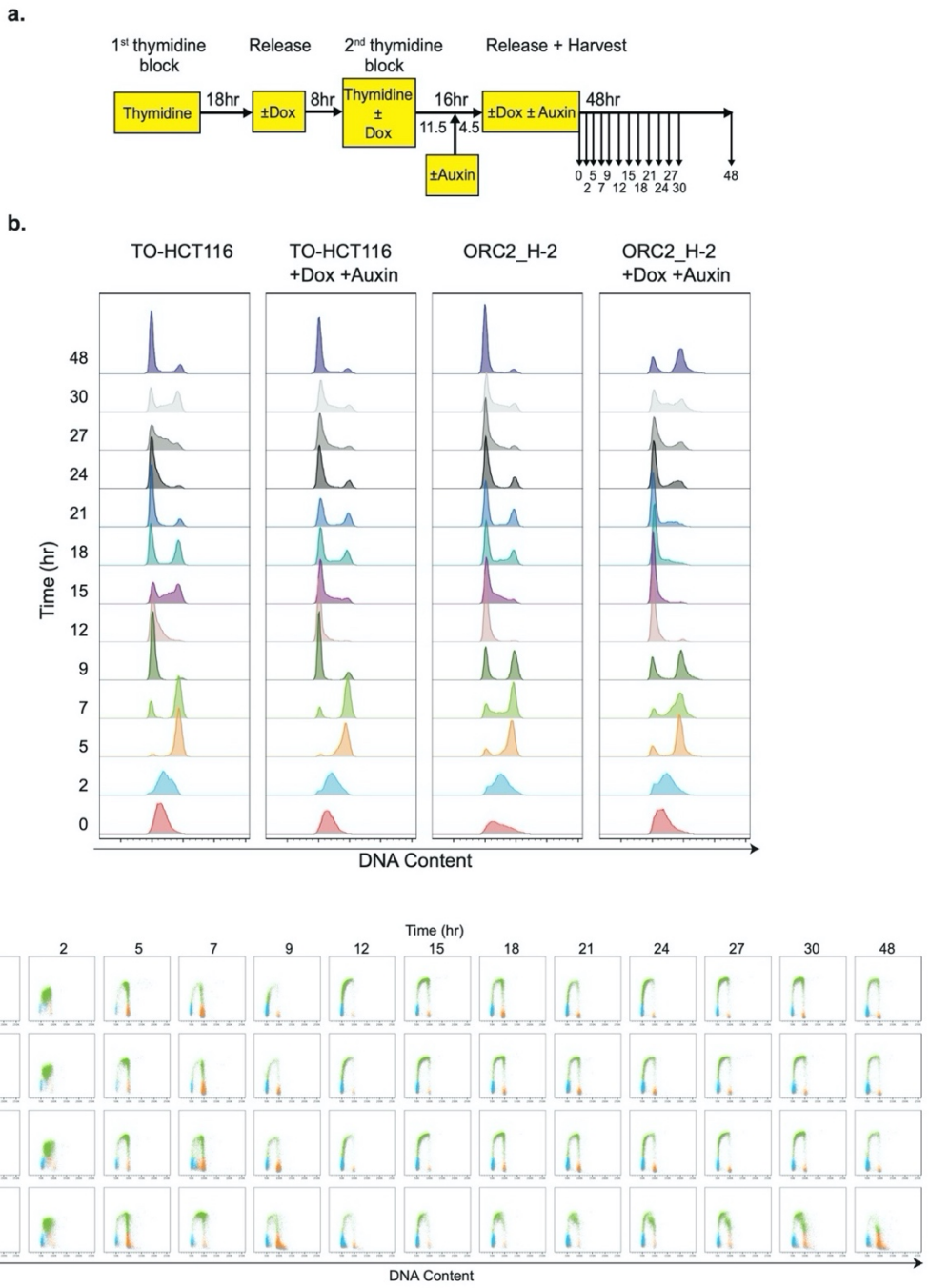

Figure 3-27. ORC2_H-2 cells show abnormal cell cycle progression after mAID-ORC2^{gr} depletion. (a) Experimental scheme of TO-HCT116 and ORC2_H-2 cells synchronization by a double thymidine block. (b) Flow cytometry analysis of FxCycle™ Violet stained cells (singlets) released from double thymidine block in indicated treatment. (c) Cell cycle profiles of TO-HCT116 and ORC2_H-2 cells released from a double thymidine block in indicated treatment. Cells were pulse labeled with 10μM EdU for 2 hours before harvesting at different time points. X axis indicates DNA content, and y axis represents to EdU incorporation. Color legend for overlay plots of cell cycle phases - G1-blue; S-green; G2/M-orange.

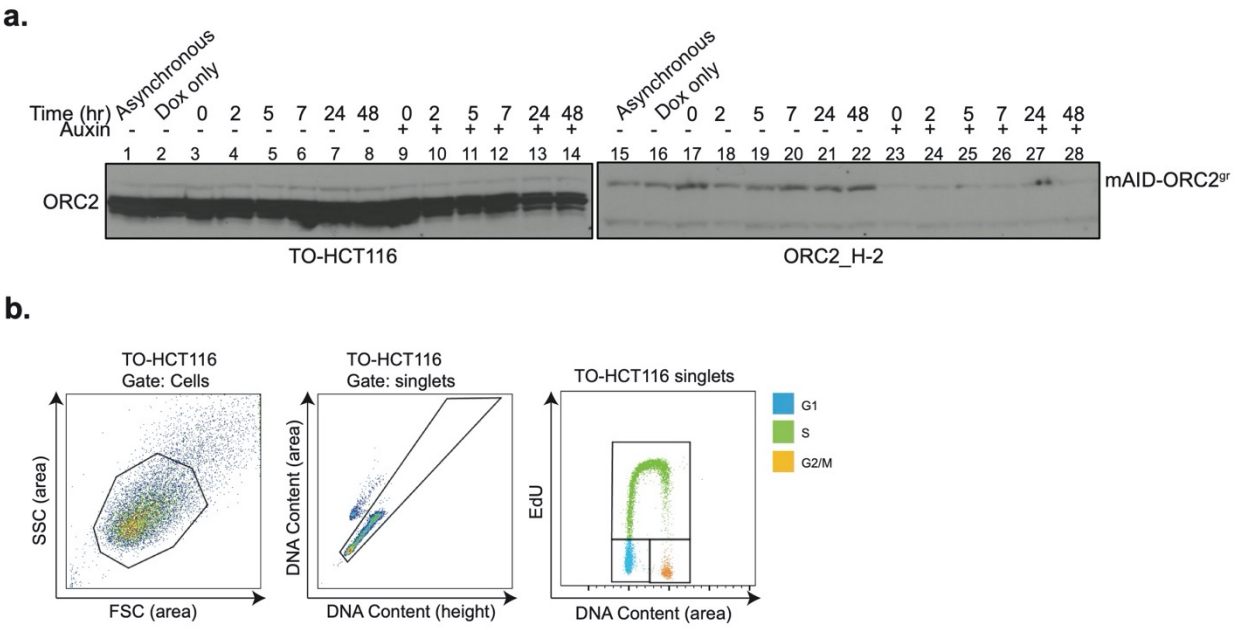

Figure 3-28. Double thymidine block and release in TO-HCT116 and ORC2_H-2 cell lines. (a) ORC2 and mAID-ORC2^{gr} protein levels in TO-HCT116 and ORC2_H-2 cells in double thymidine block and release experiments. Both blots were run and developed at the same time. (b) Flow cytometry gating strategy for Figure 3-27b and c. FSC (area) vs SSC (area) was used to exclude the cell debris and gate for cell-type population. Singlets gated on FxCycle™ Violet (DNA content) height vs area. Cell population in G1, S, and G2/M phase were gated on the FxCycle™ Violet (DNA content) area vs EdU plots.

2.5 An MCM complex loading and pre-RC assembly defect in ORC2 depleted cells

The auxin-treated, mAID-ORC2^{gr} depleted cells could not replicate normally, possibly due to insufficient ORC to form the pre-RC. To test this hypothesis, the chromatin-bound MCM2-7 was measured in asynchronous cells by flow cytometry following extraction by detergents as described previously (Matson et al., 2017). Asynchronous TO-HCT116, ORC2_H-2, and H-5 cells, with or without doxycycline and auxin treatment, were pulse-labeled with EdU, harvested and stained with anti-MCM2 antibody and DNA dye. In normal medium and without detergent extraction, nearly 100% of the cells were positive for MCM2 in all three cell lines **(Figure 3-29)**. When extracted with detergent, about 78 % of TO-HCT116, 65.2 % of ORC2_H-2, and 76.9 % of ORC2_H-5 cells were positive for MCM2. Chromatin-bound MCM2 level was not affected in untreated or doxycycline treated TO-HCT116 and ORC2 mutant cells **(Figure 3-30a)**. When treated with both doxycycline and auxin for 20 hr, chromatin-bound MCM2 levels decreased significantly in mutant cells, especially in the ORC2-H-2 cell line **(Figure 3-29a,c, Figure 3-30a)**. Focusing on the G1 population, 93.7 % of TO-HCT116 cells, 80.4 % of ORC2_H-2 cells, and 89.3 % of ORC2_H-5 cells were positive for MCM2 **(Figure 3-30b)** in untreated cells. When doxycycline was added, MCM2 level in ORC2 H-2 cells dropped slightly to 62.2 %, while the other two cell lines remained at similar level, 96.8 % in TO-HCT116 and 82.5 % in ORC2_H-5 cells. When treated with both doxycycline and auxin, 97.5 % of TO-HCT116 G1 phase cells stained for chromatin-bound MCM2, but this decreased to only 4.6 % and 22.4 % cells in ORC2_H-2 and ORC2_H-5 G1 phase cells, respectively. Importantly, the doxycycline and auxin treated ORC2_H-2 and ORC2 H-5 G1 phase cells had very low levels of MCM2 compared to the MCM2 levels in cells that did not receive auxin **(Figure 3-30b)**. The different degrees of reduction in MCM2 loading between doxycycline and auxin treated H-2 and H-5 cells reflected the relative levels of mAID-ORC2^{gr}. Therefore, ORC2 depletion prevented MCM2 loading onto G1 phase chromatin.

We also analyzed chromatin-bound MCM2 levels in TO-HCT116, ORC2_H-2, and ORC2_H-5 cells following a double thymidine block and release experiment **(Figure 3-31a)**. Flow cytometry analysis showed that at the 0 hr time point with cells arrested at the G1-early S boundary, the percentage of cells with chromatin-bound MCM2 were unchanged, whether or not

doxycycline or auxin was added. At 12 hr time point, with the cell cycle mostly back at G1 phase again, cells with chromatin-bound MCM2 level decreased significantly in doxycycline and auxin treated ORC2_H-2 and ORC2_H-5 cells **(Figure 3-31)**. This result also confirmed that since pre-RCs were already formed during the double thymidine block, ORC2 depletion did not have an effect, but new pre-RCs could not form in the next cell cycle.

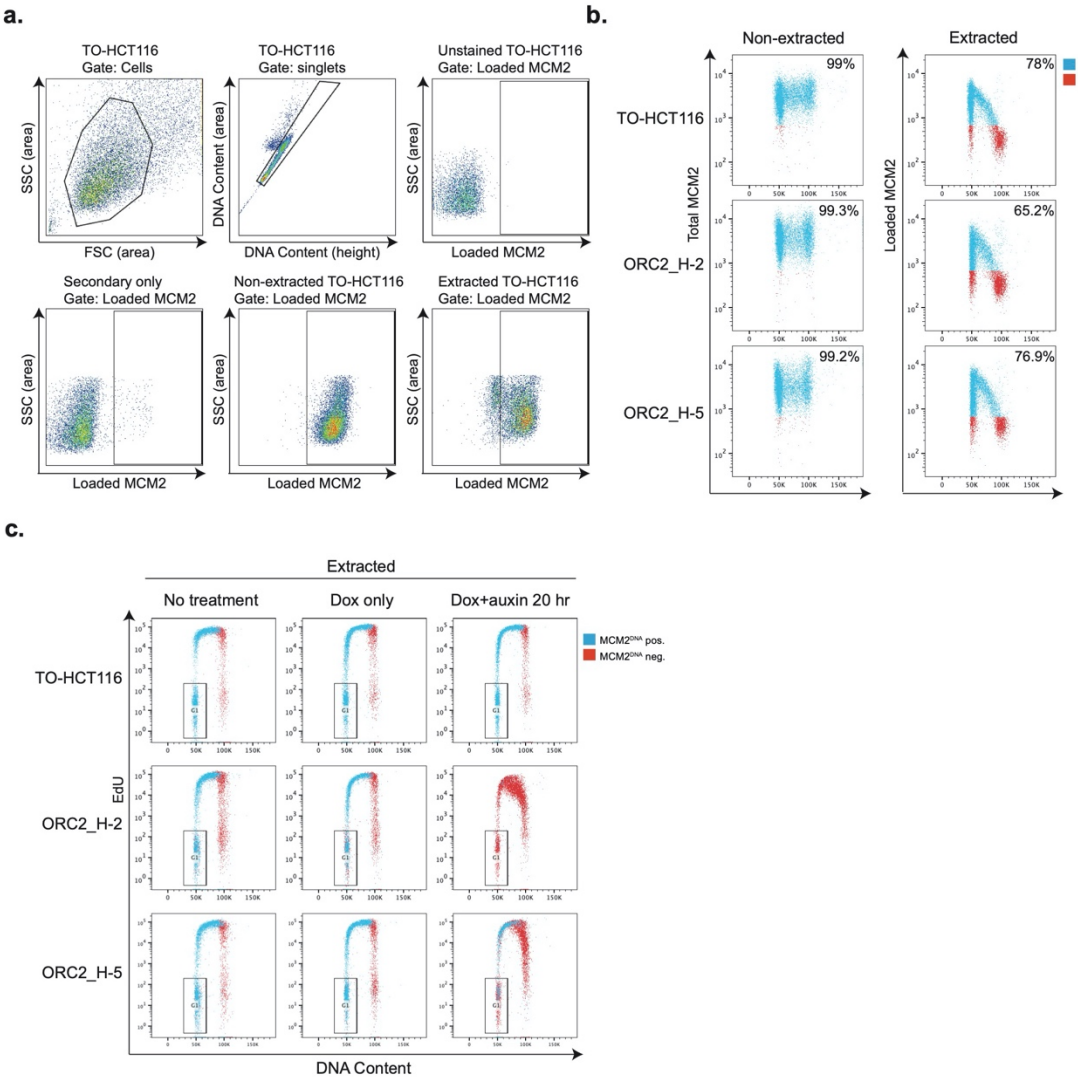

Figure 3-29. (a) Flow cytometry gating strategy for Figure 3-30. FSC (area) vs SSC (area) gating was used to exclude the cell debris and gate for cell-type population. Singlets were gated on FxCycle™ Violet (DNA content) height vs area. MCM2 positive population was gated on the loaded MCM2 (area) vs SSC (area) of the unstained negative control. Cells stained for secondary Donkey anti-Mouse Alexa Fluor 647 antibody only showed minimum background for loaded MCM2. (b) Flow cytometry analysis of DNA-bound MCM2 and total MCM2 in asynchronous cells. Extracted: Cells were treated with nonionic detergent to wash off unbound MCM2 before fixation, and then stained with anti-MCM2 antibody and Alexa Fluor 647-conjugated secondary antibody. Non-extracted: Cells were fixed right after harvest and stained with for MCM2 as before. Blue cells are MCM2 positive, and red cells are MCM2 negative. The x axis indicates DNA content, and the y axis refers to MCM2 level. Numbers at the upper right corner indicates percentage of MCM2 positive population. (c) Flow cytometry measuring DNA content, EdU incorporation, and DNA-bound MCM2 in asynchronous cells in different condition. Cells were pulse labeled with 10 μM EdU for 2 hours before harvesting. The x axis indicates DNA content, and the y axis refers to EdU incorporation. MCM2 positive and negative cells are shown as blue and red respectively. Gated area represents G1 phase cells for Fig 3-30.

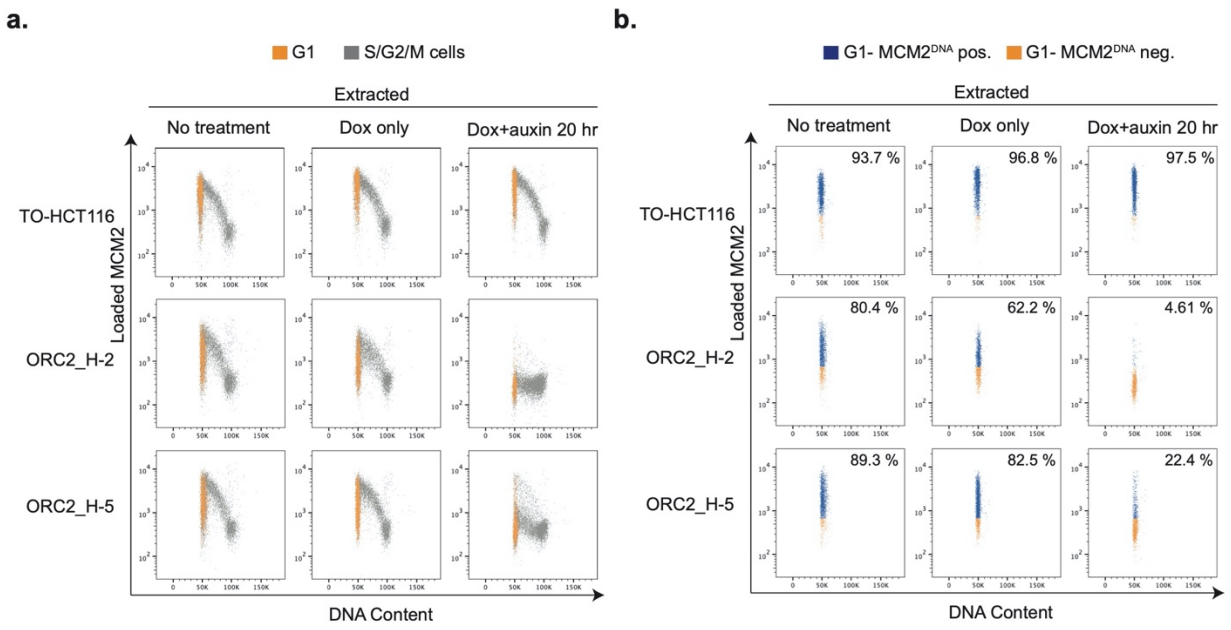

Figure 3-30. Depletion of mAID-ORC2^{gr} in ORC2_H-2 and H-5 cells results in decreased DNA-loaded MCM. (a) Flow cytometry analysis of DNA content and chromatin-bound MCM2 in asynchronous TO-HCT116, ORC2_H-2, and ORC2_H-5 cells in different conditions. The x axis indicates DNA content, and the y axis represents cells positive for chromatin-bound MCM2 as a function of its fluorescence intensity. G1 population (gated from DNA content vs EdU plot (Figure 3-29c) is shown in orange. The rest of the cells in S/G2/M phase are shown in grey. (b) Only G1 cell populations from (a) are shown here, with DNA-bound MCM2 positive cells colored in blue and negative cells in orange. Numbers at the upper right corner indicates percentage of MCM2 positive cells. The x axis indicates DNA content, and the y axis represents cells positive for chromatin-bound MCM2 as a function of its fluorescence intensity.

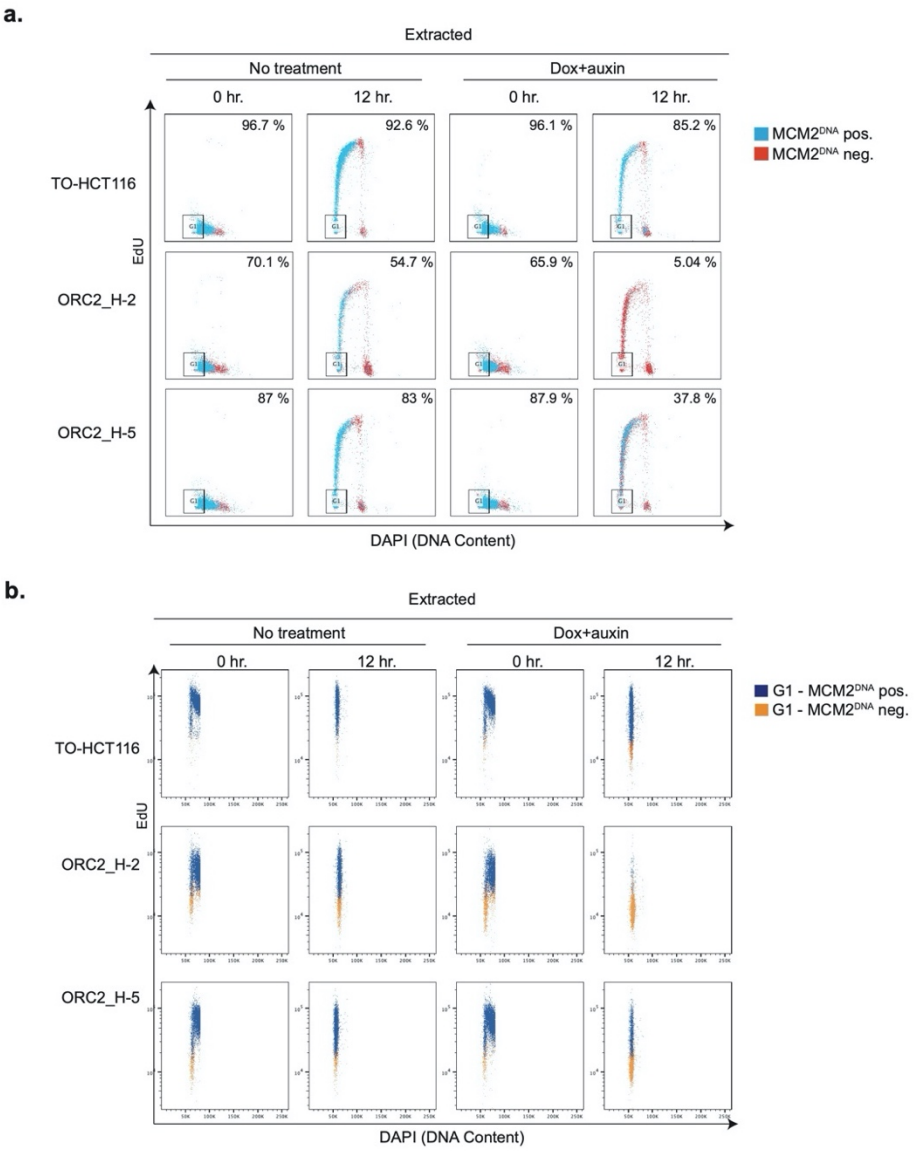

Figure 3-31. Chromatin-loaded MCM2 decrease after mAID-ORC2^{gr} depletion. The cells were synchronized with a double thymidine block and released as described in Fig 5a, and we harvested cells at 0 hr and 12 hr timepoints after release in the condition of no treatment or Dox+auxin. Cells were pulse-labeled with EdU for 2 hr before harvest. The 12 hr time point is the start of the second cell cycle after release as shown in Fig 5b. Cell cycle profiles and chromatin-loaded MCM2 were then measured the same way as described in Fig 6. (a) Flow cytometry measuring DNA content, EdU incorporation, and chromatin-bound MCM2 at 0 hr and 12 hr timepoints in either auxin-treated or non-treated TO-HCT116, ORC2_H-2, and ORC2_H-5 cells. The x axis indicates DNA content, and the y axis refers to EdU incorporation. MCM2 positive and negative cells are shown as blue and red respectively. Numbers at the upper right corner indicates percentage of MCM2 positive population. (b) G1 cell population (orange) gated from (a) is shown here, with chromatin-bound MCM2 positive cells colored in blue and negative cells in orange. The x axis indicates DNA content, and the y axis refers to MCM2 level.

2.6. ORC2 depletion in cells leads to aberrant mitosis

In order to know if the mAID-ORC2^{gr} depleted ORC2_H-2 cells entered mitosis, we evaluated the mitotic index by staining cells for phospho-Histone H3(S10) (pH3S10) followed by flow cytometry analysis **(Figure 3-32a; Figure 3-33,** n=3 biological repeats**)**. In the untreated asynchronous population, about 4.53 ± 0.59 % and 1.57 ± 0.33 % were pH3S10-positive in TO-HCT116 and ORC2_H-2 cells respectively, while 31.4 ± 2.88 % of TO-HCT116 cells and 15.6 ± 1.25 % of ORC2_H-2 cells were at G2/M. When only doxycycline was added, there was no significant change. When treated with doxycycline and auxin for 28 hr, the pH3S10-positive cell population percentage was about 2.39± 0.26 in TO-HCT116 and only 0.79 ± 0.09 in ORC2_H-2, while 17.23 ± 0.78 % of TO-HCT116 cells and 36.7 ± 1.61 % of ORC2_H-2 cells were at G2/M. After 50 hr of doxycycline and auxin treatment, the pH3S10-positive cell population percentage was 3.95 ± 0.16 in TO-HCT116 and only 0.96 ± 0.15 in ORC2_H-2, while 20.77 ± 1.76 % of TO-HCT116 cells and 79.57 ± 1.2 % of ORC2_H-2 cells were at G2/M phase. In normal medium condition, TO-HCT116 already had 2.9 times as many mitotic cells as ORC2_H-2. When treated with doxycycline and auxin, although the G2/M population increased 2.3-fold and 5-fold at 28 hr and 50 hr, respectively, the number of mitotic cells in ORC2_H-2 reduced by 50 – 80 % compared to the non-treated H-2 cells. This showed that most ORC2_H-2 cells that accumulated at the 4C DNA peak after ORC2 depletion were indeed stuck in the G2 stage and did not enter into mitosis.

Nevertheless, mitosis did occur at a very low frequency. To observe mitotic phenotypes and mitotic progression following ORC2 depletion, we constitutively expressed H2B-mCherry in TO-HCT116 and ORC2_H-2 cells via lentiviral transduction and performed time lapse fluorescent imaging of the mitotic chromosomes. Cells were synchronized using a single thymidine block and auxin was added or omitted 2 hr before releasing into fresh medium with or without doxycycline and auxin. As expected, in either treated or untreated TO-HCT116 cells, the first cell cycle after release from the thymidine block was normal and cells progressed through mitosis into the second cell cycle (data not shown). During the second cell cycle, in the absence or presence of doxycycline and auxin, it took TO-HCT116 cells about 35-50 min to progress from early prophase to chromosome segregation **(Figure 3-32b and c,** n=10 for each**)**. In the

absence of doxycycline and auxin, ORC2_H-2 cells also progressed through mitosis like the parental cells **(Figure 3-32d,** n=10**)**. In stark contrast, in presence of doxycycline and auxin ORC2_H-2 cells showed condensed chromatin and attempted to congress chromosomes at the metaphase plate but never achieved correct metaphase alignment of chromosomes even after six to thirteen hours **(Figure 3-32e,** n=5**)**. Those few cells that did attempt anaphase had abnormal chromosome segregation, producing lagging chromosomes, micronuclei and became apoptotic.

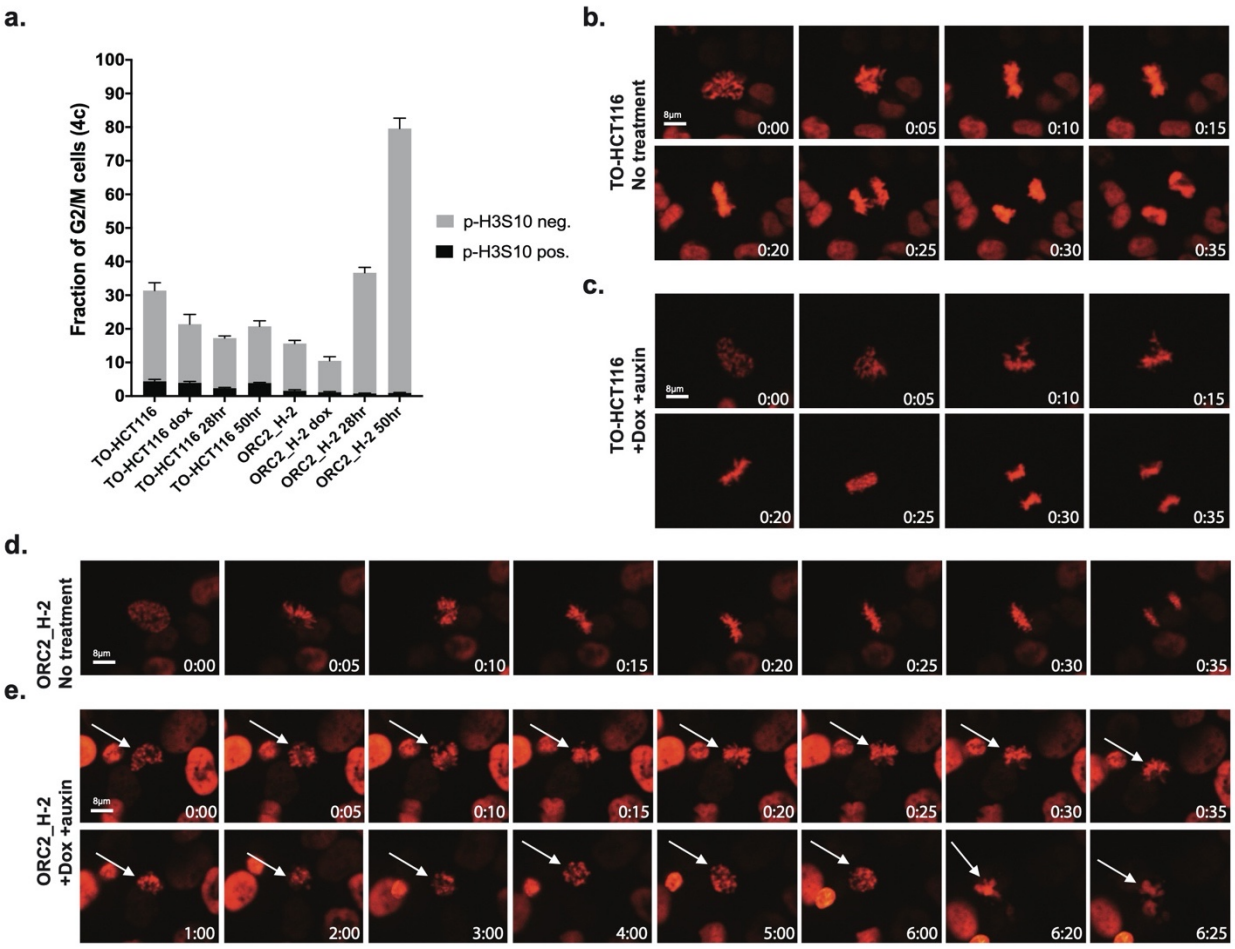

Figure 3-32. ORC2_H-2 cells have aberrant mitosis after auxin treatment. (a) Mitotic index of TO-HCT116 and ORC2_H-2 G2/M cells with or without auxin. 0.75 μg/ml Doxycycline were added for 24 hr before auxin treatment. Cells were harvested after 0, 28, or 50 hr of auxin treatment followed by staining with anti-pH3S10 antibody for mitotic cells and FxCycle™ Violet for DNA content. Histograms on x axis represent each cell line under different conditions, including no treatment, doxycycline only, dox+auxin for 28 hr, and dox+auxin for 50 hr. The y axis is the fraction of 4C G2/M cells. Cell population positive or negative for p-H3S10 were shown as black or grey color respectively. n=3 (biological repeats). (b-e) Time lapse imaging of TO-HCT116 and ORC2_H-2 cell lines following a single thymidine block (± dox) and release into the second cell cycle (i.e., > 30 hr following release). Time shown in lower left corner indicates time (hr : min) since early prophase. (b) Images of TO-HCT116 cells without auxin. (c) Auxin treated TO-HCT116 cells. (d) ORC2_H-2 cells without auxin. (e) Dox and auxin treated ORC2_H-2 cells. White arrows in (e) point to the same cell. Scale bars indicate 8 μM.

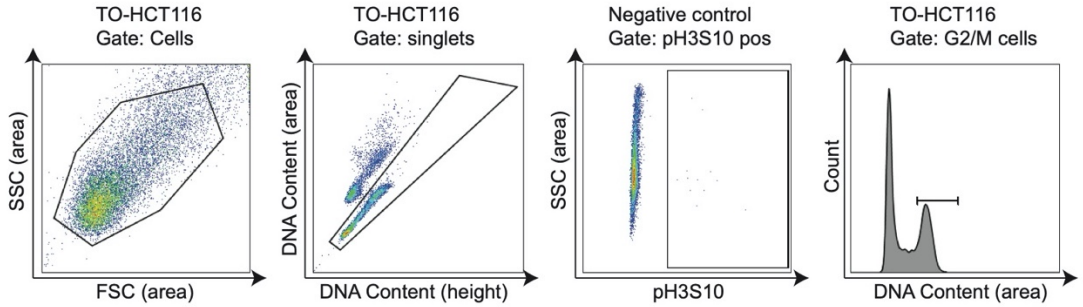

Figure 3-33. Flow cytometry gating strategy for Figure 3-32a. FSC (area) vs SSC (area) gating was used to exclude the cell debris and gate for cell-type population. Next, singlets were gated on FxCycle™ Violet (DNA content) height vs area. Phospho-H3S10 positive population was gated on pH3S10 Alexa Fluor 647 (area) vs SSC (area) of the unstained negative control cells. G2/M cell population was gated on the DNA content (area) histogram.

2.7. Characterization of previously published *ORC1*$^{-/-}$ and *ORC2*$^{-/-}$ cell lines

The results so far confirm previous observations that ORC is essential for cell proliferation in differentiated human cells, but there remained the curious case of previously reported viable knockout of *ORC1* and *ORC2* genes in p53$^{-/-}$ HCT116 cells (Shibata et al., 2016). We obtained the *ORC1*$^{-/-}$ (B14 clone) and *ORC2*$^{-/-}$ (P44 clone) cell lines described in this study as a gift from Dr. Anindya Datta and performed several experiments on them. Using the ORC2 validated sgRNAs (different target site from Shibata et al.), we first tested if the *ORC2*$^{-/-}$ cell line was sensitivity to the four *ORC2* sgRNAs we used in our study **(Figure 3-4)**. The negative-selection GFP depletion assay surprisingly showed that both the parental HCT116 *p53*$^{-/-}$ and the *ORC2*$^{-/-}$ cell line were both sensitive to CRISPR/Cas9 knockout of *ORC2* compared to control sgRNA **(Figure 3-34a-b)**. More importantly, when both cell lines were transduced to express mAID-ORC2^{gr} that was resistant to the ORC2-1 and ORC2-2 sgRNAs, this effect was rescued in HCT116 *p53*$^{-/-}$ and to a slightly lesser extent in *ORC2*$^{-/-}$ cell line **(Figure 3-34c-d)**. This suggested that there may be some form of functional ORC2 in the *ORC2*$^{-/-}$ cells that was being targeted by the tested sgRNAs. In addition, an immunoblot of the cell lysates showed a reduced level of ORC3 in the *ORC2*$^{-/-}$ cells **(Figure 3-35a)**, and since ORC2 and ORC3 form stable heterodimers in cells, this result again indicated that some form of ORC2 was expressed in cells, albeit at a lower level. When immunoprecipitated with an antibody against ORC3, we detected ORC3 and a putative truncated form of ORC2 which was seen only in *ORC2*$^{-/-}$ cells **(Figure 3-35b)**. Next, we designed primer pairs that span exon junctions for each exon in *ORC2* and performed quantitative RT-PCR (qPCR) to determine the nature of the *ORC2* transcripts in the *ORC2*$^{-/-}$ cells **(Figure 3-34e)**. The calculated fold change (FC) indicated that in the *ORC2*$^{-/-}$ cells, about 60% of the mRNAs had exon 7 skipped, whereas other exons remained the same **(Figure 3-34e, Figure 3-36)**.

We further speculated that these cell lines, in the absence of or mutations within either *ORC1* or *ORC2* may exhibit genomic instability giving rise to copy number variations (CNVs). To determine the CNV status we performed SMASH (Wang et al., 2016) analysis on the two parental HCT116 cell lines with the *p53*$^{+/+}$ and *p53*$^{-/-}$ background as well as the Shibata et al. *ORC1*$^{-/-}$ and *ORC2*$^{-/-}$ deficient lines. Both the parental cell lines showed very similar

chromosome copy number, characteristic of HCT116, while both *ORC1* deficient and *ORC2* deficient cell lines had additional CNVs in chromosomes unrelated to those harboring either *ORC1* or *ORC2* **(Figure 3-37)**. The significance of these specific loci which showed alterations in copy number when either *ORC1* or *ORC2* was deleted remains to be investigated. However, it was in this analysis that we noticed that in *ORC2*$^{-/-}$ cells a part of the *ORC2* gene locus that was hugely amplified **(Figure 3-37 solid arrow)**. To study in detail the *ORC2* gene region on chromosome 2 in these cells, we performed long-read Oxford Nanopore sequencing analysis. Compared to the reference allele sequence, *ORC2*$^{-/-}$ cells showed highly mutated and heterogenous allele distribution near the CRISPR targeting site used in the Shibata et al. study **(Figure 3-34f, Figure 3-38)**. In addition, this *ORC2*$^{-/-}$ cell line contained many copies of the plasmid with ORC2 homology arms, used for integration of a disruptive blasticidin cassette into the ORC2 gene locus (Shibata et al., 2016). In fact, it was the *ORC2* homology arms in the plasmid that showed up as the massive amplification in the CNV analysis by SMASH **(Figure 3-38a, b, c)**. Based on RT-PCR data, aside from the expected heterozygous deletions in exon 7, exon 4 also exhibited multiple heterozygous SNPs at 3 different sites. Among them, SNP1 resulted in a novel stop codon, while SNP3/4/5 were missense mutations, and SNP2/6 were silent mutations **(Figure 3-34f)**. Next, we determined the haplotype phasing information between the heterozygous exon 7 deletion and the potential novel stop codons. One allele of ORC2 contained various mutations in exon 4, in combination with the deleted exon 7, showing that the cell line was heterogeneous to start with. The other allele of *ORC2* that had an intact exon 7 also had either wild type or SNPs in exon 4. Since there is a methionine in exon 5, it is possible the truncated ORC2 protein we observed was translated from this internal start site **(Figure 3-35b)**. Although substantially altered, based on the sequencing data and the sensitivity of the cells to ORC2-1 and ORC2-2 sgRNAs, we conclude that the cell strain is not a true *ORC2* knockout.

With regard to the HCT116 *ORC1*$^{-/-}$ cell line, we confirmed that they lacked ORC1 protein using multiple antibodies and confirmed that they duplicated at a much slower rate than the parental line, as previously reported **(Figure 3-35c)** (Shibata et al., 2016). The doubling time of the *ORC1*$^{-/-}$ cells was four-times longer than the parental cells and we were unable to passage these cells for many generations (by 20-30 generations they stopped proliferating). We also compared HCT116 *ORC1*$^{-/-}$ (B14) and HCT116 *ORC2*$^{-/-}$ (P44) cell lines with the parental lines,

i.e. either *p53*$^{+/+}$ and *p53*$^{-/-}$ background by confocal microscopy **(Figure 3-34g (1-4), h; Figure 3-39a-e, Figure 3-40a-c)**. There was a myriad of nuclear morphology defects in the *ORC1*$^{-/-}$ cell line. When the nuclei were stained with Hoechst dye, up to 10 percent contained abnormally large nuclei or sometimes what seemed to be multiple nuclei aggregated together in single cell, while other cells appeared normal. When probed further by staining for F-actin and Lamin B1 to observe overall cellular morphology and nuclear membrane integrity respectively, we observed that despite the staining for DNA content looking normal, up to 50 percent of the *ORC1*$^{-/-}$ cells showed highly abnormal, involuted nuclear membranes **(Figure 3-34i)**. In addition, most of the gigantic nuclei seemed to have lost the nuclear membrane altogether, while those cells that had Lamin B1 staining displayed abnormal nuclear membrane integrity.

The chromatin organization in the cells was observed by transmission electron microscopy (TEM) and revealed huge differences in cell size and nuclear structure between the wild type HCT116 *p53*$^{+/+}$ and *ORC1*$^{-/-}$ cells **(Figure 3-40d-f)**. About 35 % of *ORC1*$^{-/-}$ cells were grossly larger than wild type cells. Those multinucleate/polyploid giant cells were full of membrane invagination and vacuoles, and also exhibit significant apoptotic activities. Most likely they were formed due to extensive DNA damage and nuclear structural defects and underwent a different type of cell division called neosis, in which intracellular cytokinesis occurs and some mononuclear cells are produced from nuclear budding or asymmetric cell division (Sundaram et al., 2004). All these phenotypes pointed to the fact that although *ORC1*$^{-/-}$ cells do not survive in culture long term, for the duration that they do grow, they proliferate extremely slowly and are grossly abnormal. It may well be the case that *p53*$^{-/-}$ status of the parental HCT116 was required for these cells to be produced in the first place.

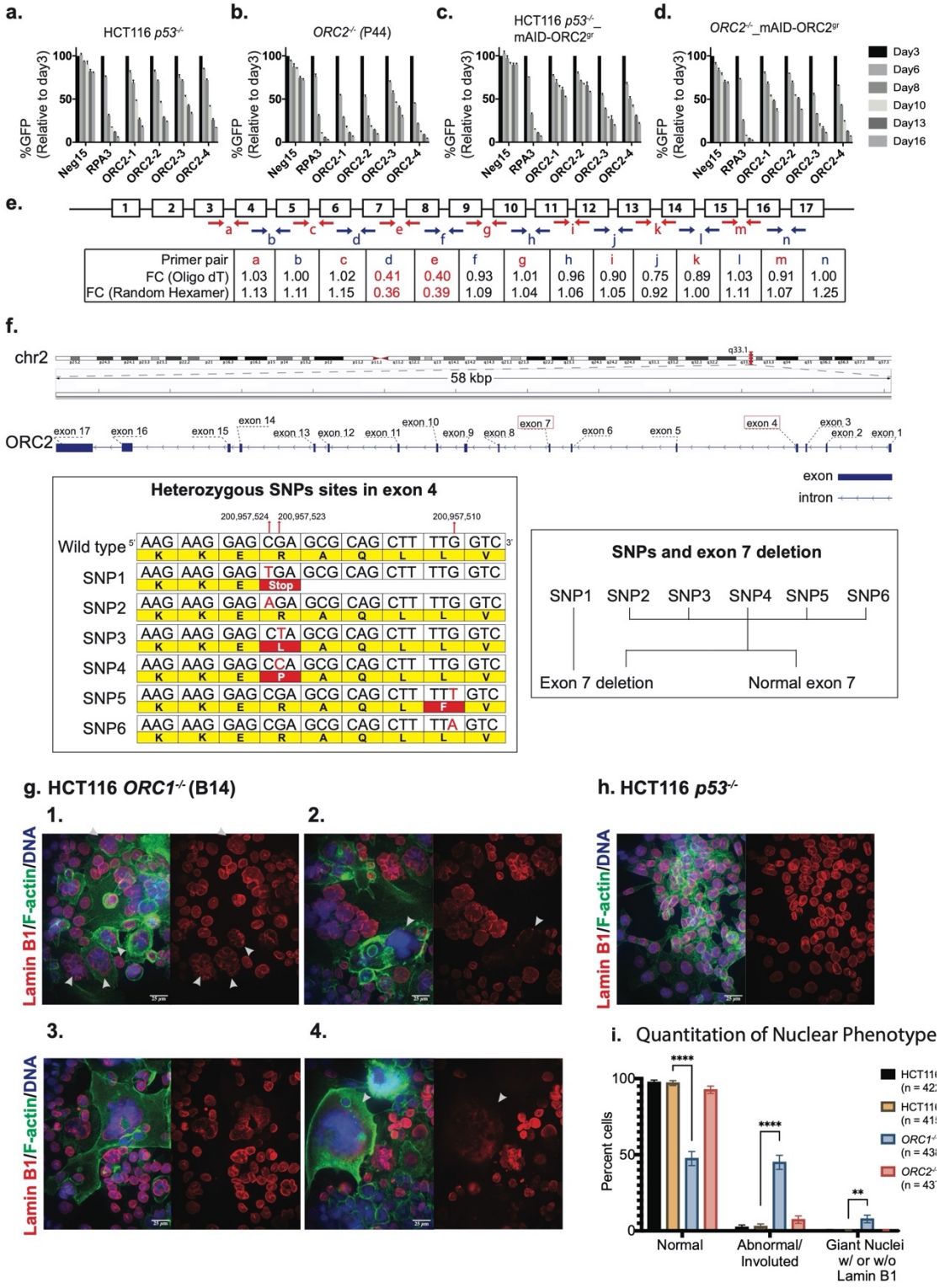
a.
HCT116 p53-/-
b.
ORC2-/- (P44)
c.
HCT116 p53-/-_ mAID-ORC2gr
d.
ORC2-/-_mAID-ORC2gr
%GFP (Relative to day3)
Neg15
RPA3
ORC2-1
ORC2-2
ORC2-3
ORC2-4
Day3
Day6
Day8
Day10
Day13
Day16
e.
Primer pair a b c d e f g h i j k l m n
FC (Oligo dT) 1.03 1.00 1.02 0.41 0.40 0.93 1.01 0.96 0.90 0.75 0.89 1.03 0.91 1.00
FC (Random Hexamer) 1.13 1.11 1.15 0.36 0.39 1.09 1.04 1.06 1.05 0.92 1.00 1.11 1.07 1.25
f.
chr2
58 kbp
ORC2
exon
intron
Heterozygous SNPs sites in exon 4
200,957,524
200,957,523
200,957,510
Wild type
SNP1
SNP2
SNP3
SNP4
SNP5
SNP6
Stop
SNPs and exon 7 deletion
Exon 7 deletion
Normal exon 7
g. HCT116 ORC1-/- (B14)
h. HCT116 p53-/-
Lamin B1/F-actin/DNA
i. Quantitation of Nuclear Phenotype
Percent cells
Normal
Abnormal/ Involuted
Giant Nuclei w/ or w/o Lamin B1

Figure 3-34. Characterization of previously published *ORC1*$^{-/-}$ and *ORC2*$^{-/-}$ cell lines. (a-d) Negative-selection time course assays that plot the percentages of GFP positive cells over time following transduction with the indicated sgRNAs/Cas9. Experiments were performed in HCT116 *p53*$^{-/-}$, *ORC2*$^{-/-}$, HCT116 *p53*$^{-/-}$_mAID-ORC2^{gr}, and *ORC2*$^{-/-}$_mAID-ORC2^{gr} cell lines. The GFP positive percentage was normalized to the Day3 measurement. n=3. Error bars, mean ± SD. (e) Calculated fold change (FC) for each primer pairs in *ORC2*$^{-/-}$ cells compared to HCT116 *p53*$^{-/-}$ cells. The red and blue arrows indicate each primer pair. Two kinds of primers, Oligo dT and Random Hexamer, were used in the reverse transcription step. Bar diagram view is shown in Figure 3-36. (f) Structural Variations (SVs) in the *ORC2* gene. Three SNP sites were among the 6 heterozygous mutations found in the 4th exon. Heterozygous deletion of exon 7 is also found in *ORC2*$^{-/-}$ cells. Long ONT reads that span both the heterozygous deletion site in exon 7 and the heterozygous SNP site in exon 4 show that SNP1 is on the same haplotype that contains the deletion of exon 7. The other haplotype contains a complete copy of exon 7 with heterozygous SNPs in exon 4. (g) (Provided by Dr. Kuhulika Bhalla) 1-4: Immunofluorescence of HCT116 *ORC1*$^{-/-}$ (B14) cell line stained with Anti-Lamin B1 antibody (Red), Phalloidin (F-actin) (Green), Hoechst Dye (Blue). Images show either merge of all three channels or Lamin-B1 staining of the nuclei. White arrows indicate abnormal and involuted nuclei in image g1. White arrows also show extremely large (nuclear giants) that have lost nuclear membrane integrity (g2, g4). (h) (Provided by Dr. Kuhulika Bhalla) Parental cell line for the *ORC1*$^{-/-}$ line as representative control for quantitative and qualitative comparison. More fields of control cells HCT116 *p53*$^{+/+}$ and *p53*$^{-/-}$ background and *ORC1*$^{-/-}$ and *ORC2*$^{-/-}$ cell lines are shown in Figure 3-39,40. Scale bar is 25 μm (i) (Provided by Dr. Kuhulika Bhalla) Quantitation of abnormal nuclei between cell lines. Nuclei per field were classified as Normal, Abnormal/Involuted or Nuclear giants (with or without Lamin B1). Multiple fields were counted to classify >400 cells for each cell line (n = sample size indicated in legend). Significance calculated using two-way ANOVA for multiple comparisons keeping HCT116 *p53*$^{-/-}$ as control. **** $p < 0.0001$, ** $p = 0.0014$.

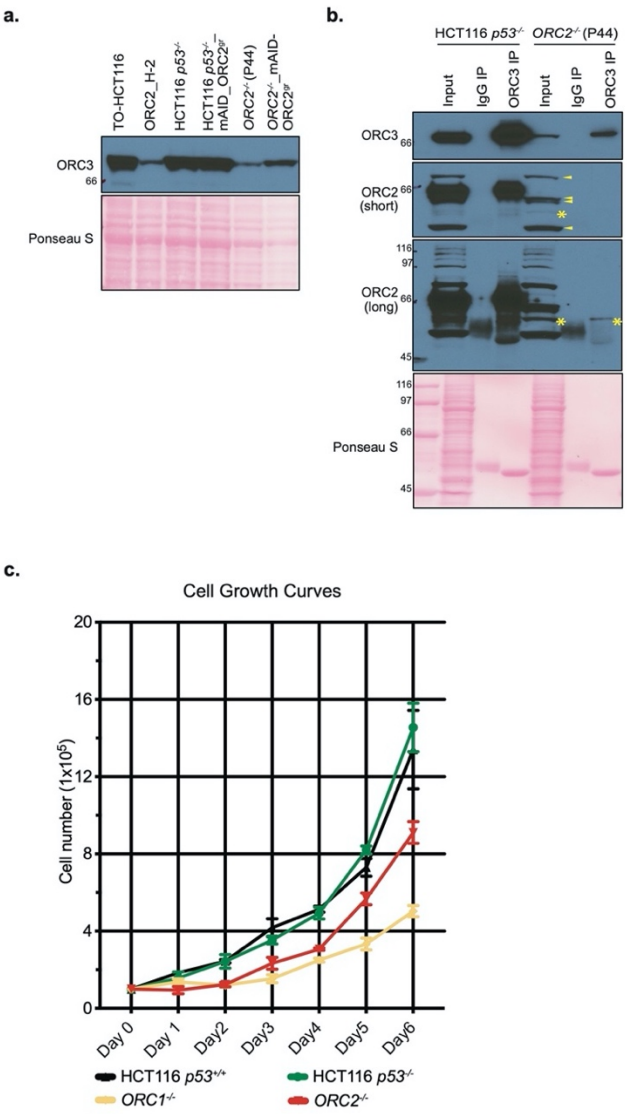

Figure 3-35. ORC3 exists in *ORC2*$^{-/-}$ cell line. (a) ORC3 expression in TO-HCT116, ORC2_H-2, HCT116 *p53*$^{-/-}$, HCT116 *p53*$^{-/-}$_mAID-ORC2^{gr}, *ORC2*$^{-/-}$, and *ORC2*$^{-/-}$_mAID-ORC2^{gr} cell lines. Whole cell lysates were made in Laemmli buffer followed by western blotting with anti-ORC3 antibody. (b) ORC3 immunoprecipitation (IP) in HCT116 *p53*$^{-/-}$ and *ORC2*$^{-/-}$ cell lines. Cells were lysed in lysis buffer and incubated with mouse IgG or ORC3 mouse monoclonal antibody for immunoprecipitation, followed by western blotting detection with antibodies against ORC2 and ORC3. Input ~2.5% and IP ~30% of total was loaded for analysis. Both short and long exposure of ORC2 detection were shown here. Asterisks (*) indicate the putative truncated ORC2 which was only found in *ORC2*$^{-/-}$ cell line. In the short exposure only, arrows point to nonspecific bands detected by the anti-ORC2 antibody. (c) (Provided by Dr. Kuhulika Bhalla) Cell growth curves of HCT116 *p53*$^{+/+}$, HCT116 *p53*$^{-/-}$, *ORC1*$^{-/-}$, and *ORC2*$^{-/-}$ cell lines. The x axis indicates days after cell seeding (Day 0 to Day 6). The y axis reflects the cell number (x10^5). n=3 (biological repeats). Error bars, mean ± SD.

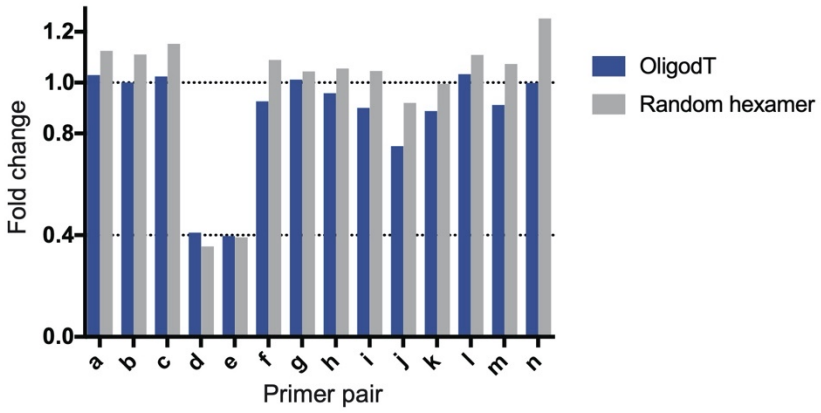

Figure 3-36. Real time quantitative PCR fold change represented as bar plot for Figure 3-34e. Blue, fold change of OligodT primer sample. Grey, fold change of random hexamer sample. Fold change (FC) for each primer pair in *ORC2*$^{-/-}$ cells compared to HCT116 *p53*$^{-/-}$ cells was calculated as FC = 2(to the power of ΔΔCt).

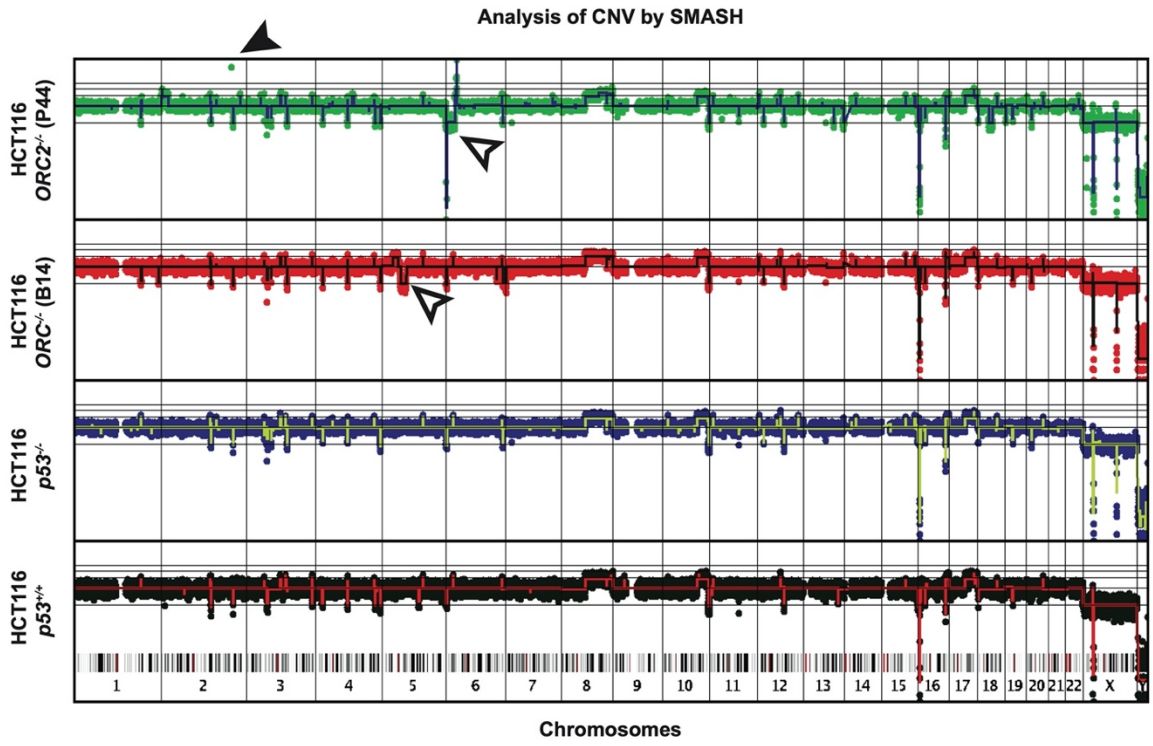

Figure 3-37. Copy number analysis of the genomes of four cell lines using the SMASH method. (Provided by Dr. Kuhulika Bhalla) The amplification of the ORC2 gene sequences in HCT116 *ORC2*$^{-/-}$ (P44) cells is shown by the green dot and filled arrow. The open arrows show acquired CNVs in the *ORC1*$^{-/-}$ and *ORC2*$^{-/-}$ cells compared to the parental cells.

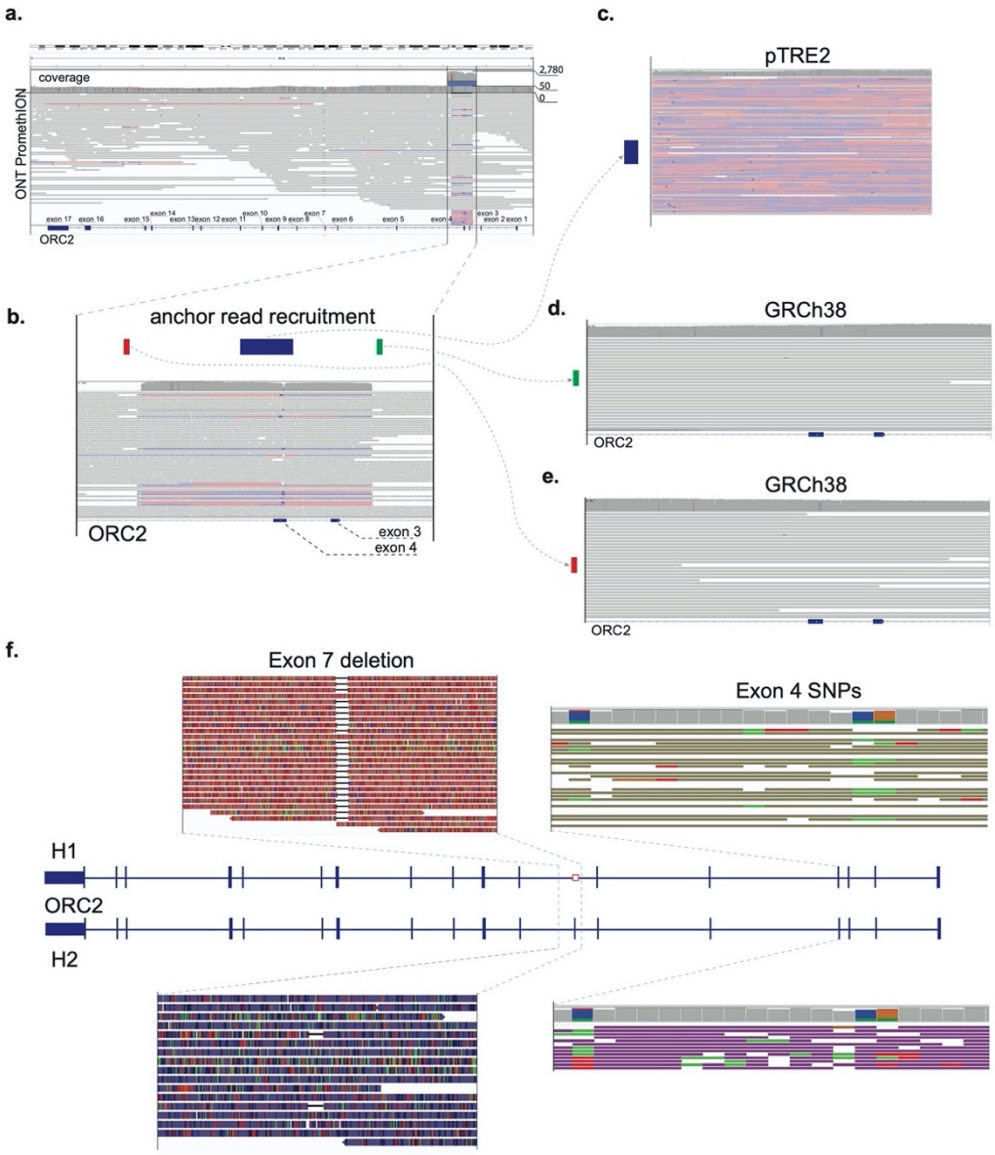

Figure 3-38. ONT PromethION long reads analysis. (Provided by Dr. Sergey Aganezov) (a) Alignment of ONT PromethION long reads to *ORC2* locus in GRCh38 with an average read-depth coverage of 50x only altered in a single highlighted reads alignment pileup (encompassing exons 3 and 4) with a coverage increase to ~2,500x. (b) Reads alignment pileup encompassing exons 3 and 4 of *ORC2* locus with schematic locations of two 100bp-long flanking anchor regions (red and green) located 200bp outside of the pileup beginning/end coordinates, respectively, and a 1Kbp internal anchor region (blue). (c) (re)alignment of long ONT reads spanning an internal (blue) anchor region in the pileup show in panel b) to pTRE2 reference with resulting average read depth coverage of ~2,955x. In panels (d) and (e) we show (re)alignments of ONT reads spanning the "green" and "red" pileup-flanking anchors to the same *ORC2* locus in GRCh38 with an observed read-depth coverage of ~50x. f) Phased alignments of reads which overlap the genomic region between exon 7 and a red pileup-flanking anchor, with highlights of the observed SNPs in Exon 4 and a deletion encompassing Exon 7.

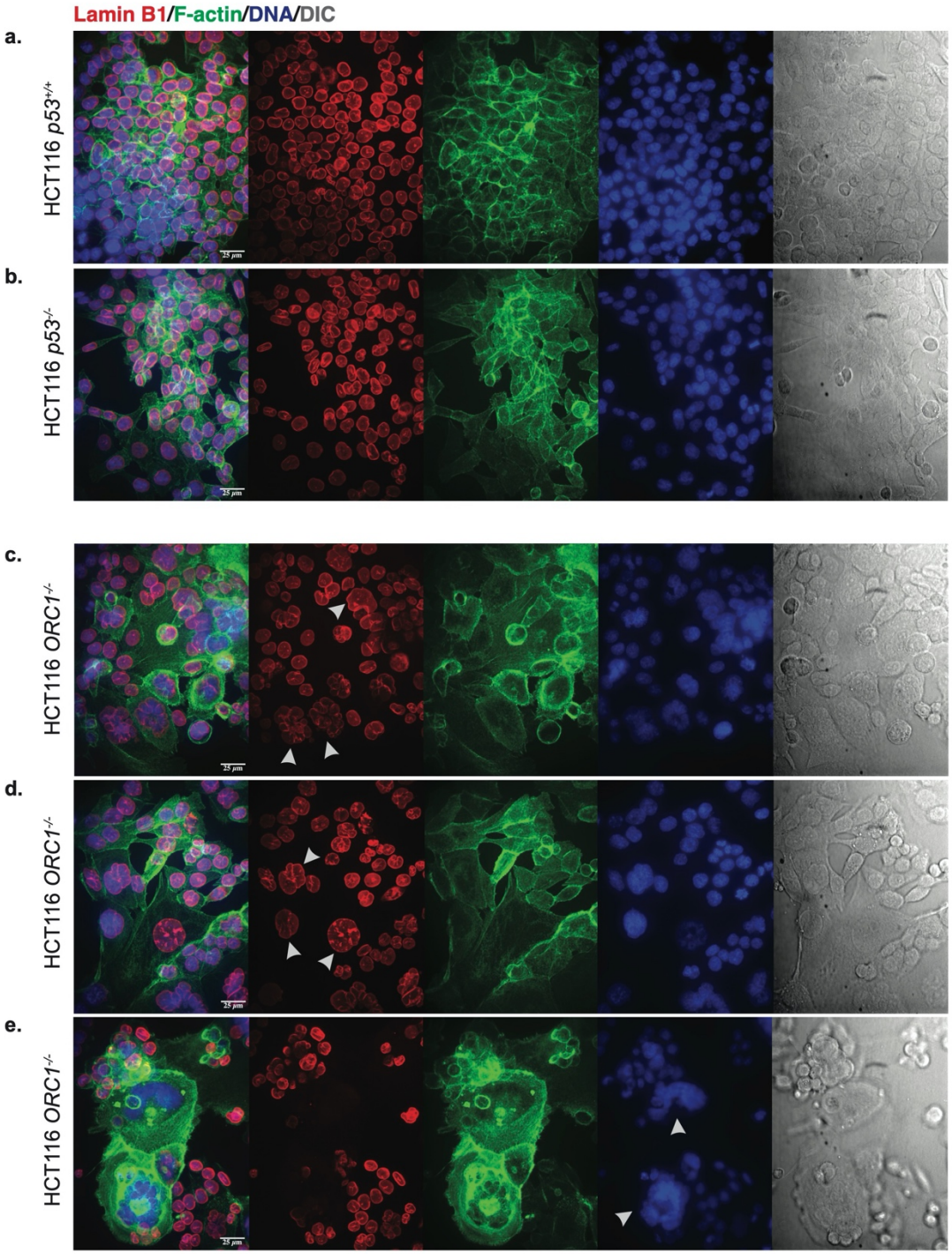

Figure 3-39. Confocal Microscopy images of HCT116 cell lines. (Provided by Dr. Kuhulika Bhalla) Images acquired as z-stacks of 25 µm (z = 1µm each). Images presented maximum intensity projections in the merge and average intensity projections in single channel images. Channel reference: Lamin B1 (Red), F-actin (Green), DNA (blue), DIC (grey) (a) HCT116 *p53*$^{+/+}$. (b) HCT116 *p53*$^{-/-}$. (c-e) HCT116 *ORC1*$^{-/-}$ (B14). Scale bar is 25 µm.

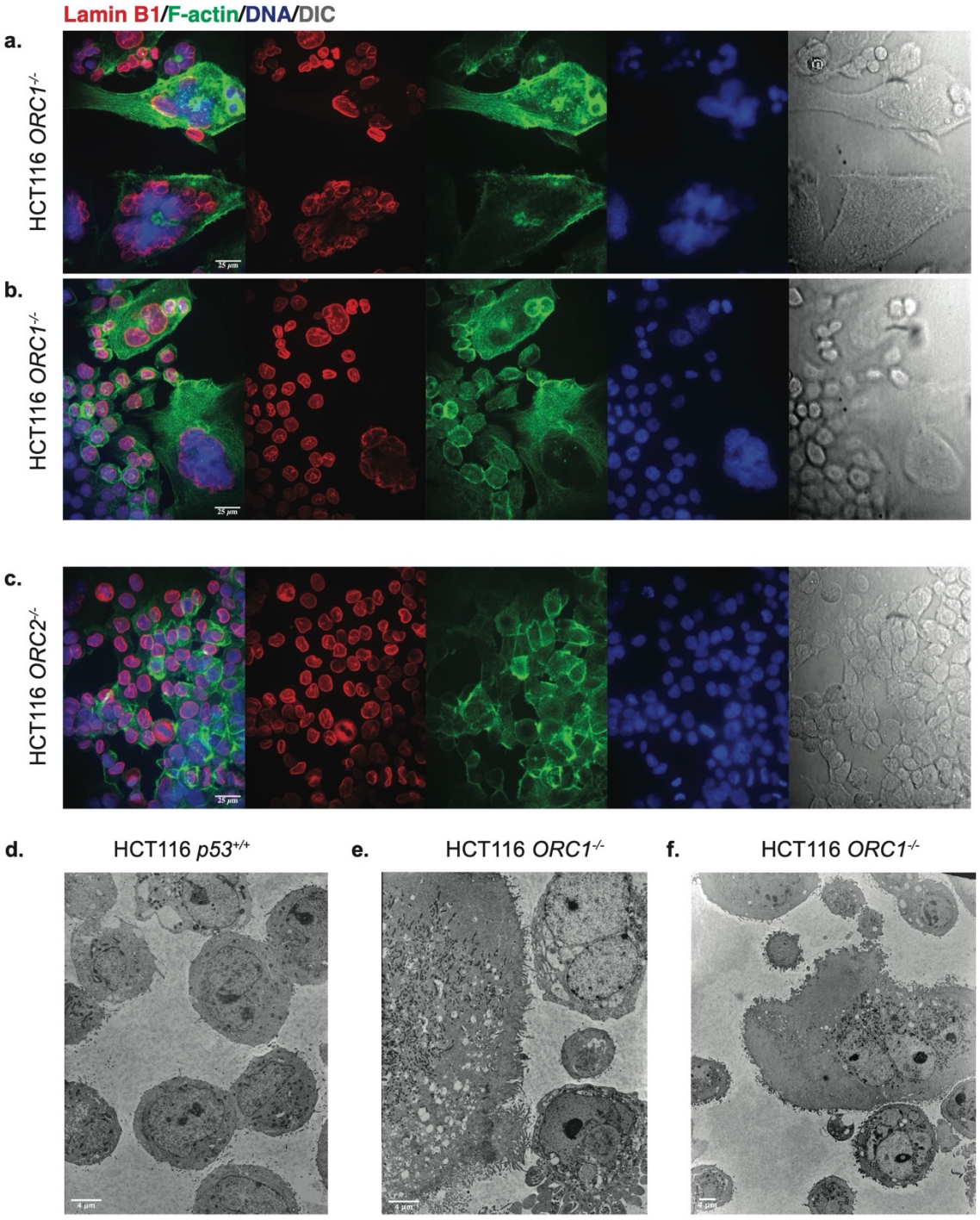

Figure 3-40. Confocal (a-c) and Transmission electron microscopy (d-f) (TEM) images of HCT116 cell lines. Confocal (Provided by Dr. Kuhulika Bhalla): (a-b) HCT116 *ORC1*$^{-/-}$ (B14), (c) HCT116 *ORC2*$^{-/-}$. Scale bar is 25 µm. TEM (Provided by Dr. Habeeb Alsudani): (d) HCT116 *p53*$^{+/+}$ cells with 2000x magnification. (e) *ORC1*$^{-/-}$ cells with 2000x magnification. (f) *ORC1*$^{-/-}$ cells with 1000x magnification. Scale bar in (d-e) is 4 µm.

3. Discussion

The *ORC2*$^{-/-}$ cell line believed to be a complete knockout via the use of 3 sgRNAs, one targeting the exon 4, and the others targeting the 6th and 7th introns retained a truncated form of ORC2 that could interact with ORC3 and was expressed from a mutated gene. These cells were still susceptible to *ORC2* knockdown using four sgRNAs selected from our CRISPR screens and also partially rescued the phenotype with two sgRNAs using a CRISPR-sgRNA resistant mAID-ORC2^{gr}. Similar to what we found for *ORC2*$^{-/-}$ cells, CRISPR-induced frameshifts in cells often generate truncated proteins that, although may not be recognized by western blot, still preserve whole or partial protein function (Smits et al., 2019). Based on these observations with ORC2 and the results with *ORC1*$^{-/-}$ lines, cells were unable to proliferate for many generations and produced abnormally structured cells, as well as data analyzed by tiling-sgRNA CRISPR screens, we conclude that ORC is essential in human cells. This conclusion is consistent with existing literature (Hemerly et al., 2009; McKinley and Cheeseman, 2017; Ohta et al., 2003; Prasanth et al., 2010, 2004) and is not surprising since ORC has multiple functions in human cells.

The fact that *ORC1*$^{-/-}$ cells could be obtained might suggest that ORC1 is not essential, but these cells did proliferate very slowly and only for a limited number of generations, and yielded cells with grossly abnormal nuclear structures. Thus, we suggest that it is unlikely to obtain cells that are viable over many generations in the absence of all ORC subunits. The *ORC1*$^{-/-}$ cells have excess levels of CDC6 protein bound to chromatin (Shibata et al., 2016) and since CDC6 is related to ORC1 and can bind to the other ORC subunits, we suggest that CDC6 might compensate, albeit poorly, for the absence of ORC1 in loading MCM2-7 proteins and establishing pre-RCs. A recent report described human cells that proliferated in the absence of ORC2 or ORC5 (Shibata and Dutta, 2020), but we suggest that a detailed molecular and phenotypic analysis of these cells be examined in greater detail as described in this report.

The pooled CRISPR/Cas9 domain-focused screen has become a common and powerful tool for uncovering genes that are essential for cell proliferation, cell survival, and for identification of essential functional domains in proteins (Adelmann et al., 2018; Park et al., 2017; Shi et al., 2015; So et al., 2019). However, if the screens use only a handful of guides targeting annotated essential regions, it may still result in data which may or may not score a gene as essential. Tiling-

sgRNA CRISPR-Cas9 screens on the other hand test 'functional' or 'essential' domains in a more rigorous and unbiased way (He et al., 2019). Using this approach, sgRNAs tiled across entire open reading frames of ORC1-6 and CDC6 enabled us to correlate the negative selection phenotype to functional domains within these proteins. The combined results also confirmed that all ORC1-6 and CDC6 proteins were essential in cancer cells as well as a human diploid cell line, including ORC2 that was characterized as non-essential based on multiple shRNA and whole genome CRIPSR/Cas9 screens in numerous types of cells in the DepMap portal (https://depmap.org/portal/). We were able to identify many sgRNAs that targeted *ORC2* in the tiling-sgRNA CRISPR screen and the two chosen cloned sgRNAs that killed cells were successfully complemented using a *mAID-ORC2^{gr}* transgene, demonstrating specificity of the knockdowns. Thus, single guide experiments, especially those with negative results, should be interpreted with caution, such that the essential nature of a gene should be examined in depth as we have done here.

The known functional domains in ORC1, including the BAH, AAA+ and WHD were identified using the open reading frame tiling-sgRNA CRISPR/Cas9 screen, as well as other regions of ORC1, including the intrinsically disordered region (IDR; amino acids 180-480, **Figure 3-3e**) which we know binds to Cyclin A-CDK2 and CDC6 (Hossain et al., 2021), as well as many other proteins we have identified and characterized in detail. Additionally, this entire IDR may contribute to DNA mediated ORC liquid phase transition (Hossain et al., 2021; Parker et al., 2019). The screen also identified an essential region of ORC1 in and around amino acid 750-790 (**Figure 3-3a-b**) which may represent the pericentrin-AKAP450 centrosomal targeting (PACT) domain that localizes ORC1 to centrosomes to regulate correctly centrosome and centriole copy number (Hemerly et al., 2009).

In ORC2, multiple, essential domains were identified, including the AAA+-like domain and the WHD. The WHD of human ORC2 controls access of human ORC to DNA by inserting itself into the DNA binding channel prior to activation of the protein by binding to ORC1 and subsequent binding to CDC6 (Bleichert, 2019; Hossain et al., 2021; Jaremko et al., 2020). The ORC2-carboxy terminus binds to ORC3 and ORC2 is also known to bind to PLK1, the mitotic protein kinase (Song et al., 2011). Interestingly, ORC2 also has an IDR **(Figure 3-8d**; amino acids

30-230**)** and the sgRNA tiling screen of this region shows CKHS essential amino acids, but a relatively conserved region within this IDR amino acid is reproducibly essential in both HCT116 and RPE-1 cell lines **(Figure 3-4a-b, Figure 3-8a, Figure 3-14a-e)**. Recent studies have implicated the N-terminal region of ORC2 to interact with ORC associated (ORCA) protein and may functionally contribute to its role in DNA replication and chromatin organization (Shen et al., 2012).

The use of a mAID-ORC2^{gr} enabled rapid removal of ORC2 from cells and analysis of the resulting phenotypes in more detail. It was not surprising that ORC2 is essential for loading MCM2, and hence MCM2-7, to establish pre-RCs and origins of DNA replication across the genome. In the absence of ORC2, cells loaded very little MCM2, most likely resulting in too few origins of replication and a consequently slow S phase and arrest with a near 4C DNA content and ongoing DNA synthesis. ORC2 depletion yielded other phenotypes, including large nuclei and a failure to execute mitosis. The large nuclei, also observed in the *ORC1*$^{-/-}$ cells, have large CENP-C and HP1α foci, probably due to decompaction of the centromeric associated α-satellite DNA, as observed previously (Prasanth et al., 2010). We suggest a general role for ORC in nuclear organization and organizing chromatin domains in the nucleus, including heterochromatin. In yeast, ORC is essential for transcriptional silencing at the silent mating type heterochromatic loci *HMRa* and *HML*α loci and its function in replication are separable from that in silencing (Bell et al., 1993; DeBeer et al., 2003; Ehrenhofer-Murray et al., 1995). In *Drosophila*, ORC localizes and associates with heterochromatin protein HP1 during interphase and mitosis, and heterozygous recessive lethal mutations in *DmORC2* suppress position effect variegation (Huang et al., 1998; Pak et al., 1997). In humans, ORC1 interacts with RB and SUV39H1, a histone methyltransferase that tri-methylates histone H3K9 which HP1 binds to repress E2F1-dependent CCNE1 transcription (Hossain and Stillman, 2016) . ORC1 and ORC3 (a tight ORC2 binding partner) directly interact with HP1, and depletion of ORC subunits disrupt localization of HP1 and the compaction of chromosome 9 α-satellite repeats DNA (Pak et al., 1997; Prasanth et al., 2010). Furthermore, ORC1 binds to the histone H3K9me3 and H4K20me2 methylation marks and co-localizes with histone H2A.Z, suggesting ORC may organize higher order chromatin structures via direct interactions with modified histones (Hossain and Stillman, 2016; Kuo et al., 2012; Long et al., 2019). The

mechanism by which the nuclei become large as a result of ORC depletion is under further investigation.

A final phenotype we observed in the acute removal of ORC2 is that the cells that replicate DNA and enter into mitosis attempt chromosome congression at the metaphase plate, but never make it, even after 7 hours. Eventually the cells die of apoptosis. We had observed abnormal mitotic cells following long term (72 hr) treatment of cells with shRNAs that targeted *ORC2* but it was not clear if this phenotype was due to incomplete DNA replication (Prasanth et al., 2004). However, in the current study, acute removal of ORC2 captured some cells with a clear defect in chromosome congression during mitosis. Moreover, both ORC2 and ORC3 localize to centromeres (Craig et al., 2003; Prasanth et al., 2004), suggesting that they play a role in spindle attachment or centromeric DNA organization, particularly the centromere associated satellite repeat sequences. We speculate that in ancestral species, ORC localized at origins of DNA replication and this ORC also functioned in organization of chromosomes and in chromosome segregation, but upon separation of DNA replication and chromosome segregation with the advent of mitosis, separate functions of ORC in DNA replication, chromatin or nuclear organization and chromosome segregation were retained, but executed at different times during the cell division cycle.

Chapter four: Additional results

In this chapter, I included some results that were not published but were important for the ORC2 research. Here I showed the result of (1) analysis the mouse monoclonal ORC2 antibody previously used in our lab for immunoprecipitation, (2) protein-protein interactions characterized by IP-MS using rabbit polyclonal ORC2 antibody, (3) more cell cycle analysis of rapid ORC2 depletion ORC2_H-2 cell line, (4) characterization of lentiviral expressed mAID-ORC2^{gr} cell line, and (5) CRISPR/Cas9 depletion of endogenous ORC3 in TO-HCT116 and TO-U2OS TRex cell lines.

1. Anti-ORC2 antibody mAb920 cross-reacts with CENP-E

ORC2 binds to the ORC3 subunit and both are co-immunoprecipitated using antibodies against ORC2 or ORC3. There were two antibodies against human ORC2 that were most widely used in our lab, the first being the mouse monoclonal mAb#9-20, and the second being the rabbit polyclonal #CS205. Both antibodies were used by previous lab members in immunofluorescence staining and ORC2 immunoprecipitation (IP) experiments. To identify ORC2 binding partners in mitosis, I blocked the cells with nocodazole, and then collected mitotic cells by mitotic shake-off method. To compare the IP results between the two antibodies, after lysing cells in lysis buffer, the antibodies against ORC2 were added into separate lysates to perform immunoprecipitation. We found out that Centromere protein E (CENP-E) was strongly co-immunoprecipitated with mAb#9-20 antibody, but not with #CS205 antibody, or the anti-ORC3 mouse monoclonal mAb#PKS16 antibody. We suspected that the CENP-E co-IP was a result of a cross-reactivity of mAb#9-20 antibody. Because the epitope of mAb#9-20 antibody (LKNDPEITI) has been identified by peptide competition previously (Prasanth et al., 2004), I performed a blast search of the peptide sequence in CENP-E protein and discovered a region in CENP-E (LKENIEMTI, 1073-1081aa) that might be responsible for the possible cross-reactivity **(Figure 4-1a)**. Next, I

cloned five different fragments of CENP-E protein into IPTG induced expression vector and expressed them in bacteria (data not shown). MBP-tagged 1-667 aa, 501-1173 aa, 1001-1667 aa, 1501-2167 aa, and 2001-2605 aa CENP-E fragments were induced by IPTG and I confirmed that ORC2 mAb#9-20 antibody can recognize the CENP-E 1001-1667 aa fragment which contains 1073-1081 aa by doing western blotting **(Figure 4-1b)**.

This was an important finding since CENP-E is a motor-like protein responsible for spindle elongation and chromosome movement during mitosis (Abrieu et al., 2000; Gudimchuk et al., 2013). Using this mouse monoclonal mAb#9-20 antibody for experiments might co-IP many other CENP-E associated proteins which are unrelated to ORC2 protein. Therefore, this mAb#9-20 antibody was not used for subsequent immunoprecipitation experiments.

a.

ORC2 antibody epitope: 124 aa - SLKNDPEITINVPQSSKGHS -143 aa

Protein blast:

	Query	2	LKNDPEITI	10
			LK + E TI	
hCENP-E	Sbjct	1073	LKENIEMTI	1081

b.

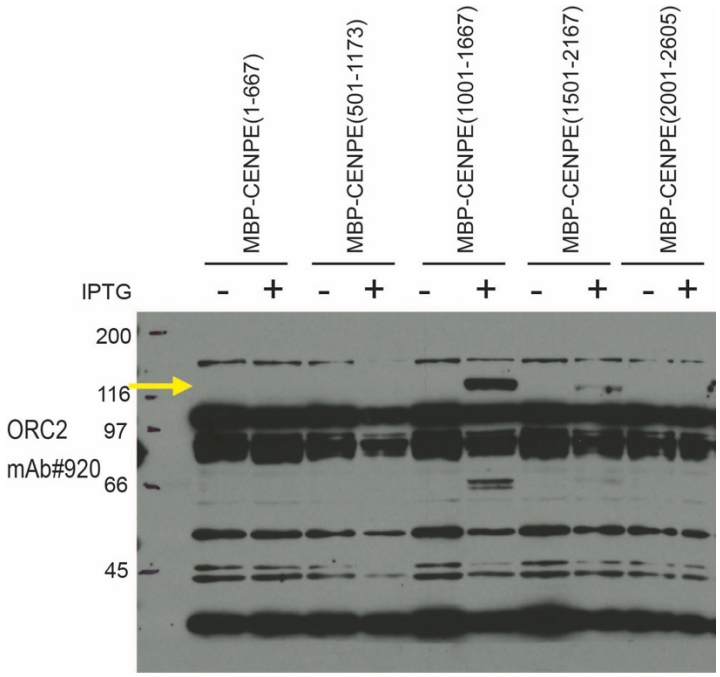

Figure 4-1. ORC2 mouse monoclonal mAb#920 antibody cross-reacts with CENP-E. (a) The ORC2 monoclonal antibody epitope was within ORC2 124-143aa. The BLAST result showed the sequence similarity between ORC2 and CENP-E. (b) Five different fragments of MBP-CENP-E were induced in E. coli respectively. Yellow arrow points to the detected CENP-C protein fragment by ORC2 antibody.

2. IP-MS with anti-ORC2 rabbit polyclonal CS205 antibody

The study by Prasanth et al., 2004 suggested that ORC2 might play an important role in heterochromatin structure, kinetochore-microtubule alignments and chromosome congression (Prasanth et al., 2004). In order to explore its function and identify ORC2 binding partners during mitosis, I treated HeLa cells with nocodazole for 16 hr and harvested interphase (G2) and mitotic cells separately for immunoprecipitation experiment with anti-ORC2 #CS205 antibody. After lysing cells in lysis buffer, the lysates were centrifuged and the supernatant 1 (sup1) was collected. The pellet was treated with MNase, and centrifuged again to collect the supernatant 2 (sup2) and the final pellet (P). Sup1 or Sup2 were incubated with rabbit IgG or ORC2 antibody-conjugated GammaBind G Sepharose and then washed with washing buffer containing 100 mM NaCl. Half of the Sepharose beads were boiled for protein gel loading followed by western blot analysis **(Figure 4-2)**. Antibodies against ORC1, ORC2, ORC3, HP1, and several mitotic proteins were used for detection. The results showed ORC1, ORC2, and ORC3 co-IP well with ORC2. PLK1, HP1, and BUB3 protein also interact with ORC2, although they were also detected in the IgG IP control. To improve the result in the future, more detergent or salt can be added into the wash buffer to reduce background binding to the IgG beads.

Another half of the beads were sent for iTRAQ-based proteomics analysis. **(Table 4-1)** and **(Table 4-2)** contain proteins names that have enriched > 1.6 fold (FC > 1.6) with ORC2 antibody. Several proteins, including ORC2, ORC3, ORC5 and LRWD1/ORCA appeared to be in the top ten candidates of the ORC2-interacting proteins suggested that the experiment worked well. Many other proteins enriched with ORC2 and appeared on both tables. One of these proteins is the Phosphatidylinositol 3,4,5-trisphosphate 5-phosphatase 2 (INPPL1, SHIP2), which ranks number four in both G2 and M phase cells. INPPL1 is a phosphatidylinositol phosphatase and plays an important role in regulating the insulin signaling PI3K pathway (Gupta and Dey, 2009). It also participates in endocytosis, remodeling cytoskeleton and actin structures, regulating cell adhesion and spreading, etc. (Dyson et al., 2001; Habib et al., 1998; Pesesse et al., 2001; Prasad et al., 2002; Zhuang et al., 2007). It will be very interesting to find out how and why ORC and INPPL1 interacts in cells. Transferrin receptor protein 1 (TFRC) is responsible for importing iron-transferrin complex to endosomes by receptor-mediated endocytosis (Senyilmaz

et al., 2015). Retinoblastoma-binding protein 5 (RBBP5) plays an important role in embryonic stem cell differentiation potential and involves in methylation of H3K4 which marks the active genes (Avdic et al., 2011; Garapaty et al., 2009; Patel et al., 2009). Phosphatidylglycerophosphatase and protein-tyrosine phosphatase 1 (PTPMT1) is a lipid phosphatase that phosphorylates PGP, an essential phospholipid regulating the membrane integrity in mitochondria, and it potentially plays a role in insulin secretion (Mugabo et al., 2016; Niemi et al., 2014). Functions of many other proteins shown in both tables were not studied in detail but would be interesting to have a closer look after hypothesizing a possible new role of ORC2 based on other interactions.

Septin-2 (SEPT2) interacts with ORC2 during G2 but not mitosis **(Table 4-1)**. Septin-2 is essential for organization of actin cytoskeleton and also required for mitosis during spindle elongation, movement and chromosome segregation (Kremer et al., 2007; Spiliotis et al., 2008, 2005). It is interesting that Septin-2 is enriched with ORC2 during G2 phase but not M phase, suggesting that ORC2 might have a role by recruiting Septin before cells entering mitosis. Nestin (NES) promotes assembly and disassembly of intermediate filament protein during mitosis (Guérette et al., 2007; Michalczyk and Ziman, 2005) and the IP-MS results showed that Nestin binds with ORC2 during mitosis but not interphase (G2/M ratio = 1.63) **(Table 4-3)**. This interaction suggested that ORC2 might play a role in distributing intermediate filaments and providing support for cellular structure during mitosis. Mitotic checkpoint serine/threonine-protein kinase BUB1 beta (BUB1B) was also slightly enriched with ORC2 IP during mitosis (G2/M ratio = 1.53), suggesting that ORC2 might participate in mitotic checkpoint function, which is entirely possible since ORC2 localize to kinetochore/centromere during M phase.

The western blot showed mostly negative result, but I can try to optimize the IP condition to get a clearer result with more detecting antibodies. The IP-MS result uncovered a few potential interacting proteins to study in the future, and these interacting proteins lists provide us a new path to uncover possible functions of ORC2, which also support the current findings that ORC2 are essential for normal M phase progression, although the mechanism has yet to be investigated.

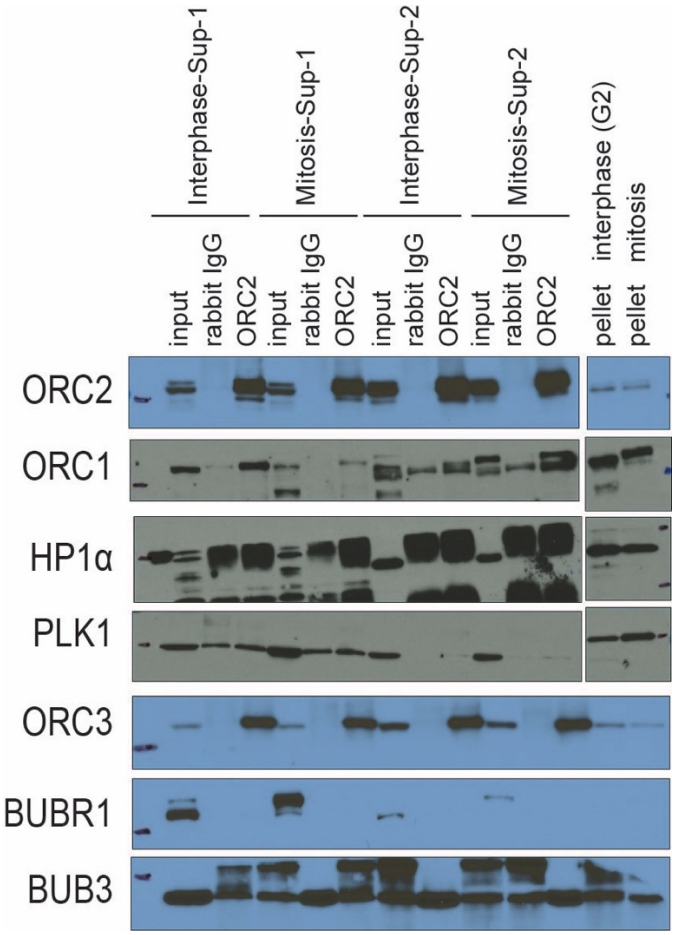

Figure 4-2. ORC2 immunoprecipitation in interphase (G2) and mitotic cells.
Immunoprecipitation was done by IgG or ORC2 antibodies from HeLa cell lysates. Immunoblots were detected with several ORC antibodies, heterochromatin protein HP1 antibody, or kinetochore protein antibodies. I: Interphase; M: mitosis. Interphase: Input: 2.5 %; IP: 25%. Mitosis: Input: 3 %; IP: 30%. Immunoblots for each protein were developed at the same time.

	G2 FC	Protein	
1	9.018	ORC3	Origin recognition complex subunit 3
2	6.060	ALB	Serum albumin
3	5.765	LRWD1	Leucine-rich repeat and WD repeat-containing protein 1
4	4.693	INPPL1	Phosphatidylinositol 3,4,5-trisphosphate 5-phosphatase 2
5	4.054	ORC5	Origin recognition complex subunit 5
6	3.710	RNF220	E3 ubiquitin-protein ligase RNF220 (Fragment)
7	3.670	PDLIM7	PDZ and LIM domain protein 7
8	3.284	ORC2	Origin recognition complex subunit 2
9	2.994	ABTB2	Ankyrin repeat and BTB/POZ domain-containing protein 2
10	2.802	TFRC	Transferrin receptor protein 1
11	2.366	ANKRD26	Ankyrin repeat domain-containing protein 26
12	2.361	TSTD2	Thiosulfate sulfurtransferase/rhodanese-like domain-containing protein 2
13	2.058	RPLP2	60S acidic ribosomal protein P2
14	2.051	RANGAP1	Ran GTPase-activating protein 1
15	2.004	SRBD1	S1 RNA-binding domain-containing protein 1
16	1.993	WDR11	WD repeat-containing protein 11 (Fragment)
17	1.968	ERICH3	Glutamate-rich protein 3
18	1.929	RBBP5	Retinoblastoma-binding protein 5
19	1.898	SEC16A	Protein transport protein Sec16A (Fragment)
20	1.851	HBS1L	HBS1-like protein (Fragment)
21	1.795	ACOX1	Peroxisomal acyl-coenzyme A oxidase 1
22	1.789	MLLT1	Protein ENL
23	1.785	SYNE3	Nesprin-3
24	1.758	PHF2	Lysine-specific demethylase PHF2
25	1.734	RSBN1L	Round spermatid basic protein 1-like protein
26	1.721	RPLP1	60S acidic ribosomal protein P1
27	1.697	BABAM2	BRISC and BRCA1 A complex member 2 (Fragment)
28	1.690	NCAPG2	Condensin-2 complex subunit G2 (Fragment)
29	1.680	ARRDC1	Arrestin domain-containing protein 1
30	1.671	ELP3	Elongator complex protein 3 (Fragment)
31	1.662	SEC13	Protein SEC13 homolog
32	1.662	ALDH18A1	Delta-1-pyrroline-5-carboxylate synthase
33	1.662	TECR	Very-long-chain enoyl-CoA reductase (Fragment)
34	1.662	TUBG1	Tubulin gamma-1 chain
35	1.660	RPL32	60S ribosomal protein L32 (Fragment)
36	1.639	RPS26	40S ribosomal protein S26

37	1.638	RIOX1	Ribosomal oxygenase 1
38	1.636	PTPMT1	Phosphatidylglycerophosphatase and protein-tyrosine phosphatase 1
39	1.619	EIF3F	Eukaryotic translation initiation factor 3 subunit F (Fragment)
40	1.616	PPIB	Peptidyl-prolyl cis-trans isomerase B
41	1.607	EIF4B	Eukaryotic translation initiation factor 4B
42	1.601	CUTA	Protein CutA
43	1.591	SEPT2	Septin-2

Table 4-1. ORC2-interacting proteins in G2 phase analyzed by iTRAQ. Each IP was done in duplicate, and one sample of the ORC2 IP in G2 cells were set at enrichment score=1. Average enrichment score of the duplicate was calculated for IgG IP or ORC2 IP in G2 cells. Fold change (FC) was calculated by G2 cells ORC2 IP average enrichment score divided by G2 cells IgG IP average enrichment score. Proteins listing here have fold change ≥ 1.6. Protein names in the red color overlapped with table 4-2.

	M FC	Protein	
1	7.985	ALB	Serum albumin
2	6.857	ORC3	Origin recognition complex subunit 3
3	5.191	LRWD1	Leucine-rich repeat and WD repeat-containing protein 1
4	5.095	INPPL1	Phosphatidylinositol 3,4,5-trisphosphate 5-phosphatase 2
5	4.036	ORC5	Origin recognition complex subunit 5
6	4.006	TFRC	Transferrin receptor protein 1
7	3.984	PDLIM7	PDZ and LIM domain protein 7
8	3.887	ORC2	Origin recognition complex subunit 2
9	3.823	RNF220	E3 ubiquitin-protein ligase RNF220 (Fragment)
10	3.231	ABTB2	Ankyrin repeat and BTB/POZ domain-containing protein 2
11	2.504	NES	Nestin
12	2.460	SRBD1	S1 RNA-binding domain-containing protein 1
13	2.248	SHCBP1	SHC SH2 domain-binding protein 1
14	2.235	TUBG1	Tubulin gamma-1 chain
15	2.234	ACOX1	Peroxisomal acyl-coenzyme A oxidase 1
16	2.153	ALDH18A1	Delta-1-pyrroline-5-carboxylate synthase
17	2.122	ELP3	Elongator complex protein 3 (Fragment)
18	2.112	RBBP5	Retinoblastoma-binding protein 5
19	2.106	TF	Serotransferrin (Fragment)
20	2.091	TUBGCP3	Gamma-tubulin complex component 3
21	2.017	HECTD4	Probable E3 ubiquitin-protein ligase HECTD4
22	1.976	BABAM2	BRISC and BRCA1 A complex member 2 (Fragment)
23	1.954	NF1	Neurofibromin (Fragment)
24	1.949	LSM14B	Protein LSM14 homolog B
25	1.943	ANKRD26	Ankyrin repeat domain-containing protein 26
26	1.928	PTPMT1	Phosphatidylglycerophosphatase and protein-tyrosine phosphatase 1
27	1.860	PLS3	Plastin-3
28	1.851	KRT6C	Keratin, type II cytoskeletal 6C
29	1.850	MLLT1	Protein ENL
30	1.823	SEC16A	Protein transport protein Sec16A (Fragment)
31	1.808	TUBGCP4	Gamma-tubulin complex component (Fragment)
32	1.776	TUBGCP2	Gamma-tubulin complex component
33	1.711	DDX49	Probable ATP-dependent RNA helicase DDX49
34	1.700	HBS1L	HBS1-like protein (Fragment)
35	1.697	PRKAR2A	cAMP-dependent protein kinase type II-alpha regulatory subunit
36	1.688	RASAL2	Ras GTPase-activating protein nGAP (Fragment)

37	1.684	RPL32	60S ribosomal protein L32 (Fragment)
38	1.679	U2SURP	U2 snRNP-associated SURP motif-containing protein
39	1.678	PML	Protein PML (Fragment)
40	1.668	TOMM20	Mitochondrial import receptor subunit TOM20 homolog
41	1.654	KIF23	Kinesin-like protein KIF23
42	1.653	RPL14	60S ribosomal protein L14
43	1.653	TECR	Very-long-chain enoyl-CoA reductase (Fragment)
44	1.649	CYP4B1	Cytochrome P450 4B1
45	1.641	PUS1	tRNA pseudouridine synthase A, mitochondrial (Fragment)
46	1.635	PPFIA1	Liprin-alpha-1
47	1.618	SRSF11	Serine/arginine-rich-splicing factor 11 (Fragment)
48	1.617	WDR5	WD repeat-containing protein 5
49	1.616	CYR61	Protein CYR61
50	1.613	KRT2	Keratin, type II cytoskeletal 2 epidermal
51	1.613	RPLP1	60S acidic ribosomal protein P1
52	1.610	NF2	Merlin
53	1.610	PUM3	Pumilio homolog 3
54	1.602	HAUS8	HAUS augmin-like complex subunit 8
55	1.600	RPL36	60S ribosomal protein L36
56	1.596	PTRH1	Probable peptidyl-tRNA hydrolase (Fragment)
57	1.593	DDX50	ATP-dependent RNA helicase DDX50

Table 4-2. ORC2-interacting proteins in M phase analyzed by iTRAQ. Each IP was done in duplicate, and one sample of the ORC2 IP in G2 cells were set at enrichment score=1. Average enrichment score of the duplicate was calculated for IgG IP or ORC2 IP in mitotic cells. Fold change (FC) was calculated by mitotic cells ORC2 IP average enrichment score divided by mitotic cells IgG IP average enrichment score. Proteins listing here have fold change ≥ 1.6. Protein names in the red color overlapped with table 4-1.

	G2 FC	M FC	G2/M ratio	Protein	
1	1.537	2.504	1.629	NES	Nestin
2	1.331	2.248	1.689	SHCBP1	SHC SH2 domain-binding protein 1
3	1.292	1.954	1.512	NF1	Neurofibromin (Fragment)
4	0.903	1.613	1.787	KRT2	Keratin, type II cytoskeletal 2 epidermal
5	0.910	1.596	1.753	PTRH1	Probable peptidyl-tRNA hydrolase (Fragment)
6	1.007	1.547	1.536	CXorf56	UPF0428 protein CXorf56
7	0.980	1.618	1.651	SRSF11	Serine/arginine-rich-splicing factor 11 (Fragment)
8	0.861	1.564	1.816	KRT5	Keratin, type II cytoskeletal 5
9	1.032	1.577	1.528	BUB1B	Mitotic checkpoint serine/threonine-protein kinase BUB1 beta
10	0.874	1.851	2.117	KRT6C	Keratin, type II cytoskeletal 6C
11	0.937	1.528	1.630	PCMTD1	Protein-L-isoaspartate O-methyltransferase domain-containing protein 1 (Fragment)
12	1.043	1.610	1.544	NF2	Merlin
13	0.818	2.017	2.465	HECTD4	Probable E3 ubiquitin-protein ligase HECTD4
14	0.811	1.568	1.932	SELENOF	Selenoprotein F
15	0.752	1.519	2.021	HELLS	Helicase, lymphoid-specific, isoform CRA_d
16	0.747	1.505	2.015	DGCR8	Microprocessor complex subunit DGCR8
17	0.722	1.535	2.127	PHAX	Phosphorylated adapter RNA export protein
18	0.893	1.641	1.838	PUS1	tRNA pseudouridine synthase A, mitochondrial (Fragment)

Table 4-3. ORC2-interacting proteins enriched in M phase analyzed by iTRAQ. G2/M ratio was calculated by mitotic cells ORC2 IP FC divided by G2 cells ORC2 IP FC. The list contains proteins that have M FC>1.5 with G2/M ratio >1.5.

3. Additional Cell cycle analysis of ORC2_H-2 cells

To explore whether ORC2 has a direct role in mitosis, I arrested TO-HCT116 cells or ORC2_H-2 cells with nocodazole to see whether depleting mAID-ORC2^{gr} at this arrest point in mitosis can prevent cells entering into G1. Cells were first treated with doxycycline for 24 hrs for OsTIR1 expression and then arrested the cells at G1/S phase with 2 mM thymidine for 24 hours. Next, I released the cells into fresh media for 3 hours, and then treated them with 50ng/ml nocodazole for 12 hours. 4.5 hours before harvesting the mitotic cells, I added auxin to the cells. To collect mitotic arrested cells, I performed mitotic shake-off, washed the cells with PBS, and re-seeded the cells in fresh media with or without auxin and doxycycline. After the cells were re-seeded, I harvested them at 0, 2, 4, 6, 8, 9, and 28-hour time points, indicating the period of time released from nocodazole. Depleting mAID-ORC2^{gr} during mitosis did not affect cells entering G1. However, auxin treatment caused slower cell progression into S phase at 6, 8, 9-hour time points. At the 28-hour time point, some auxin treated ORC2_H-2 cells that have a near 4C DNA content still seemed to be incorporating EdU **(Figure 4-3c arrow)**. This experiment showed that once cells entered M phase, ORC2 is not required for completing mitosis. Cells entered G1 phase normally and begun to accumulate errors and arrest in 4c DNA content **(Figure 4-3b,c arrow)**.

Next, to see how depletion of mAID-ORC2^{gr} during G1 phase affects cell cycle progression, I arrested cells with a double thymidine block and followed progression upon release from the thymidine block. Cells were first treated with 2 mM thymidine for 18 hours, released into fresh medium for 8 hours, and then incubated with second thymidine (with or without doxycycline) for another 16 hours. For cells treated with auxin, auxin was added 4.5 hours before release. After a second thymidine block, cells were released into medium containing 100 ng/ml nocodazole and doxycycline, with or without auxin. Nocodazole was added to arrest cells when they progressed to mitosis in order to observe one replication event. I then harvested cells at 0, 2, 4, 6, 8, 9 -hr time points. After nine hours of nocodazole arrest, I washed the cells in PBS and released them into fresh medium with or without doxycycline and auxin and harvest at 24 and 48 hr time points.

The results showed that both auxin-treated cell lines had much slower S phase progression and progressed to mitosis slower. Importantly, there was a population of auxin treated ORC2_H-2 cells arrested in G1 that never progressed through S phase to mitosis **(Figure 4-4b, c)**. At the 24-hr time point, which is 15 hours after washing off nocodazole, some auxin treated ORC2_H-2 cells progressed through mitosis and entered G1, but had very slow S phase progression, implying that cells may be struggling to finish replicating the DNA. Eventually, cells arrest at either G1 or late S/G2 phase as shown in the 48 hr timepoint.

Although depleting mAID-ORC2^{gr} during final 4.5 hr of nocodazole block or upon released from thymidine block did not have an obvious effect on cells entering or exiting mitosis phase in both experiments, we still cannot rule out that ORC2 has a function in mitosis. ORC2 may still play an important role in mitosis by recruiting essential mitotic proteins during M-G1 phase before mAID-ORC2^{gr} was depleted by auxin.

a.

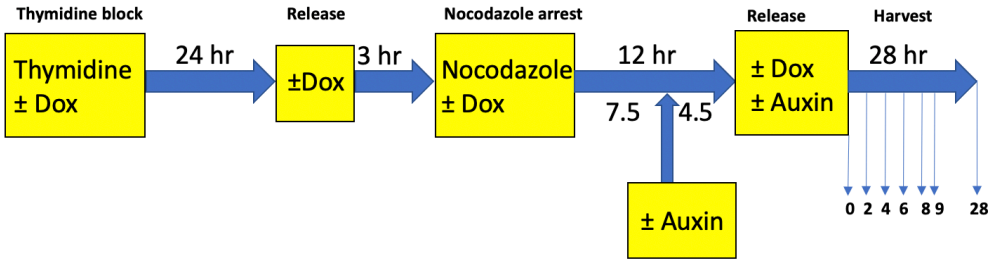
Thymidine block
Thymidine
± Dox
24 hr
Release
±Dox
3 hr
Nocodazole arrest
Nocodazole
± Dox
12 hr
7.5
4.5
± Auxin
Release
± Dox
± Auxin
Harvest
28 hr
0 2 4 6 8 9
28

b.

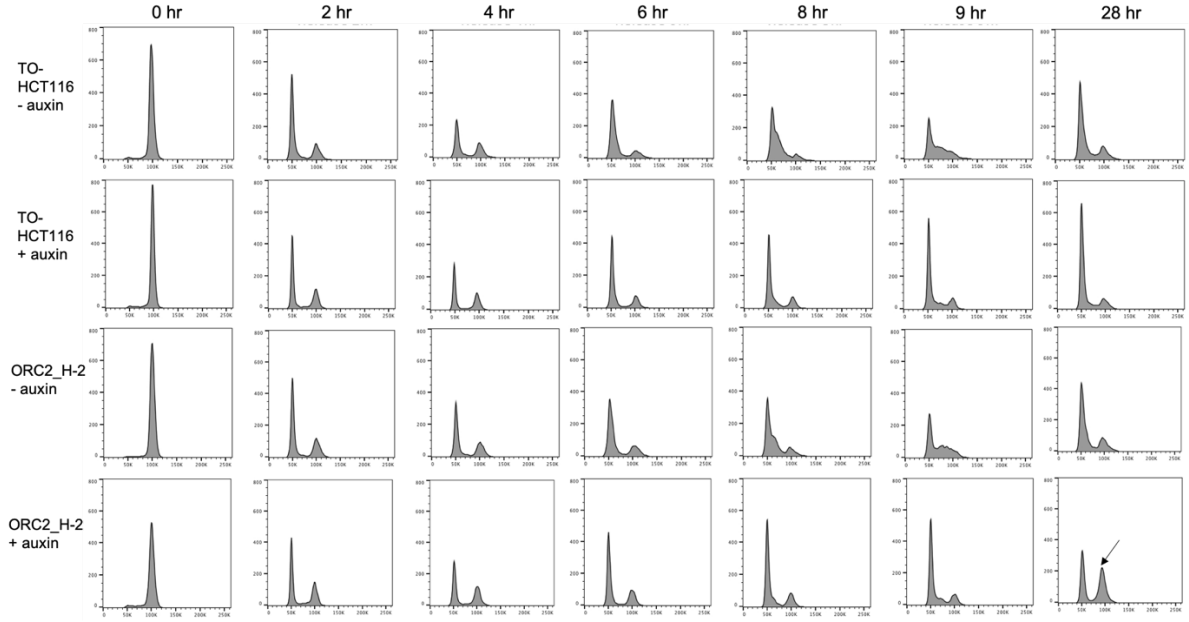
0 hr
2 hr
4 hr
6 hr
8 hr
9 hr
28 hr
TO-HCT116 - auxin
TO-HCT116 + auxin
ORC2_H-2 - auxin
ORC2_H-2 + auxin

c.

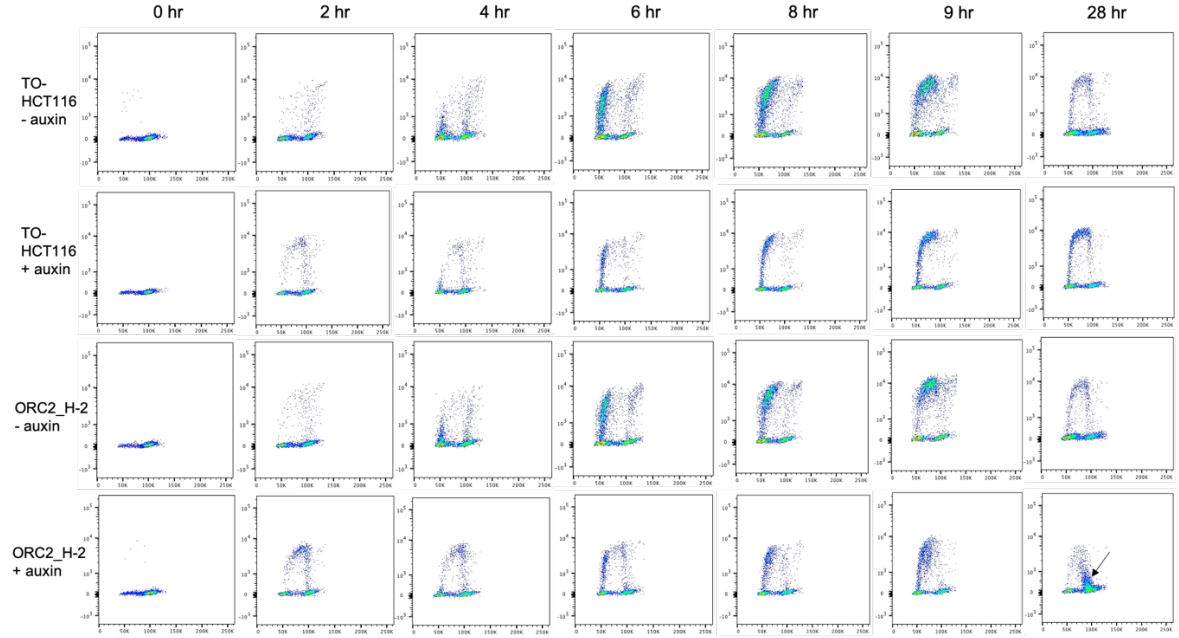
0 hr
2 hr
4 hr
6 hr
8 hr
9 hr
28 hr
TO-HCT116 - auxin
TO-HCT116 + auxin
ORC2_H-2 - auxin
ORC2_H-2 + auxin

Figure 4-3. Cell cycle profile of TO-HCT116 and ORC2_H-2 cells after thymidine-nocodazole arrest and release. (a) Experimental scheme of TO-HCT116 and ORC2_H-2 cells synchronization by a thymidine-nocodazole block. (b) Flow cytometry analysis of FxCycle™ Violet stained cells (singlets) released from nocodazole in indicated treatment. DNA content was detected with a 405/407 nm laser and collected in the 450/50 BP filter at a linear range. (c) Cell cycle profiles of TO-HCT116 and ORC2_H-2 cells released from a thymidine-nocodazole block in indicated treatment. Cells were pulse labeled with 10 μM EdU for 2 hours before harvesting at different time points. The x axis indicates DNA content, and the y axis represents to EdU incorporation.

a.

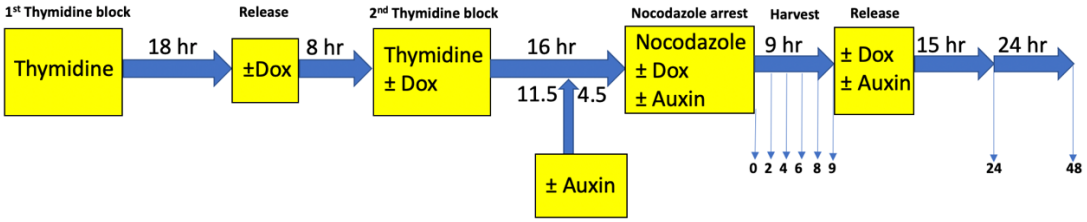
1st Thymidine block
Thymidine
18 hr
Release
±Dox
8 hr
2nd Thymidine block
Thymidine
± Dox
16 hr
11.5
4.5
± Auxin
Nocodazole arrest
Nocodazole
± Dox
± Auxin
Harvest
9 hr
0 2 4 6 8 9
Release
± Dox
± Auxin
15 hr
24 hr
24
48

b.

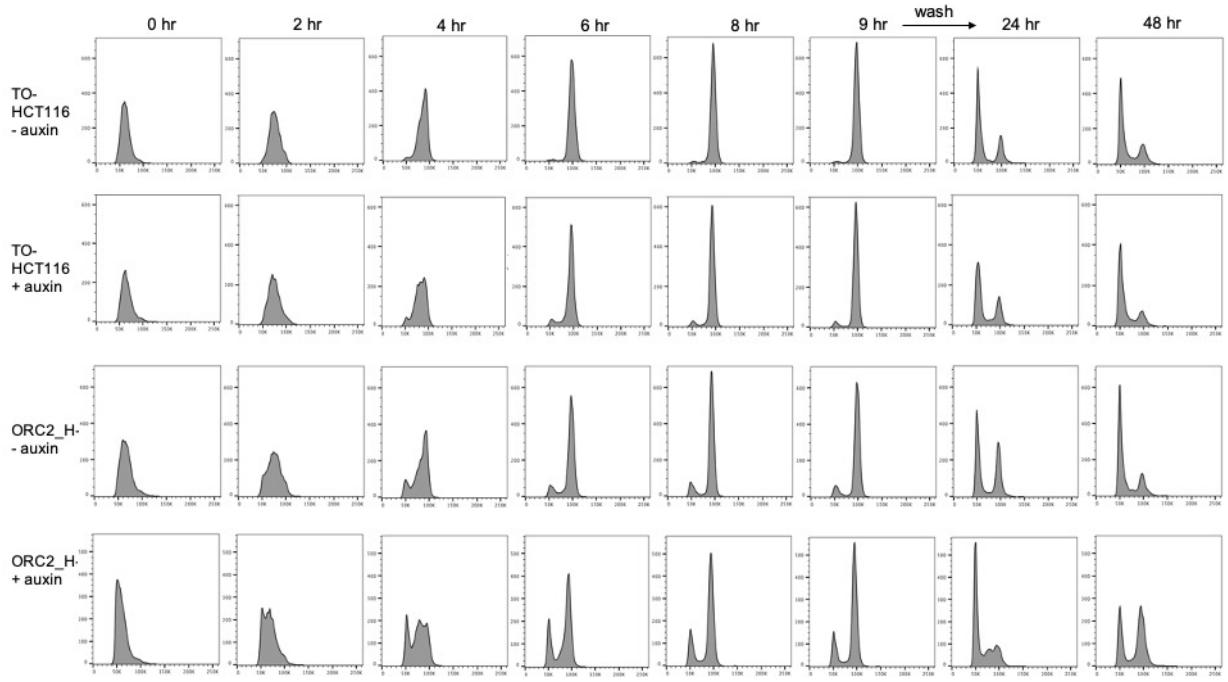
0 hr
2 hr
4 hr
6 hr
8 hr
9 hr
wash
24 hr
48 hr
TO-HCT116 - auxin
TO-HCT116 + auxin
ORC2_H- auxin
ORC2_H- + auxin

c.

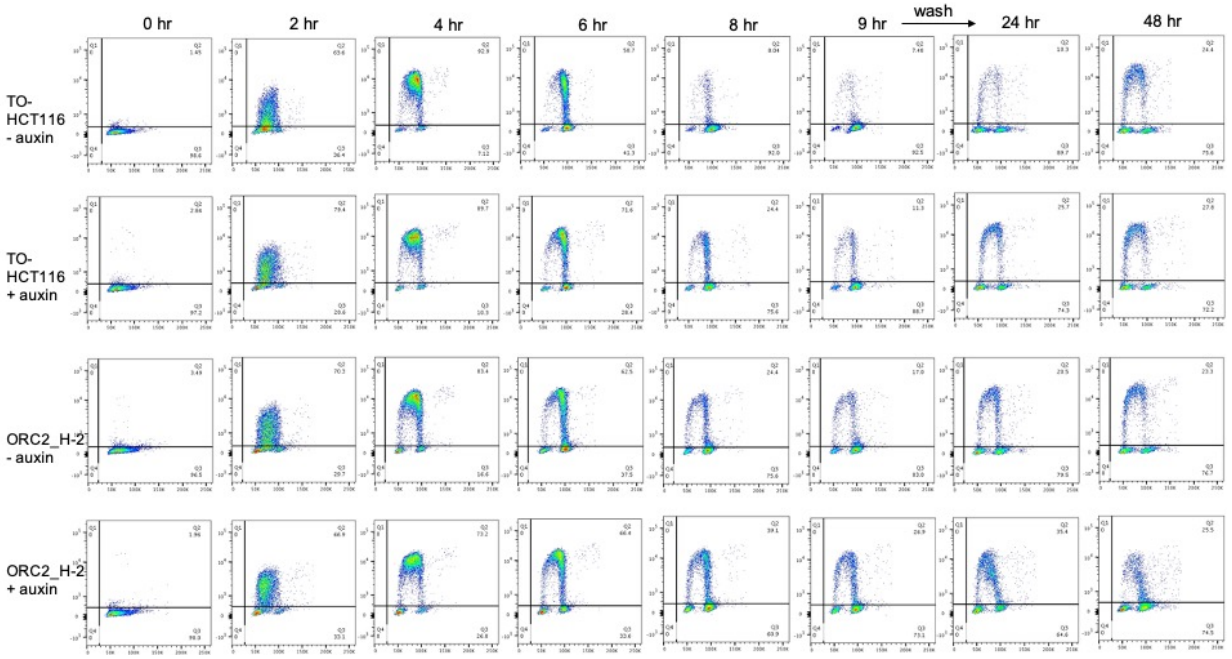
0 hr
2 hr
4 hr
6 hr
8 hr
9 hr
wash
24 hr
48 hr
TO-HCT116 - auxin
TO-HCT116 + auxin
ORC2_H-2 - auxin
ORC2_H-2 + auxin

Figure 4-4. Cell cycle profile of TO-HCT116 and C2 after a double thymidine block and released into nocodazole. (a) Experimental scheme of TO-HCT116 and ORC2_H-2 cells synchronization by a thymidine-nocodazole block and released into medium containing nocodazole. (b) Flow cytometry analysis of FxCycle™ Violet stained cells (singlets) released from thymidine block and nocodazole block in indicated treatment. DNA content was detected with a 405/407 nm laser and collected in the 450/50 BP filter at a linear range. (c) Cells were pulse labeled with 10μM EdU for 2 hours before harvesting at different time points. Cells stained for EdU-DNA and total DNA are subjected to dual-parameter processing (total DNA vs EdU). The x axis indicates DNA content, and the y axis represents EdU incorporation. The horizontal line divides the cell population with or without EdU incorporation.

4. Rapid ORC2 depletion in CMV-mAID-ORC2^{gr} cell lines

The LTR-retroviral system used above expressed mAID-ORC2^{gr} about 5-10% of the endogenous ORC2 level, and the anti-mAID antibody was not sensitive enough to detect the protein. We wanted to construct cell lines that express the exogenous protein at the endogenous level and see if the knockdown results in similar phenotypes. I cloned the mAID-ORC2^{gr} sequence into the lentiviral vector that express from the CMV promoter. Next, the viral vector encoding CMV-mAID-ORC2^{gr} or CMV-ORC3^{gr}-mAID-mCherry was transduced into TO-U2OS TRex and the TO-HCT116 cell lines. U2OS TRex has an FRT site in the genome which I inserted the OsTIR1-V5 gene into. After I co-transfected the U2OS TRex cells with pcDNA5/FRT/TO plasmid encoding OsTIR1-V5 and FLP recombinase into the cells and selected with puromycin, every cell expressed OsTIR1 at the same locus under control of the Tet repressor. Therefore, Tet-OsTIR1 U2OS TRex and Tet-OsTIR1 HCT116 will be very similar to work with in terms of experimental procedures. Next, endogenous ORC2 was targeted by using sgRNA ORC2-1 (targeting 525aa) via the CRISPR/Cas9 technique. Four new cell lines were obtained following single cell sorting after targeting endogenous ORC2 by sgRNA. C3 and C4 were derived from TO-HCT116, and C5 and C6 were derived from TO-U2OS TRex cell line **(Figure 4-5a)**.

The expression levels of mAID-ORC2^{gr} in C3, C4, C5, and C6 cell lines are similar to the protein level of endogenous ORC2 **(Figure 4-5a)**. I went on to investigate whether the C4 cell line had the same phenotypes as ORC2_H-2 cell line upon adding doxycycline and auxin. After incubating C4 cells with doxycycline and different concentration of auxin for 48 hours, I harvested the cells for western blot and flow cytometry analysis **(Figure 4-5b,c)**. The cell cycle profile of C4 cells showed that after 48 hours of doxycycline and auxin treatment, slightly more cells are at the 4C peak and less cells are in S phase. There was no obvious cell cycle profile difference observed in the 250, 500 or 1000 μM auxin-treated cells. The level of residual mAID-ORC2^{gr} protein after knockdown in C4 cells was higher than mAID-ORC2^{gr} expression level in the untreated ORC2_H-2 cells **(Figure 4-5a,b)**. Because auxin-induced degradation was not 100 % efficient, the residual mAID-ORC2^{gr} in C4 cells, which was about 15% of endogenous ORC2 level, was enough to support cell growth, and therefore there was no obvious phenotype or

abnormal cell cycle profile observed. I concluded that lentiviral expression system is not an ideal system for my study.

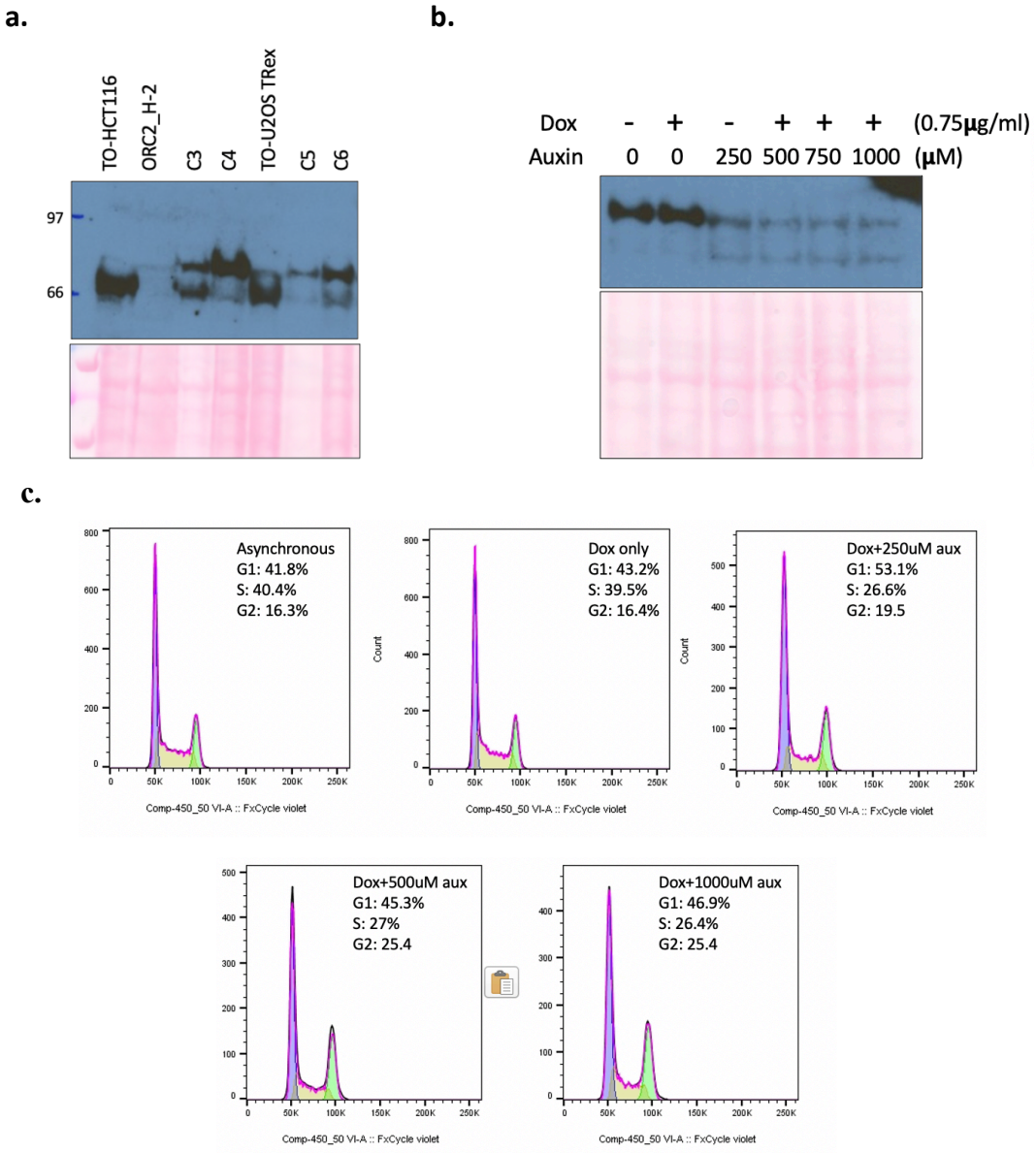

Figure 4-5. Detection of mAID-ORC2^{gr} fusion protein and cell cycle profile of C4 after auxin treatment. (a) New endogenous ORC2 knockout and mAID-ORC2^{gr} expressed cell lines derived from TO-HCT116 and TO-U2OS TRex cell line. Cells were pelleted and boiled in Laemmli buffer and followed by western blot to detect ORC2 protein, both endogenous and mAID-ORC2^{gr}. (b) Cells were incubated with 0.75µ g/ml doxycycline and indicated amount of auxin. After 48 hours, cells were pelleted, boiled in Laemmli buffer, and followed by western blot to detect mAID-ORC2^{gr} using antibody against ORC2. (c) C4 cells were treated with different concentration of auxin and doxycycline for 48 hr, stained with propidium iodide and analyzed by flow cytometry. Two peaks indicate 2c and 4c DNA content. Percentage of cell population in each phase was calculated with FlowJo software by the Watson univariate model.

5. CRISPR/Cas9 depletion of endogenous ORC3 in TO-HCT116 and TO-U2OS TRex cell lines

ORC3 forms a stable complex with ORC2, and also directly interacts with heterochromatin protein 1 α subunit (HP1α) via the N-terminal coiled-coil region and the MIR. To establish rapid ORC3 knockdown cell line, I first tested the targeting effects of two sgRNA, ORC3_123 and ORC3_256 (targeting ORC3 123 aa and 256 aa respectively). GFP depletion assay showed that both sgRNAs targeting in TO-HCT116 and TO-U2OS TRex cell lines affect cell proliferation **(Figure 4-6a,e)**. Expression of CMV-ORC3^{gr}-mAID-mCherry that are resistant to ORC3_123 and ORC3_256 sgRNAs in both cell lines rescued or partially rescued the negative selection phenotype **(Figure 4-6b,f)**. The level of ORC3^{gr}-mAID-mCherry fusion protein was similar or higher than the endogenous ORC3. The effects of sgRNAs target could be rescued by ORC3^{gr}-mAID-mCherry in both TO-HCT116_ ORC3^{gr}-mAID-mCherry and U2OS_mAID-ORC2^{gr} cell lines confirming sgRNA target specificity **(Figure 4-6a,b,e,f)**.

Previous studies in our lab have shown that ORC3 interacts with HP1α via the coiled-coil domain at the N-terminus (45-65aa) and the MOD1-interacting region (MIR;213-218aa). The ORC3 MIR domain is composed of consensus sequence PXVXL that is highly conserved in animals and plants. Deleting either region will not abolish the interaction between ORC3 and HP1α but the mutants fail to localize ORC3 to the heterochromatin foci and therefore both regions are essential *in vivo*. To investigate whether these two regions are essential for cell survival, ORC3^{gr}(ΔMIR)-mAID-mCherry or ORC3^{gr}(Δcoiled-coil)-mAID-mCherry that are resistant to both ORC3_123 and ORC3_256 sgRNAs were expressed in both cell lines via lentiviral transduction. The result showed that both ORC3^{gr}(ΔMIR)-mAID-mCherry or ORC3 ^{gr}(Δcoiled-coil) could not compliment the ORC3 knockout **(Figure 4-6c,d,g)**. In other words, the MIR domain and the coiled-coil domain are both essential for cell proliferation and survival. Since HP1α was shown to interact independently with each of these two domains, I preliminarily conclude that HP1α interaction with both domains of ORC3 is essential.

Next, I tested if the ORC3^{gr}-mAID-mCherry fusion protein will be degraded upon adding doxycycline and auxin. The western blot result showed that the expression level of ORC3^{gr}-

mAID-mCherry in TO- HCT116 was similar to the endogenous ORC3, and upon adding auxin, ORC3^{gr}-mAID-mCherry can be degraded **(Figure 4-7)**. On the other hand, the level of ORC3^{gr}-mAID-mCherry in the TO-U2OS TRex cell line was much higher than the endogenous ORC3 and was not degraded efficiently after auxin treatment. The reason why it was not knockdown efficiently could be because the level of OsTIR1-V5 expressed in U2OS TRex cells from the FRT locus was too low and cannot degrade that huge amount of mAID-tagged protein. In summary, the TO-U2OS TRex cell line is not an idea system for future study.

In addition, as mentioned in part 4, because lentiviral expression of mAID-ORC2 or ORC3 wouldn't work well in the auxin depletion system due to its high expression level, this TO-HCT116_ORC3^{gr}-mAID-mCherry cells were not suitable for knockdown study. To efficiently knockdown ORC3 by auxin, the ORC3^{gr}-mAID should be expressed under a weak promoter, and retroviral LTR expression system provides a better way for generating the auxin-induced knockdown cell line.

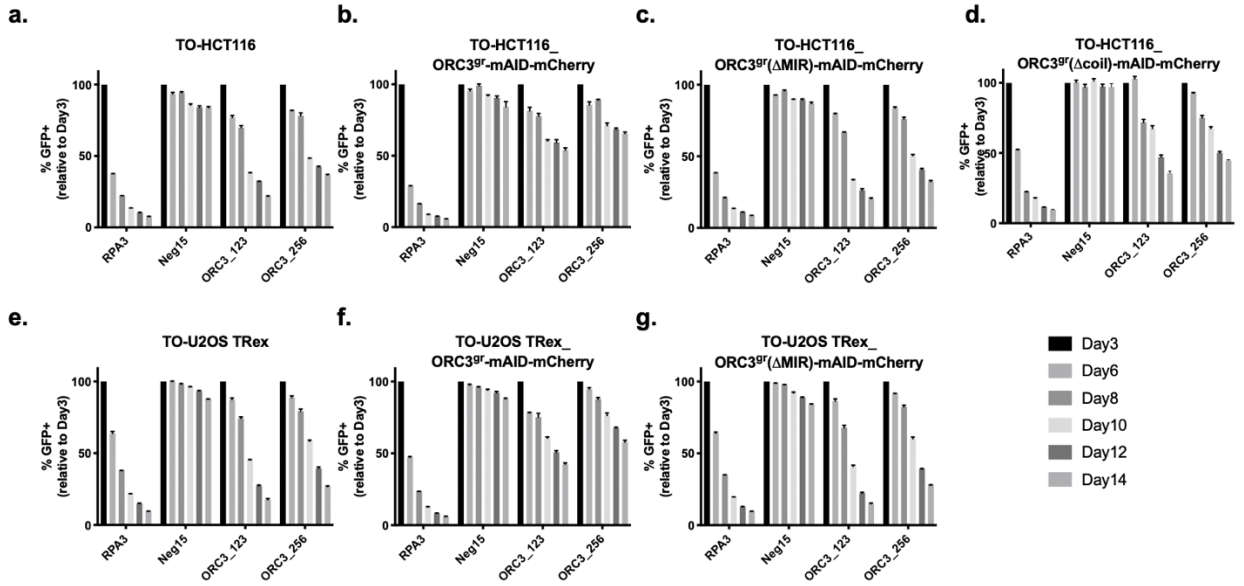

Figure 4-6. ORC3^{gr}-mAID-mCherry fusion protein partially rescues endogenous ORC3 knockout by sgRNA but not ORC3^{gr} (ΔMIR)-mAID-mCherry or ORC3^{gr} (Δcoiled-coil)-mAID-mCherry protein. Negative-selection time course assay that plots the percentage of GFP-positive cells over time following transduction with the indicated sgRNAs with Cas9. Experiments were performed in seven cell lines. The GFP-positive percentage is normalized to the day3 measurement. n = 3. Error bars, mean ± SEM.

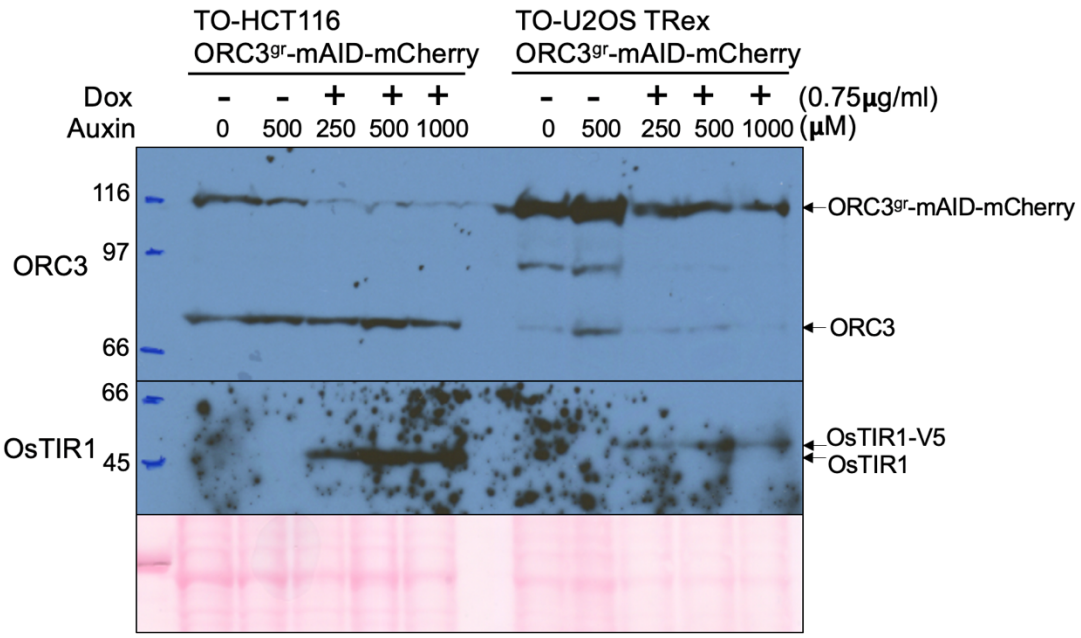

Figure 4-7. ORC3^{gr}-mAID-mCherry can be knockdown upon adding auxin and doxycycline in TO-HCT116 but not in TO-U2OS TRex cell line. Cells were incubated with 0.75 µg/ml doxycycline and indicated concentration of auxin for 26 hours. Cells were then pelleted, boiled in Laemmli buffer, and followed by western blot to detect endogenous ORC3, ORC3^{gr}-mAID-mCherry, OsTIR1 in TO-HCT116, or OsTIR-V5 in TO-U2OS TRex cells using antibody against ORC3 or OsTIR1.

Chapter Five- Discussion and future directions

ORC serves as one of the most important components in DNA replication initiation, acting as a platform to recruit other factors to form pre-RC complexes at origins after exit from mitosis and into G1 phase. In contrast to yeast ORC that remains as a complex binding to the chromatin during the cell division cycle, human ORC subunits dissociate from chromatin while cells progress through S phase (Méndez et al., 2002; Ohta et al., 2003; Siddiqui and Stillman, 2007). In human, ORC subunits are found at centrosomes, centromeres, kinetochores, the cytokinesis cleavage furrow and at heterochromatin foci. However, besides its function in regulating centriole duplication, its mechanism or functions in other locations has not been fully uncovered. The auxin-induced, rapid degradation system has enabled us to deplete ORC2 in 4 hr in synchronized cells to study the outcome. We showed that ORC2 depletion in human HCT116 cells resulted in replication defects, G2 arrest with DNA damage checkpoint activation, aberrant mitosis, and heterochromatin decompaction. We suggested that besides the essential function in replication initiation, ORC2 is also required for normal mitosis progression and nuclear organization. In this section I will discuss about the rapid degradation cell lines, the phenotypes linked to ORC2 depletion, and propose some future experiments to investigate the function of ORC.

1. What happened to the prolonged-arrested cells in auxin-containing medium?

From the cell synchronization and release experiments I showed that when ORC2 was depleted in cells, some of the cells arrested in G1, some cells progressed into an extended S phase, and the rest arrested in late S/G2 phase. In addition, in the time-lapse imaging experiments I found that only a small number of cells entered a prolonged mitosis and ended up progressing in apoptosis. The remaining cells seemed to arrest in interphase for the duration of the experiment. During treatment of ORC2 mutant cells with doxycycline and auxin to deplete mAID-ORC2^{gr} I noticed that most of the interphase cells remained attached to the culture dish even on the fifth day of treatment and no significant cell death was observed. At the same time,

cells were counted every day and the cell number remained unchanged **(Figure 3-20e)**. This observation raised the interesting question of why the ORC2 depleted cells did not die, how long could the cells remain in the apparently arrested state, and were those cells senescent or quiescent? Follow up experiments on such cells should be completed.

In addition to the replication senescence caused by shortening of telomeres, stress-induced premature senescence (SIPS) can be caused by DNA damage or prolonged cell cycle arrest (Hayashi et al., 2012; Lou and Chen, 2006; Sikora et al., 2016). Senescent cells will become enlarged and flattened morphologically, undergo chromatin remodeling and metabolic reprogramming, exhibit DNA damage response factors foci, and also secrete signaling molecules to the cells nearby (Herranz and Gil, 2018; Lou and Chen, 2006; Sikora et al., 2016). In one experiment I cultured various cell lines in the medium containing doxycycline and auxin for different lengths of time and observed them using phase contrast light microscopy. After culturing ORC2_H-2 cells with doxycycline and auxin for 72 hr, more mitotic cells were found, but in addition to these rounded mitotic cells, the morphology of adherent cells became elongated and some cells showed long and thin extensions similar to neuronal axons **(Figure 5-1)**. At 96 hr, a few polynucleated cells were found, a few cells were enlarged and flattened with an irregular shape. At 120 hr, more morphologically abnormal cells were observed. Based on the phenotypes observed, it is possible that DNA damage and replication defects in ORC2-depleted cells triggered irreversible cell cycle arrest, also known as cellular senescence.

To test if ORC2-depleted cells became senescence, the activity of senescence-associated β-galactosidase (SA-β-gal) in auxin-treated ORC2 mutant cells could be measured, since SA-β-gal is not present in quiescent or non-senescent immortal cells. The auxin and doxycycline could be removed from the culture medium to determine if the cells re-entered into the cell cycle and continued to proliferate. If the cells already had become senescence, re-expressing ORC2 in the cells should not facilitate re-entry into the cell cycle. In contrast, if cells enter into quiescence phase, removing auxin might rescue the cell cycle arrest.

2. How to further investigate the function of ORC in mitosis?

In the time-lapse live imaging experiment of TO-HCT116_H2B-mCherry and ORC2_H-2_H2B-mCherry cell lines, I found that a small number of cells adapted to the G2 checkpoint function and thus, had entered into mitosis **(Figure 3-32e)**. However, those cells either entered apoptosis after prolonged metaphase, or showed cytokinesis defects and resulted in polyploid cells. In another live imaging experiment taken with differential interference contrast (DIC) microscopy, rounded-mitotic ORC2-depleted cells were monitored for several hours, and eventually the cells entered into apoptosis or exited mitosis without cytokinesis and became multi-nuclear. It has been shown that when treating cells with bleomycin to induce DNA damage, cells that escaped from the G2 checkpoint entered mitosis with various phenotypes including chromatin decondensation, elongated spindles, kinetochore alignment defect, and the lack of cells in anaphase and telophase (Varmark et al., 2009). Cells with DNA damage have high rates of cytokinesis failure, but if those damaged cells completed cytokinesis, they died at higher rates than the cells that failed to complete cytokinesis (Varmark et al., 2009). In the case of ORC2 depleted cells, aberrant mitosis can be explained by various reasons.

DNA damage generated from incomplete replication might led to cytokinesis failure, resulting in polyploidy and multi-nucleated cells. In addition, ORC2 might be required for proper kinetochore-microtubule alignment and chromatid segregation during mitosis, as we saw persistent of lagging chromosomes at the metaphase plate. Lagging chromosomes are formed mostly because of merotelic attachment of the kinetochore and the spindles, which are often found in multipolar cells and cells with abnormal number of centrosomes (Cimini et al., 2004, 2003; Gregan et al., 2011). In addition, micronuclei, which could be the result of the segregation of the lagging chromosome (Cimini et al., 2002), were also observed in auxin-treated ORC2-depleted cells. Since ORC2 localize to centrosomes and kinetochore/centromere during mitosis, and depletion of ORC2 via siRNA knockdown led to a subpopulation with mitotic defects and multiple centrosomes (Prasanth et al., 2004), it is possible that ORC2 is involved in regulating centrosome number, cellular polarity and spindle attachment although the mechanism has yet to be uncovered. In yeast, *Xenopus*, *Drosophila* and human cells, the ring-shaped cohesin which links sister chromatids together play an important role in chromosome segregation during

mitosis, is loaded onto chromatin starting from G1 throughout S phase by Scc2 and Scc4 proteins which bind stably to the chromatin (Ciosk et al., 2000; Gillespie and Hirano, 2004; Guacci et al., 1997; Lengronne et al., 2004; Losada et al., 1998; Michaelis et al., 1997; Misulovin et al., 2008; Takahashi et al., 2004). In *Xenopus*, pre-RCs and DDK recruit Scc2 and Scc4 to bind to chromatin, which then facilitate the loading of cohesin (Gillespie and Hirano, 2004; Takahashi et al., 2008, 2004; Walter et al., 2007). Moreover, in *Drosophila*, genome-wide chromatin immunoprecipitation studies showed that ORC colocalizes with cohesin, suggesting that ORC and pre-RC might regulate the loading of cohesin, although the mechanism is not yet clear (MacAlpine et al., 2009). In human, it has been shown that during DNA replication cohesin binds to MCM proteins and is enriched at DNA origins to stabilize the chromatin loops, and MCM2-7 complex is essential for loading cohesin during S phase (Guillou et al., 2010; Zheng et al., 2018). These studies suggested that ORC2 might play a direct or indirect role in regulating the cohesion between sister chromatids.

To further dissect the function of ORC2 in mitosis, the first thing we could try is to isolate the doxycycline and auxin-treated ORC2_H-2 mitotic cells and remove auxin from the medium to see if mitosis can then progress smoothly. The Proximity-dependent biotin identification (BioID) method followed by mass spectrometry also provides a good way to decipher the pathways and regulatory networks ORC2 participates in since it is able to capture weak or transient interaction (Roux et al., 2013, 2012). To improve the IP-MS result from previous experiments, cells collected for BioID analysis should be synchronized and then released to harvest multiple timepoints in cell cycle. Since depleting ORC2 in mitosis did not affect mitosis progression **(Figure 4-3)**, timepoints before mitosis might be crucial for uncovering the mitotic function of ORC2.

Once identified the protein-protein interactions by BioID-MS, it should be possible to validate the direct protein-protein interactions using bimolecular fluorescence molecular complementation (BiFC) (Kerppola, 2009, 2008; Lin et al., 2010) by fusing complementary fluorescent protein (FC) fragments to ORC2 and the interacting protein and monitor the interactions using time-lapse microscopy. Since BiFC is irreversible, once the complementary FC fragments interact, they will be covalently associated with each other. Therefore, if

monitoring temporal dynamics of ORC2 and the interacting proteins is needed, perform fluorescence resonance energy transfer (FRET) experiments can be performed to measure cellular activities.

It would also be interesting to know if the domain required for replication initiation can be separated from its mitotic function. Based on the tiling-sgRNA CRISPR screens, in addition to the AAA+ and WHD regions, ORC2 amino acid sequence near the 50 aa and 200 aa also showed significant negative selection phenotype. The amino-terminal 234 amino acids of ORC2 are likely to form intrinsically disordered regions within which there are essential regions **(Fig. 3-14)**. To determine the essential or sufficient regions for mitotic functions, different ORC2 fragments could be overexpressed in ORC2 depleted cells to find out deletion which region leads to the highest rate of mitotic arrest cells.

3. The possible role of ORC in heterochromatin organization.

In human, ORC subunits localize to pericentric heterochromatin foci, depletion of ORC subunits also results in defects in HP1 protein localization. Using small interfering RNA (siRNA) to target ORC1 or ORC5 in HeLa cells caused HP1 to localize to only the periphery of the nucleoli and also led to clustering of centromeres (Prasanth et al., 2010). When targeting ORC2 or ORC3 subunits with siRNA, HP1 protein distribution in HeLa cells became homogeneous instead of foci, and DNA FISH experiment also showed decompaction of chromosome 9 satellite region in those ORC knockdown cells. In ORC2_H-2 cells, depletion of ORC2 by auxin-induced degradation system resulted in nuclear enlargement and decondensation of heterochromatin protein HP1 foci and centromeric protein CENP-C foci (Chou et al., 2021). We suggested that ORC subunits are important for heterochromatin and nuclear organization, but the regulatory mechanisms are yet to be investigated.

In the ORC2 IP-MS experiment, ORCA protein was strongly enriched with anti-ORC2 antibody (Shen et al., 2010). ORCA interacts with ORC complex and stabilize its binding to the chromatin and also shows similar cell cycle dynamics and distribution especially to ORC2 (Shen et al., 2010). ORC-ORCA complex interacts with histone hallmarks H3K9me3, H3K27me3, and H4K20me3 located at the silenced heterochromatic regions (Bartke et al., 2010; Vermeulen et al., 2010). The ORC-ORCA complex binds to G9a (EHMT2) and GLP (EHMT1) histone methyltransferases that are responsible for di-methylation of H3K9, and ORCA and ORC1 protein bind directly to SUV39H1 which is responsible for establishing H3K9me3 and recruiting HP1 to heterochromatin (Fritsch et al., 2010; Giri et al., 2015; Rea et al., 2000; Robin et al., 2007; Shinkai and Tachibana, 2011; Stewart et al., 2005; Tachibana et al., 2005). Depletion of ORCA by siRNA knockdown led to significant reduction of H3K9me3 marks at the satellite repeats at the heterochromatic region (Giri et al., 2015). On the other hand, siRNA mediated knockdown of ORC didn't affect H3K9me3 marks at the heterochromatin but disrupted localization of HP1 to the heterochromatin foci (Prasanth et al., 2010). Together these studies support the role of ORC in recruiting HP1 to the heterochromatin and can potentially stabilize the structure.

HP1 is also involved in DNA damage repair and is phosphorylated in response to DNA damage (Baldeyron et al., 2011; Dinant and Luijsterburg, 2009; Luijsterburg et al., 2009; Quivy et al., 2008; Zarebski et al., 2009). When double strand break (DSB) occurs in cells, a complex consists of KAP-1, HP1 and SUV39H1 is loaded and enriched at the chromatin to mediate tri-methylation of H3K9 (Ayrapetov et al., 2014). This chromatin-associated complex leads to spreading of H3K9me3 and activation of Tip60 histone acetyltransferase, which can then bind to and activate ATM kinase (Ayrapetov et al., 2014; Sun et al., 2005). In ORC2_H-2 cells, phosphorylation of ATM(S1981), CHK1(S345), ATR(T1989) and CHK2(T68) were detected by western blot or immunofluorescent (IF) staining after 48 hr of doxycycline and auxin treatment. IF staining of HP1 and CENP-C showed more diffused and enlarged pattern rather than discrete foci. It will be interesting to find out whether those DNA damage protein foci colocalize with HP1 distribution in nucleus and where they located in the genome after ORC2 depletion. It has been shown that during S/G2 phase, double strand break (DSB) can relocate to the periphery of heterochromatin (Tsouroula et al., 2016). If HP1 colocalize with DNA damage response proteins,

the diffusing HP1 IF staining phenotype we observed after ORC2 depletion might be due to HP1 detaching from heterochromatin in order to enrich at the DNA damage sites, regardless of whether the damage sites are at heterochromatic or not. To study the relationship between ORC2 knockdown and HP1 at the DNA damage sites, we should test whether HP1 is phosphorylated in ORC2 depleted cells. Next, IF staining can be performed to analyze the colocalization of HP1 and the DNA damage response proteins. Finally, Chromatin Immunoprecipitation (ChIP)-Seq experiment can be done to identify the genome-wide binding sites of DNA damage response proteins and HP1 protein after ORC2 depletion in cells.

If HP1 is recruited to DNA damage foci following ORC2 depletion, this still does not explain why the centromere protein CENP-C foci were enlarged and showed more intense signal after ORC2 depletion. When cells encounter DNA damage, heterochromatin is decondensed or relaxed to facilitate DNA damage repair process in certain chromosomal regions (Chiolo et al., 2011), but no obvious change of heterochromatic histone marks such as H3K9me3 or H4K20me3 was found, suggesting that the basic characteristic of heterochromatin is not altered (Natale et al., 2017; Tsouroula et al., 2016). For example, the ATM-dependent KAP-1 activation led to chromatin relaxation following DSB formation (Ziv et al., 2006). Similarly, when ORC2 is depleted by siRNA knockdown, HP1 is removed from heterochromatin foci and showed homogeneous distribution, while H3K9me3 level was unaffected at the heterochromatin region (Prasanth et al., 2010). To assess the level of heterochromatin decondensation, we could perform Assay for Transposase Accessible Chromatin with high-throughput sequencing (ATAC-seq) to detect genome-wide chromatin accessibility of ORC2-depleted cells. This could result in a better understanding about the how ORC2 affects heterochromatin organization and where in the genome it has the largest effect. Moreover, it might also answer our question of why the centromere protein was clustered and showed an intense signal, and why the volume of the nucleus increased significantly after ORC2 depletion (Chou et al., 2021; Prasanth et al., 2010).

4. Concluding remarks

I have studied the outcome of ORC2 depletion in human HCT116 cells and showed that ORC is essential for initiation of DNA replication, progression of mitosis, and is also involved in heterochromatin organization. Since human ORC subunits not only localize to DNA replication origins, but also to pericentromeric heterochromatin, centrosomes, kinetochore/ centromere, cleavage furrow (Bernal and Venkitaraman, 2011; Chesnokov et al., 2009, 2003; Gillingham and Munro, 2000; Hemerly et al., 2009; Pflumm and Botchan, 2001; Popova et al., 2018; Prasanth et al., 2010, 2004, 2002; Shimada and Gasser, 2007) it is not surprising that it has so many other functions in the chromosome cycle. With the success of tiling-sgRNA CRISPR screens and the auxin-induced rapid degradation cell line, this study has provided a comprehensive way to study protein functions, especially cell cycle protein since cells can be arrested first and then had protein of interest degraded in a short time. Although most regulating mechanisms remain unsolved, it has provided us with directions to look into more deeply in the future.

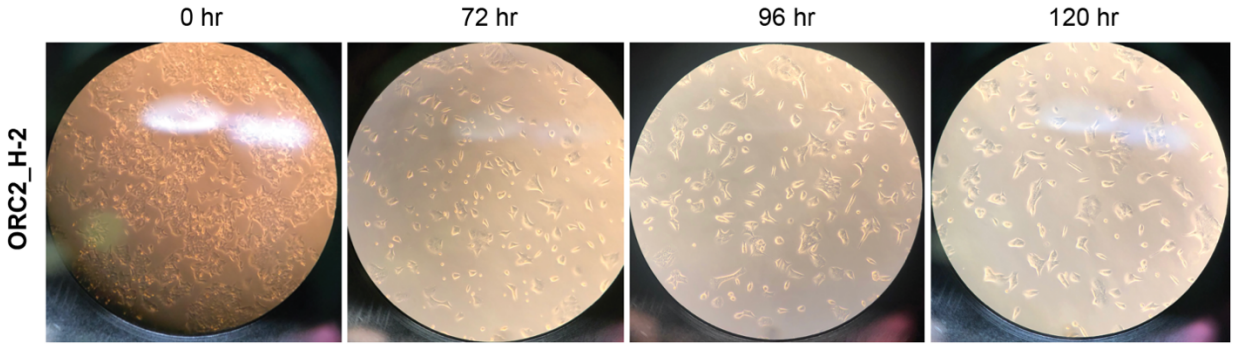

Figure 5-1. ORC2_H-2 cells display abnormal morphologies after growing in medium containing doxycycline and auxin for 0, 72, 96, and 120 hr. Cells were observed with phase contrast light microscopy with 20x magnification.

Cited literatures

Aagaard L, Laible G, Selenko P, Schmid M, Dorn R, Schotta G, Kuhfittig S, Wolf A, Lebersorger A, B.Singh P, Jenuwein GR and T. 1999. Functional mammalian homologues of the Drosophila PEV-modifier Su(var)3-9 encode centromere-associated proteins which complex with the heterochromatin component M31. *Embo J* **18**:1923–1938. doi:10.1093/emboj/18.7.1923

Aasland R, Gibson TJ, Stewart AF. 1995. The PHD finger: Implications for chromatin-mediated transcriptional regulation. *Trends Biochem Sci* **20**:56–59. doi:10.1016/s0968-0004(00)88957-4

Abrieu A, Kahana JA, Wood KW, Cleveland DW. 2000. CENP-E as an Essential Component of the Mitotic Checkpoint In Vitro. *Cell* **102**:817–826. doi:10.1016/s0092-8674(00)00070-2

Adamczak R, Porollo A, Meller J. 2004. Accurate prediction of solvent accessibility using neural networks-based regression. *Proteins Struct Funct Bioinform* **56**:753–767. doi:10.1002/prot.20176

Adelmann CH, Wang T, Sabatini DM, Lander ES. 2018. Cancer Driver Genes, Methods and Protocols. *Methods Mol Biology* **1907**:125–136. doi:10.1007/978-1-4939-8967-6_10

Akhmetova K, Balasov M, Huijbregts RPH, Chesnokov I. 2014. Functional insight into the role of Orc6 in septin complex filament formation in Drosophila. *Mol Biol Cell* **26**:15–28. doi:10.1091/mbc.e14-02-0734

Allshire RC, Madhani HD. 2018. Ten principles of heterochromatin formation and function. *Nat Rev Mol Cell Bio* **19**:229–244. doi:10.1038/nrm.2017.119

Amin A, Hei CM, Liang C. 2019. DNA Replication-Initiation Proteins in Eukaryotic Cells. *Biomed J Sci Technical Res* **23**. doi:10.26717/bjstr.2019.23.003830

Andrews PA, Iossifov I, Kendall J, Marks S, Muthuswamy L, Wang Z, Levy D, Wigler M. 2016. MUMdex: MUM-based structural variation detection. *Biorxiv* 078261. doi:10.1101/078261

Aparicio OM, Weinstein DM, Bell SP. 1997. Components and Dynamics of DNA Replication Complexes in S. cerevisiae: Redistribution of MCM Proteins and Cdc45p during S Phase. *Cell* **91**:59–69. doi:10.1016/s0092-8674(01)80009-x

Araki H. 2016. Elucidating the DDK-dependent step in replication initiation. *Embo J* **35**:907–8. doi:10.15252/embj.201694227

Araki H. 2011. Initiation of chromosomal DNA replication in eukaryotic cells; contribution of yeast genetics to the elucidation. *Genes & Genetic Systems* **86**:141–149. doi:10.1266/ggs.86.141

Araki H, Hirai K, Li Y, Tanaka T, Muramatsu S, Tanaka S. 2009. CDK-dependent assembly of replication proteins at the initiation step of chromosomal DNA replication. *Faseb J* **23**:78.3-78.3. doi:10.1096/fasebj.23.1_supplement.78.3

Araki H, Leem SH, Phongdara A, Sugino A. 1995. Dpb11, which interacts with DNA polymerase II(epsilon) in Saccharomyces cerevisiae, has a dual role in S-phase progression and at a cell cycle checkpoint. *Proc Natl Acad Sci USA* **92**:11791–11795. doi:10.1073/pnas.92.25.11791

Ashkenazy H, Abadi S, Martz E, Chay O, Mayrose I, Pupko T, Ben-Tal N. 2016. ConSurf 2016: an improved methodology to estimate and visualize evolutionary conservation in macromolecules. *Nucleic Acids Res* **44**:W344–W350. doi:10.1093/nar/gkw408

Atanasiu C, Deng Z, Wiedmer A, Norseen J, Lieberman PM. 2006. ORC binding to TRF2 stimulates OriP replication. *Embo Rep* **7**:716–721. doi:10.1038/sj.embor.7400730

Avdic V, Zhang P, Lanouette S, Groulx A, Tremblay V, Brunzelle J, Couture J-F. 2011. Structural and Biochemical Insights into MLL1 Core Complex Assembly. *Structure* **19**:101–108. doi:10.1016/j.str.2010.09.022

Ayrapetov MK, Gursoy-Yuzugullu O, Xu C, Xu Y, Price BD. 2014. DNA double-strand breaks promote methylation of histone H3 on lysine 9 and transient formation of repressive chromatin. *Proc National Acad Sci* **111**:9169–9174. doi:10.1073/pnas.1403565111

Balasov M, Akhmetova K, Chesnokov I. 2020. Humanized Drosophila Model of the Meier-Gorlin Syndrome Reveals Conserved and Divergent Features of the Orc6 Protein. *Genetics* genetics.303698.2020. doi:10.1534/genetics.120.303698

Balasov M, Akhmetova K, Chesnokov I. 2015. Drosophila model of Meier-Gorlin syndrome based on the mutation in a conserved C-Terminal domain of Orc6: Drosophila model of Meier-Gorlin syndrome. *Am J Med Genet A* **167**:2533–2540. doi:10.1002/ajmg.a.37214

Balasov M, Huijbregts RPH, Chesnokov I. 2009. Functional analysis of an Orc6 mutant in Drosophila. *Proc National Acad Sci* **106**:10672–10677. doi:10.1073/pnas.0902670106

Balasov M, Huijbregts RPH, Chesnokov I. 2007. Role of the Orc6 Protein in Origin Recognition Complex-Dependent DNA Binding and Replication in Drosophila melanogaster ▿ . *Mol Cell Biol* **27**:3143–3153. doi:10.1128/mcb.02382-06

Baldeyron C, Soria G, Roche D, Cook AJL, Almouzni G. 2011. HP1α recruitment to DNA damage by p150CAF-1 promotes homologous recombination repair. *J Cell Biology* **193**:81–95. doi:10.1083/jcb.201101030

Ballabeni A, Zamponi R, Moore JK, Helin K, Kirschner MW. 2013. Geminin deploys multiple mechanisms to regulate Cdt1 before cell division thus ensuring the proper execution of DNA replication. *Proc National Acad Sci* **110**:E2848–E2853. doi:10.1073/pnas.1310677110

Bannister AJ, Zegerman P, Partridge JF, Miska EA, Thomas JO, Allshire RC, Kouzarides T. 2001. Selective recognition of methylated lysine 9 on histone H3 by the HP1 chromo domain. *Nature* **410**:120–124. doi:10.1038/35065138

Bartke T, Vermeulen M, Xhemalce B, Robson SC, Mann M, Kouzarides T. 2010. Nucleosome-Interacting Proteins Regulated by DNA and Histone Methylation. *Cell* **143**:470–484. doi:10.1016/j.cell.2010.10.012

Bell SP. 2017. Rethinking origin licensing. *eLife* **6**:1027. doi:10.7554/elife.24052

Bell SP, Kobayashi R, Stillman B. 1993. Yeast origin recognition complex functions in transcription silencing and DNA replication. *Science* **262**:1844–1849. doi:10.1126/science.8266072

Bell SP, Labib K. 2016. Chromosome Duplication in Saccharomyces cerevisiae. *Genetics* **203**:1027–67. doi:10.1534/genetics.115.186452

Bell SP, Stillman B. 1992. ATP-dependent recognition of eukaryotic origins of DNA replication by a multiprotein complex. *Nature* **357**:128–134. doi:10.1038/357128a0

Bernal JA, Venkitaraman AR. 2011. A vertebrate N-end rule degron reveals that Orc6 is required in mitosis for daughter cell abscission. *J Cell Biology* **192**:969–978. doi:10.1083/jcb.201008125

Bicknell LS, Bongers EMHF, Leitch A, Brown S, Schoots J, Harley ME, Aftimos S, Al-Aama JY, Bober M, Brown PAJ, Bokhoven H van, Dean J, Edrees AY, Feingold M, Fryer A, Hoefsloot LH, Kau N, Knoers NVAM, MacKenzie J, Opitz JM, Sarda P, Ross A, Temple IK, Toutain A, Wise CA, Wright M, Jackson AP. 2011a. Mutations in the pre-replication complex cause Meier-Gorlin syndrome. *Nat Genet* **43**:356–359. doi:10.1038/ng.775

Bicknell LS, Walker S, Klingseisen A, Stiff T, Leitch A, Kerzendorfer C, Martin C-A, Yeyati P, Sanna NA, Bober M, Johnson D, Wise C, Jackson AP, O'Driscoll M, Jeggo PA. 2011b. Mutations in ORC1, encoding the largest subunit of the origin recognition complex, cause microcephalic primordial dwarfism resembling Meier-Gorlin syndrome. *Nat Genet* **43**:350–355. doi:10.1038/ng.776

Bleichert F. 2019. Mechanisms of replication origin licensing: a structural perspective. *Curr Opin Struc Biol* **59**:195–204. doi:10.1016/j.sbi.2019.08.007

Bleichert F, Botchan MR, Berger JM. 2017. Mechanisms for initiating cellular DNA replication. *Science* **355**:eaah6317. doi:10.1126/science.aah6317

Bleichert F, Leitner A, Aebersold R, Botchan MR, Berger JM. 2018. Conformational control and DNA-binding mechanism of the metazoan origin recognition complex. *Proc Natl Acad Sci USA* **115**:E5906–E5915. doi:10.1073/pnas.1806315115

Blin M, Tallec BL, Nähse V, Schmidt M, Brossas C, Millot GA, Prioleau M-N, Debatisse M. 2019. Transcription-dependent regulation of replication dynamics modulates genome stability. *Nat Struct Mol Biol* **26**:58–66. doi:10.1038/s41594-018-0170-1

Bonaccorsi S, Giansanti MG, Gatti M. 1998. Spindle Self-organization and Cytokinesis During Male Meiosis in asterless Mutants of Drosophila melanogaster. *J Cell Biology* **142**:751–761. doi:10.1083/jcb.142.3.751

Bowers JL, Randell JCW, Chen S, Bell SP. 2004. ATP Hydrolysis by ORC Catalyzes Reiterative Mcm2-7 Assembly at a Defined Origin of Replication. *Mol Cell* **16**:967–978. doi:10.1016/j.molcel.2004.11.038

Broach JR, Li YY, Feldman J, Jayaram M, Abraham J, Nasmyth KA, Hicks JB. 1983. Localization and Sequence Analysis of Yeast Origins of DNA Replication. *Cold Spring Harbor Symposia on Quantitative Biology* **47**:1165–1173. doi:10.1101/sqb.1983.047.01.132

Buchan DWA, Jones DT. 2019. The PSIPRED Protein Analysis Workbench: 20 years on. *Nucleic Acids Res* **47**:W402–W407. doi:10.1093/nar/gkz297

Burke TW, Cook JG, Asano M, Nevins JR. 2001. Replication Factors MCM2 and ORC1 Interact with the Histone Acetyltransferase HBO1*. *J Biol Chem* **276**:15397–15408. doi:10.1074/jbc.m011556200

Canudas S, Houghtaling BR, Bhanot M, Sasa G, Savage SA, Bertuch AA, Smith S. 2011. A role for heterochromatin protein 1γ at human telomeres. *Gene Dev* **25**:1807–1819. doi:10.1101/gad.17325211

Canzio D, Larson A, Narlikar GJ. 2014. Mechanisms of functional promiscuity by HP1 proteins. *Trends Cell Biol* **24**:377–386. doi:10.1016/j.tcb.2014.01.002

Castel SE, Ren J, Bhattacharjee S, Chang A-Y, Sánchez M, Valbuena A, Antequera F, Martienssen RA. 2014. Dicer Promotes Transcription Termination at Sites of Replication Stress to Maintain Genome Stability. *Cell* **159**:572–583. doi:10.1016/j.cell.2014.09.031

Celniker SE, Sweder K, Srienc F, Bailey JE, Campbell JL. 1984. Deletion mutations affecting autonomously replicating sequence ARS1 of Saccharomyces cerevisiae. *Molecular and Cellular Biology* **4**:2455–2466. doi:10.1128/mcb.4.11.2455

Chang F, Riera A, Evrin C, Sun J, Li H, Speck C, Weinreich M. 2015. Cdc6 ATPase activity disengages Cdc6 from the pre-replicative complex to promote DNA replication. *Elife* **4**:e05795. doi:10.7554/elife.05795

Chen Y, Caldwell JM, Pereira E, Baker RW, Sanchez Y. 2009. ATRMec1 Phosphorylation-independent Activation of Chk1 in Vivo *. *J Biol Chem* **284**:182–190. doi:10.1074/jbc.m806530200

Chen Z, Speck C, Wendel P, Tang C, Stillman B, Li H. 2008. The architecture of the DNA replication origin recognition complex in Saccharomyces cerevisiae. *Proc National Acad Sci* **105**:10326–10331. doi:10.1073/pnas.0803829105

Chesnokov I, Balasov M, Huijbregts R, Svitin A. 2009. Multiple functions of the Drosophila Orc6 protein. *Faseb J* **23**:481.6-481.6. doi:10.1096/fasebj.23.1_supplement.481.6

Chesnokov IN. 2007. Multiple functions of the origin recognition complex. *International review of cytology* **256**:69–109. doi:10.1016/s0074-7696(07)56003-1

Chesnokov IN, Chesnokova ON, Botchan M. 2003. A cytokinetic function of Drosophila ORC6 protein resides in a domain distinct from its replication activity. *Proc National Acad Sci* **100**:9150–9155. doi:10.1073/pnas.1633580100

Cheutin T, McNairn AJ, Jenuwein T, Gilbert DM, Singh PB, Misteli T. 2003. Maintenance of Stable Heterochromatin Domains by Dynamic HP1 Binding. *Science* **299**:721–725. doi:10.1126/science.1078572

Chiolo I, Minoda A, Colmenares SU, Polyzos A, Costes SV, Karpen GH. 2011. Double-Strand Breaks in Heterochromatin Move Outside of a Dynamic HP1a Domain to Complete Recombinational Repair. *Cell* **144**:732–744. doi:10.1016/j.cell.2011.02.012

Chou H-C, Bhalla K, El Demerdesh O, Klingbeil O, Hanington K, Aganezov S, Andrews P, Alsudani H, Chang K, Vakoc CR, Schatz MC, McCombie WR, Stillman B. 2021. The human Origin Recognition Complex is essential for pre-RC assembly, mitosis and maintenance of nuclear structure. *Elife* **10**:e61797. doi:10.7554/elife.61797

Chow TT, Shi X, Wei J-H, Guan J, Stadler G, Huang B, Blackburn EH. 2018. Local enrichment of HP1alpha at telomeres alters their structure and regulation of telomere protection. *Nat Commun* **9**:3583. doi:10.1038/s41467-018-05840-y

Chuang R-Y, Chrétien L, Dai J, Kelly TJ. 2002. Purification and characterization of the Schizosaccharomyces pombe origin recognition complex: Interaction with origin DNA and Cdc18 protein. *J Biol Chem* **277**:16920–16927. doi:10.1074/jbc.m107710200

Chuang R-Y, Kelly TJ. 1999. The fission yeast homologue of Orc4p binds to replication origin DNA via multiple AT-hooks. *Proc National Acad Sci* **96**:2656–2661. doi:10.1073/pnas.96.6.2656

Cimini D, Cameron LA, Salmon ED. 2004. Anaphase Spindle Mechanics Prevent Mis-Segregation of Merotelically Oriented Chromosomes. *Curr Biol* **14**:2149–2155. doi:10.1016/j.cub.2004.11.029

Cimini D, Fioravanti D, Salmon ED, Degrassi F. 2002. Merotelic kinetochore orientation versus chromosome mono-orientation in the origin of lagging chromosomes in human primary cells. *J Cell Sci* **115**:507–15.

Cimini D, Moree B, Canman JC, Salmon ED. 2003. Merotelic kinetochore orientation occurs frequently during early mitosis in mammalian tissue cells and error correction is achieved by two different mechanisms. *J Cell Sci* **116**:4213–4225. doi:10.1242/jcs.00716

Ciosk R, Shirayama M, Shevchenko Anna, Tanaka T, Toth A, Shevchenko Andrej, Nasmyth K. 2000. Cohesin's Binding to Chromosomes Depends on a Separate Complex Consisting of Scc2 and Scc4 Proteins. *Mol Cell* **5**:243–254. doi:10.1016/s1097-2765(00)80420-7

Clarke DJ, Giménez-Abián JF. 2000. Checkpoints controlling mitosis. *Bioessays* **22**:351–363. doi:10.1002/(sici)1521-1878(200004)22:4<351::aid-bies5>3.0.co;2-w

Clyne RK, Kelly TJ. 1995. Genetic analysis of an ARS element from the fission yeast Schizosaccharomyces pombe. *Embo J* **14**:6348–6357. doi:10.1002/j.1460-2075.1995.tb00326.x

Craig JM, Earle E, Canham P, Wong LH, Anderson M, Choo KHA. 2003. Analysis of mammalian proteins involved in chromatin modification reveals new metaphase centromeric proteins and distinct chromosomal distribution patterns. *Hum Mol Genet* **12**:3109–3121. doi:10.1093/hmg/ddg330

Davey NE, Edwards RJ, Shields DC. 2007. The SLiMDisc server: short, linear motif discovery in proteins. *Nucleic Acids Res* **35**:W455–W459. doi:10.1093/nar/gkm400

Davey NE, Roey KV, Weatheritt RJ, Toedt G, Uyar B, Altenberg B, Budd A, Diella F, Dinkel H, Gibson TJ. 2011. Attributes of short linear motifs. *Mol Biosyst* **8**:268–281. doi:10.1039/c1mb05231d

DeBeer MAP, Müller U, Fox CA. 2003. Differential DNA affinity specifies roles for the origin recognition complex in budding yeast heterochromatin. *Gene Dev* **17**:1817–1822. doi:10.1101/gad.1096703

Deng Z, Dheekollu J, Broccoli D, Dutta A, Lieberman PM. 2007. The Origin Recognition Complex Localizes to Telomere Repeats and Prevents Telomere-Circle Formation. *Curr Biol* **17**:1989–1995. doi:10.1016/j.cub.2007.10.054

Deng Z, Norseen J, Wiedmer A, Riethman H, Lieberman PM. 2009. TERRA RNA Binding to TRF2 Facilitates Heterochromatin Formation and ORC Recruitment at Telomeres. *Mol Cell* **35**:403–413. doi:10.1016/j.molcel.2009.06.025

DePamphilis ML. 2004. Cell Cycle Dependent Regulation of the Origin Recognition Complex. *Cell Cycle* **4**:70–79. doi:10.4161/cc.4.1.1333

DePamphilis ML. 2003. The 'ORC cycle': a novel pathway for regulating eukaryotic DNA replication. *Gene* **310**:1–15. doi:10.1016/s0378-1119(03)00546-8

Deshpande AM, Newlon CS. 1992. The ARS consensus sequence is required for chromosomal origin function in Saccharomyces cerevisiae. *Mol Cell Biol* **12**:4305–4313. doi:10.1128/mcb.12.10.4305

Dhar SK, Yoshida K, Machida Y, Khaira P, Chaudhuri B, Wohlschlegel JA, Leffak M, Yates J, Dutta A. 2001. Replication from oriP of Epstein-Barr Virus Requires Human ORC and Is Inhibited by Geminin. *Cell* **106**:287–296. doi:10.1016/s0092-8674(01)00458-5

Diffley JF. 1996. Once and only once upon a time: specifying and regulating origins of DNA replication in eukaryotic cells. *Genes & Development* **10**:2819–2830.

Diffley JF. 1994. Eukaryotic DNA replication. *Current opinion in cell biology* **6**:368–372.

Dillin A, Rine J. 1998. Roles for ORC in M Phase and S Phase. *Science* **279**:1733–1737. doi:10.1126/science.279.5357.1733

Dinant C, Luijsterburg MS. 2009. The Emerging Role of HP1 in the DNA Damage Response ▿ . *Mol Cell Biol* **29**:6335–6340. doi:10.1128/mcb.01048-09

Donovan S, Diffley JF. 1996. Replication origins in eukaroytes. *Current opinion in genetics & development* **6**:203–207.

Drinnenberg IA, Weinberg DE, Xie KT, Mower JP, Wolfe KH, Fink GR, Bartel DP. 2009. RNAi in Budding Yeast. *Science* **326**:544–550. doi:10.1126/science.1176945

Drosopoulos WC, Deng Z, Twayana S, Kosiyatrakul ST, Vladimirova O, Lieberman PM, Schildkraut CL. 2020. TRF2 Mediates Replication Initiation within Human Telomeres to Prevent Telomere Dysfunction. *Cell Reports* **33**:108379. doi:10.1016/j.celrep.2020.108379

Duursma AM, Agami R. 2005. CDK-Dependent Stabilization of Cdc6: Linking Growth and Stress Signals to Activation of DNA Replication. *Cell Cycle* **4**:1725–1728. doi:10.4161/cc.4.12.2193

Dyson JM, O'Malley CJ, Becanovic J, Munday AD, Berndt MC, Coghill ID, Nandurkar HH, Ooms LM, Mitchell CA. 2001. The SH2-containing inositol polyphosphate 5-phosphatase, SHIP-2, binds filamin and regulates submembraneous actin. *J Cell Biology* **155**:1065–1080. doi:10.1083/jcb.200104005

Eaton ML, Galani K, Kang S, Bell SP, MacAlpine DM. 2010. Conserved nucleosome positioning defines replication origins. *Gene Dev* **24**:748–753. doi:10.1101/gad.1913210

Ehrenhofer-Murray AE, Gossen M, Pak DTS, Botchan MR, Rine J. 1995. Separation of Origin Recognition Complex Functions by Cross-Species Complementation. *Science* **270**:1671–1674. doi:10.1126/science.270.5242.1671

Ellahi A, Rine J. 2016. Evolution and Functional Trajectory of Sir1 in Gene Silencing. *Mol Cell Biol* **36**:1164–1179. doi:10.1128/mcb.01013-15

Evrin C, Clarke P, Zech J, Lurz R, Sun J, Uhle S, Li H, Stillman B, Speck C. 2009. A double-hexameric MCM2-7 complex is loaded onto origin DNA during licensing of eukaryotic DNA replication. *Proc National Acad Sci* **106**:20240–20245. doi:10.1073/pnas.0911500106

Eymery A, Callanan M, Vourc'h C. 2009. The secret message of heterochromatin: new insights into the mechanisms and function of centromeric and pericentric repeat sequence transcription. *Int J Dev Biol* **53**:259–268. doi:10.1387/ijdb.082673ae

Fanti L, Giovinazzo G, Berloco M, Pimpinelli S. 1998. The Heterochromatin Protein 1 Prevents Telomere Fusions in Drosophila. *Mol Cell* **2**:527–538. doi:10.1016/s1097-2765(00)80152-5

Fernández-Cid A, Riera A, Tognetti S, Herrera MC, Samel S, Evrin C, Winkler C, Gardenal E, Uhle S, Speck C. 2013. An ORC/Cdc6/MCM2-7 Complex Is Formed in a Multistep Reaction to Serve as a Platform for MCM Double-Hexamer Assembly. *Mol Cell* **50**:577–588. doi:10.1016/j.molcel.2013.03.026

Fischer JD, Mayer CE, Söding J. 2008. Prediction of protein functional residues from sequence by probability density estimation. *Bioinformatics* **24**:613–620. doi:10.1093/bioinformatics/btm626

Fischer T, Cui B, Dhakshnamoorthy J, Zhou M, Rubin C, Zofall M, Veenstra TD, Grewal SIS. 2009. Diverse roles of HP1 proteins in heterochromatin assembly and functions in fission yeast. *Proc National Acad Sci* **106**:8998–9003. doi:10.1073/pnas.0813063106

Foss M, McNally F, Laurenson P, Rine J. 1993. Origin recognition complex (ORC) in transcriptional silencing and DNA replication in S. cerevisiae. *Science* **262**:1838–1844. doi:10.1126/science.8266071

Fox CA, Loo S, Dillin A, Rine J. 1995. The origin recognition complex has essential functions in transcriptional silencing and chromosomal replication. *Gene Dev* **9**:911–924. doi:10.1101/gad.9.8.911

Fritsch L, Robin P, Mathieu JRR, Souidi M, Hinaux H, Rougeulle C, Harel-Bellan A, Ameyar-Zazoua M, Ait-Si-Ali S. 2010. A Subset of the Histone H3 Lysine 9 Methyltransferases Suv39h1, G9a, GLP, and SETDB1 Participate in a Multimeric Complex. *Mol Cell* **37**:46–56. doi:10.1016/j.molcel.2009.12.017

Frydrychova RC, Mason JM, Archer TK. 2008. HP1 Is Distributed Within Distinct Chromatin Domains at Drosophila Telomeres. *Genetics* **180**:121–131. doi:10.1534/genetics.108.090647

Garapaty S, Xu C-F, Trojer P, Mahajan MA, Neubert TA, Samuels HH. 2009. Identification and Characterization of a Novel Nuclear Protein Complex Involved in Nuclear Hormone Receptor-mediated Gene Regulation*. *J Biol Chem* **284**:7542–7552. doi:10.1074/jbc.m805872200

Gardner KA, Fox CA. 2001. The Sir1 protein's association with a silenced chromosome domain. *Gene Dev* **15**:147–157. doi:10.1101/gad.852801

Gatei M, Sloper K, Sörensen C, Syljuäsen R, Falck J, Hobson K, Savage K, Lukas J, Zhou B-B, Bartek J, Khanna KK. 2003. Ataxia-telangiectasia-mutated (ATM) and NBS1-dependent Phosphorylation of Chk1 on Ser-317 in Response to Ionizing Radiation. *J Biol Chem* **278**:14806–14811. doi:10.1074/jbc.m210862200

Gibson DG, Bell SP, Aparicio OM. 2006. Cell cycle execution point analysis of ORC function and characterization of the checkpoint response to ORC inactivation in Saccharomyces cerevisiae. *Genes Cells* **11**:557–573. doi:10.1111/j.1365-2443.2006.00967.x

Gillespie PJ, Hirano T. 2004. Scc2 Couples Replication Licensing to Sister Chromatid Cohesion in Xenopus Egg Extracts. *Curr Biol* **14**:1598–1603. doi:10.1016/j.cub.2004.07.053

Gillingham AK, Munro S. 2000. The PACT domain, a conserved centrosomal targeting motif in the coiled-coil proteins AKAP450 and pericentrin. *Embo Rep* **1**:524–529. doi:10.1093/embo-reports/kvd105

Giri S, Aggarwal V, Pontis J, Shen Z, Chakraborty A, Khan A, Mizzen C, Prasanth KV, Ait-Si-Ali S, Ha T, Prasanth SG. 2015. The preRC protein ORCA organizes heterochromatin by assembling histone H3 lysine 9 methyltransferases on chromatin. *eLife* **4**:332. doi:10.7554/elife.06496

Giri S, Chakraborty A, Sathyan KM, Prasanth KV, Prasanth SG. 2016. Orc5 induces large-scale chromatin decondensation in a GCN5-dependent manner. *J Cell Sci* **129**:417–429. doi:10.1242/jcs.178889

Goto H, Natsume T, Kanemaki MT, Kaito A, Wang S, Gabazza EC, Inagaki M, Mizoguchi A. 2019. Chk1-mediated Cdc25A degradation as a critical mechanism for normal cell-cycle progression. *J Cell Sci* **132**:jcs.223123. doi:10.1242/jcs.223123

Gregan J, Polakova S, Zhang L, Tolić-Nørrelykke IM, Cimini D. 2011. Merotelic kinetochore attachment: causes and effects. *Trends Cell Biol* **21**:374–381. doi:10.1016/j.tcb.2011.01.003

Greil F, Kraan I van der, Delrow J, Smothers JF, Wit E de, Bussemaker HJ, Driel R van, Henikoff S, Steensel B van. 2003. Distinct HP1 and Su(var)3-9 complexes bind to sets of developmentally coexpressed genes depending on chromosomal location. *Genes & Development* **17**:2825–2838. doi:10.1101/gad.281503

Grewal SIS, Jia S. 2007. Heterochromatin revisited. *Nat Rev Genet* **8**:35–46. doi:10.1038/nrg2008

Groth A, Corpet A, Cook AJL, Roche D, Bartek J, Lukas J, Almouzni G. 2007. Regulation of Replication Fork Progression Through Histone Supply and Demand. *Science* **318**:1928–1931. doi:10.1126/science.1148992

Guacci V, Koshland D, Strunnikov A. 1997. A Direct Link between Sister Chromatid Cohesion and Chromosome Condensation Revealed through the Analysis of MCD1 in S. cerevisiae. *Cell* **91**:47–57. doi:10.1016/s0092-8674(01)80008-8

Gudimchuk N, Vitre B, Kim Y, Kiyatkin A, Cleveland DW, Ataullakhanov FI, Grishchuk EL. 2013. Kinetochore kinesin CENP-E is a processive bi-directional tracker of dynamic microtubule tips. *Nat Cell Biol* **15**:1079–1088. doi:10.1038/ncb2831

Guérette D, Khan PA, Savard PE, Vincent M. 2007. Molecular evolution of type VI intermediate filament proteins. *Bmc Evol Biol* **7**:164. doi:10.1186/1471-2148-7-164

Guernsey DL, Matsuoka M, Jiang H, Evans S, Macgillivray C, Nightingale M, Perry S, Ferguson M, LeBlanc M, Paquette J, Patry L, Rideout AL, Thomas A, Orr A, McMaster CR, Michaud JL, Deal C, Langlois S, Superneau DW, Parkash S, Ludman M, Skidmore DL, Samuels ME. 2011. Mutations in origin recognition complex gene ORC4 cause Meier-Gorlin syndrome. *Nat Genet* **43**:360–364. doi:10.1038/ng.777

Guillou E, Ibarra A, Coulon V, Casado-Vela J, Rico D, Casal I, Schwob E, Losada A, Méndez J. 2010. Cohesin organizes chromatin loops at DNA replication factories. *Gene Dev* **24**:2812–2822. doi:10.1101/gad.608210

Gupta A, Dey CS. 2009. PTEN and SHIP2 regulates PI3K/Akt pathway through focal adhesion kinase. *Mol Cell Endocrinol* **309**:55–62. doi:10.1016/j.mce.2009.05.018

Haapaniemi E, Botla S, Persson J, Schmierer B, Taipale J. 2018. CRISPR-Cas9 genome editing induces a p53-mediated DNA damage response. *Nat Med* **19**:1. doi:10.1038/s41591-018-0049-z

Habib T, Hejna JA, Moses RE, Decker SJ. 1998. Growth Factors and Insulin Stimulate Tyrosine Phosphorylation of the 51C/SHIP2 Protein*. *J Biol Chem* **273**:18605–18609. doi:10.1074/jbc.273.29.18605

Hayashi MT, Cesare AJ, Fitzpatrick JAJ, Lazzerini-Denchi E, Karlseder J. 2012. A telomere-dependent DNA damage checkpoint induced by prolonged mitotic arrest. *Nat Struct Mol Biol* **19**:387–394. doi:10.1038/nsmb.2245

He W, Zhang L, Villarreal OD, Fu R, Bedford E, Dou J, Patel AY, Bedford MT, Shi X, Chen T, Bartholomew B, Xu H. 2019. De novo identification of essential protein domains from CRISPR-Cas9 tiling-sgRNA knockout screens. *Nat Commun* **10**:4541. doi:10.1038/s41467-019-12489-8

Heller RC, Kang S, Lam WM, Chen S, Chan CS, Bell SP. 2011. Eukaryotic Origin-Dependent DNA Replication In Vitro Reveals Sequential Action of DDK and S-CDK Kinases. *Cell* **146**:80–91. doi:10.1016/j.cell.2011.06.012

Hemerly AS, Prasanth SG, Siddiqui K, Stillman B. 2009. Orc1 controls centriole and centrosome copy number in human cells. *Sci New York N Y* **323**:789–93. doi:10.1126/science.1166745

Herranz N, Gil J. 2018. Mechanisms and functions of cellular senescence. *J Clin Invest* **128**:1238–1246. doi:10.1172/jci95148

Higa M, Kushiyama T, Kurashige S, Kohmon D, Enokitani K, Iwahori S, Sugimoto N, Yoshida K, Fujita M. 2017. TRF2 recruits ORC through TRFH domain dimerization. *Biochimica Et Biophysica Acta Bba - Mol Cell Res* **1864**:191–201. doi:10.1016/j.bbamcr.2016.11.004

Hornig NCD, Knowles PP, McDonald NQ, Uhlmann F. 2002. The Dual Mechanism of Separase Regulation by Securin. *Curr Biol* **12**:973–982. doi:10.1016/s0960-9822(02)00847-3

Hossain M, Bhalla K, Stillman B. 2021. Multiple, short protein binding motifs in ORC1 and CDC6 control the initiation of DNA replication. *Mol Cell*. doi:10.1016/j.molcel.2021.03.003

Hossain M, Stillman B. 2016. Opposing roles for DNA replication initiator proteins ORC1 and CDC6 in control of Cyclin E gene transcription. *Elife* **5**:4294. doi:10.7554/elife.12785

Hossain M, Stillman B. 2012. Meier-Gorlin syndrome mutations disrupt an Orc1 CDK inhibitory domain and cause centrosome reduplication. *Gene Dev* **26**:1797–810. doi:10.1101/gad.197178.112

Hou Z, Bernstein DA, Fox CA, Keck JL. 2005. Structural basis of the Sir1-origin recognition complex interaction in transcriptional silencing. *Proc National Acad Sci* **102**:8489–8494. doi:10.1073/pnas.0503525102

Hsu JY, Fulco CP, Cole MA, Canver MC, Pellin D, Sher F, Farouni R, Clement K, Guo JA, Biasco L, Orkin SH, Engreitz JM, Lander ES, Joung JK, Bauer DE, Pinello L. 2018. CRISPR-SURF: discovering regulatory elements by deconvolution of CRISPR tiling screen data. *Nat Methods* **15**:992–993. doi:10.1038/s41592-018-0225-6

Hsu PD, Scott DA, Weinstein JA, Ran FA, Konermann S, Agarwala V, Li Y, Fine EJ, Wu X, Shalem O, Cradick TJ, Marraffini LA, Bao G, Zhang F. 2013. DNA targeting specificity of RNA-guided Cas9 nucleases. *Nat Biotechnol* **31**:827–832. doi:10.1038/nbt.2647

Hu Y, Tareen A, Sheu Y-J, Ireland WT, Speck C, Li H, Joshua-Tor L, Kinney JB, Stillman B. 2020. Evolution of DNA Replication Origin Specification and Gene Silencing Mechanisms. *Biorxiv* 2020.07.04.187286. doi:10.1101/2020.07.04.187286

Huang DW, Fanti L, Pak DTS, Botchan MR, Pimpinelli S, Kellum R. 1998. Distinct Cytoplasmic and Nuclear Fractions of Drosophila Heterochromatin Protein 1: Their Phosphorylation Levels and Associations with Origin Recognition Complex Proteins. *J Cell Biol* **142**:307–318. doi:10.1083/jcb.142.2.307

Huang H, Yu Z, Zhang S, Liang X, Chen J, Li C, Ma J, Jiao R. 2010. Drosophila CAF-1 regulates HP1-mediated epigenetic silencing and pericentric heterochromatin stability. *J Cell Sci* **123**:2853–2861. doi:10.1242/jcs.063610

Iizuka M, Stillman B. 1999. Histone Acetyltransferase HBO1 Interacts with the ORC1 Subunit of the Human Initiator Protein*. *J Biol Chem* **274**:23027–23034. doi:10.1074/jbc.274.33.23027

Inoue A, Hyle J, Lechner MS, Lahti JM. 2008. Perturbation of HP1 localization and chromatin binding ability causes defects in sister-chromatid cohesion. *Mutat Res Genetic Toxicol Environ Mutagen* **657**:48–55. doi:10.1016/j.mrgentox.2008.08.010

Jackson JR, Gilmartin A, Imburgia C, Winkler JD, Marshall LA, Roshak A. 2000. An indolocarbazole inhibitor of human checkpoint kinase (Chk1) abrogates cell cycle arrest caused by DNA damage. *Cancer Res* **60**:566–72.

Janssen A, Colmenares SU, Karpen GH. 2018. Heterochromatin: Guardian of the Genome. *Annual review of cell and developmental biology* **34**:265–288. doi:10.1146/annurev-cellbio-100617-062653

Jaremko MJ, On KF, Thomas DR, Stillman B, Joshua-Tor L. 2020. The dynamic nature of the human Origin Recognition Complex revealed through five cryoEM structures. *Elife* **9**:e58622. doi:10.7554/elife.58622

Jiang W, Wells NJ, Hunter T. 1999. Multistep regulation of DNA replication by Cdk phosphorylation of HsCdc6. *Proc National Acad Sci* **96**:6193–6198. doi:10.1073/pnas.96.11.6193

Jones DO, Cowell IG, Singh PB. 2000. Mammalian chromodomain proteins: their role in genome organisation and expression. *Bioessays* **22**:124–137. doi:10.1002/(sici)1521-1878(200002)22:2<124::aid-bies4>3.0.co;2-e

Jones DT, Cozzetto D. 2015. DISOPRED3: precise disordered region predictions with annotated protein-binding activity. *Bioinformatics* **31**:857–863. doi:10.1093/bioinformatics/btu744

Jørgensen S, Schotta G, Sørensen CS. 2013. Histone H4 Lysine 20 methylation: key player in epigenetic regulation of genomic integrity. *Nucleic Acids Res* **41**:2797–2806. doi:10.1093/nar/gkt012

Kamimura Y, Masumoto H, Sugino A, Araki H. 1998. Sld2, Which Interacts with Dpb11 in Saccharomyces cerevisiae, Is Required for Chromosomal DNA Replication. *Molecular and Cellular Biology* **18**:6102–6109. doi:10.1128/mcb.18.10.6102

Kang J, Chaudhary J, Dong H, Kim S, Brautigam CA, Yu H. 2011. Mitotic centromeric targeting of HP1 and its binding to Sgo1 are dispensable for sister-chromatid cohesion in human cells. *Mol Biol Cell* **22**:1181–1190. doi:10.1091/mbc.e11-01-0009

Kara N, Hossain M, Prasanth SG, Stillman B. 2015. Orc1 Binding to Mitotic Chromosomes Precedes Spatial Patterning during G1 Phase and Assembly of the Origin Recognition Complex in Human Cells. *J Biol Chem* **290**:12355–12369. doi:10.1074/jbc.m114.625012

Karnani N, Taylor CM, Malhotra A, Dutta A. 2010. Genomic Study of Replication Initiation in Human Chromosomes Reveals the Influence of Transcription Regulation and Chromatin Structure on Origin Selection. *Mol Biol Cell* **21**:393–404. doi:10.1091/mbc.e09-08-0707

Kawakami H, Ohashi E, Kanamoto S, Tsurimoto T, Katayama T. 2015. Specific binding of eukaryotic ORC to DNA replication origins depends on highly conserved basic residues. *Sci Rep-uk* **5**:14929. doi:10.1038/srep14929

Kerppola TK. 2009. Visualization of molecular interactions using bimolecular fluorescence complementation analysis: Characteristics of protein fragment complementation. *Chem Soc Rev* **38**:2876–2886. doi:10.1039/b909638h

Kerppola TK. 2008. Bimolecular Fluorescence Complementation (BiFC) Analysis as a Probe of Protein Interactions in Living Cells. *Biophysics* **37**:465–487. doi:10.1146/annurev.biophys.37.032807.125842

Khodjakov A, Cole RW, Oakley BR, Rieder CL. 2000. Centrosome-independent mitotic spindle formation in vertebrates. *Curr Biol* **10**:59–67. doi:10.1016/s0960-9822(99)00276-6

Khodjakov A, Rieder CL. 2001. Centrosomes Enhance the Fidelity of Cytokinesis in Vertebrates and Are Required for Cell Cycle Progression. *J Cell Biology* **153**:237–242. doi:10.1083/jcb.153.1.237

Kose HB, Xie S, Cameron G, Strycharska MS, Yardimci H. 2019. Mechanism of RPA-Facilitated Processive DNA Unwinding by the Eukaryotic CMG Helicase. *Biorxiv* 796003. doi:10.1101/796003

Kreitz S, Ritzi M, Baack M, Knippers R. 2001. The Human Origin Recognition Complex Protein 1 Dissociates from Chromatin during S Phase in HeLa Cells. *J Biol Chem* **276**:6337–6342. doi:10.1074/jbc.m009473200

Kremer BE, Adang LA, Macara IG. 2007. Septins Regulate Actin Organization and Cell-Cycle Arrest through Nuclear Accumulation of NCK Mediated by SOCS7. *Cell* **130**:837–850. doi:10.1016/j.cell.2007.06.053

Kueh AJ, Eccles S, Tang L, Garnham AL, May RE, Herold MJ, Smyth GK, Voss AK, Thomas T. 2019. HBO1 (KAT7) Does Not Have an Essential Role in Cell Proliferation, DNA Replication, or Histone 4 Acetylation in Human Cells. *Mol Cell Biol* **40**. doi:10.1128/mcb.00506-19

Kumar A, Kono H. 2020. Heterochromatin protein 1 (HP1): interactions with itself and chromatin components. *Biophysical Rev* **12**:387–400. doi:10.1007/s12551-020-00663-y

Kuo AJ, Song J, Cheung P, Ishibe-Murakami S, Yamazoe S, Chen JK, Patel DJ, Gozani O. 2012. The BAH domain of ORC1 links H4K20me2 to DNA replication licensing and Meier–Gorlin syndrome. *Nature* **484**:115–119. doi:10.1038/nature10956

Kwon SH, Workman JL. 2011. The changing faces of HP1: From heterochromatin formation and gene silencing to euchromatic gene expression. *Bioessays* **33**:280–289. doi:10.1002/bies.201000138

Lachner M, O'Carroll D, Rea S, Mechtler K, Jenuwein T. 2001. Methylation of histone H3 lysine 9 creates a binding site for HP1 proteins. *Nature* **410**:116–120. doi:10.1038/35065132

Larson AG, Elnatan D, Keenen MM, Trnka MJ, Johnston JB, Burlingame AL, Agard DA, Redding S, Narlikar GJ. 2017. Liquid droplet formation by HP1α suggests a role for phase separation in heterochromatin. *Nature* **547**:236–240. doi:10.1038/nature22822

Lee CSK, Cheung MF, Li J, Zhao Y, Lam WH, Ho V, Rohs R, Zhai Y, Leung D, Tye B-K. 2021. Humanizing the yeast origin recognition complex. *Nat Commun* **12**:33. doi:10.1038/s41467-020-20277-y

Lengronne A, Katou Y, Mori S, Yokobayashi S, Kelly GP, Itoh T, Watanabe Y, Shirahige K, Uhlmann F. 2004. Cohesin relocation from sites of chromosomal loading to places of convergent transcription. *Nature* **430**:573–578. doi:10.1038/nature02742

Li H, Stillman B. 2012. The origin recognition complex: a biochemical and structural view. *Sub-cellular biochemistry* **62**:37–58. doi:10.1007/978-94-007-4572-8_3

Li N, Lam WH, Zhai Y, Cheng J, Cheng E, Zhao Y, Gao N, Tye B-K. 2018. Structure of the origin recognition complex bound to DNA replication origin. *Nature* **559**:217–222. doi:10.1038/s41586-018-0293-x

Li W, Xu H, Xiao T, Cong L, Love MI, Zhang F, Irizarry RA, Liu JS, Brown M, Liu XS. 2014. MAGeCK enables robust identification of essential genes from genome-scale CRISPR/Cas9 knockout screens. *Genome Biol* **15**:554. doi:10.1186/s13059-014-0554-4

Liang F, Wang Y. 2007. DNA Damage Checkpoints Inhibit Mitotic Exit by Two Different Mechanisms ▿ . *Mol Cell Biol* **27**:5067–5078. doi:10.1128/mcb.00095-07

Lidonnici MR, Rossi R, Paixão S, Mendoza-Maldonado R, Paolinelli R, Arcangeli C, Giacca M, Biamonti G, Montecucco A. 2004. Subnuclear distribution of the largest subunit of the human origin recognition complex during the cell cycle. *J Cell Sci* **117**:5221–5231. doi:10.1242/jcs.01405

Lin H-P, Vincenz C, Eliceiri KW, Kerppola TK, Ogle BM. 2010. Bimolecular fluorescence complementation analysis of eukaryotic fusion products. *Biol Cell* **102**:525–537. doi:10.1042/bc20100033

Liu Q, Guntuku S, Cui X-S, Matsuoka S, Cortez D, Tamai K, Luo G, Carattini-Rivera S, DeMayo F, Bradley A, Donehower LA, Elledge SJ. 2000. Chk1 is an essential kinase that is regulated by Atr and required for the G2/M DNA damage checkpoint. *Gene Dev* **14**:1448–1459. doi:10.1101/gad.14.12.1448

Liu S, Balasov M, Wang H, Wu L, Chesnokov IN, Liu Y. 2011. Structural analysis of human Orc6 protein reveals a homology with transcription factor TFIIB. *Proc National Acad Sci* **108**:7373–7378. doi:10.1073/pnas.1013676108

Long H, Zhang L, Lv M, Wen Z, Zhang W, Chen X, Zhang P, Li T, Chang L, Jin C, Wu G, Wang X, Yang F, Pei J, Chen P, Margueron R, Deng H, Zhu M, Li G. 2019. H2A.Z facilitates licensing and activation of early replication origins. *Nature* **577**:1–18. doi:10.1038/s41586-019-1877-9

Losada A, Hirano M, Hirano T. 1998. Identification of Xenopus SMC protein complexes required for sister chromatid cohesion. *Gene Dev* **12**:1986–1997. doi:10.1101/gad.12.13.1986

Lou Z, Chen J. 2006. Cellular senescence and DNA repair. *Exp Cell Res* **312**:2641–2646. doi:10.1016/j.yexcr.2006.06.009

Loupart M-L, Krause S, Heck MS. 2000. Aberrant replication timing induces defective chromosome condensation in Drosophila ORC2 mutants. *Curr Biol* **10**:1547–1556. doi:10.1016/s0960-9822(00)00844-7

Lu B, Klingbeil O, Tarumoto Y, Somerville TDD, Huang Y-H, Wei Y, Wai DC, Low JKK, Milazzo JP, Wu XS, Cao Z, Yan X, Demerdash OE, Huang G, Mackay JP, Kinney JB, Shi J, Vakoc CR. 2018. A Transcription Factor Addiction in Leukemia Imposed by the MLL Promoter Sequence. *Cancer Cell* **34**:970-981.e8. doi:10.1016/j.ccell.2018.10.015

Luijsterburg MS, Dinant C, Lans H, Stap J, Wiernasz E, Lagerwerf S, Warmerdam DO, Lindh M, Brink MC, Dobrucki JW, Aten JA, Fousteri MI, Jansen G, Dantuma NP, Vermeulen W, Mullenders LHF, Houtsmuller AB, Verschure PJ, Driel R van. 2009. Heterochromatin protein 1 is recruited to various types of DNA damage. *J Cell Biology* **185**:577–586. doi:10.1083/jcb.200810035

MacAlpine HK, Gordân R, Powell SK, Hartemink AJ, MacAlpine DM. 2009. Drosophila ORC localizes to open chromatin and marks sites of cohesin complex loading. *Genome Res* **20**:201–11. doi:10.1101/gr.097873.109

Mailand N, Diffley JFX. 2005. CDKs promote DNA replication origin licensing in human cells by protecting Cdc6 from APC/C-dependent proteolysis. *Cell* **122**:915–926. doi:10.1016/j.cell.2005.08.013

Maison C, Almouzni G. 2004. HP1 and the dynamics of heterochromatin maintenance. *Nat Rev Mol Cell Bio* **5**:296–305. doi:10.1038/nrm1355

Marahrens Y, Stillman B. 1992. A yeast chromosomal origin of DNA replication defined by multiple functional elements. *Science* **255**:817–823. doi:10.1126/science.1536007

Martienssen R, Moazed D. 2015. RNAi and Heterochromatin Assembly. *Csh Perspect Biol* **7**:a019323. doi:10.1101/cshperspect.a019323

Matson JP, Dumitru R, Coryell P, Baxley RM, Chen W, Twaroski K, Webber BR, Tolar J, Bielinsky A-K, Purvis JE, Cook JG. 2017. Rapid DNA replication origin licensing protects stem cell pluripotency. *eLife* **6**:114. doi:10.7554/elife.30473

Matthies HJ, McDonald HB, Goldstein LS, Theurkauf WE. 1996. Anastral meiotic spindle morphogenesis: role of the non-claret disjunctional kinesin-like protein. *J Cell Biology* **134**:455–464. doi:10.1083/jcb.134.2.455

McFarland JM, Ho ZV, Kugener G, Dempster JM, Montgomery PG, Bryan JG, Krill-Burger JM, Green TM, Vazquez F, Boehm JS, Golub TR, Hahn WC, Root DE, Tsherniak A. 2018. Improved estimation of cancer dependencies from large-scale RNAi screens using model-based normalization and data integration. *Nat Commun* **9**:4610. doi:10.1038/s41467-018-06916-5

McGarry TJ, Kirschner MW. 1998. Geminin, an Inhibitor of DNA Replication, Is Degraded during Mitosis. *Cell* **93**:1043–1053. doi:10.1016/s0092-8674(00)81209-x

McKinley KL, Cheeseman IM. 2017. Large-Scale Analysis of CRISPR/Cas9 Cell-Cycle Knockouts Reveals the Diversity of p53-Dependent Responses to Cell-Cycle Defects. *Dev Cell* **40**:405-420.e2. doi:10.1016/j.devcel.2017.01.012

McNairn AJ, Gilbert DM. 2005. Overexpression of ORC subunits and increased ORC-chromatin association in transformed mammalian cells. *J Cell Biochem* **96**:879–887. doi:10.1002/jcb.20609

Meehan RR, Kao C, Pennings S. 2003. HP1 binding to native chromatin in vitro is determined by the hinge region and not by the chromodomain. *Embo J* **22**:3164–3174. doi:10.1093/emboj/cdg306

Megraw TL, Kao L-R, Kaufman TC. 2001. Zygotic development without functional mitotic centrosomes. *Curr Biol* **11**:116–120. doi:10.1016/s0960-9822(01)00017-3

Méndez J, Zou-Yang XH, Kim S-Y, Hidaka M, Tansey WP, Stillman B. 2002. Human Origin Recognition Complex Large Subunit Is Degraded by Ubiquitin-Mediated Proteolysis after Initiation of DNA Replication. *Mol Cell* **9**:481–491. doi:10.1016/s1097-2765(02)00467-7

Meyers RM, Bryan JG, McFarland JM, Weir BA, Sizemore AE, Xu H, Dharia NV, Montgomery PG, Cowley GS, Pantel S, Goodale A, Lee Y, Ali LD, Jiang G, Lubonja R, Harrington WF, Strickland M, Wu T, Hawes DC, Zhivich VA, Wyatt MR, Kalani Z, Chang JJ, Okamoto M, Stegmaier K, Golub TR, Boehm JS, Vazquez F, Root DE, Hahn WC, Tsherniak A. 2017. Computational correction of copy number effect improves specificity of CRISPR-Cas9 essentiality screens in cancer cells. *Nat Genet* **49**:1779–1784. doi:10.1038/ng.3984

Michaelis C, Ciosk R, Nasmyth K. 1997. Cohesins: Chromosomal Proteins that Prevent Premature Separation of Sister Chromatids. *Cell* **91**:35–45. doi:10.1016/s0092-8674(01)80007-6

Michalczyk K, Ziman M. 2005. Nestin structure and predicted function in cellular cytoskeletal organisation. *Histol Histopathol* **20**:665–71.

Miles LA, Garippa RJ, Poirier JT. 2016. Design, execution, and analysis of pooledin vitroCRISPR/Cas9 screens. *Febs J* **283**:3170–3180. doi:10.1111/febs.13770

Miller TCR, Locke J, Greiwe JF, Diffley JFX, Costa A. 2019. Mechanism of head-to-head MCM double-hexamer formation revealed by cryo-EM. *Nature* **575**:704–710. doi:10.1038/s41586-019-1768-0

Minc E, Allory Y, Worman HJ, Courvalin JC, Buendia B. 1999. Localization and phosphorylation of HP1 proteins during the cell cycle in mammalian cells. *Chromosoma* **108**:220–234.

Miotto B, Ji Z, Struhl K. 2016. Selectivity of ORC binding sites and the relation to replication timing, fragile sites, and deletions in cancers. *Proc National Acad Sci* **113**:E4810–E4819. doi:10.1073/pnas.1609060113

Miotto B, Struhl K. 2008. HBO1 histone acetylase is a coactivator of the replication licensing factor Cdt1. *Genes Dev* . doi:10.1101/gad.1674108

Misulovin Z, Schwartz YB, Li X-Y, Kahn TG, Gause M, MacArthur S, Fay JC, Eisen MB, Pirrotta V, Biggin MD, Dorsett D. 2008. Association of cohesin and Nipped-B with transcriptionally active regions of the Drosophila melanogaster genome. *Chromosoma* **117**:89–102. doi:10.1007/s00412-007-0129-1

Montalbano A, Canver MC, Sanjana NE. 2017. High-Throughput Approaches to Pinpoint Function within the Noncoding Genome. *Mol Cell* **68**:44–59. doi:10.1016/j.molcel.2017.09.017

Motamedi MR, Hong E-JE, Li X, Gerber S, Denison C, Gygi S, Moazed D. 2008. HP1 Proteins Form Distinct Complexes and Mediate Heterochromatic Gene Silencing by Nonoverlapping Mechanisms. *Mol Cell* **32**:778–790. doi:10.1016/j.molcel.2008.10.026

Mugabo Y, Zhao S, Seifried A, Gezzar S, Al-Mass A, Zhang D, Lamontagne J, Attane C, Poursharifi P, Iglesias J, Joly E, Peyot M-L, Gohla A, Madiraju SRM, Prentki M. 2016. Identification of a mammalian glycerol-3-phosphate phosphatase: Role in metabolism and signaling in pancreatic β-cells and hepatocytes. *Proc National Acad Sci* **113**:E430–E439. doi:10.1073/pnas.1514375113

Müller P, Park S, Shor E, Huebert DJ, Warren CL, Ansari AZ, Weinreich M, Eaton ML, MacAlpine DM, Fox CA. 2010. The conserved bromo-adjacent homology domain of yeast Orc1 functions in the selection of DNA replication origins within chromatin. *Gene Dev* **24**:1418–1433. doi:10.1101/gad.1906410

Munnik Sonja A de, Bicknell LS, Aftimos S, Al-Aama JY, Bever Y van, Bober MB, Clayton-Smith J, Edrees AY, Feingold M, Fryer A, Hagen JM van, Hennekam RC, Jansweijer MCE, Johnson D, Kant SG, Opitz JM, Ramadevi AR, Reardon W, Ross A, Sarda P, Schrander-Stumpel CTRM, Schoots J, Temple IK, Terhal PA, Toutain A, Wise CA, Wright M, Skidmore DL, Samuels ME, Hoefsloot LH, Knoers NVAM, Brunner HG, Jackson AP, Bongers EMHF. 2012. Meier–Gorlin syndrome genotype–phenotype studies: 35 individuals with pre-replication complex gene mutations and 10 without molecular diagnosis. *Eur J Hum Genet* **20**:598–606. doi:10.1038/ejhg.2011.269

Munnik SA de, Hoefsloot EH, Roukema J, Schoots J, Knoers NV, Brunner HG, Jackson AP, Bongers EM. 2015. Meier-Gorlin syndrome. *Orphanet J Rare Dis* **10**:114. doi:10.1186/s13023-015-0322-x

Munnik Sonja A. de, Otten BJ, Schoots J, Bicknell LS, Aftimos S, Al-Aama JY, Bever Y van, Bober MB, Borm GF, Clayton-Smith J, Deal CL, Edrees AY, Feingold M, Fryer A, Hagen JM van, Hennekam RC, Jansweijer MCE, Johnson D, Kant SG, Opitz JM, Ramadevi AR, Reardon W, Ross A, Sarda P, Schrander-Stumpel CTRM, Sluiter AE, Temple IK, Terhal PA, Toutain A, Wise CA, Wright M, Skidmore DL, Samuels ME, Hoefsloot LH, Knoers NVAM, Brunner HG, Jackson AP, Bongers EMHF. 2012. Meier–Gorlin syndrome: Growth and secondary sexual development of a microcephalic primordial dwarfism disorder. *Am J Med Genet A* **158A**:2733–2742. doi:10.1002/ajmg.a.35681

Munoz DM, Cassiani PJ, Li L, Billy E, Korn JM, Jones MD, Golji J, Ruddy DA, Yu K, McAllister G, DeWeck A, Abramowski D, Wan J, Shirley MD, Neshat SY, Rakiec D, Beaumont R de, Weber O, Kauffmann A, McDonald ER, Keen N, Hofmann F, Sellers WR, Schmelzle T, Stegmeier F, Schlabach MR. 2016. CRISPR Screens Provide a Comprehensive Assessment of Cancer Vulnerabilities but Generate False-Positive Hits for Highly Amplified Genomic Regions. *Cancer Discov* **6**:900–913. doi:10.1158/2159-8290.cd-16-0178

Muramatsu S, Hirai K, Tak Y-S, Kamimura Y, Araki H. 2010. CDK-dependent complex formation between replication proteins Dpb11, Sld2, Pol ε, and GINS in budding yeast. *Gene Dev* **24**:602–612. doi:10.1101/gad.1883410

Nasmyth K. 2001. DISSEMINATING THE GENOME: Joining, Resolving, and Separating Sister Chromatids During Mitosis and Meiosis **35**:673–745. doi:10.1146/annurev.genet.35.102401.091334

Natale F, Rapp A, Yu W, Maiser A, Harz H, Scholl A, Grulich S, Anton T, Hörl D, Chen W, Durante M, Taucher-Scholz G, Leonhardt H, Cardoso MC. 2017. Identification of the

elementary structural units of the DNA damage response. *Nat Commun* **8**:15760. doi:10.1038/ncomms15760

Natsume T, Kiyomitsu T, Saga Y, Kanemaki MT. 2016. Rapid Protein Depletion in Human Cells by Auxin-Inducible Degron Tagging with Short Homology Donors. *Cell reports* **15**:210–218. doi:10.1016/j.celrep.2016.03.001

Neufeld TP, Rubin GM. 1994. The Drosophila peanut gene is required for cytokinesis and encodes a protein similar to yeast putative bud neck filament proteins. *Cell* **77**:371–379. doi:10.1016/0092-8674(94)90152-x

Newlon CS, Theis JF. 1993. The structure and function of yeast ARS elements. *Curr Opin Genet Dev* **3**:752–758. doi:10.1016/s0959-437x(05)80094-2

Nguyen VQ, Co C, Li JJ. 2001. Cyclin-dependent kinases prevent DNA re-replication through multiple mechanisms. *Nature* **411**:1068–1073. doi:10.1038/35082600

Nielsen AL, Oulad-Abdelghani M, Ortiz JA, Remboutsika E, Chambon P, Losson R. 2001. Heterochromatin Formation in Mammalian Cells Interaction between Histones and HP1 Proteins. *Mol Cell* **7**:729–739. doi:10.1016/s1097-2765(01)00218-0

Niemi NM, Sacoman JL, Westrate LM, Gaither LA, Lanning NJ, Martin KR, MacKeigan JP. 2014. The Pseudophosphatase MK-STYX Physically and Genetically Interacts with the Mitochondrial Phosphatase PTPMT1. *Plos One* **9**:e93896. doi:10.1371/journal.pone.0093896

Nishibuchi G, Nakayama J -i. 2014. Biochemical and structural properties of heterochromatin protein 1: understanding its role in chromatin assembly. *J Biochem* **156**:11–20. doi:10.1093/jb/mvu032

Nishimura K, Fukagawa T, Takisawa H, Kakimoto T, Kanemaki M. 2009. An auxin-based degron system for the rapid depletion of proteins in nonplant cells. *Nature methods* **6**:917–922. doi:10.1038/nmeth.1401

Noguchi K, Vassilev A, Ghosh S, Yates JL, DePamphilis ML. 2006. The BAH domain facilitates the ability of human Orc1 protein to activate replication origins in vivo. *Embo J* **25**:5372–5382. doi:10.1038/sj.emboj.7601396

Ocaña-Pallarès E, Vergara Z, Desvoyes B, Tejada-Jimenez M, Romero-Jurado A, Galvan A, Fernandez E, Ruiz-Trillo I, Gutierrez C. 2020. Origin recognition complex (ORC) evolution is influenced by global gene duplication/loss patterns in eukaryotic genomes. *Genome Biol Evol* **12**:3878–3889. doi:10.1093/gbe/evaa011

Ohta S, Tatsumi Y, Fujita M, Tsurimoto T, Obuse C. 2003. The ORC1 Cycle in Human Cells. *J Biol Chem* **278**:41535–41540. doi:10.1074/jbc.m307535200

O'Keefe RT, Henderson SC, Spector DL. 1992. Dynamic organization of DNA replication in mammalian cell nuclei: spatially and temporally defined replication of chromosome-specific alpha-satellite DNA sequences. *J Cell Biology* **116**:1095–1110. doi:10.1083/jcb.116.5.1095

Okuno Y, McNairn AJ, Elzen N den, Pines J, Gilbert DM. 2001. Stability, chromatin association and functional activity of mammalian pre-replication complex proteins during the cell cycle. *Embo J* **20**:4263–4277. doi:10.1093/emboj/20.15.4263

O'Leary NA, Wright MW, Brister JR, Ciufo S, Haddad D, McVeigh R, Rajput B, Robbertse B, Smith-White B, Ako-Adjei D, Astashyn A, Badretdin A, Bao Y, Blinkova O, Brover V, Chetvernin V, Choi J, Cox E, Ermolaeva O, Farrell CM, Goldfarb T, Gupta T, Haft D, Hatcher E, Hlavina W, Joardar VS, Kodali VK, Li W, Maglott D, Masterson P, McGarvey KM, Murphy MR, O'Neill K, Pujar S, Rangwala SH, Rausch D, Riddick LD, Schoch C, Shkeda A, Storz SS, Sun H, Thibaud-Nissen F, Tolstoy I, Tully RE, Vatsan AR, Wallin C, Webb D, Wu W, Landrum MJ, Kimchi A, Tatusova T, DiCuccio M, Kitts P, Murphy TD, Pruitt KD. 2016. Reference sequence (RefSeq) database at NCBI: current status, taxonomic expansion, and functional annotation. *Nucleic Acids Res* **44**:D733–D745. doi:10.1093/nar/gkv1189

Pak DTS, Pflumm M, Chesnokov I, Huang DW, Kellum R, Marr J, Romanowski P, Botchan MR. 1997. Association of the Origin Recognition Complex with Heterochromatin and HP1 in Higher Eukaryotes. *Cell* **91**:311–323. doi:10.1016/s0092-8674(00)80415-8

Palzkill TG, Oliver SG, Newlon CS. 1986. DNA sequence analysis of ARS elements from chromosome III of Saccharomyces cerevisiae: identification of a new conserved sequence. *Nucleic Acids Res* **14**:6247–6264. doi:10.1093/nar/14.15.6247

Park RJ, Wang T, Koundakjian D, Hultquist JF, Lamothe-Molina P, Monel B, Schumann K, Yu H, Krupzcak KM, Garcia-Beltran W, Piechocka-Trocha A, Krogan NJ, Marson A, Sabatini DM, Lander ES, Hacohen N, Walker BD. 2017. A genome-wide CRISPR screen identifies a restricted set of HIV host dependency factors. *Nat Genet* **49**:193–203. doi:10.1038/ng.3741

Parker MW, Bell M, Mir M, Kao JA, Darzacq X, Botchan MR, Berger JM. 2019. A new class of disordered elements controls DNA replication through initiator self-assembly. *Elife* **8**:e48562. doi:10.7554/elife.48562

Paro R, Hogness DS. 1991. The Polycomb protein shares a homologous domain with a heterochromatin-associated protein of Drosophila. *Proc National Acad Sci* **88**:263–267. doi:10.1073/pnas.88.1.263

Patel A, Dharmarajan V, Vought VE, Cosgrove MS. 2009. On the Mechanism of Multiple Lysine Methylation by the Human Mixed Lineage Leukemia Protein-1 (MLL1) Core Complex* ♦. *J Biol Chem* **284**:24242–24256. doi:10.1074/jbc.m109.014498

Perkins G, Diffley JFX. 1998. Nucleotide-Dependent Prereplicative Complex Assembly by Cdc6p, a Homolog of Eukaryotic and Prokaryotic Clamp-Loaders. *Mol Cell* **2**:23–32. doi:10.1016/s1097-2765(00)80110-0

Perkins G, Drury LS, Diffley JFX. 2001. Separate SCFCDC4 recognition elements target Cdc6 for proteolysis in S phase and mitosis. *Embo J* **20**:4836–4845. doi:10.1093/emboj/20.17.4836

Perrini B, Piacentini L, Fanti L, Altieri F, Chichiarelli S, Berloco M, Turano C, Ferraro A, Pimpinelli S. 2004. HP1 Controls Telomere Capping, Telomere Elongation, and Telomere Silencing by Two Different Mechanisms in Drosophila. *Mol Cell* **15**:467–476. doi:10.1016/j.molcel.2004.06.036

Pesesse X, Dewaste V, Smedt FD, Laffargue M, Giuriato S, Moreau C, Payrastre B, Erneux C. 2001. The Src Homology 2 Domain Containing Inositol 5-Phosphatase SHIP2 Is Recruited to the Epidermal Growth Factor (EGF) Receptor and Dephosphorylates Phosphatidylinositol 3,4,5-Trisphosphate in EGF-stimulated COS-7 Cells*. *J Biol Chem* **276**:28348–28355. doi:10.1074/jbc.m103537200

Petersen BO, Lukas J, Sørensen CS, Bartek J, Helin K. 1999. Phosphorylation of mammalian CDC6 by Cyclin A/CDK2 regulates its subcellular localization. *Embo J* **18**:396–410. doi:10.1093/emboj/18.2.396

Petersen BO, Wagener C, Marinoni F, Kramer ER, Melixetian M, Denchi EL, Gieffers C, Matteucci C, Peters J-M, Helin K. 2000. Cell cycle– and cell growth–regulated proteolysis of mammalian CDC6 is dependent on APC–CDH1. *Gene Dev* **14**:2330–2343. doi:10.1101/gad.832500

Pflumm MF, Botchan MR. 2001. Orc mutants arrest in metaphase with abnormally condensed chromosomes. *Dev Camb Engl* **128**:1697–707.

Piatti S, Böhm T, Cocker JH, Diffley JF, Nasmyth K. 1996. Activation of S-phase-promoting CDKs in late G1 defines a “point of no return” after which Cdc6 synthesis cannot promote DNA replication in yeast. *Gene Dev* **10**:1516–1531. doi:10.1101/gad.10.12.1516

Popova VV, Brechalov AV, Georgieva SG, Kopytova DV. 2018. Nonreplicative Functions of the Origin Recognition Complex. *Nucleus (Austin, Tex)* 19491034.2018.1516484. doi:10.1080/19491034.2018.1516484

Prasad N, Topping RS, Decker SJ. 2002. Src family tyrosine kinases regulate adhesion-dependent tyrosine phosphorylation of 5′-inositol phosphatase SHIP2 during cell attachment and spreading on collagen I. *J Cell Sci* **115**:3807–3815. doi:10.1242/jcs.00070

Prasanth SG, Prasanth KV, Siddiqui K, Spector DL, Stillman B. 2004. Human Orc2 localizes to centrosomes, centromeres and heterochromatin during chromosome inheritance. *The EMBO Journal* **23**:2651–2663. doi:10.1038/sj.emboj.7600255

Prasanth SG, Prasanth KV, Stillman B. 2002. Orc6 Involved in DNA Replication, Chromosome Segregation, and Cytokinesis. *Science* **297**:1026–1031. doi:10.1126/science.1072802

Prasanth SG, Shen Z, Prasanth KV, Stillman B. 2010. Human origin recognition complex is essential for HP1 binding to chromatin and heterochromatin organization. *Proc Natl Acad Sci USA* **107**:15093–15098. doi:10.1073/pnas.1009945107

Quivy J, Roche D, Kirschner D, Tagami H, Nakatani Y, Almouzni G. 2004. A CAF-1 dependent pool of HP1 during heterochromatin duplication. *Embo J* **23**:3516–3526. doi:10.1038/sj.emboj.7600362

Quivy J-P, Gérard A, Cook AJL, Roche D, Almouzni G. 2008. The HP1–p150/CAF-1 interaction is required for pericentric heterochromatin replication and S-phase progression in mouse cells. *Nat Struct Mol Biol* **15**:972–979. doi:10.1038/nsmb.1470

Randell JCW, Bowers JL, Rodríguez HK, Bell SP. 2006. Sequential ATP Hydrolysis by Cdc6 and ORC Directs Loading of the Mcm2-7 Helicase. *Mol Cell* **21**:29–39. doi:10.1016/j.molcel.2005.11.023

Rao H, Stillman B. 1995. The origin recognition complex interacts with a bipartite DNA binding site within yeast replicators. *Proc National Acad Sci* **92**:2224–2228. doi:10.1073/pnas.92.6.2224

Rea S, Eisenhaber F, O'Carroll D, Strahl BD, Sun Z-W, Schmid M, Opravil S, Mechtler K, Ponting CP, Allis CD, Jenuwein T. 2000. Regulation of chromatin structure by site-specific histone H3 methyltransferases. *Nature* **406**:593–599. doi:10.1038/35020506

Remus D, Beuron F, Tolun G, Griffith JD, Morris EP, Diffley JFX. 2009. Concerted loading of Mcm2-7 double hexamers around DNA during DNA replication origin licensing. *Cell* **139**:719–30. doi:10.1016/j.cell.2009.10.015

Richart AN, Brunner CIW, Stott K, Murzina NV, Thomas JO. 2012. Characterization of Chromoshadow Domain-mediated Binding of Heterochromatin Protein 1α (HP1α) to Histone H3*. *J Biological Chem* **287**:18730–18737. doi:10.1074/jbc.m111.337204

Robin P, Fritsch L, Philipot O, Svinarchuk F, Ait-Si-Ali S. 2007. Post-translational modifications of histones H3 and H4 associated with the histone methyltransferases Suv39h1 and G9a. *Genome Biol* **8**:R270. doi:10.1186/gb-2007-8-12-r270

Romanowski P, Madine MA, Rowles A, Blow JJ, Laskey RA. 1996. The Xenopus origin recognition complex is essential for DNA replication and MCM binding to chromatin. *Curr Biol* **6**:1416–1425. doi:10.1016/s0960-9822(96)00746-4

Roux KJ, Kim DI, Burke B. 2013. BioID: A Screen for Protein-Protein Interactions. *Curr Protoc Protein Sci* **74**:19.23.1-19.23.14. doi:10.1002/0471140864.ps1923s74

Roux KJ, Kim DI, Raida M, Burke B. 2012. A promiscuous biotin ligase fusion protein identifies proximal and interacting proteins in mammalian cells. *J Cell Biology* **196**:801–810. doi:10.1083/jcb.201112098

Rowley A, Cocker JH, Harwood J, Diffley JF. 1995. Initiation complex assembly at budding yeast replication origins begins with the recognition of a bipartite sequence by limiting amounts of the initiator, ORC. *Embo J* **14**:2631–2641. doi:10.1002/j.1460-2075.1995.tb07261.x

Saha P, Chen J, Thome KC, Lawlis SJ, Hou Z, Hendricks M, Parvin JD, Dutta A. 1998. Human CDC6/Cdc18 Associates with Orc1 and Cyclin-cdk and Is Selectively Eliminated from the Nucleus at the Onset of S Phase. *Mol Cell Biol* **18**:2758–2767. doi:10.1128/mcb.18.5.2758

Saksouk N, Simboeck E, Déjardin J. 2015. Constitutive heterochromatin formation and transcription in mammals. *Epigenet Chromatin* **8**:3. doi:10.1186/1756-8935-8-3

Sanchez Y, Bachant J, Wang H, Hu F, Liu D, Tetzlaff M, Elledge SJ. 1999. Control of the DNA Damage Checkpoint by Chk1 and Rad53 Protein Kinases Through Distinct Mechanisms. *Science* **286**:1166–1171. doi:10.1126/science.286.5442.1166

Sanjana NE, Shalem O, Zhang F. 2014. Improved vectors and genome-wide libraries for CRISPR screening. *Nat Methods* **11**:783–784. doi:10.1038/nmeth.3047

Sasaki T, Gilbert DM. 2007. The many faces of the origin recognition complex. *Current opinion in cell biology* **19**:337–343. doi:10.1016/j.ceb.2007.04.007

Schleker T, Shimada K, Sack R, Pike BL, Gasser SM. 2010. Cell cycle-dependent phosphorylation of Rad53 kinase by Cdc5 and Cdc28 modulates checkpoint adaptation. *Cell Cycle Georget Tex* **9**:350–63. doi:10.4161/cc.9.2.10448

Schueler MG, Sullivan BA. 2006. Structural and Functional Dynamics of Human Centromeric Chromatin. *Annu Rev Genom Hum G* **7**:301–313. doi:10.1146/annurev.genom.7.080505.115613

Sedlazeck FJ, Rescheneder P, Smolka M, Fang H, Nattestad M, Haeseler A von, Schatz MC. 2018. Accurate detection of complex structural variations using single-molecule sequencing. *Nat Methods* **15**:461–468. doi:10.1038/s41592-018-0001-7

Semple JW, Da-Silva LF, Jervis EJ, Ah-Kee J, Al-Attar H, Kummer L, Heikkila JJ, Pasero P, Duncker BP. 2006. An essential role for Orc6 in DNA replication through maintenance of pre-replicative complexes. *Embo J* **25**:5150–5158. doi:10.1038/sj.emboj.7601391

Senyilmaz D, Virtue S, Xu X, Tan CY, Griffin JL, Miller AK, Vidal-Puig A, Teleman AA. 2015. Regulation of mitochondrial morphology and function by stearoylation of TFR1. *Nature* **525**:124–128. doi:10.1038/nature14601

Shen Z, Chakraborty A, Jain A, Giri S, Ha T, Prasanth KV, Prasanth SG. 2012. Dynamic Association of ORCA with Prereplicative Complex Components Regulates DNA Replication Initiation. *Mol Cell Biol* **32**:3107–3120. doi:10.1128/mcb.00362-12

Shen Z, Prasanth SG. 2012. Orc2 protects ORCA from ubiquitin-mediated degradation. *Cell cycle (Georgetown, Tex)* **11**:3578–3589. doi:10.4161/cc.21870

Shen Z, Sathyan KM, Geng Y, Zheng R, Chakraborty A, Freeman B, Wang F, Prasanth KV, Prasanth SG. 2010. A WD-Repeat Protein Stabilizes ORC Binding to Chromatin. *Mol Cell* **40**:99–111. doi:10.1016/j.molcel.2010.09.021

Shi J, Wang E, Milazzo JP, Wang Z, Kinney JB, Vakoc CR. 2015. Discovery of cancer drug targets by CRISPR-Cas9 screening of protein domains. *Nat Biotechnol* **33**:661–7. doi:10.1038/nbt.3235

Shibata E, Dutta A. 2020. A human cancer cell line initiates DNA replication normally in the absence of ORC5 and ORC2 proteins. *J Biol Chem* jbc.RA120.015450. doi:10.1074/jbc.ra120.015450

Shibata E, Kiran M, Shibata Y, Singh S, Kiran S, Dutta A. 2016. Two subunits of human ORC are dispensable for DNA replication and proliferation. *Elife* **5**:1844. doi:10.7554/elife.19084

Shimada K, Gasser SM. 2007. The origin recognition complex functions in sister-chromatid cohesion in Saccharomyces cerevisiae. *Cell* **128**:85–99. doi:10.1016/j.cell.2006.11.045

Shinkai Y, Tachibana M. 2011. H3K9 methyltransferase G9a and the related molecule GLP. *Gene Dev* **25**:781–788. doi:10.1101/gad.2027411

Shirahige K, Iwasaki T, Rashid MB, Ogasawara N, Yoshikawa H. 1993. Location and characterization of autonomously replicating sequences from chromosome VI of Saccharomyces cerevisiae. *Mol Cell Biol* **13**:5043–5056. doi:10.1128/mcb.13.8.5043

Siddiqui K, On KF, Diffley JFX. 2013. Regulating DNA replication in eukarya. *Csh Perspect Biol* **5**:a012930–a012930. doi:10.1101/cshperspect.a012930

Siddiqui K, Stillman B. 2007. ATP-dependent Assembly of the Human Origin Recognition Complex. *J Biol Chem* **282**:32370–32383. doi:10.1074/jbc.m705905200

Sikora E, Mosieniak G, Sliwinska MA. 2016. Morphological and Functional Characteristic of Senescent Cancer Cells. *Curr Drug Targets* **17**:377–387. doi:10.2174/1389450116666151019094724

Singh PB, Miller JR, Pearce J, Kothary R, Burton RD, Paro R, James TC, J.Gaunt S. 1991. A sequence motif found in a Drosophila heterochromatin protein is conserved in animals and plants. *Nucleic Acids Res* **19**:789–794. doi:10.1093/nar/19.4.789

Smits AH, Ziebell F, Joberty G, Zinn N, Mueller WF, Clauder-Münster S, Eberhard D, Savitski MF, Grandi P, Jakob P, Michon A-M, Sun H, Tessmer K, Bürckstümmer T, Bantscheff M, Steinmetz LM, Drewes G, Huber W. 2019. Biological plasticity rescues target activity in CRISPR knock outs. *Nat Methods* **16**:1087–1093. doi:10.1038/s41592-019-0614-5

So RWL, Chung SW, Lau HHC, Watts JJ, Gaudette E, Al-Azzawi ZAM, Bishay J, Lin LT-W, Joung J, Wang X, Schmitt-Ulms G. 2019. Application of CRISPR genetic screens to investigate neurological diseases. *Mol Neurodegener* **14**:41. doi:10.1186/s13024-019-0343-3

Song B, Liu XS, Davis K, Liu X. 2011. Plk1 Phosphorylation of Orc2 Promotes DNA Replication under Conditions of Stress. *Mol Cell Biol* **31**:4844–4856. doi:10.1128/mcb.06110-11

Speck C, Chen Z, Li H, Stillman B. 2005. ATPase-dependent cooperative binding of ORC and Cdc6 to origin DNA. *Nat Struct Mol Biol* **12**:965–971. doi:10.1038/nsmb1002

Spiliotis ET, Hunt SJ, Hu Q, Kinoshita M, Nelson WJ. 2008. Epithelial polarity requires septin coupling of vesicle transport to polyglutamylated microtubules. *J Cell Biology* **180**:295–303. doi:10.1083/jcb.200710039

Spiliotis ET, Kinoshita M, Nelson WJ. 2005. A Mitotic Septin Scaffold Required for Mammalian Chromosome Congression and Segregation. *Science* **307**:1781–1785. doi:10.1126/science.1106823

Stewart MD, Li J, Wong J. 2005. Relationship between histone H3 lysine 9 methylation, transcription repression, and heterochromatin protein 1 recruitment. *Molecular and Cellular Biology* **25**:2525–2538. doi:10.1128/mcb.25.7.2525-2538.2005

Stinchcomb DT, Struhl K, Davis RW. 1979. Isolation and characterisation of a yeast chromosomal replicator. *Nature* **282**:39–43. doi:10.1038/282039a0

Strom AR, Emelyanov AV, Mir M, Fyodorov DV, Darzacq X, Karpen GH. 2017. Phase separation drives heterochromatin domain formation. *Nature* **547**:241–245. doi:10.1038/nature22989

Sun Y, Jiang X, Chen S, Fernandes N, Price BD. 2005. A role for the Tip60 histone acetyltransferase in the acetylation and activation of ATM. *P Natl Acad Sci Usa* **102**:13182–13187. doi:10.1073/pnas.0504211102

Sundaram M, Guernsey DL, Rajaraman MM, Rajaraman R. 2004. Neosis: A Novel Type of Cell Division in Cancer. *Cancer Biol Ther* **3**:207–218. doi:10.4161/cbt.3.2.663

Tachibana M, Ueda J, Fukuda M, Takeda N, Ohta T, Iwanari H, Sakihama T, Kodama T, Hamakubo T, Shinkai Y. 2005. Histone methyltransferases G9a and GLP form heteromeric

complexes and are both crucial for methylation of euchromatin at H3-K9. *Gene Dev* **19**:815–826. doi:10.1101/gad.1284005

Tak Y, Tanaka Y, Endo S, Kamimura Y, Araki H. 2006. A CDK-catalysed regulatory phosphorylation for formation of the DNA replication complex Sld2–Dpb11. *Embo J* **25**:1987–1996. doi:10.1038/sj.emboj.7601075

Takahashi TS, Basu A, Bermudez V, Hurwitz J, Walter JC. 2008. Cdc7–Drf1 kinase links chromosome cohesion to the initiation of DNA replication in Xenopus egg extracts. *Gene Dev* **22**:1894–1905. doi:10.1101/gad.1683308

Takahashi TS, Yiu P, Chou MF, Gygi S, Walter JC. 2004. Recruitment of Xenopus Scc2 and cohesin to chromatin requires the pre-replication complex. *Nat Cell Biol* **6**:991–996. doi:10.1038/ncb1177

Takayama Y, Kamimura Y, Okawa M, Muramatsu S, Sugino A, Araki H. 2003. GINS, a novel multiprotein complex required for chromosomal DNA replication in budding yeast. *Genes & Development* **17**:1153–1165. doi:10.1101/gad.1065903

Tarumoto Y, Lu B, Somerville TDD, Huang Y-H, Milazzo JP, Wu XS, Klingbeil O, Demerdash OE, Shi J, Vakoc CR. 2018. LKB1, Salt-Inducible Kinases, and MEF2C Are Linked Dependencies in Acute Myeloid Leukemia. *Mol Cell* **69**:1017-1027.e6. doi:10.1016/j.molcel.2018.02.011

Tatsumi Y, Ezura K, Yoshida K, Yugawa T, Narisawa-Saito M, Kiyono T, Ohta S, Obuse C, Fujita M. 2008. Involvement of human ORC and TRF2 in pre-replication complex assembly at telomeres. *Genes Cells* **13**:1045–1059. doi:10.1111/j.1365-2443.2008.01224.x

Tatsumi Y, Ohta S, Kimura H, Tsurimoto T, Obuse C. 2003. The ORC1 Cycle in Human Cells. *J Biol Chem* **278**:41528–41534. doi:10.1074/jbc.m307534200

Tennakoon C, Purbojati RW, Sung W-K. 2012. BatMis: a fast algorithm for k-mismatch mapping. *Bioinformatics* **28**:2122–2128. doi:10.1093/bioinformatics/bts339

Theis JF, Newlon CS. 1997. The ARS309 chromosomal replicator of Saccharomyces cerevisiae depends on an exceptional ARS consensus sequence. *Proc National Acad Sci* **94**:10786–10791. doi:10.1073/pnas.94.20.10786

Thiru A, Nietlispach D, Mott HR, Okuwaki M, Lyon D, Nielsen PR, Hirshberg M, Verreault A, Murzina NV, Laue ED. 2004. Structural basis of HP1/PXVXL motif peptide interactions and HP1 localisation to heterochromatin. *The EMBO Journal* **23**:489–499. doi:10.1038/sj.emboj.7600088

Ticau S, Friedman LJ, Ivica NA, Gelles J, Bell SP. 2015. Single-Molecule Studies of Origin Licensing Reveal Mechanisms Ensuring Bidirectional Helicase Loading. *Cell* **161**:513–525. doi:10.1016/j.cell.2015.03.012

Tiengwe C, Marcello L, Farr H, Gadelha C, Burchmore R, Barry JD, Bell SD, McCulloch R. 2012. Identification of ORC1/CDC6-Interacting Factors in Trypanosoma brucei Reveals Critical Features of Origin Recognition Complex Architecture. *Plos One* **7**:e32674. doi:10.1371/journal.pone.0032674

Tocilj A, On KF, Yuan Z, Sun J, Elkayam E, Li H, Stillman B, Joshua-Tor L. 2017. Structure of the active form of human origin recognition complex and its ATPase motor module. *Elife* **6**:1822. doi:10.7554/elife.20818

Triolo T, Sternglanz R. 1996. Role of interactions between the origin recognition complex and SIR1 in transcriptional silencing. *Nature* **381**:251–253. doi:10.1038/381251a0

Tsherniak A, Vazquez F, Montgomery PG, Weir BA, Kryukov G, Cowley GS, Gill S, Harrington WF, Pantel S, Krill-Burger JM, Meyers RM, Ali L, Goodale A, Lee Y, Jiang G, Hsiao J, Gerath WFJ, Howell S, Merkel E, Ghandi M, Garraway LA, Root DE, Golub TR, Boehm JS, Hahn WC. 2017. Defining a Cancer Dependency Map. *Cell* **170**:564-576.e16. doi:10.1016/j.cell.2017.06.010

Tsouroula K, Furst A, Rogier M, Heyer V, Maglott-Roth A, Ferrand A, Reina-San-Martin B, Soutoglou E. 2016. Temporal and Spatial Uncoupling of DNA Double Strand Break Repair Pathways within Mammalian Heterochromatin. *Mol Cell* **63**:293–305. doi:10.1016/j.molcel.2016.06.002

Uhlmann F. 2001. Chromosome cohesion and segregation in mitosis and meiosis. *Curr Opin Cell Biol* **13**:754–761. doi:10.1016/s0955-0674(00)00279-9

Varmark H, Sparks CA, Nordberg JJ, Koppetsch BS, Theurkauf WE. 2009. DNA damage-induced cell death is enhanced by progression through mitosis. *Cell Cycle* **8**:2952–2964. doi:10.4161/cc.8.18.9539

Vashee S. 2003. Sequence-independent DNA binding and replication initiation by the human origin recognition complex. *Genes & Development* **17**:1894–1908. doi:10.1101/gad.1084203

Vashee S, Simancek P, Challberg MD, Kelly TJ. 2001. Assembly of the Human Origin Recognition Complex. *J Biol Chem* **276**:26666–26673. doi:10.1074/jbc.m102493200

Vermeulen M, Eberl HC, Matarese F, Marks H, Denissov S, Butter F, Lee KK, Olsen JV, Hyman AA, Stunnenberg HG, Mann M. 2010. Quantitative Interaction Proteomics and Genome-wide Profiling of Epigenetic Histone Marks and Their Readers. *Cell* **142**:967–980. doi:10.1016/j.cell.2010.08.020

Walter D, Hoffmann S, Komseli E-S, Rappsilber J, Gorgoulis V, Sørensen CS. 2016. SCFCyclin F-dependent degradation of CDC6 suppresses DNA re-replication. *Nat Commun* **7**:10530. doi:10.1038/ncomms10530

Walter JC, Takahashi TS, Bermudez VP, Hurwitz J. 2007. Mechanism of pre-RC-dependent cohesin loading in Xenopus egg extracts. *Faseb J* **21**:A94–A94. doi:10.1096/fasebj.21.5.a94-c

Wang Y, Zhong Y, Zhou Y, Tanaseichuk O, Li Z, Zhao JC. 2019. Identification of a Xist silencing domain by Tiling CRISPR. *Sci Rep-uk* **9**:2408. doi:10.1038/s41598-018-36750-0

Wang Z, Andrews P, Kendall J, Ma B, Hakker I, Rodgers L, Ronemus M, Wigler M, Levy D. 2016. SMASH, a fragmentation and sequencing method for genomic copy number analysis. *Genome Res* **26**:844–851. doi:10.1101/gr.201491.115

Weinreich M, Liang C, Stillman B. 1999. The Cdc6p nucleotide-binding motif is required for loading mcm proteins onto chromatin. *Proc Natl Acad Sci USA* **96**:441–446. doi:10.1073/pnas.96.2.441.

Wilsker D, Petermann E, Helleday T, Bunz F. 2008. Essential function of Chk1 can be uncoupled from DNA damage checkpoint and replication control. *P Natl Acad Sci Usa* **105**:20752–7. doi:10.1073/pnas.0806917106

Wohlschlegel JA, Dwyer BT, Dhar SK, Cvetic C, Walter JC, Dutta A. 2000. Inhibition of Eukaryotic DNA Replication by Geminin Binding to Cdt1. *Science* **290**:2309–2312. doi:10.1126/science.290.5500.2309

Xu N, You Y, Liu C, Balasov M, Lun LT, Geng Y, Fung CP, Miao H, Tian H, Choy TT, Shi X, Fan Z, Zhou B, Akhmetova K, Din RU, Yang H, Hao Q, Qian P, Chesnokov I, Zhu G. 2020. Structural basis of DNA replication origin recognition by human Orc6 protein binding with DNA. *Nucleic Acids Res* gkaa751-. doi:10.1093/nar/gkaa751

Yan H, Xiang X, Chen Q, Pan X, Cheng H, Wang F. 2018. HP1 cooperates with CAF-1 to compact heterochromatic transgene repeats in mammalian cells. *Sci Rep-uk* **8**:14141. doi:10.1038/s41598-018-32381-7

Ye Q, Callebaut I, Pezhman A, Courvalin J-C, Worman HJ. 1997. Domain-specific Interactions of Human HP1-type Chromodomain Proteins and Inner Nuclear Membrane Protein LBR*. *J Biol Chem* **272**:14983–14989. doi:10.1074/jbc.272.23.14983

Yeeles JTP, Deegan TD, Janska A, Early A, Diffley JFX. 2015. Regulated eukaryotic DNA replication origin firing with purified proteins. *Nature* **519**:431–435. doi:10.1038/nature14285

Yi Q, Chen Q, Liang C, Yan H, Zhang Z, Xiang X, Zhang M, Qi F, Zhou L, Wang F. 2018. HP1 links centromeric heterochromatin to centromere cohesion in mammals. *Embo Rep* **19**. doi:10.15252/embr.201745484

Yuan Z, Riera A, Bai L, Sun J, Nandi S, Spanos C, Chen ZA, Barbon M, Rappsilber J, Stillman B, Speck C, Li H. 2017. Structural basis of Mcm2-7 replicative helicase loading by ORC-Cdc6 and Cdt1. *Nature structural & molecular biology* **24**:316–324. doi:10.1038/nsmb.3372

Zarebski M, Wiernasz E, Dobrucki JW. 2009. Recruitment of heterochromatin protein 1 to DNA repair sites. *Cytom Part A* **75A**:619–625. doi:10.1002/cyto.a.20734

Zeng W, Jr ARB, Yokomori K. 2010. HP1: Heterochromatin binding proteins working the genome. *Epigenetics* **5**:287–292. doi:10.4161/epi.5.4.11683

Zheng G, Kanchwala M, Xing C, Yu H. 2018. MCM2–7-dependent cohesin loading during S phase promotes sister-chromatid cohesion. *Elife* **7**:e33920. doi:10.7554/elife.33920

Zhuang G, Hunter S, Hwang Y, Chen J. 2007. Regulation of EphA2 Receptor Endocytosis by SHIP2 Lipid Phosphatase via Phosphatidylinositol 3-Kinase-dependent Rac1 Activation*. *J Biol Chem* **282**:2683–2694. doi:10.1074/jbc.m608509200

Ziv Y, Bielopolski D, Galanty Y, Lukas C, Taya Y, Schultz DC, Lukas J, Bekker-Jensen S, Bartek J, Shiloh Y. 2006. Chromatin relaxation in response to DNA double-strand breaks is modulated by a novel ATM- and KAP-1 dependent pathway. *Nat Cell Biol* **8**:870–876. doi:10.1038/ncb1446